Population Balance Modelling and Experimental Studies of Emulsion Polymerisation

Stephen John Sweetman

May 2008

A thesis submitted for the degree of

Doctor of Philosophy of the University of London

and for the

Diploma of Membership of Imperial College

Centre for Process Systems Engineering

Department of Chemical Engineering and Chemical Technology

Imperial College London,

South Kensington Campus,

London SW7 2AZ



Abstract

Emulsion polymerisation is a process of considerable technological and industrial significance. The process presents many challenges in respect to design, optimisation and multi-objective distribution control. The quality of latex is determined by the final product properties, i.e. viscosity, mechanical strength and film-forming ability, which are in turn a function of the latex attributes of PSD and MWD. This motivates an inferential control scheme utilising these distributions. This research addresses model development and controllability analysis towards model-based control.

A population balance model for PSD and MWD is developed. The PSD information is incorporated via a one-dimensional population distribution of the polymer particles with respect to their size, in conjunction with a population distribution of the total live polymer radicals/particle. MWD information is incorporated via one-dimensional population distributions of the live radicals and dead polymer chains with respect to their length (in different sized particles). The model solution is facilitated by a number of algorithmic developments, including a decomposition algorithm coupled with a multi-level discretisation for PSD and the application of the method of moments for MWD. This model is compared to extensive experimental data for its validation. Improvements in the form of a two-dimensional version of this model enable better prediction of compartmentalisation and hence the growth rates, thereby improving model match with experiments.

This work presents a study into the simultaneous controllability of PSD and MWD, assessed through an experimental sensitivity analysis on the main process manipulations: initiator, CTA, monomer and surfactant. The work analyses the practical limitations on the attainability of PSD and MWD. The range of experiments carried out clearly indicates the operation of individual mechanisms in the simultaneous formation of PSD and MWD.

Acknowledgments

I owe a debt of gratitude to my supervisor, Dr. Charles Immanuel. His sound advice and careful guidance were invaluable.

For their efforts and assistance, a special thanks as well to Tahir (Tom) Malik, Simon Emmett and Neal Williams of ICI.

Finally, I would be remiss without mentioning my friends inside and outside of university for their support and motivation.

To each of the above, I extend my deepest appreciation.

DEDICATION

For my family, who offered me unconditional love and support throughout the course of my Ph.D.

Contents

Abstract 2

Acknowledgments 3

Contents 5

List of Figures 9

List of Tables 9

1 Introduction, Motivation and Aims 14

1.1 Emulsion Polymerisation 14

1.1.1 Theory 16

1.2 Control of Particulate Processes: A Model-Based Approach 27

1.2.1 Process Modelling 28

1.2.2 Population Balance Models 29

1.3 Thesis Objectives & Structure 32

2 Literature Review 34

2.1 Introduction 34

2.2 Early Process Modelling 34

2.3 Lumped Parameter Modelling 36

2.4 PSD Modelling 37

2.5 MWD Modelling 41

2.6 Compartmentalisation Modelling 44

2.7 Controllability 46

3 PSD & MWD Model **49**

3.1 PSD Model Structure 49

3.1.1 Kinetic Scheme 50

3.1.2 Pseudo-homopolymerisation Approximation 51

3.1.3 Aqueous Phase Radical Balances 51

3.1.4 Monomer Balance 54

3.1.5 Surfactant Balance 55

3.1.6 CTA Balance 56

3.1.7 System Population Balance 56

3.1.8 Average Radicals per Particle 57

3.1.9 Particle Entry 58

3.1.10 Desorption from Particles 58

3.1.11 Termination within Particles 59

3.1.12 Particle Growth 59

3.1.13 Particle Nucleation 59

3.1.14 Coagulation Framework 60

3.1.15 Coagulation Rate Kernel 61

3.2 PSD Model Solution 65

3.3 MWD Model Structure 69

3.4 Method of Moments for MWD 71

3.5 Semi-batch Emulsion Polymerisation Simulation: PSD Results 77

3.5.1 PSD and Nucleation 80

3.5.2 PSD and Coagulation 81

3.5.3 PSD and Average Number of Radicals/Particle 83

3.6 MWD: Semi-batch Simulation Results 85

3.6.1 Effect of Particle Growth on MWD 87

3.6.2 Effect of Compartmentalisation on Termination Rates: Sensitivity on PSD and MWD 88

3.7 Macroscopic Process Sensitivities to Process Manipulations 91

3.8 Chapter Summary 96

4 Experimental Studies & Model Validation **97**

4.1 **Introduction** 97

4.2 Experimental System 98

4.3 Recipe and Operating Conditions 101

4.3.1 Latex Characterisation 104

4.4 Experimental Results & Discussions 105

4.4.1 Repeatability Analysis: PSD, solids content and number of particles 105

4.4.2 Repeatability Analysis: Molecular weight 106

4.4.3 Initiator Perturbation: effect on PSD, solids content and number of particles 107

4.4.4 Initiator Perturbation: effect on MWD 111

4.4.5 Summary of Initiator Effects 112

4.4.6 CTA Perturbation: effect on PSD & MWD 113

4.4.7 Summary of CTA Effects 115

4.4.8 Monomer Perturbation: effect on PSD, solids content and number of particles 116

4.4.9 Monomer Perturbation: effect on MWD 117

4.4.10 Summary of Monomer Effects 118

4.4.11 Surfactant Perturbation: effect on PSD, solids content and number of particles 119

4.4.12 Surfactant Perturbation: effect on MWD 121

4.4.13 Summary of Surfactant Effects 122

4.4.14 Comparison of Component Addition Policies 122

4.5 Preliminary Model Validation Results 123

4.5.1 Effect of Initiator 126

4.5.2 Effect of CTA 127

4.5.3 Effect of Monomer 128

4.5.4 Effect of Surfactant 130

4.6 Chapter Summary 133

5 Compartmentalisation Analysis **135**

5.1 Introduction 135

5.2 2D PSD Model Framework 137

5.2.1 PSD Model: System PBE 137

5.2.2 PSD Model: Component Balances 138

5.2.3 Aqueous Phase Oligomer Balance 139

5.2.4 Average Radical Number per Particle 140

5.3 2D PSD Model Solution 141

5.4 MWD Model and Solution 146

5.5 PSD/MWD Results and Discussion 147

5.5.1 Convergence of n 147

5.5.2 PSD and MWD Model Results 148

5.5.3 1D Model, 2D Model and Experiment Comparison 153

5.6 Chapter Summary 155

6 Conclusions and Future Work **156**

6.1 Thesis Conclusions 156

6.2 Future work 160

Bibliography **164**

A Nomenclature **184**

B Experimental Studies **190**

B.1 Emulsion Polymerisation Equipment 190

B.2 Capillary Hydrodynamic Fractionation: Measurement of PSD 191

B.2.1 Materials and Methods 191

B.3 Gel Permeation Chromatography: Measurement of MWD 192

B.3.1 Materials and Methods 192

List of Tables

3.1 Nominal values for kinetic parameters used in model. 78

3.2 Nominal values for physical constants used in model. 79

4.1 Experimental inputs for initial reactants and feeds. 103

4.2 Tuned values for kinetic parameters used in model. 125

4.3 Tuned values for physical constants used in model. 125

List of Figures

1.1 Decomposition of a peroxide to produce radicals. 17

1.2 Addition of a primary free radical to the double bond of ethene. 17

1.3 Propagation of ethane. 17

1.4 Termination via *combination* of polyethene radicals. 18

1.5 Termination via *disproportionation* of polyethene radicals. 18

1.6 Chain transfer from a growing polymer radical (polyethene) to monomer (ethene). 18

1.7 Schematic of basic reactions and physical transport mechanisms occurring during an emulsion polymerisation reaction. 19

1.8 Thermodynamic schematic of a lyophilic system, where $\Delta G_f^o = \gamma \Delta A$, with γ and ΔA being the solid-liquid interface tension and the increase in interfacial area, respectively. 21

1.9 Illustration of the charge layers surrounding a particle with adsorbed ionic surfactant in an ionic medium. 23

3.1 a) Discretisation of particle size domain and b) time domain 65

3.2 Hierarchical 2-tier algorithm for PSD/MWD model solution 67

3.3 Simulation base-case input flow rates 77

3.4 PSD evolution and the corresponding trends of surfactant concentration, nucleation rates and particle number. 80

3.5 Net interaction potential between particles of size r_{nuc} at 0.6 s and 1800 s. 82

3.6 Coagulation rate constants corresponding to critical changes in surfactant concentration. 83

3.7 The average number of radicals/particle, the rate of entry, the rate of termination and the rate of desorption. 84

3.8 The ratio of entry to termination and the global average number of radicals/particle. 85
3.9 Number-average and Weight-average MWD evolution. 86
3.10 Global Number-average and Global Weight-average MW evolution and an initial time plot of the Global number-average MW evolution. 86
3.11 Global average molecular weight evolutions analysing the effect of particle growth. 87
3.12 The effect of introducing a termination correction factor in the calculation of $\bar{n}$ on the global average number of radicals per particle and the end-point PSD. 89
3.13 The effect of introducing a termination correction factor in the calculation of $\bar{n}$ on the global average molecular weight evolutions. 90
3.14 The effect of perturbations in monomer flow rates on end-time PSD and MWD. . . 91
3.15 The effect of perturbations in surfactant flow rate on end-time PSD and MWD. . . 93
3.16 The effect of perturbations in initiator flow rate on end-time PSD and MWD. . . . 94
3.17 The effect of perturbations in CTA flowrate on end-time PSD and MWD. 95

4.1 Schematic of experimental facility and impeller design. 100
4.2 Experimental feed rates. 102
4.3 Number and weight-averaged end-time PSD profiles for medium initiator case with 1 wt% CTA. 105
4.4 Solids content and particle number evolutions for medium initiator case with 1 wt% CTA. 106
4.5 a) Number-averaged MW evolutions and b) End-time MWD profiles for medium initiator case with 1 wt% CTA. 106
4.6 Number and weight-averaged PSD evolution profiles for medium initiator case with 1 wt% CTA. 108
4.7 Number and weight-averaged end-time PSD profiles for initiator perturbation experiment set with 1 wt% CTA. 110
4.8 Solids content and particle number evolutions for initiator perturbation experiment set with 1 wt% CTA. 111
4.9 a) Number-averaged MW evolution and b) End-time MWD profiles for medium and low initiator cases: with 1 wt% CTA. 112
4.10 End-time PSD profiles for CTA perturbation experiment set. 114

4.11 a) Number-averaged MW evolution and b) End-time MWD profiles for 1 and 3 wt% CTA cases. 115
4.12 End-time PSD profiles for monomer perturbation experiment set with 1 wt% CTA. 116
4.13 Solids content and particle number evolution for monomer perturbation experiment set with 1 wt% CTA. 117
4.14 a) Weight-averaged MW evolution and b) End-time MWD profiles for monomer perturbation experiment set with 1 wt% CTA. 118
4.15 End-time PSD profiles for surfactant perturbation experiment set with 1 wt% CTA.119
4.16 Solids content and particle number evolution for surfactant perturbation experiment set with 1 wt% CTA. 120
4.17 a) Weight-averaged MW evolution and b) End-time MWD profiles for surfactant perturbation experiment set with 1 wt% CTA. 121
4.18 a) Simulation and b) Experimental results for end-time weight-averaged PSD for initiator perturbation set. 126
4.19 a) Simulation and b) Experimental results for particle number for initiator perturbation set. 127
4.20 a) Simulation and b) Experimental results for number-averaged MW for initiator perturbation set. 127
4.21 a) Simulation and b) Experimental results for end-time weight-averaged PSD for CTA perturbation set. 128
4.22 a) Simulation and b) Experimental results for number-averaged MW evolution for CTA perturbation set. 128
4.23 a) Simulation and b) Experimental results for end-time weight-averaged PSD for monomer perturbation set. 129
4.24 a) Simulation and b) Experimental results for particle number for monomer perturbation set. 130
4.25 a) Simulation and b) Experimental results for weight-averaged MW evolution for monomer perturbation set. 130
4.26 a) Simulation and b) Experimental results for end-time weight-averaged PSD for surfactant perturbation set. 131

4.27 a) Simulation and b) Experimental results for particle number for surfactant perturbation set. 132
4.28 a) Simulation and b) Experimental results for weight-averaged MW for surfactant perturbation set. 132

5.1 2D discretisation grid for $F_n(r,t)$. 141
5.2 Adapted Hierarchical 2-Tier algorithm for 2D PSD/MWD model solution. 142
5.3 2D grid update considerations. 145
5.4 Convergence of weight-average PSD for increasing values of $n_{\max}$. 147
5.5 End-time 2D model output for density of particles distributed over r and n. 148
5.6 Comparison of 1D and 2D model results for a) Weight-average PSD b) Particle number c) Rate of homogenous nucleation and c) Rate of micellar nucleation. . . . 150
5.7 Comparison of 1D and 2D model results for a) end-time $\bar{n}(r,t)$ and b) n_{glob}. . . . 151
5.8 Comparison of 1D and 2D model results for a) VAc and b) BuA consumption rates. 151
5.9 Comparison of 1D and 2D model results for the amount of a) VAc and b) BuA in the system. 152
5.10 Comparison of 1D and 2D model results for global number-average MW. 152
5.11 Comparison of 1D and 2D model and experimental results for weight-averaged PSD for a) case S1 b) case S2 and c) case S3. 154

B.1 Emulsion Polymerisation Experimental System system. 190
B.2 Diagrammatic representation of CHDF system. 191

Chapter 1

Introduction, Motivation and Aims

1.1 Emulsion Polymerisation

The inception of emulsion polymerisation can be traced back to the early twentieth century, with the Goodyear Tire & Rubber Company and the I.G. Farbenindustrie Ludwigshafen laboratories being amongst the first to patent processes involving emulsified monomer solutions and thermal initiator. The initial development of emulsion polymerisation has been reviewed in detail by others.[1,2] The early process evolved around the copolymerisation of butadiene and styrene. Since then, the technology has advanced to incorporate a range of monomers and has application in a number of fields including but not limited to water-borne paints, paper coatings, adhesives and novel biotechnological applications.

Emulsion polymerisation has received increasing attention due to a number of factors. As a viable alternative to solvent-based polymerisation processes, emulsion polymerisation has aided in the compliance with legislation aiming to reduce the use of volitive organic compounds. Due to its segregated nature, emulsion polymerisation offers a practical method of producing high molecular weight polymers, without compromising on reaction rates unlike bulk or solution polymerisation techniques. The reaction medium promotes efficient heat transfer and acts to maintain a low viscosity.[3] In addition to these technological advantages the principle of heterogeneous polymerisation offers unique

opportunities not possible in homogeneous systems. These include the intrinsic capabilities of exploiting the heterogeneity of the system to control molecular level architecture (i.e. copolymer composition) as well as to control the heterogeneity at the particle size level.

Notable disadvantages of the process include those related to post processing of the latex product. Where latex purity is a concern, difficulties may arise in the polymerisation of the final fraction of free monomer or the complete removal of any unwanted adjuvant residues. Recovery techniques such as filtration can prove both complicated and problematic. For example, where microfiltration is applied to colloidal paints, concentration polarisation and membrane fouling can effect both the permeation flux and the retention of desirable and undesirable solutes.[4] However, much interest[5] exists in facilitating such filtration processes. The complexity of the reaction scheme and heterogeneous nature that characterises emulsion polymerisation present many challenges in terms of theoretical understanding, and hence control of the process and resulting product attributes is regarded as a classical and challenging problem.

The latex material produced by emulsion polymerisation has many complex and interrelated characteristics. The so-called 'quality' of a latex is usually dependent on a number of these characteristics, and directly impacts the performance of an end-product. The quality of a latex is defined by a combination of molecular properties (molecular weight distribution (MWD), copolymer composition distribution (CCD), long and short chain branching (LCB, SCB), stereoregularity, etc.) as well as morphological properties, such as particle size distribution (PSD) and bulk density. These molecular and morphological properties underpin latex processing and end-product application governing physical, thermal, mechanical, rheological and chemical properties. The effect of the particle size distribution (PSD) on end-use properties such as rheology is well known. Luckham and Ukeje[6] demonstrated the effect of PSD on the rheology of latexes. Greenwood et al.[7] described the effect of a bimodal PSD on the rheological properties of a latex. Amaral et al.[8] demonstrated the effect of PSD on the viscosity of high solid content latexes. In addition, the molecular weight distribution (MWD) has been shown[9] to influence mechanical strength. It has been shown[10] that significant improvements can be made to latex rheology by manipulating the distribution of long and short chain polymers. A

quantitative link[11] has been established between latex MWD and its adhesive properties (resistance to shear and peel). Furthermore, the fourth moment of the MWD is expected to be correlated with the rheology.[12]

The objectives of this thesis relate to the feasibility of simultaneous control, given process limitations, of PSD and MWD. The possibility and practicality of adopting a model-based approach to design, optimise and control the process will be assessed. The evaluation of a suitable modelling framework will also be given.

The remainder of this introductory chapter details process theoretics, as well as providing the motivations for this study, followed by a more specific description of the thesis content.

1.1.1 Theory

Emulsion polymerisation is a heterogeneous process, the final product of which is a colloidal dispersion of sub-micron polymer particles in an aqueous medium also known as a latex. It is a special type of free radical process, wherein the main locus for polymerisation is within a segregated polymer particle phase.

The basic components required to carry out an emulsion polymerisation are monomer, water, stabilising agent and a free radical source. Additional components may be added to the formulation to modify the process dynamics or product, e.g. rheological modifiers, chain transfer agents (CTA), buffers, biocides and fungicides, antioxidants and UV absorbers. Several different phases coexist during a process: water as a continuous phase, monomer droplets, polymer particles and, above the critical micelle concentration, a micellar phase.

Chemistry

The most commonly used monomers are alkenes; these include chloroethene, vinyl acetate, styrene and butadiene. Free radical type polymerisation can be classified into three main parts: *initiation*, wherein free radicals react with monomer to initiate the polymerisation; *propagation*, wherein live polymer chains undergo concatenation via monomer addition; and *termination*, a reaction that stops further propagation. A brief overview of the process kinetics will now be given:

- **Initiation**: This stage commences with the generation of primary free radicals, either by homolysis, redox reaction, or a combination of both. Homolysis can be achieved by the application of heat or light (UV) radiation. Water soluble initiator molecules, with peroxide or azo groups, readily undergo homolysis to produce free radicals via application of heat (thermolysis). An example of a peroxide initiator cleaving into alkoxy radicals (decomposition) is shown in Figure 1.1.

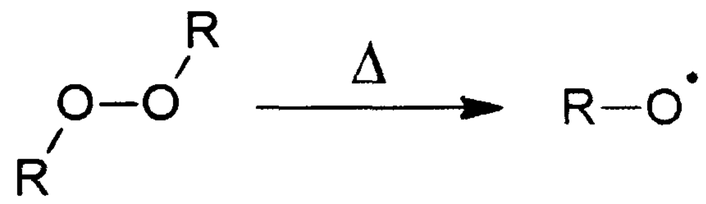


Figure 1.1: Decomposition of a peroxide to produce radicals.

Initiation is completed when the primary radical generated in the first part of the initiation process reacts, via addition, with the double bond of an alkene monomer as shown in Figure 1.2



Figure 1.2: Addition of a primary free radical to the double bond of ethene.

- **Propagation**: Propagation involves attack of the carbon double bond of an alkene monomer molecule by a radical. The radical centre created will migrate along the chain length as further monomer units are added via propagation [Figure 1.3]



Figure 1.3: Propagation of ethane.

- **Termination**: The termination reaction stops radical growth and can occur via two main mechanisms: (1) *combination* [Figure 1.4]- where the active centres of two growing chains combine, resulting in a single dead chain of length equal to the sum of reacting chain lengths.

(2) *disproportionation* [Figure 1.5]- where a hydrogen atom is abstracted from one

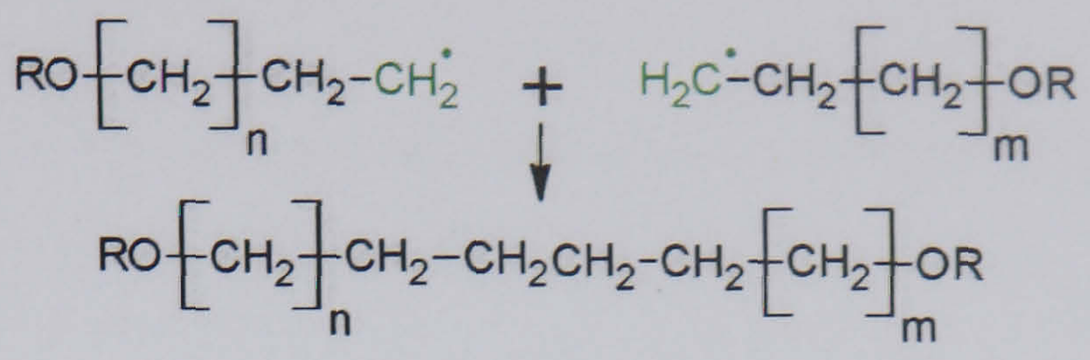


Figure 1.4: Termination via *combination* of polyethene radicals.

growing chain by another, resulting in two separate dead chains, each undergoing no change in length.

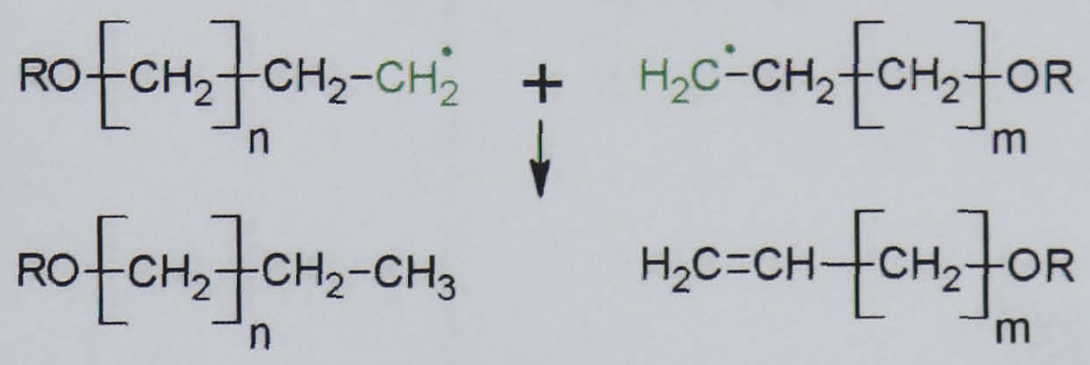


Figure 1.5: Termination via *disproportionation* of polyethene radicals.

- **Chain Transfer**: Chain transfer involves the active centre from a radical being abstracted by a hydrogen atom donating recipient molecule. Recipients of the active centre may include polymer chains (resulting in branching), monomer or CTA.[13] Chain transfer to monomer is shown in Figure 1.6.

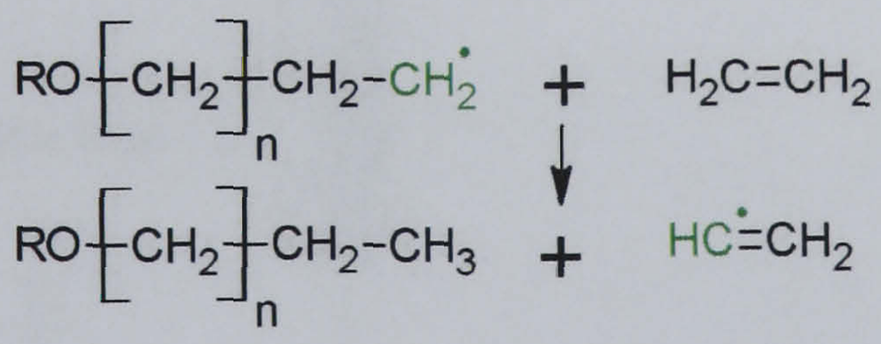


Figure 1.6: Chain transfer from a growing polymer radical (polyethene) to monomer (ethene).

Particle Formation, Growth and Stabilisation

This section will detail mechanisms for particle generation, stabilisation once created and continuous growth. Figure 1.7 gives an overview of the reactions and mechanisms that are described in this and the previous section.

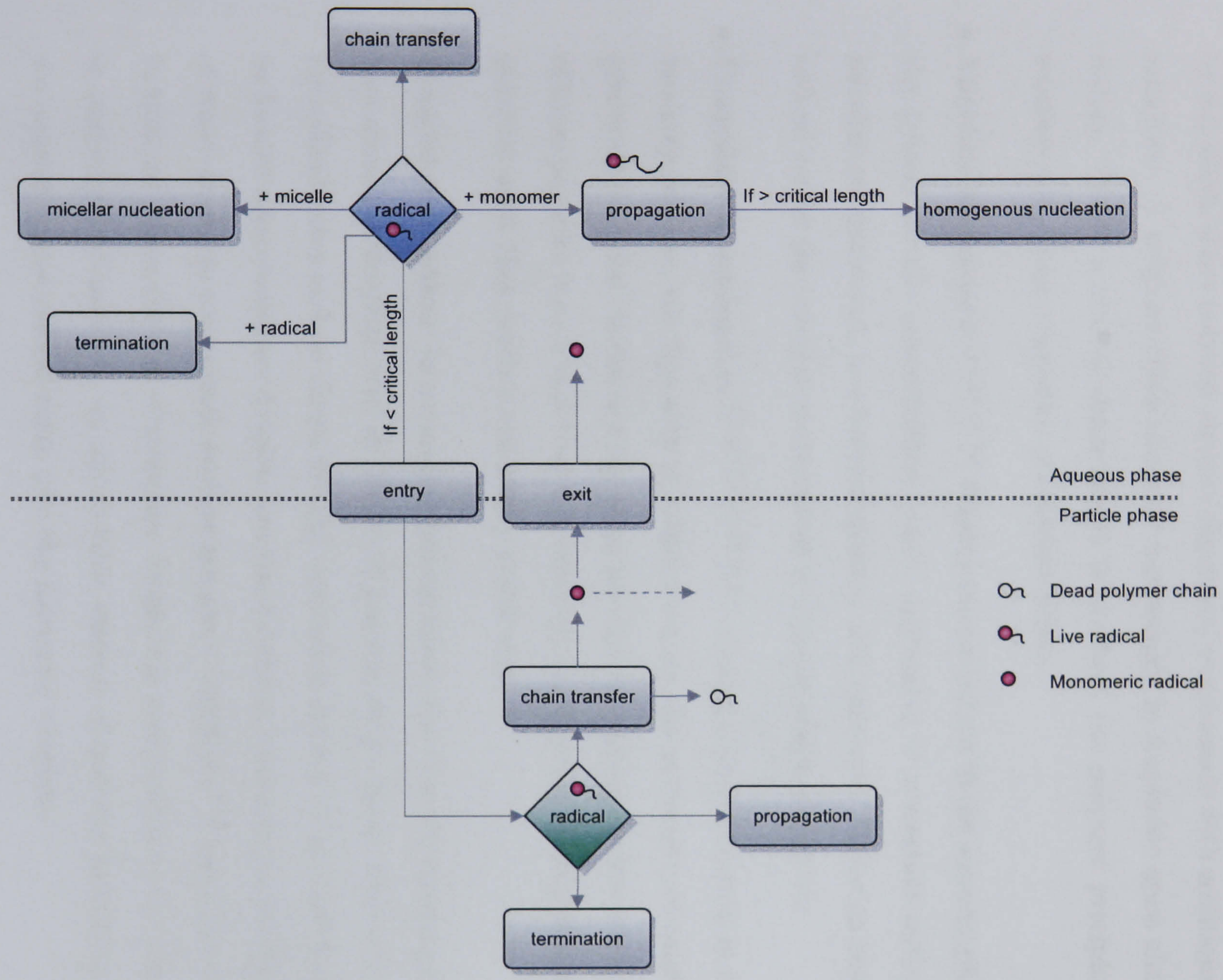


Figure 1.7: Schematic of basic reactions and physical transport mechanisms occurring during an emulsion polymerisation reaction.

Nucleation

Nucleation involves to the creation of polymer particles within the polymerisation system. Different nucleation theories have been proposed:

- **Homogenous nucleation**:[14,15,16,17,18] Having been formed in the aqueous phase by initiation, short polymer chains (oligomers) concatenate with additional monomer molecules. A polymer chain becomes increasingly hydrophobic upon chain concatenation. When a critical chain length is reached, the polymer precipitates out of solution and forms a separate particulate phase.

- **Micellar nucleation**:[14,18,19,20] When ionic surfactant in the aqueous phase exceeds the critical micelle concentration (cmc), aggregates of surfactant molecules called micelles are generated, and become swollen with monomer. When an aqueous phase radical enters the micellar environment it forms a polymer particle.

- **Coagulative nucleation**:[21,22,23,24,25,26,27] Coagulative nucleation is a sequential two-step process, the first step of which involves the nucleation of small, unstable, precursor particles via the homogenous/micellar nucleation mechanisms. The nature of these particles is such that they subsequently undergo rapid coagulation with other particles until they reach a colloidally stable size.

- **Droplet nucleation**: In a conventional emulsion, the Ostwald ripening effect means that monomer droplets exist in the 10-50 μm size range, hence they do not compete for radical entry and no direct droplet nucleation occurs. A miniemulsion[28,29] can be formed when monomer droplets are maintained at a sub-micron size by dissolution of water-insoluble compounds such as hexadecyl sulphate,[30] known as costabilisers. In systems where the size of monomer droplets is comparable to the size of micelles or particles (sub-micron), an appreciable amount of particle formation may occur via aqueous phase radical entry into the monomer droplets.

Particle Growth

The main locus of reaction in an emulsion polymerisation system is within monomer swollen particles. Newly formed particles will increase in volume due to the polymerisation of radicals contained therein. The rate of growth is proportional to the number of

live radicals contained. The coagulation mechanism also causes particles to increase in volume. Coagulation and the associated inter-particle dynamics are described in the next section.

Particle Stabilisation

Colloidal particle systems of the kind relevant to this work (e.g. polystyrene in water) are inherently unstable, that is, the standard free energy of the system, ΔG_f^o, is positive, thermodynamically favouring the process of particle agglomeration as shown in Figure 1.8, indicated by the left-to-right process. In this kind of *lyophobic* colloidal system the free energy is thus minimised. Conversely, in a *lyophilic* system ΔG_f^o is negative, thus favouring the reverse process shown in figure 1.8

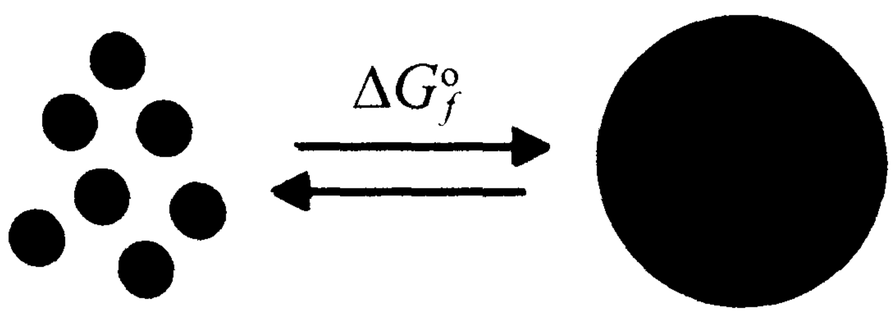


Figure 1.8: Thermodynamic schematic of a lyophilic system, where $\Delta G_f^o = \gamma \Delta A$, with γ and ΔA being the solid-liquid interface tension and the increase in interfacial area, respectively.

Coagulation and *flocculation* are terms used to describe an agglomeration process between particles. Coagulation refers to an irreversible pairing between particles, whereas flocculation describes a reversible process with weaker interactions, usually resulting in larger loosely bound 'flocs' of particles. In a typical application, such as paint or film production, it is generally desirable to minimise or control the rate of coagulation, with the aim to retain the colloidal nature of the system. The attraction between particles that causes coagulation is attributable to van der Waals force. Van der Waals force arises due to attractions between transient dipoles in neighboring molecules. To counteract this force and thus inhibit the coagulation process, a repulsive force, comparable in range and magnitude, is required.

Surfactants are used to induce a large enough energy barrier to inhibit the tendency for particles to coagulate. Surfactants are amphipathic molecules operating at interfaces and thereby altering the physico-chemical properties of such. Surfactants act to reduce the surface tension of an interface to which they are adsorbed. In addition to stabilising

particles, surfactants also act to stabilise oil-water emulsions by reducing the interfacial tension between liquids.

Surfactants can be classified into two main groups: ionic and non-ionic. Ionic surfactants have a charged head region and can be further classified in terms of their net charge. If positively charged, the surfactant is termed cationic e.g. cetyl trimethylammonium bromide. If negatively charged, the surfactant is termed anionic e.g. sodium dodecyl sulphate (SDS). If two opposing charged groups are present, the surfactant is termed zwitterionic e.g. cocamidopropyl betaine. Non-ionic surfactants are those which do not form ions in aqueous solution e.g. poly(ethylene oxide).

The degree of colloidal stability and the mechanism by which it arises is different for ionic and non-ionic surfactants. Ionic surfactants impart an electrostatic stabilisation, with a repulsive force arising from the Columbic interaction between electrical double layers that exist due to the arrangement of ionic molecules at the particle surface. Persulphate initiated systems can produce surface active oligomers, which invoke a similar kind of stability (facilitating emulsifier-free polymerisations). The stabilisation mechanism involves the accumulation at the particle surface of a uniform layer of ions, with opposing charge to the particle. The adsorbed surface charge, together with the diffuse outer ionic layer are referred to as the *double layer* [see Figure 1.9]. The thickness of the double layer is important when considering particle stability and is strongly effected by the presence of electrolytes. The structure and dynamics of this shielding layer have been studied in great detail.[31,32] The DLVO theory quantifies these interactions, and provides a basis to model particle coagulation rates (covered in more detail in Chapter 3). Where ionic stabilisers are used, the colloidal environment is important in determining the interaction between particles, greatly influencing particle stability. Such environmental factors include, monomer concentration, surfactant concentration, electrolyte concentration, surfactant type, temperature.

The mechanism by which non-ionic surfactants impart stability is known as *steric* stabilisation. Non-ionic stabilisers are lyophilic materials, of polymeric nature, which graft to the surface of polymer particles. The interaction between the adsorbed chains of two approaching particles results in a repulsive force, that may counteract the van der Waals attractive force. As the particles move closer together, the number of contacts between

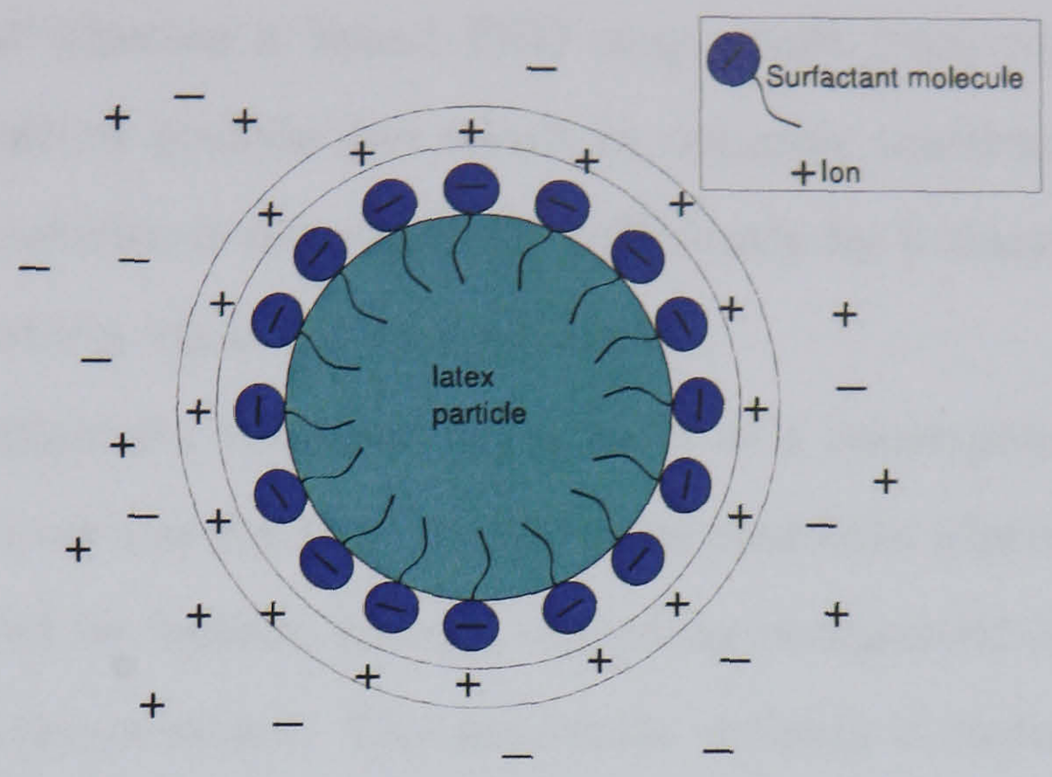


Figure 1.9: Illustration of the charge layers surrounding a particle with adsorbed ionic surfactant in an ionic medium.

polymer chains is increased, whilst the number of contacts between polymer chain and solvent (water) decreases. For a lyophilic molecule, this results in an increase in free energy and a repulsive force, which forms the basis of the steric stabilisation mechanism. Steric stabilisers have a number of advantages over ionic stabilisers, for instance they may be used in a range of medias, whereas ionic stabilisers are only suitable in aqueous solution. Steric stabilisers are insensitive to electrolyte, whereas ionic stabilisers are highly sensitive. Steric stabilisers prove effective at both high and low volume fractions, whereas ionic stabilisers are only suitable for low volume fractions. Reversible flocculation is possible using steric stabilisers, whereas only irreversible coagulation is possible with ionic stabilisers. A disadvantage of using steric stabilisers is that they tend to be required in far larger quantities than their ionic counterparts (typically 10 times more). Furthermore, absorption of steric stabiliser tends to be so strong that migration over the colloid particle surface is prevented, which makes the film forming process very difficult.

Latex Characterisation

The PSD arises from the differential growth rates exhibited by particles. The balance over radicals in particles due to entry, desorption and termination is dependant on the particle size, which in turn means that growth rates, dictated by the number of radicals per particle, is also affected. Differences in length of nucleation period can also result in different distributions of particle sizes. For example, a narrow distribution is associated with a

short nucleation period whereas a broad PSD may result from a prolonged nucleation period. Multiple nucleation periods can result in complex multimodal distributions.[33] Therefore, the size of particles is not captured sufficiently by a simple average metric but necessitates characterisation via a distributed metric.

The molecular architecture exhibited by a latex is a consequence of the interaction between chemical reactions and physical mechanisms that take place during a polymerisation, and can be effected by various factors, including component feed trajectories.[34,35] reaction mode,[36] and temperature. The molecular weights of chains produced during a polymerisation may present several different classes of distribution, for example, narrow, long tailed and multimodal.[37]

An increasing requirement for accurately specified latex characteristics motivates the development of latex characterisation techniques. An account will now be given of the measurement techniques used to determine important latex characteristics, starting with conversion, followed by latex particle size and molecular properties.

Monomer Conversion

Measuring monomer conversion gives an indication of the extent of reaction. Furthermore, it allows the tailoring of monomer feed profiles to prevent copolymer composition drift. Techniques for measuring monomer conversion are listed below:

1. **Gravimetry** [off-line]
2. **Gas Chromatography** [on-line][38]
3. **Calorimetry** [on-line][39]
4. **Latex Density Measurement** [on-line] via dilatometry,[40] densitometry,[33] ultrasound velocity measurements[41] and Raman spectroscopy (utilising fibre optics)[42]

Particle Size

There are many techniques that enable the characterisation of particles in terms of size and shape. Underlying such measurements are several complications. The deviation of particle shape from perfect sphericity may necessitate the use of certain approximations.[43] such as Stokes diameter and the projected area diameter. Another often problematic

aspect is ensuring that representative sample of reactor contents is obtained. Preparation of samples may require dilution, therefore it is essential that suitable dilution agents and conditions are used, in order to avoid particle coagulation. Of the techniques that exist for measurement of particle size, those giving average size seem inadequate and possibly misleading when considering that latex particles will be distributed. perhaps with multimodal distributions. The concept of average size seems even more inadequate when considering the relationship that exists between the *full* distributions and important end-product attributes.

Particle size measurement techniques can be categorised into 6 main groups, shown below. Some illustrative examples are given.

1. **Light scattering**: classical e.g. turbidity,[44] quasi-elastic,[45] and neutron scattering

2. **Microscopy**:[46]

3. **Particle transport**: sedimentation,[47] hydrodynamic chromatography (HC), capillary hydrodynamic fractionation, CHDF[48] and field flow fractionation (FFF)

4. **Acoustics**

5. **Surface area**: gas adsorption, soap titration

6. **Classification**: sieving, filtration

Of these devices, the few that directly measure the full PSD include CHDF, microscopy and light scattering. When evaluating different methods it is pertinent to consider measurement resolution, time, complexity and equipment cost. A thorough description of these aspects can be found in.[49] Recent advances in PSD measurement have included improvements in ease of sample dilution, direct management of high solids content latex and devices that offer on-line measurement capability suitable for closed-loop control application.

Molecular Weight & MWD

A brief account will be provided of the techniques for measuring the average molecular

weight and MWD of a latex. Depending on the sample requirements for molecular characterisation, isolation of the pure polymer fraction from a raw latex may be important. Isolation of a particular polymer fraction involves separation from the other residual molecular compounds such as surfactant, initiator and electrolyte. Separation methods include destabilisation via electrolyte addition, dialysis and ion-exchange. This situation is further complicated by having to ensure that a representative reactor sample is obtained.

Similar to the consideration of particle size measurement. it is important to capture the full MWD due to the inherent link between the the distribution and important end-product properties. The following techniques are used to measure latex molecular weight and are classified in terms of their ability to capture average molecular weight or full distribution information:

1. **Osmometry** [average MW]: based on equilibrium balance between a polymer solution in different solvents[50]

2. **Scattering Methods** [average MW]: based on the degree of scattering of electromagnetic radiation or neutrons effected by the latex[51]

3. **Ultracentrifugation** [average MW]: based on size dependant molecule separation under centrifugal acceleration[50]

4. **Viscometry** [average MW]: based on the dependence of viscosity on MW[50]

5. **Size Exclusion Chromatography** [average MW/MWD]: based on size-based separation of molecules combined with various detectors e.g. refractive index (RI), viscometry and light scattering[50]

6. **Matrix assisted laser desorption ionisation mass spectrometry** (MALDI-MS) [average MW/MWD]: based on dissolution of polymer in a UV absorbing compound, followed by ionisation via a UV-laser pulse and acceleration within an electric field. Mass spectrometry is used then to record the resultant time-of-flight spectrum, which yields MWD data[52]

The full account of molecular level architecture in a polymer is significantly more complicated than can be described by MWD alone. Branching and crosslinking reactions

create various network structures, strongly effecting polymer properties. and as such can be measured via NMR[53] and gel permeation chromatography (GPC). Copolymerisation systems produce polymer that may be further classified in terms of copolymer composition distribution, measurable via infrared, UV and NMR[53] spectroscopy and pyrolysis gas chromatography (PGC).

Intramolecular structure analysis such as tacticity measurement is important from the point of view of understanding the relationship between molecular structure and polymer properties. This kind of analysis is facilitated by measurement techniques such as X-ray diffraction, IR spectroscopy and NMR.

1.2 Control of Particulate Processes: A Model-Based Approach

The control of dynamic process systems represents a challenging task when considering the multi-objective, distributed control associated with emulsion polymerisation. An account will be given of the various approaches that have been adopted to control and optimise the emulsion polymerisation process.

Before effective control measures can be put in place, the controllability of the system is an aspect that need to be addressed. Controllability analysis relates to the identification of suitable manipulated variables, assessment of the availability of sensors for critical product attributes that need control, and the quantification of the limitations in these two respects and their effect on the desired control.

The simplest control strategy might involve defining a set of conditions that give the desired product quality. These conditions e.g. temperature and component feed trajectories, are maintained as close as possible to their set points using PID control. There is no feed back involved for the specific product attributes, which in a process like emulsion polymerisation can lead to sub-optimal operation. The technique is based on the assumption that a set of chosen process conditions is ultimately correct and that accurate enough control of these is possible.

An improved control strategy would employ a suitable dynamic process model to determine optimal conditions, motivating batch to batch optimisation studies.[54,55] Closed-loop

control may be applied, involving the on-line manipulation of process inputs. The difficulty in obtaining frequent enough measurements of end-use properties such as viscosity to enable online control corrections, motivates inferential control via easier to monitor and suitably related online variables, such as PSD/MWD. As a further step, model predictive control (MPC) can be employed, which involves the determination of manipulated variable trajectories at the same time as evaluating uncertain parameters.[56,57]

Indirect process monitoring parameters can be incorporated into control schemes using a fusion of hardware sensors and software-based models, the so-called soft-sensor.[58] State estimation techniques[59,60,61] are used in control applications and offer the potential to estimate system states from noisy data sources, also to provide estimates of parameters that cannot be measured using hardware sensors.

1.2.1 Process Modelling

The need to operate processes more efficiently to satisfy economic, safety and environmental constraints motivates a model-based approach. Models can be used to study process mechanisms allowing improved understanding to underpin more robust model-based product and process design. By performing process sensitivity analysis models facilitate the establishment of process controllability. Models are also used for off-line optimisation, in doing so helping to circumvent trail and error techniques, as well as for on-line process monitoring and control requirements.

One type of model is the so-called 'black box' model, where parameters in a general model structure, usually not of a mechanistic basis, are 'fitted' to actual plant data. The advantages of this type of model are associated with the relatively short amount of time it takes to construct, which is balanced somewhat with the time spent generating experimental data. This type of model does not rely on an understanding of the underlying process mechanisms and can therefore present a useful solution to generating a model for a controller. Use of 'black box' models is limited to the range of process data from which it was constructed.

In contrast, mechanistic models involve a description of the physical and chemical principles that constitute the process. They are considerably more complex and time consuming to develop than their 'black box' counterparts. However, motivation for their

development lies in the range of application and mechanistic understanding they allow. Parameter fitting is also needed for mechanistic models. wherein they are compared to experimental data and uncertain parameters are tuned.

Moreover, the dynamic modelling and validation of PSD and MWD in emulsion polymerisation in a mechanistic sense is a difficult task. This represents a multi-scale problem in terms of both length and time, with a need to incorporate particle nucleation, growth and coagulation into a coherent framework. The process encompasses highly interacting kinetics, thermodynamics, heat and mass transfer phenomena, which take place over a heterogeneous landscape. Furthermore, the physical properties (e.g., viscosity, density, transport coefficients, interfacial tension, etc.) of the various phases typically vary by several orders of magnitude during the course of polymerisation.

1.2.2 Population Balance Models

Of specific interest to modelling of distributions is the framework based on the population balance concept. Population balances are ideally suited to capturing the dynamics of distributed systems and are widely used in process systems engineering.[62] A comprehensive review of population balances and their application can be found in the book, Population Balances by Ramkrishna.[63] This section will provide some of the basics regarding population balances and their solution. Population balance equations (PBE) are non-linear integro-partial differential equations, which can account for a distributed entity by tracking the interchange with respect to a representative feature (internal coordinate). The balance is able to capture the growth dynamic of classes of the population with respect to this internal coordinate. It also represents birth and death events, which account for arrival or depletion of the dispersed entity from the population. In the case of emulsion polymerisation, PBEs provide a framework to capture the important process features. The general form of a population balance is shown below:

$$\frac{\partial}{\partial t}\zeta(\eta,t) + \frac{\partial}{\partial \eta}\left(\zeta(\eta,t)\frac{d\eta}{dt}\right) = \Re_{nuc}(\eta,t) + \Re_{internal}(\eta,t) \tag{1.1}$$

where $\zeta(\eta,t)$ is the population density function, η is the internal coordinate, t is time, $\Re_{nuc}(\eta,t)$ is a discrete term that accounts for the 'birth' of dispersed entities within the

system, $\frac{\partial}{\partial \eta}\left(\zeta(\eta,t)\frac{d\eta}{dt}\right)$ and $\Re_{internal}(\eta,t)$ are two terms that account for realignment of the internal coordinate, the first of which accounts for a continuous growth process i.e. polymerisation. The second term accounts for discrete processes involving coagulation or breakage. Coagulation describes the non-continuous growth of polymer particles.

The numerical techniques used to solve PBEs can be classified into the method of moments and discretisation-based methods. To derive the moments of a PBE the following definition is used:

$$\mu_k = \int_{\eta_{min}}^{\eta_{max}} \eta^k \zeta(\eta,t) d\eta \tag{1.2}$$

where μ_k is the kth moment. Thus for each moment of the whole PBE an ordinary differential equation (ODE) results.[64] Although solution of the resulting ODEs is straightforward, the number of moments used must be limited and where lower order moments depend on higher order moments the closure conditions must be carefully chosen. Also, the construction of the distribution from its moments is faced with numerical instability.

Discretisation methods seek to satisfy the PBE only at certain discrete points along the internal coordinate. One class of discretisation techniques is the finite difference methods (FD) wherein a difference approximation is used to evaluate the PBE solution, thus creating a set of ODEs or algebraic equations. Numerical dispersion and spurious oscillations are common in this method due to the truncation error that stems from the approximation method for the derivatives. In the solution of a PBE describing a crystalliser, Ma et al.[65] proposed a customised FD approximation method to avoid these problems. Studies by Crowley et al.[66] using FD methods prevented backtracking of errors by considering a wide range for the internal coordinate.

The method of weighted residuals (MWR) aims to solve the PBE by approximating it by a polynomial basis function in the internal coordinate domain. The residuals of the PBE are multiplied by weighting factors and then forced to zero at certain points. The weighting factors are dependant on the particular method used. In Galerkin's method the weighting factor is identical to the basis function. Collocation techniques employ the Dirac Delta function as the weighting function. The points at which the weighted residuals are driven to zero are called collocation points, the error involved with the positioning of

which can be optimised by choosing the points to be the zeros of an orthogonal polynomial. Using a single polynomial to cover the entire internal coordinate domain in the collocation technique would necessitate the use of a very high order polynomial, therefore it is more efficient to split up the domain into finite elements and employ a different polynomial (of lower order) for each finite element. This method, called orthogonal collocation on finite elements (OCFE), has been used by various researchers.[67,68,69] Wavelet-based collocation methods,[70] have also been employed to solve PBEs. with the ability to deal with steep moving profiles.

A probabilistic method for the solution of PBEs is the Monte Carlo method. This can be applied to either directly evaluate difficult functions or to artificially realise the system behaviour.[63]

A recent method for the solution of PBEs was developed by Immanuel et al.,[71] wherein a multilevel[72] discretisation is applied to the internal coordinate. A decomposition technique involving decoupling of sub-process rate models (nucleation, growth and coagulation) resulted in a considerable reduction in the numerical stiffness associated with the difference in time scales. The overall PBE is then solved using a hierarchical update strategy.

For application to a special class of aggregation/breakge only PBEs, for example in the case of granulation, there are number of discretisation techniques available. Hounslow et al.[73] used a geometrical discretisation grid based on particle length, instead of the usual volume coordinate. The particles were assumed to exist at a single pivotal point within the element of a discretisation grid, whilst their mass and number were conserved. Kumar and Ramkrisna[74] developed a volume based discretisation method, with a more general and flexible grid with fine or coarse discretisations possible.

1.3 Thesis Objectives & Structure

This thesis is concerned with the experimental controllability analysis and the detailed mechanistic modelling of the emulsion polymerisation process. The salient questions that will be addressed by the research are:

1. Can PSD and MWD be simultaneously controlled given process limitations, since these are both important controlled variables for the emulsion polymerisation process?

2. Is it *possible* and *practical* to model the emulsion polymerisation reactor, accounting simultaneously for both PSD and MWD? This question will be addressed in light of previous works elaborated on in the next chapter, the most relevant of which being that of Ray and coworkers.[75,76,77]

3. What is the ideal framework to formulate such a model?

It is an objective to experimentally analyse the simultaneous controllability of the process in terms of PSD and MWD. The objectives are also to build, solve and analyse a dynamic process model and to validate this model with experimental data, towards providing for a model-based approach to process control applications. The practicality of model solution in combination with availability of process measurements, will be considered. The strong dependance of latex end-use properties on PSD and MWD forms the basis for the selection of PSD and MWD model output variables.

The thesis is organised as follows:

Chapter 2 contains a literature review pertaining to the elements of the above questions. Discussion evolves around modelling of the emulsion polymerisation process to date with regard to early empirical models, such as the classical Smith and Ewart theory, lumped models and distributed models. Particular attention will be paid to the aspect of compartmentalisation and studies into the effect of this phenomena on the process. Furthermore, a review of efforts to establish the state of controllability of the process will be given.

Chapter 3 presents the development of a combined PSD and MWD model. The chapter will detail the development of both parts of the model together with their solution. An analysis of the model results will be given, including a preliminary insight into the effect of compartmentalisation in this heterogenous process.

Chapter 4 presents an experimental study into the controllability of PSD and MWD. Four main inputs: initiator, monomer, surfactant and CTA are perturbed and the resultant latex characteristics are analysed in detail, including PSD, MWD and solids fraction. Following on from the experimental studies is a model validation exercise, wherein the model developed in chapter 3 is compared to the experimental data.

Chapter 5 aims to give an insight into the effect of compartmentalisation on the process model predictions through the development of a more rigorous version of the PSD model, which differentiates between individual particles based on the number of radicals instead of assigning the same average value of radicals/particle to all particles. This model is solved and simulation results are compared to experimental results, together with results from the model developed in chapter 3, in a bid to elucidate the effect of compartmentalisation on growth, a factor highlighted in chapter 3 as being at least partly responsible for some of the model validation mismatches.

Chapter 6 concludes the work, drawing together learnings and addressing the extent to which the above thesis objectives have been answered. It is followed by a description of corollary work.

Chapter 2

Literature Review

2.1 Introduction

This review covers emulsion polymerisation modelling, starting with the early models and lumped parameter models, followed by a more in depth review of models that account for full PSD, MWD or both together. An account of works that investigate the compartmentalisation phenomena will also be given. The final section covers the aspect of controllability in emulsion polymerisation.

2.2 Early Process Modelling

The first notable descriptions of emulsion polymerisation were made by Harkins,[78,79,14] owing to work carried out at the Research Laboratory of the United States Rubber Company at Passaic, New Jersey. These descriptions provided a framework for future quantitative modelling. The different phases arising in a emulsion polymerisation were distinguished and evidence was presented for the initiation process occurring in the aqueous phase. Nucleation was defined as occurring either in the aqueous phase (homogenous nucleation) or in micelles (micellar nucleation). The principal locus for polymerisation was defined as being in monomer swollen polymer particles. The work also indicated that the emulsified droplets of monomer did not serve as loci for nucleation, but as 'reservoirs' supplying monomer to particles.

Based on the Harkins' framework and experimental data, Smith and Ewart[80] con-

structed an empirical model for the process. The model encompassed the kinetics of polymerisation reactions occurring in isolated loci. Particle number was derived based on micelles being the origin of new particles. Owing to the difficulty of providing a general solution to the model, three limiting cases were defined:

I Number of radicals per particle << 1

II Number of radicals per particle = 0.5

III Number of radicals per particle >> 1

Case II was particularly of interest as it applied to the polymerisation of styrene under normal conditions. Smith and Ewart derived an empirical relationship between the number of particles, the rate of polymerisation and the surfactant concentration:

$$N = k(\rho/\mu)^{2/5}(a_s S)^{3/5} \tag{2.1}$$

$$0.37 \leq k \leq 0.53$$

where N is the number of particles per litre of water, a_s is the surface area occupied by unit weight of emulsifier, S is the weight concentration of surfactant, ρ is the rate of aqueous radical generation by initiation and μ is the volumetric growth rate of particles.

Gardon produced a series of papers[81,82,83,84,85] which were to review and subsequently modify the theory of Smith and Ewart. Key assumptions were retained; most importantly that polymerisation occurred within monomer swollen polymer particles, initiation occurred in the aqueous phase and micelles provided a loci for particle nucleation. Parameters were chosen with bias towards those that could be experimentally verified. The kinetics of slow termination were studied by relaxing the condition that implied the instantaneous termination of radicals upon particle entry. A varying particle volume was modelled by considering the growth of particles to be a function of the number of radicals contained. A more general solution to the Smith-Ewart formulation was later provided by Stockmayer,[86] which was further modified by O'Toole.[87]

Harada[88] developed a model of emulsion polymerisation, again based on the Smith-Ewart theory. A more accurate estimation of the number of particles was achieved and the nucleation events were analysed in detail. Many commercially important monomers did not fit the classical Smith-Ewart theory, such as vinyl chloride, vinyl acetate and butyl acrylate. Also, the early models based on Smith-Ewart theory did not give accurate predictions at the extremes for the number of radicals per particle, i.e. $<<0.5$ or $>>1$.

2.3 Lumped Parameter Modelling

A lumped model contains parameters that are assumed to apply over the entire region being modelled. When applied to model particles in emulsion polymerisation, such a model assumes all particles to be of the same average size. Moments can be used to approximate the full PSD or MWD. The advantage of using a lumped parameter modelling approach lies in its relative computational simplicity. The following models involve mass balances over the system components and evaluate the number of particles. Particle growth rate is calculated based on a consideration of the Smith-Ewart theory.

Dimitratos et al.[89,90] recognised the problem of controlling copolymer composition in emulsion polymerisation and formulated a model of the process, to act as a state estimator via a Kalman filter. The model incorporated Smith-Ewart case 3 kinetics, and solved for monomer partitioning using a rigorous thermodynamic approach. Urretabizkaia[91] also modelled polymer composition, but for a terpolymer system, assuming thermodynamic equilibrium and using an approach involving partition coefficients.

Nomura et al.[92,93] showed that the Smith-Ewart theory could not properly predict the rate of polymerisation exhibited by a styrene/methyl methacrylate copolymer system and attributed it to the lack of desorption information. Based on this idea, they developed an expression for the rate of radical desorption from polymer particles and incorporated it into a seeded copolymerisation model. An average number of radicals per particle of ≤ 0.5 was assumed. They demonstrated that desorption did not affect copolymer composition, whilst desorption of methyl methacrylate, due to its solubility, effected the rate of polymerisation and hence the particle growth rate. The highly insoluble monomer, styrene, did not have such an effect. Forcada and Asua[94] studied a similar copolymerisation system, albeit

unseeded. They modified the desorption kernel to properly account for experimental data, where the previous model had failed.

Richards et al.[95] developed a model that accounted for partial PSD, monomer conversion, copolymer composition and molecular weight in an emulsion system. The model was validated by comparison to styrene and styrene/methyl methacrylate systems, and covered both batch and continuous modes of reactor operation. Casella et al.[96] employed a lumped parameter modelling approach to create a simplified yet general model, with a reduced number of adjustable parameters, applicable to a range of copolymerization systems.

Gao and Penlidis[97] developed a lumped parameter model incorporating Smith-Ewart type kinetics, able to simulate average particle diameter, conversion, and average molecular weight. They gave a thorough review of the modelling literature, compiling their model equations from the best parts of the literature as they proceeded, with the aim to balance modelling detail and solution efficiency. The model incorporated a detailed thermodynamic description of monomer partitioning. The model was made available as a software simulation package, a notable feature being the extensive database of parameters for several systems that was appended to the simulator. The model was used to successfully simulate a range of experimental conditions.

2.4 PSD Modelling

Among the pioneering efforts to model the full PSD, using a population balance framework, was the work of Min and Ray.[75] Their model accounted for PSD, together with MWD. The model covered batch and continuous systems. The kinetics of single monomer systems were incorporated. They considered monomers with a good range of solubilities. Polymer particle volume was taken as the internal coordinate for the population balance. The number of radicals per particle was modelled based on a mechanistic balance over polymer particles. The inclusion of particle coagulation made this work a more realistic account of the emulsion polymerisation process. The model was based on the assumption that PSD influenced MWD, but no reverse influence was accounted for. The results were shown to be insensitive to the application of the steady-state approximation to the complex equations

describing the aqueous-phase radicals. In the absence of experimental validation, they showed that their model could be reduced to the form of previously studied systems, such as that of Sundberg and Eliassen,[98] whose model, in their opinion was the most general of it's time. They also showed that a reduced instance of their model approximated to a classical Smith-Ewart case.

Kiparissides et al.[99] studied continuous emulsion polymerisation systems and formulated a PSD model via particle age distribution. The model was able to simulate particle number, particle surface area, free surfactant concentration and from this the amount of homogenous and micellar nucleation. Sustained oscillation behaviour, assumed to be caused by periodic nucleation, was captured.

Stevens and Funderburk[100] developed a model for continuous systems. They used three different rate kernels, which enabled model application over a range of conversions. The model was able to predict PSD, with analytical solutions given to the population densities based on Smith-Ewart, Medvedev or Stockmayer kinetics. Araujo et al.[101] also developed a continuous emulsion polymerisation model accounting for PSD in copolymerisation systems. The model encompassed the mechanism of coagulation, based on the assumption that two distinct particle populations existed: one that coagulated and another stable. The model enabled simulation of complex dynamic behaviour, typical of continuous reactors.

Rawlings and Ray[76,102] extended the work of Min and Ray. They retained the general form of the previous model and explicitly solved for the entire PSD using a collocation technique. They were able to model continuous steady-state multiplicity, sustained oscillations, and ignition and extinction dynamics, advancing the theoretical understanding of these phenomena. Experimental accord was achieved under a variety of monomers and over a range of operating conditions, with minimal parameter manipulation. Despite the many complex reactions that constitute emulsion polymerisation, until this time very little progress had been made in elucidating the sensitivity of the system to each reaction. With this in mind, Rawlings and Ray carried out a parametric sensitivity study using their model, and concluded that the system was particularly sensitive to the gel effect as well as the propagation, termination and initiator decomposition kinetic constants. It was also noted that although alternative mechanistic approaches yielded similar overall conver-

sions, they computed very different PSDs– evidence of the need for further understanding with regard to the underlying mechanisms that determined PSD.

Lichti et al.[103] developed a model, encompassing the effect of PSD on growth. They extended the Smith-Ewart equations to account for the size dependence of particle growth. They demonstrated analytical solutions to the partial differential equations that constituted their model. Two cases were studied: (1) constant ab-initio nucleation (Smith-Ewart case I) and (2) Seeded polymerisation (Smith-Ewart case II). The equations developed were generalised to describe the growth of colloids, in which the kinetics could be defined in terms of some property of the particles.

Although lumped models of *copolymerisation* existed, Chen and Wu[104] were the first to publish a theory of copolymerisation in a distributed framework. They used an analogous model structure to that developed by Lichti,[103] which incorporated Smith-Ewart kinetics and dynamically described particles with respect to the number of radicals they contained and the volume of the particles. The homopolymerisation model of Lichti was modified to account for reactions occurring as a result of the presence of two different monomers, resulting in an intractable balance over particles with respect to the number and *type* of radicals contained and the volume of the particle. This balance was simplified by assuming that propagation was rate limiting (Ballard[105]) and ignoring other kinetic events. The model was used to explore seeded 0-1 and 0-1-2 systems, and was able to simulate complex bimodal PSDs. With a similar objective to Chen and Wu, Storti et al.[106] developed the pseudo-homopolymerisation approach, which was designed to simplify the consideration of multi-monomer systems. Working with balances that characterised particles by the number and type of radicals contained in each particle, Storti et al. provided a basis to simplify the balances with respect to those accounting for polymer type. It was reasoned that the interchange between polymer types, due to cross-propagation, was much faster than transitions occurring between radical number based populations due to entry, exit and termination reactions. Therefore, a measure of the degree of polymerisation of a particular polymer type could be approximated via steady state relationship involving the ratios of polymer reactivity. This approximation was considered reasonable for most systems, and thereby considerably reduced the work load in solving for the complete PSD. Experimental data for polymer composition and conversion was used to validate

this theory. The principles developed by these authors were instrumental in the future development of models, specifically those accounting for multiple monomers.

The model of Saldvar et al.[77,107] was a most comprehensive extension of Min and Ray's model. Its population balance framework incorporated copolymer composition distribution, PSD and MWD. The model exhaustively accounted for process kinetics. As in Min and Ray's model, a one-way dependence of MWD on PSD was assumed. The complexity of the model made it fairly intractable, therefore two main simplification techniques were applied to the model, which enabled its solution: the pseudo-homopolymerisation approach was employed to simplify balances over radical type, and an average radical number per particle equation was derived, which simplified balances over radical number, eliminating the use of discrete radical coordinate in the PBE. The simplifications thereby reduced the dimensionality of the population balance, whilst retaining the mechanistic description of the process. Solution of the simplified model was achieved via a modified discretisation technique based on that of Rawlings et al.[76] Comparison of the model predictions for particle size distribution and conversion were made with several experimental styrene-based copolymer systems, with manipulation of initiator and surfactant concentrations, water to monomer ratio, monomer composition, and temperature. The practical applicability of the model was demonstrated, but as the authors pointed out, due to the highly complex system, dynamic model validation over a set of experimental data was difficult.

Immanuel et al.[69] developed an efficient PSD model, drawing on the computation saving model reductions made by Saldvar et al. The homopolymerisation approach was implemented, together with a mechanistic balance over the number of radicals per particle. The PBE was solved using a collocation-based discretisation technique, and resulting data compared to a semi-batch copolymer system, with good overall accord between solids fraction, conversion and PSD. Through a parametric sensitivity analysis, key surfactant. monomer and initiator properties, together with their non-linear influence on the process were highlighted. Immanuel and Doyle[71] also incorporated the dynamics of coagulation into their model. They developed a solution algorithm, applicable to population balances in general, that effectively decomposed the process into the substituent processes of growth, nucleation and coagulation, thus removing the stiffness associated with the

differences of time-scale of these processes. The model was geared towards control application, with a further reduction in computational time brought about by the work of Sun and Immanuel[72] A multi-level discretisation of the particle size domain was effected, and tailored based on sensitivity towards each of the growth, nucleation and coagulation mechanisms.

Coen et al.[108] developed a model for PSD and particle number, incorporating a comprehensive radical balance and transient nucleation dynamics (homogenous and micellar nucleation). They adopted a 0-1 approach, compared to the more general approach of the previous two models. The model contained a detailed kernel accounting for particle coagulation. The kernel accounted for the presence of ionic surfactant and was based on the precepts of the DLVO theory. Good accord was obtained between model and experiment. It was also found, via experimentation, that by substituting non-ionic surfactant for ionic surfactant, for an otherwise identical system, led to appreciably different results. Immanuel et al.[109] developed a coagulation rate kernel for systems with steric stabilisers and implemented it in the framework previously discussed.[71,69]

A methodology for modelling PSD in a seeded emulsion polymerisation was developed by Reynhout,[110,111] using the 'radical-particle size distribution approach'. Radicals were described in terms of their chain length and the class (size and total radicals) of particle containing them. The equations describing the polymerisation system were solved using the Galerkin finite element method. The model was able to simulate PSD and chain length distribution over discrete radical classes. The model was also able to simulate conditions wherein the gel effect was predominant. Validation was carried out for a seeded styrene system and a styrene/methyl acrylate copolymer system. The model is available in a commercial emulsion polymerisation simulation package (PREDICI).

2.5 MWD Modelling

MWD models in the literature fall into two categories; ones that rely on an average particle size to evaluate the relevant entry and desorption kinetics and ones that incorporate the interaction that underlies the description of PSD and MWD. The latter category consists of only a few works, albeit valuable and necessary contributions. One of the reasons for

the lack of papers that account for the MWD dependence on PSD is the increase in model complexity and hence solution time required when considering such a dependence.

Sayer et al.[112] formulated a model for MWD. They assumed that the polymer particles were monodisperse and that pseudo-bulk kinetics applied, that is. the radical number within particles is large and that an average measure of the number of radicals per particle was sufficient to capture termination dynamics. The model was solved using a polynomial approximation technique. Experimental validation was carried out using a methyl methacrylate/butylacrylate copolymer system.

Tobita et al.[113] utilised a probabilistic method, namely the Monte Carlo technique, to simulate MWD. They incorporated detailed kinetics, and exploited the ease of incorporation of mechanistic detail within the Monte Carlo technique to model the chain length dependence of kinetic parameters. Smith-Ewart kinetics were used to obtain the average number of radicals present in particles and consequently evaluate a size independent particle entry rate. An efficient algorithm was used to deal with the various decisions regarding the fates of radicals. Influx times were calculated, followed by calculation of growth time based on the probabilities of chain transfer and termination. This calculation continued until radical desorption, and then restarted via an entry event. In accounting for detailed individual molecular level events, this work presented a confirmation that chain transfer to polymer indeed had a strong effect on the MWD of the simplified systems studied.

Gianetti et al.[114] presented a MWD model incorporating Smith-Ewart kinetics for a 0-1 system. They reformulated the Smith-Ewart equations for a copolymer system using the pseudohomopolymer[106] approach. The model output consisted of a three dimensional distribution of chain length and chemical composition. Average molecular weight was calculated with comparison to experimental data.

Storti et al.[115,116] modelled MWD using the probabilistic approach of Markov chains. A system consisting of monodisperse particles was assumed. Due to the adopted approach, which allowed a coordination of the time distribution of the Markov process with the MWD, the model could be applied to systems with any number of reacting species or any number of radicals per particle. The complexity of the resulting equations limited application to 0-1 and 0-1-2 systems, and also precluded accurate modelling of chain transfer reactions.

Of the second class of MWD models, that account for the interaction between PSD and MWD, is that developed by Min and Ray.[75] The homopolymerisation model consisted of two parts: a PSD model (described in section 2.4) and a dependent MWD formulation based on a population balance framework. The live and dead polymer chains were described in terms of length and the total number of radicals contained within the particle that housed them. A wide range of reactions were accounted for. The model was applicable to batch and semi-batch systems. The full framework was found to be intractable and no solutions were offered. Min[117] addressed the solution of a similar set of MWD equations by applying the method of moments. He was able to independently solve the equations for live and dead chain balances.

Saldívar et al.[77] further refined the aforementioned model, comprehensively accounting for process kinetics, and also addressing copolymerisation systems. A complete framework for MWD was developed, as well as a simplified pseudohomopolymer version of the MWD model. A similar modelling framework to that of Min and Ray was derived for the polymer chains, with the addition of a chain branching function. A most complete range of kinetics were covered, including reverse propagation, transfer to monomer/CTA/polymer, reinitiation, termination, inhibition, micellar/homogenous nucleation, backbiting and scission after intramolecular transfer, and the creation of terminal and internal double bonds. Like in the PSD case, no solution was offered to the full MWD model. Also, having identified the complexity of the pseudo-homopolymer MWD equations, a dimensionality reduction in the form of the method of moments was used. Problems arose due to the dependance of lower order moments on the higher order moments. Min[117] circumvented the problem by not taking moments for the radical index. This was not however possible in the model of Saldívar et al.[77] because the live and dead polymer populations could not be solved independently; the partial moments were thus derived. The model of Saldívar et al. was compared to several experimental copolymer systems, including methyl methacrylate/styrene, wherein an acceptable level of accord between average molecular weights resulted. This work not only served as a detailed and thorough basis for future works, but highlighted the importance of accounting for at least a one-way dependence of MWD on PSD.

2.6 Compartmentalisation Modelling

Compartmentalisation is the phenomenon that allows high molecular weights to be obtained in an emulsion polymerisation system, without having to sacrifice polymer growth rate. In a bulk polymerisation a polymer radical that is growing may terminate via bimolecular termination with any other radical that exists in the system (at least at low viscosities). The segregation provided in emulsion polymerisation precludes termination between two radicals contained in separate particles, the effect of which may be to decrease the amount of termination that occurs, in comparison to an equivalent unsegregated system. In theory, as a segregated system approaches very high numbers of radicals per particle, the relationship between radicals may be approximated by using average radical numbers. However, in systems, where the number of radicals per particle is low, this assumption may not be valid. This section will focus on MWD models developed with a specific interest in analysing the compartmentalisation phenomenon.

Arzamendi et al.[118] developed a copolymerisation MWD model that accounted for chain transfer dynamics leading to branching. The model was based on the tendency model of Villermaux and Blavier,[119] with influence from the probabilistic approach developed by Storti et al.[115,116] based on Markov chains. The average molecular weight was calculated based on the leading moments of the distribution. It was found that large disparities in molecular weight resulted from not accounting for compartmentalisation.

In a subsequent paper, and as a departure from the classical modelling approach of resolving intraparticle molecular structure in terms of individual polymer chain units. Arzamendi et al.[120] developed a model based on the so-called 'partial distinction approach'. In this approach, radicals were lumped into one of two groups; 'short' and 'long'. Smith-Ewart kinetics for a 0-1-2 system were applied. Criteria were established to determine the numbers of short and long chains present in particle, based on an appreciation of the kinetics of the system. The MWD equations resulting from this treatment were somewhat complicated and therefore subjected to a dimensionality reduction via the method of moments, to yield weight and number average molecular weights. An attempt was made to determine the conditions where compartmentalisation became evident. Four models were assessed, each accounting for the compartmentalisation phenomena to a different degree:

1 Psuedo-bulk

2 Semi-compartmentalised

3 Partial distinction (Arzamendi et al.)

4 Lichti double-distinction

The comparison between models showed that the predictive capacity of the pseudo-bulk model was accurate only where compartmentalisation was negligible (i.e. the number of radicals per particle was large). The predictions of the semi-compartmentalised models were accurate in all but highly compartmentalised cases. Experimental error in measuring MWD was deemed to be an appreciable factor in evaluating the models, where differences due to compartmentalisation were small.

In an effort to rigorously account for compartmentalisation in emulsion polymerisation, Lichti et al.[121] introduced the concept of the singly and doubly-distinguished particle. Equations were derived for singly-distinguished particles, with $N_i'(t,t')$ being the distribution of 'distinguished' latex particles. These particles were defined as those inside which a polymer chain (a 'distinguished' chain) *began* growing at time t and was still growing at time $t+t'$, the state of the particle (number of radicals contained) at this time being i. This formulation was enough to account for all chains in systems where bimolecular termination was absent, however the dependance of termination on compartmentalisation was an important factor to consider. Therefore, to incorporate bimolecular termination, the doubly distinguished particle was introduced: $N_i'(t,t',t'')$, specifying the number of particles which at time $t+t'+t''$ were in state i and contained two distinguishing polymer chains– the longer of which began growing at time t, and the shorter, at time $t+t'$. The resultant equations were solved analytically for a case wherein particle growth and concentration were negligible, giving the chain growth time distribution (proportional to MWD). The results of this analysis were thought to be equally applicable to a system in which these conditions were relaxed. It was found that polydispersity was increased due to compartmentalisation, however not so in the case where chain transfer was dominant.

Ghielmi et al.[122,123] and Butte et al.[124,125,126] developed models for MWD. Butte et al. reformulated the singly and doubly-distinguished particle equations using chain length

instead of growth time. The importance of directly solving for the entire distribution was demonstrated by simulation of a bimodal MWD, resulting from short-long polymer chain bimolecular termination, a characteristic of 0-1 systems. Ghielmi extended Lichti's model structure by incorporating a further coordinate to account for branching. It was shown that significant errors in MWD estimation could be made in neglecting the compartmentalisation phenomenon. This effect was particularly apparent when the number of radicals per particle was small.

As mentioned in Section 2.4, Reynhout et al.[110,111] modelled PSD in a seeded system using the 'radical-particle size distribution approach'. They modelled chain length distribution with respect to 9 discrete radical classes, that is, up to 9 radicals per particle were allowed. A key model feature was the compartmentalisation factor, a lumped parameter, which accounted for the degree of segregation on the overall polymerisation rate and therefore the average chain length by using several moments of the PSD. The compartmentalisation factor was derived for several scenarios, including Smith-Ewart case I, II and III. Results showed that compartmentalisation strongly effected the PSD. It was also noted that for some cases, the maximum value of 9 radicals per particle was insufficient to capture the process dynamics.

2.7 Controllability

Emulsion polymerisation presents a classical problem in multi-objective and distribution control. Several candidate manipulable variables exist, which influence the main subprocesses of nucleation, growth and coagulation in a complex and often non-intuitive manner. The difficulty in controlling the system lies in the coupling effects between PSD and MWD. The feasible range of control of output variables is therefore limited, making it necessary to understand further these coupling effects and elucidate feasible operational regions in a practical sense.

Formal PSD controllability studies on a continuous emulsion polymerisation system by Semino and Ray[127] identified that surfactant, initiator and inhibitor ensured a wide system controllability in an unconstrained case. They discussed the coupling of initiator and inhibitor to create a manipulated variable with effective positive as well as negative

values. In a subsequent paper,[128] they developed successful control strategies for the constrained case using choices for pairings of the manipulated variables (previously identified) and controlled variables. In industry, complex PSDs are often desired, for example to maximise packing fractions in a latex. In practice, the maximum attainable packing fraction is limited to that generated by a bimodal particle distribution. The disparities between theoretical possibilities and actual attainable product specifications can be addressed by control studies relating to generation of complex PSDs. Crowley et al.[129] studied the optimisation of surfactant feed profile to drive the process towards a bimodal target distribution. They were successful in reaching a bimodal distribution and found that using a variable most closely related to nucleation (free surfactant concentration above the critical micelle concentration) gave the best results. In a later paper, Meadows et al.[130] developed a model for emulsion polymerisation under non-isothermal conditions. They highlight the advantages of utilising semi-batch experimental data for more accurate parameter identification compared to using batch systems. Furthermore, they identified temperature as a variable with the ability to direct the process towards a specified PSD. Liotta et al.[131] developed and validated a model for a bidisperse system, with two overlaid monodisperse PSDs. With constrained monomer concentrations, they specified the reachable regions for different diameter ratios of seed particles. Growth was determined to be a suitable tool for manipulation of particle size, with semi-batch systems giving the maximum possible diameter ratio trajectories. Based on this bidisperse system, they also developed a control algorithm[57] using a Kalman filter and a nonlinear model predictive controller (MPC).

Towards advanced MWD control analysis, Ahn et al.[132] studied solution polymerisation, in which an extended Kalman filter-based non-linear MPC was used to control average molecular weight and conversion via manipulation of temperature and feed flow rate of a continuous reactor. Crowley et al.[133] studied the effect of using temperature as a control variable in a similar manner. An MWD model of emulsion polymerisation was developed by Echevarria et al.[134] and implemented within a non-linear control scheme to calculate the optimised feed profiles for monomer and CTA feeds. They were able to achieve complex bimodal MWDs. Vicente et al.[135] controlled the MWD of copolymers by maintaining calculated trajectories of monomers and CTA. Vicente et al.[136] also im-

plemented dynamically optimised monomer and CTA feed profiles for the simultaneous control of copolymer composition and MWD.

A recent paper by Immanuel et al.[137] addressed the controllability of PSD in emulsion polymerisation for a vinyl acetate/butyl acrylate (VAc/BuA) copolymer system with a redox initiator pair and non-ionic surfactant. The main conclusions to come from this work were that control of multiple process inputs i.e. monomer and surfactant, were essential to tailor the PSD and that a hierarchial control strategy exploiting the sub-processes of nucleation, growth and coagulation was possible. Aspects of irreversibility were demonstrated, such as those arising from enhanced coagulation, and limitations with respect to the kind of PSDs that could be produced were highlighted. A continuation on the theme of types of PSD amenable for feedback control was presented in a paper by Immanuel et al.[138] The context of the paper was multiscale inferential control of latex rheology via PSD. Herein, certain feedback controllable cases were assessed as well as those cases where process corrections were not possible, therefore motivating use of a detailed process model for batch-to-batch control. This work however did not consider MWD influence.

The interaction between PSD and MWD in emulsion polymerisation has received very little attention. Of the few works addressing this important aspect. Zeaiter et al.[139] developed and experimentally validated a dynamic population balance model for a semi-batch system employing 0-1 kinetics. Model sensitivity analysis, supported by experiments, showed that monomer feed rate affected growth and PSD, however had little effect on MWD. Furthermore, temperature had a profound influence on MWD. In a later paper, Zeaiter et al.[140] carried out a comprehensive multiobjective control study of emulsion polymerisation. They developed an MPC algorithm using a dynamic model as a soft-sensor for on-line control of polymer PSD and MWD, implementation of which was carried out using capillary hydrodynamic fractionation (CHDF) to measure PSD and gel permeation chromatography (GPC) to measure MWD.

Chapter 3

PSD & MWD Model

This Chapter presents the theoretical development of a combined PSD/MWD model. The general chapter layout will be as follows: Firstly, the PSD model structure and solution technique will be presented, followed by the MWD model and solution technique. A sensitivity analysis of the model will then be presented, including a preliminary analysis of the model response to effects of compartmentalisation. The contents of this chapter were partly published in Macromolecular Symposia.[141]

3.1 PSD Model Structure

The model developed in this section has been developed with particular reference to the modelling work by Saldivar et al.[77] and Immanual et al.[71] A vinyl acetate/butyl acrylate (VAc/BuA) copolymer system with thermal initiator, ionic surfactant and CTA is modelled. A difference in this work is that it develops and incorporates a coagulation kernel for ionic surfactants[108] within the overall coagulation scheme.[71]

The PSD model is formulated based on a PBE framework. Semi-batch component addition is modelled for initiator, monomer, surfactant and CTA. Isothermal conditions are assumed. The overall kinetic scheme is given first. It should be noted that chain transfer reactions to polymer are not considered due to the computational intractability that this reaction would lead to in terms of the MWD model described later. When CTA is present the effect of this assumption is considered to be minimal, but may lead to errors where CTA is not present. An account of the pseudo-homopolymer approximation is then

BIRK LONDON UNIV.

given. Dynamic mass balances over the system components are then developed, including a consideration of partitioning effects in the heterogenous system. PSD information is then incorporated via a one-dimensional population distribution of the polymer particles with respect to their size, in combination with a population distribution of the total live polymer radicals/particle. Finally, the solution technique for the PSD model is given.

3.1.1 Kinetic Scheme

Kinetics	**Mechanism**
Aqueous Phase:	
$I_{\mathrm{w}} \xrightarrow{k_{\mathrm{d}}} 2R_{\mathrm{w}}$	Thermal decomposition
$R_{\mathrm{w}} + M_{\mathrm{w}j} \xrightarrow{k_{\mathrm{r}j}} P^1_{\mathrm{w}j} \quad (j = 1, 2)$	Initiation
$P^l_{\mathrm{w}i} + M_{\mathrm{w}j} \xrightarrow{k^{\mathrm{w}}_{\mathrm{p}ij}} P^{l+1}_{\mathrm{w}j}$ $(l = 1, 2, ..., J_{cr} - 1 \;\; i, j = 1, 2)$	Propagation
$P^l_{\mathrm{w}i} + M_{\mathrm{w}j} \xrightarrow{k^{\mathrm{w}}_{\mathrm{tr}ij}} P^0_{\mathrm{w}i} + D^l_{\mathrm{w}} \quad (i, j = 1, 2)$	Chain transfer to monomer
$P^l_{\mathrm{w}i} + A_{\mathrm{w}} \xrightarrow{k^{\mathrm{w}}_{\mathrm{trA}i}} P^0_{\mathrm{w}A} + D^l_{\mathrm{w}} \quad (i = 1, 2)$	Chain transfer to CTA
$P^l_{\mathrm{w}i} + P^m_{\mathrm{w}j} \xrightarrow{k^{\mathrm{w}}_{\mathrm{tc}ij}} D^{l+m}_{\mathrm{w}} \quad (i, j = 1, 2)$	Combination
$P^l_{\mathrm{w}i} + P^m_{\mathrm{w}j} \xrightarrow{k^{\mathrm{w}}_{\mathrm{td}ij}} D^l_{\mathrm{w}} + D^m_{\mathrm{w}} \quad (i, j = 1, 2)$	Disproportionation
$P^0_{\mathrm{w}i} + M_{\mathrm{w}j} \xrightarrow{k^{\mathrm{w}}_{\mathrm{p}ij}} P^1_{\mathrm{w}j} \quad (i, j = 1, 2)$	Reinitiation
$P^0_{\mathrm{w}A} + M_{\mathrm{w}j} \xrightarrow{k^{\mathrm{w}}_{\mathrm{p}ij}} P^1_{\mathrm{w}j} \quad (j = 1, 2)$	Reinitiation (CTA radical)
$P^l_{\mathrm{w}i} \xrightarrow{e^l_i} N^l_{\mathrm{p}i} \quad (l = 0, ..., J_{cr} - 1 \quad i = 1, 2)$	Entry into a particle
$P^l_{\mathrm{w}i} + \mathrm{micelle} \xrightarrow{e^l_{\mathrm{m},i}} N^l_{\mathrm{p}i}$ $(l = 0, 1, ..., J_{cr} - 1 \quad i = 1, 2)$	Micellar nucleation
$P^{j_{cr}-1}_{\mathrm{w}i} + M_{\mathrm{w}j} \xrightarrow{k^{\mathrm{w}}_{\mathrm{p}ij}} N^{j_{\mathrm{cr}}}_{\mathrm{p}j} \quad (i, j = 1, 2)$	Homogenous nucleation
Particle Phase:	
$N^l_{\mathrm{p}i} + M_{\mathrm{p}j} \xrightarrow{k_{\mathrm{p}ij}} N^{l+1}_{\mathrm{p}j} \quad (i, j = 1, 2)$	Propagation
$N^l_{\mathrm{p}i} + M_{\mathrm{p}j} \xrightarrow{k_{\mathrm{tr}ij}} N^0_{\mathrm{p}j} + D^l_{\mathrm{p}} \quad (i, j = 1, 2)$	Chain transfer to monomer
$N^l_{\mathrm{p}i} + A_{\mathrm{p}} \xrightarrow{k_{\mathrm{trA}i}} N^0_{\mathrm{p}A} + D^l_{\mathrm{p}} \quad (i = 1, 2)$	Chain transfer to CTA
$N^l_{\mathrm{p}i} + N^m_{\mathrm{p}j} \xrightarrow{k_{\mathrm{tc}ij}} D^{l+m}_{\mathrm{p}} \quad (i, j = 1, 2)$	Combination
$N^l_{\mathrm{p}i} + N^m_{\mathrm{p}j} \xrightarrow{k_{\mathrm{td}ij}} D^l_{\mathrm{p}} + D^m_{\mathrm{p}} \quad (i, j = 1, 2)$	Disproportionation
$N^0_{\mathrm{p}i} \xrightarrow{k_{\mathrm{dM}i}} P^0_{\mathrm{w}i} \quad (i = 1, 2)$	Desorption from a particle

where w denotes aqueous phase, p denotes particle phase, I is initiator molecules, R is free-radicals, M_i is monomer of type i, A is chain transfer agent, $P^l_{\mathrm{w}i}$ is live aqueous phase

polymer chains of type i and length l, $P^0_{\mathrm{w}A}$ is aqueous phase monomeric radicals derived from transfer to CTA, $N^l_{\mathrm{p}i}$ is live particle phase polymer chains of type i and length l, $N^0_{\mathrm{p}A}$ is polymer phase monomeric radicals derived from transfer to CTA. D^l is dead polymer chains of length l, j_{cr} is the critical chain length required for an aqueous phase oligomer to homogenously nucleate [see nomenclature for full list of kinetic constants].

3.1.2 Pseudo-homopolymerisation Approximation

The kinetics of copolymerisation systems (containing two monomers) are incorporated by using the pseudo-homopolymerisation approximation developed by.[106,77] The pseudo-homopolymerisation equation for the aqueous phase is given as:

$$p_{\mathrm{w}1} = \frac{k^{\mathrm{w}}_{\mathrm{p}21} + k^{\mathrm{w}}_{\mathrm{tr}21}[M_{\mathrm{w}1}]}{k^{\mathrm{w}}_{\mathrm{p}21} + k^{\mathrm{w}}_{\mathrm{tr}21}[M_{\mathrm{w}1}] + k^{\mathrm{w}}_{\mathrm{p}12} + k^{\mathrm{w}}_{\mathrm{tr}12}[M_{\mathrm{w}2}]} \tag{3.1}$$

where $k^{\mathrm{w}}_{\mathrm{p}ij}$ and $k^{\mathrm{w}}_{\mathrm{tr}ij}$ are the propagation and chain transfer constants for chains of type i with monomer of type j in the aqueous phase. $p_{\mathrm{w}2}$ is defined as $1 - p_{\mathrm{w}1}$.

The particle phase consideration of the pseudo-homopolymerisation approximation is derived analogously to that in the aqueous phase:

$$p_1 = \frac{k_{\mathrm{p}21} + k_{\mathrm{tr}21}[M_{\mathrm{p}1}]}{k_{\mathrm{p}21} + k_{\mathrm{tr}21}[M_{\mathrm{p}1}] + k_{\mathrm{p}12} + k_{\mathrm{tr}12}[M_{\mathrm{p}2}]} \tag{3.2}$$

where $k_{\mathrm{p}ij}$ and $k_{\mathrm{tr}ij}$ are the propagation and chain transfer constants for chains of type i with monomer of type j in the particle phase.

This method greatly simplifies the mass balances for system components. The pseudo-homopolymer probabilities are multiplied by the total amount of live polymer in each phase, to distinguish between the different classes of polymer i.e. that with an end group constituting either type 1 or type 2 monomer.

3.1.3 Aqueous Phase Radical Balances

Dissolved aqueous phase initiator molecules decompose under heating to produce initiator free-radicals. The free-radicals produced may either react with the sparing amount of monomer dissolved in the aqueous phase or encounter another aqueous phase species and undergo termination. The aqueous phase dynamic mass balances over initiator molecules

and initiator free-radicals are given by:[142,143]

$$\frac{d([I_{\mathrm{w}}]V_{\mathrm{aq}})}{dt} = u_i - k_{\mathrm{d}}[I_{\mathrm{w}}]V_{\mathrm{aq}} \tag{3.3}$$

$$\begin{aligned}\frac{d[R_{\mathrm{w}}]V_{\mathrm{aq}}}{dt} &= 2k_d[I_{\mathrm{w}}]V_{\mathrm{aq}} - V_{\mathrm{aq}}\sum_{i=1}^{2} k_{\mathrm{r}i}[M_{\mathrm{w}i}][R_{\mathrm{w}}] \\ &- V_{\mathrm{aq}}\bar{k}_{\mathrm{t}}^{\mathrm{w}}[R_{\mathrm{w}}]\left[\sum_{l=0}^{J_{\mathrm{cr}}-1}[P_{\mathrm{w}}^{l}] + [R_{\mathrm{w}}]\right]\end{aligned} \tag{3.4}$$

where V_{aq} is the aqueous phase volume and u_i is the molar flow rate of initiator molecules into the system.

The mass balances for the various aqueous phase oligomer species are given by:

$$\begin{aligned}\frac{d([P_{\mathrm{w}}^{1}]V_{\mathrm{aq}})}{dt} &= V_{\mathrm{aq}}\sum_{i=1}^{2} k_{\mathrm{r}i}[R_{\mathrm{w}}][M_{\mathrm{w}i}] - V_{\mathrm{aq}}\bar{k}_{t}^{\mathrm{w}}[P_{\mathrm{w}}^{1}]\left(\sum_{l=0}^{j_{\mathrm{cr}}-1}[P_{\mathrm{w}}^{l}] + [R_{\mathrm{w}}]\right) \\ &- \left(\bar{k}_{\mathrm{p}}^{\mathrm{w}} + \bar{k}_{\mathrm{tr}}^{\mathrm{w}} + \bar{k}_{\mathrm{trA}}^{\mathrm{w}}\right)[P_{\mathrm{w}}^{1}]V_{\mathrm{aq}} + \bar{k}_{\mathrm{p}}^{\mathrm{w}}[P_{\mathrm{w}}^{0}]V_{\mathrm{aq}} \\ &- \sum_{i=1}^{2} e_{\mathrm{m},i}^{1} p_{\mathrm{w}i}[P_{\mathrm{w}}^{1}]C_{\mathrm{micelle}}V_{\mathrm{aq}} - \int_{r=r_{\mathrm{nuc}}}^{r_{\mathrm{max}}}\sum_{i=1}^{2} e_i^{1}(r)[P_{\mathrm{w}}^{1}]F(r,t)dr\end{aligned} \tag{3.5}$$

The monomeric radicals produced by chain transfer to monomer and to CTA are lumped into a single variable, $P_w^{0\mathrm{T}}$:

$$P_w^{0\mathrm{T}} = P_{\mathrm{w}}^{0} + P_{\mathrm{wA}}^{0} \tag{3.6}$$

$$\begin{aligned}\frac{d([P_{\mathrm{w}}^{0\mathrm{T}}]V_{\mathrm{aq}})}{dt} &= \left(\bar{k}_{\mathrm{tr}}^{\mathrm{w}} + \bar{k}_{\mathrm{trA}}^{\mathrm{w}}\right)\sum_{l=1}^{j_{\mathrm{cr}}-1}[P_{\mathrm{w}}^{l}]V_{\mathrm{aq}} - \bar{k}_{\mathrm{p}}^{\mathrm{w}}[P_{\mathrm{w}}^{0\mathrm{T}}]V_{\mathrm{aq}} \\ &- \bar{k}_{\mathrm{t}}^{\mathrm{w}}[P_{\mathrm{w}}^{0\mathrm{T}}]\left(\sum_{l=0}^{j_{\mathrm{cr}}-1}[P_{\mathrm{w}}^{l}] + [R_{\mathrm{w}}]\right)V_{\mathrm{aq}} - \sum_{i=1}^{2} e_{\mathrm{m},i}^{0} p_{\mathrm{w}i}[P_{\mathrm{w}}^{0\mathrm{T}}]C_{\mathrm{micelle}}V_{\mathrm{aq}} \\ &- \int_{r=r_{\mathrm{nuc}}}^{r_{\mathrm{max}}}\sum_{i=1}^{2} e_i^{0}(r)p_{\mathrm{w}i}[P_{\mathrm{w}}^{0\mathrm{T}}]F(r,t)dr \\ &+ \left(\bar{k}_{\mathrm{tr}}^{\mathrm{p}} + \bar{k}_{\mathrm{trA}}^{\mathrm{p}}\right)\int_{r=r_{\mathrm{nuc}}}^{r_{\mathrm{max}}}\frac{\bar{n}(r,t)F(r,t)k_{\mathrm{dM}j}(r)dr}{k_{\mathrm{dM}j}(r) + \sum_{l=1}^{2} k_{\mathrm{p}il}[M_{\mathrm{pl}}]}\end{aligned} \tag{3.7}$$

$$\begin{aligned}\frac{d([P_{\mathrm{w}}^n]V_{\mathrm{aq}})}{dt} &= \bar{k}_{\mathrm{p}}^{\mathrm{w}}\left([P_{\mathrm{w}}^{n-1}]-[P_{\mathrm{w}}^n]\right)V_{\mathrm{aq}} - \bar{k}_{\mathrm{tr}}^{\mathrm{w}}[P_{\mathrm{w}}^n]V_{\mathrm{aq}} \\ &- e_{\mathrm{m},i}^n p_{\mathrm{w}i}[P_{\mathrm{w}}^n]C_{\mathrm{micelle}}V_{\mathrm{aq}} - \int_{r=r_{\mathrm{nuc}}}^{r_{\max}}\sum_{i=1}^{2} e_i^n(r)p_{\mathrm{w}i}[P_{\mathrm{w}}^n]F(r,t)dr \\ &- \bar{k}_t^{\mathrm{w}}[P_{\mathrm{w}}^n]\left(\sum_{l=0}^{j_{\mathrm{cr}}-1}[P_{\mathrm{w}}^l]+[R_{\mathrm{w}}]\right)V_{\mathrm{aq}} \\ &(n=2,3,...,J_{\mathrm{cr}-1}) \end{aligned} \tag{3.8}$$

where $C_{micelle}$ is the concentration of micelles. The *aqueous phase* pseudo-homopolymer rate constants are given as:

$$\bar{k}_{\mathrm{tr}}^{\mathrm{w}} = \sum_{i=1}^{2}\sum_{j=1}^{2} k_{\mathrm{tr}ij}^{\mathrm{w}} p_{\mathrm{w}i}[M_{\mathrm{w}j}] \tag{3.9}$$

$$\bar{k}_{\mathrm{p}}^{\mathrm{w}} = \sum_{i=1}^{2}\sum_{j=1}^{2} k_{\mathrm{p}ij}^{\mathrm{w}} p_{\mathrm{w}i}[M_{\mathrm{w}j}] \tag{3.10}$$

$$\bar{k}_t^{\mathrm{w}} = \sum_{i=1}^{2}\sum_{j=1}^{2}(k_{\mathrm{tc}ij}^{\mathrm{w}} + k_{\mathrm{td}ij}^{\mathrm{w}})p_{\mathrm{w}i}p_{\mathrm{w}j} \tag{3.11}$$

$$\bar{k}_{\mathrm{trA}}^{\mathrm{w}} = \sum_{i=1}^{2} k_{\mathrm{trA}i}^{\mathrm{w}} p_{\mathrm{w}i}[A_{\mathrm{w}}] \tag{3.12}$$

Analogous to those for the aqueous phase, the *particle phase* pseudo-homopolymer rate constants are given as:

$$\bar{k}_{\mathrm{tr}} = \sum_{i=1}^{2}\sum_{j=1}^{2} k_{\mathrm{tr}ij} p_i[M_{\mathrm{p}j}] \tag{3.13}$$

$$\bar{k}_{\mathrm{trA}} = \sum_{i=1}^{2} k_{\mathrm{trA}i}^{w} p_i[A_{\mathrm{p}}] \tag{3.14}$$

$$\bar{k}_{\mathrm{p}} = \sum_{i=1}^{2}\sum_{j=1}^{2} k_{\mathrm{p}ij} p_i[M_{\mathrm{p}j}] \tag{3.15}$$

$$\bar{k}_{\mathrm{t}} = \sum_{i=1}^{2}\sum_{j=1}^{2}(k_{\mathrm{tc}ij} + k_{\mathrm{td}ij})p_i p_j \tag{3.16}$$

$$\bar{k}_{\mathrm{tc}} = \sum_{i=1}^{2}\sum_{j=1}^{2} k_{\mathrm{tc}ij} p_i p_j \tag{3.17}$$

$$\bar{k}_{\mathrm{td}} = \sum_{i=1}^{2}\sum_{j=1}^{2} k_{\mathrm{td}ij} p_i p_j \tag{3.18}$$

3.1.4 Monomer Balance

The dynamic mass balance for monomers in a semi-batch copolymer **reaction** system. with monomer feed is given as:

$$\begin{aligned}\frac{dM_j}{dt} &= u_{Mj} - \sum_{i=1}^{2}(k^{\mathrm{w}}_{\mathrm{p}ij} + k^{\mathrm{w}}_{\mathrm{tr}ij}p_{\mathrm{w}i}[M_{\mathrm{w}j}]\sum_{n=o}^{j_{\mathrm{cr}}-1}[P^n_{\mathrm{w}}]V_{\mathrm{aq}} \\ &- \sum_{i=1}^{2}(k_{\mathrm{p}ij} + k_{\mathrm{tr}ij})p_i[M_{\mathrm{p}j}]\int_{r=r_{\mathrm{nuc}}}^{r_{\mathrm{max}}}\bar{n}(r,t)F(r,t)dr \\ &(j = 1, 2)\end{aligned} \tag{3.19}$$

where $u_{\mathrm{M}j}$ is the molar feed rate of monomer j, $[M_{\mathrm{w}j}]$ is the concentration of monomer j in the aqueous phase and $[M_{\mathrm{p}j}]$ is the concentration of monomer j in the particle phase.

In order to evaluate the rate of change of monomer, a value for the concentration in each phase is needed. Monomer is modelled under equilibrium conditions, wherein monomer will partition between the dispersed and aqueous phases. When equilibrium solubility is reached in the dispersed and aqueous phases, a separate monomer droplet phase is formed. The set of equations below account for the monomer throughout the system phases:

- $V_{1,\mathrm{p}} + V_{2,\mathrm{p}} + V_{\mathrm{p}} = V^{\mathrm{s}}_{\mathrm{p}}$ Particle phase balance
- $V_{1,\mathrm{w}} + V_{2,\mathrm{w}} + V_{\mathrm{w}} = V^{\mathrm{T}}_{\mathrm{w}}$ Aqueous phase balance
- $V_{1,\mathrm{d}} + V_{2,\mathrm{d}} = V_{\mathrm{d}}$ Droplet phase balance
- $V_{i,\mathrm{p}} + V_{i,\mathrm{d}} + V_{i,\mathrm{w}} = \frac{M_i \mathrm{MW}_i}{\rho_{\mathrm{M}i}}$ Total system monomer balance

where $V_{i,\mathrm{p}}$, $V_{i,\mathrm{w}}$ and $V_{i,\mathrm{d}}$ are the volume of monomer i in the particles, aqueous phase and monomer droplets, respectively, $V^{\mathrm{s}}_{\mathrm{p}}$, $V^{\mathrm{T}}_{\mathrm{w}}$ and V_{d} are the total volume of the swollen polymer, aqueous phase and droplet phase, respectively. Partitioning coefficients are used to relate these quantities: $V_{i,\mathrm{p}}/V^{\mathrm{s}}_{\mathrm{p}} = K_{\mathrm{p}i}(V_{i,\mathrm{w}}/V^{\mathrm{T}}_{\mathrm{w}})$ and $V_{i,\mathrm{d}}/V_{\mathrm{d}} = (K_{\mathrm{d}i}/K_{\mathrm{p}i})(V_{i,\mathrm{p}}/V^{\mathrm{s}}_{\mathrm{p}})$.

The total volume of unswollen particles is given by:

$$V_{\mathrm{p}} = N_{\mathrm{A}}\int_{r=r_{\mathrm{nuc}}}^{r_{\mathrm{max}}}\frac{4}{3}\pi r^3 F(r,t)dr \tag{3.20}$$

where r is the radius of the unswollen particles. The relationship between the unswollen

and swollen radii is given by:

$$r_{\mathrm{s}}^3 = \frac{r^3}{\left(1 - \frac{\mathrm{MW}_1[M_{\mathrm{p1}}]}{\rho_{\mathrm{M1}}} - \frac{\mathrm{MW}_2[M_{\mathrm{p2}}]}{\rho_{\mathrm{M1}}}\right)} \tag{3.21}$$

where $\rho_{\mathrm{M}i}$ is the density of monomer i.

3.1.5 Surfactant Balance

Surfactants play a number of roles in emulsion polymerisation: they emulsify monomer droplets, stabilise polymer particles and take part in particle nucleation. This framework incorporates *ionic* surfactants. Surfactants undergo no reaction within the emulsion polymerisation system, therefore the amount existing in the system is simply equal to the amount added. The surfactants will however be subject to partitioning amongst the heterogenous system phases. Ionic surfactants will be present mostly in the aqueous phase, as well as adsorbing to the surface of particles. Due to their charged nature, ionic surfactant molecules tend not to partition into the organic phases. The Langmuir monolayer theory is used to model the adsorption of surfactant to the surface of a particle. The partitioning of surfactant in the system is modelled under equilibrium conditions using partition coefficients. The surfactant balance is given as:

$$V_{\mathrm{w}} S_{\mathrm{w}} + K_{\mathrm{s}} S_{\mathrm{w}} V_{\mathrm{p}}^{\mathrm{s}} + K_{\mathrm{s}}^{\mathrm{d}} S_{\mathrm{w}} V_{\mathrm{d}} + \frac{\Gamma_\infty K_{\mathrm{ad}} S_{\mathrm{w}} A_{\mathrm{p}}^{\mathrm{s}}}{1 + K_{\mathrm{ad}} S_{\mathrm{w}}} = S_{\mathrm{T}} \tag{3.22}$$

where S_{T} is the total surfactant present in the system, S_{w} is the surfactant present in the aqueous phase, V_{w} is the volume of the aqueous phase. The second and third terms on the LHS account for the partitioning of surfactant into droplets and particles, respectively; $V_{\mathrm{p}}^{\mathrm{s}}$ is the volume of swollen polymer particles, V_{d} is the volume of the monomer droplets, with K_{s} and $K_{\mathrm{s}}^{\mathrm{d}}$ being the partitioning coefficients for surfactant between the particles and the aqueous phase; and between the droplets and the aqueous phase. These terms are expected to be extremely small for ionic surfactants, and are therefore set to zero in the model. The fourth term on the LHS accounts for the adsorption of surfactant onto the surface of particles, in equilibrium with that in the aqueous phase; Γ_∞ and K_{ad} are Langmuir adsorption constants and $A_{\mathrm{p}}^{\mathrm{s}}$ is the total surface area of the polymer particles.

calculated as:

$$A_{\mathrm{p}}^{\mathrm{s}} = \int_{r_{\mathrm{nuc}}}^{r_{\mathrm{max}}} 4\pi r_{\mathrm{s}}^2 N_{\mathrm{A}} F(r,t) dr \tag{3.23}$$

3.1.6 CTA Balance

The dynamic mass balance for CTA in a semi-batch reaction system with CTA feed is given as:

$$\begin{aligned} \frac{dA}{dt} &= u_{\mathrm{A}} - \sum_{i=1}^{2} k_{\mathrm{trA}i}^{\mathrm{w}} p_{\mathrm{w}i} \sum_{n=o}^{j_{\mathrm{cr}}-1} [P_{\mathrm{w}}^{n}][A_{\mathrm{w}}] V_{\mathrm{aq}} \\ &- \sum_{i=1}^{2} k_{\mathrm{trA}i} p_i [A_{\mathrm{p}}] \int_{r=r_{\mathrm{nuc}}}^{r_{\mathrm{max}}} \bar{n}(r,t) F(r,t) dr \\ &(j = 1,2) \end{aligned} \tag{3.24}$$

where $u_{\mathrm{A}j}$ is the molar feed rate of CTA and $[A_{\mathrm{w}}]/[A_{\mathrm{p}}]$ is the concentration of CTA in the aqueous/particle phase, respectively.

The partitioning of CTA through the system phases is modelled using partition coefficients, as follows:

$$[A_{\mathrm{w}}]V_{\mathrm{aq}} + [A_{\mathrm{w}}]K_{\mathrm{d}}^{\mathrm{A}} V_{\mathrm{d}} + [A_{\mathrm{w}}]K_{\mathrm{p}}^{\mathrm{A}} V_{\mathrm{p}}^{\mathrm{s}} = A^{\mathrm{T}} \tag{3.25}$$

where K_A^d is the partitioning coefficient for CTA, between the aqueous and droplet phases, K_A^p is the partitioning coefficient for CTA, between the aqueous and particle phases, V_d is the volume of droplets and A^T is the total amount of CTA existing in the system.

3.1.7 System Population Balance

The population balance equation describing the polymer particles in the system is given by:

$$\frac{\partial}{\partial t} F(r,t) + \frac{\partial}{\partial r}\left(F(r,t) \frac{dr}{dt} \right) = \Re_{\mathrm{nuc}} \delta(r - r_{\mathrm{nuc}}) + \Re_{\mathrm{coag}} \tag{3.26}$$

where $F(r,t)dr$ is the particle density, defined as the moles of particles of a size between r and $r + dr$ at time t. It is assumed that nucleation only occurs at a minimum size, r_{nuc}, as depicted by the delta function. It is assumed that r_{nuc} is equal to the radius of a micelle,

r_{mic}. The interchange of particles through coagulation is incorporated through the term, $\Re_{\text{coag}}$.

3.1.8 Average Radicals per Particle

An additional population balance is performed over the the average number of radicals (of both types combined) contained in particles:

$$\frac{\partial}{\partial t}(\bar{n}(r,t)F(r,t)) + \frac{\partial}{\partial r}\left(\bar{n}(r,t)F(r,t)\frac{dr}{dt}\right) = \Re_{\text{entry}} + \Re_{\text{des}} + \Re_{\text{termin}} + \Re_{\text{coag}} \tag{3.27}$$

where $\bar{n}(r,t)$ is the average number of live polymer chains/particle in particles of size r at time t, $\Re_{\text{entry}}$ accounts for entry from all particles of size between r and $r+dr$, $\Re_{\text{des}}$ accounts for desorption from all particles of size between r and $r+dr$, $\Re_{\text{termin}}$ accounts for termination inside particles of size between r and $r+dr$ and $\Re_{\text{coag}}$ accounts for coagulation of particles. In order to distinguish between the different types of polymer inside particles, the pseudo-homopolymerisation approximation is used, analogous to that defined for the aqueous phase. For the purposes of this work the above population balance approach can be simplified by focussing on a single particle and neglecting growth and coagulation effects, giving a fundamental balance over entry, desorption and termination:

$$\frac{\partial}{\partial t}(\bar{n}(r,t)) = \Re'_{\text{entry}}(r) + \Re'_{\text{des}}(r) - 2\Re'_{\text{termin}}(r) \tag{3.28}$$

where $\Re'_{\text{entry}}$ accounts for the rate of entry into a single particle of size between r and $r+dr$, $\Re'_{\text{des}}$ accounts for the rate of desorption from a single particles of size between r and $r+dr$ and $\Re'_{\text{termin}}$ accounts for the rate of termination within a single particle of size between r and $r+dr$. The global average number of radicals per particle is defined as:

$$n_{\text{glob}}(t) = \frac{\int_{r=r_{\text{nuc}}}^{r_{\text{max}}} \bar{n}(r,t)F(r,t)dr}{\int_{r=r_{\text{nuc}}}^{r_{\text{max}}} F(r,t)dr} \tag{3.29}$$

The individual terms that comprise the radical balance over a particle will now be detailed.

3.1.9 Particle Entry

Aqueous phase oligomers are able to enter existing polymer particles. The rate constant for this phenomena is given as:[76]

$$e_i^l(r) = 4\pi r^n N_{\mathrm{A}} D_{\mathrm{w}i}, \quad l = 0, 1 \tag{3.30}$$

$$e_i^l(r) = 4\pi r^n N_{\mathrm{A}} D_{\mathrm{w}i}/\sqrt{l-1}, \quad l = 2, 3, ..., j_{\mathrm{cr}} - 1 \tag{3.31}$$

where e_i^l is the rate coefficient for a radical of type i, $(i = 1, 2)$ and chain length l. $(l = 0, 1, ..., j_{\mathrm{cr}} - 1)$. The entry mechanism corresponds to the Fickian diffusion model when $n = 1$ or the collision model when $n = 2$ (the units and physical meaning of parameter $D_{\mathrm{w}i}$ change accordingly). All chains up to the limit $j_{\mathrm{cr}} - 1$ are assumed to be able to enter a particle, otherwise they nucleate via the homogenous mechanism. The total rate of entry into a single particle of size r is given by:

$$\Re'_{\mathrm{entry}}(r) = \sum_{l=0}^{j_{cr}-1} \sum_{i=1}^{2} e_i^l(r) p_{\mathrm{w}i} [P_{\mathrm{w}}^l] \tag{3.32}$$

3.1.10 Desorption from Particles

Chain transfer to monomer or CTA results in a monomeric radical (as shown in the table of kinetics above), which, in addition to other possible reaction routes, is able to desorb out of the particle into the aqueous phase. The rate of desorption from a particle of size between r and $r + dr$ is given by extending the approach of[69,108] for systems with CTA. A balance for the monomeric radicals within a particle is given by:

$$\begin{aligned} \frac{\partial [N_{\mathrm{p}j}^0]}{\partial t} &= \sum_{i=1}^{2} k_{\mathrm{tr}ij} \sum_{l=0}^{l_{\max}} [N_{\mathrm{p}i}^l][M_{\mathrm{p}j}] + \sum_{i=1}^{2} k_{\mathrm{trA}i} \sum_{l=0}^{l_{\max}} [N_{\mathrm{p}i}^l][A_{\mathrm{p}}] \\ &- \sum_{i=1}^{2} k_{\mathrm{p}ji} [N_{\mathrm{p}j}^0][M_{\mathrm{p}i}] - k_{\mathrm{dM}j} [N_{\mathrm{p}j}^0] \end{aligned} \tag{3.33}$$

where $k_{\mathrm{dM}j} = 3\bar{D}_{\mathrm{w}j}/r^2$, with $\bar{D}_{\mathrm{w}j}$ being the diffusion coefficient for monomer j in the aqueous phase

Assuming pseudo steady state and solving for $N^0_{\mathrm{p}j}$ gives:

$$[N^0_{\mathrm{p}j}] = \frac{\sum_{l=0}^{l_{\max}} [N^l_{\mathrm{p}i}] \sum_{i=1}^{2} (k_{\mathrm{tr}ij}[M_{\mathrm{p}j}] + k_{\mathrm{trA}i}[A_{\mathrm{p}}])}{k_{\mathrm{dM}j}(r) + \sum_{i=1}^{2} k_{\mathrm{p}ji}[M_{\mathrm{p}i}]} \tag{3.34}$$

Thus the total rate of desorption is given as:

$$\Re'_{\mathrm{des}}(r) = \sum_{j=1}^{2} k_{\mathrm{dM}j}(r) \frac{\sum_{i=1}^{2} (k_{\mathrm{tr}ij}[M_{\mathrm{p}j}] + k_{\mathrm{trA}i}[A_{\mathrm{p}}]) p_i \bar{n}(r.t)}{k_{\mathrm{dM}j}(r) + \sum_{l=1}^{2} k_{\mathrm{p}jl}[M_{\mathrm{p}l}]} \tag{3.35}$$

3.1.11 Termination within Particles

The rate of termination of radicals inside particles of size r is given by:

$$\Re'_{\mathrm{termin}}(r) = \frac{\bar{k}_{\mathrm{t}} \bar{n}(r,t)^2}{V_{\mathrm{p}} N_{\mathrm{A}}} \tag{3.36}$$

3.1.12 Particle Growth

The second term on the LHS of Eq. (3.26) accounts for the continuous particle growth via polymerisation. Rapid propagation of radicals inside particles, via the addition of monomer units, causes the length of the radicals to increase. This causes the particle size/mass to increase. The overall density of the latex will also increase as polymerisation proceeds. The growth kernel is given by:

$$\frac{dr}{dt} = \frac{1}{4\pi r^2 \rho_{\mathrm{p}}} \sum_{i=1}^{2} \sum_{j=1}^{2} k_{\mathrm{p}ij} p_i \frac{\bar{n}(r,t)}{N_{\mathrm{A}}} [M_{\mathrm{p}j}] \mathrm{MW}_j \tag{3.37}$$

where ρ_{p} is the density of polymer and MW_j is the molecular weight of monomer j.

3.1.13 Particle Nucleation

The formation of particles is modelled in respect to the mechanisms of micellar and homogenous nucleation. There is also much evidence for coagulative nucleation[24,21,144,145] playing an important part in particle formation, the modelling[26] of which could be included as a possible model improvement step.

Homogenous Nucleation

Upon reaching a critical chain length, j_{cr}, the aqueous phase radicals will become too

hydrophobic to remain dissolved in the aqueous phase, and will therefore precipitate from solution a form a new polymer particle. This particle will form a location for the adsorption of surfactant molecules, which will act to stabilise it. The rate of homogenous nucleation is given as:

$$\Re_{\text{homogenous}} = \bar{k}_{\text{p}}^{\text{w}}[P_{\text{w}}^{j_{\text{cr}}-1}]V_{\text{aq}} \tag{3.38}$$

Micellar Nucleation

Micellar nucleation occurs when an aqueous phase radical enters a micelle (aggregate of surfactant molecules), rather like entry into a small particle. However, this phenomenon will not occur unless there is enough surfactant in the system to form micelles. The free surfactant, S_w (i.e. not adsorbed to surfaces) in the aqueous phase, having exceeded its equilibrium solubility, will aggregate to form micelles. The level of equilibrium solubility is termed the critical micelle concentration (cmc). The following equation is used to determine the concentration of micelles in the system:

$$C_{\text{micelle}} = \frac{(S_{\text{w}} - \text{cmc})\alpha_{\text{ms}}}{4\pi r_{\text{micelle}}^2} \tag{3.39}$$

where C_{micelle} is the concentration of micelles, α_{ms} is the area occupied by a surfactant molecule and r_{micelle} is the radius of a micelle. The rate of entry of aqueous radicals into micelles, and hence the rate of micellar nucleation, is given by:

$$\Re_{\text{micellar}} = \sum_{l=0}^{j_{\text{cr}}-1} \sum_{i=1}^{2} e_{\text{m},i}^{l}(r) p_{\text{w}i}[P_{\text{w}}^{l}] C_{\text{micelle}} V_{\text{aq}} \tag{3.40}$$

with the entry rate constant, $e_{\text{m},i}^{l}$ being defined as:[76]

$$e_{\text{m},i}^{l}(r) = 4\pi r^n N_{\text{A}} D_{\text{w}i}, \quad l = 0, 1 \tag{3.41}$$

$$e_{\text{m},i}^{l}(r) = 4\pi r^n N_{\text{A}} D_{\text{w}i}/\sqrt{l-1}, \quad l = 2, 3, ..., j_{\text{cr}} - 1 \tag{3.42}$$

3.1.14 Coagulation Framework

The methodology used to model coagulation of polymer particles within a population balance framework is based on the work.[146,108,71] The modelling of the coagulation phe-

nomena involves integral terms as shown:

$$\Re_{\text{coag}}(r,t) = H(r_{\text{upper}} - r)\Re_{\text{formation}}(r,t) - H(r_{\text{cut-off}} - r)\Re_{\text{depletion}}(r,t) \tag{3.43}$$

where $H(.)$ is the Heaviside function (unity when argument is non-negative and 0 elsewhere), $r_{\text{cut-off}}$ is the cut-off size, below which the particles will be likely to coagulate, r_{upper} is the maximum size of particles that could result from the coagulation of smaller particles, related to $r_{\text{cut-off}}$ as $r_{\text{upper}} = 2^{1/3} r_{\text{cut-off}}$. $\Re_{\text{formation}}(r,t)$ is the rate of formation of particles of size r, due to coagulation, and is given by:

$$\begin{aligned} \Re_{\text{formation}}(r,t) &= \frac{1}{V_{\text{aq}}} \int_{r'=r_{\text{nuc}}}^{\frac{r}{2^{1/3}}} \beta(r',r'')F(r',t) \\ &\times F(r'',t)\frac{r^2}{(r^3-(r')^3)^{2/3}}dr' \end{aligned} \tag{3.44}$$

and $\Re_{depletion}(r,t)$ is the rate of depletion of particles of size r due to coagulation, given by:

$$\Re_{\text{depletion}}(r,t) = \frac{1}{V_{\text{aq}}} \int_{r_{\text{nuc}}}^{r_{\max}} \beta(r,r')F(r,t)F(r',t)dr' \tag{3.45}$$

Here, $\beta(r,r')$ is the size-dependent intrinsic coagulation rate (kernel) between particles of size r and r'. A full description of the kernel is given below.

3.1.15 Coagulation Rate Kernel

The coagulation kernel is dependent on the concentration of free surfactant, S_{w} and initiator (ionic), I_{w} and is therefore a dynamic entity. The kernel is based on the DLVO theory[31,32] for colloidal interactions in the presence of ionic species. Influential in the kernel derivation was the work by Coen et al.,[108] Hogg et al.,[147] Wiese and Healy,[148] Ottewill,[149] Hamaker,[150] and Dunn.[151]

The rate kernel is derived based on the understanding that 2 opposing forces exist between 2 approaching particles: an attractive and a repulsive force. The repulsive potential will be derived first, followed by the attractive potential.

Surface Charge

The total surface charge, σ on a particle, contains two constituent elements: the surfactant charge, σ_{surf}, arising due to adsorbed surfactant, and the initiator generated component σ_{gen},

$$\sigma = \sigma_{\text{surf}} + \sigma_{\text{gen}} \tag{3.46}$$

where σ_{surf} and σ_{gen} are given as:

$$\sigma_{\text{surf}} = \frac{z_+ e}{A_{\text{s}}} \tag{3.47}$$

$$\sigma_{\text{gen}} = \frac{R_{\text{w}} Z_+ N_{\text{A}} e}{A_{\text{p}}^{\text{s}}} \tag{3.48}$$

where z_+ is the counter-ion valence (unity for persulphate), e is charge on an electron (Coulombs), A_{p}^{s} is the total surface area of the polymer particles (m^2) and $[S_{\text{w}}]$ is the aqueous phase surfactant concentration ($\text{mol}\cdot\ell^{-1}$). A_{s} is the area occupied by surfactant (m^2), given as:

$$A_{\text{s}} = \alpha_{\text{ms}} \left(1 + \frac{1}{S_{\text{w}} k_{\text{ad}}}\right) \tag{3.49}$$

where K_{ad} is a Langmuir adsorption constant ($\ell \cdot \text{mol}^{-1}$).

Inverse Double-Layer Thickness

The inverse length, k (m^{-1}) is based on the Debye-double layer thickness (m) and is defined as:

$$k = \left(\frac{8\pi N_{\text{A}} I_{\text{s}} e^2}{\varepsilon K_{\text{B}} T}\right) \tag{3.50}$$

with:

$$I_{\text{s}} = 3[I_{\text{w}}] + S_{\text{w}} + [\text{elec}] \tag{3.51}$$

$$\varepsilon = 4\pi\varepsilon_0\varepsilon_r \tag{3.52}$$

where T is absolute temperature, K_{B} is the Boltzmann constant, S_{w} is the concentration of free surfactant (mol·ℓ^{-1}), [elec] is the concentration of added electrolyte (mol·ℓ^{-1}), ε_0 is the permittivity of free space (F·m^{-1}) and ε_r is the relative permittivity of water.

Surface and Zeta Potentials

The surface and zeta potentials are calculated for each particle size class. The product of k and the swollen particle radius r_s is used to determine the form of equation used to calculate the surface potential, ψ (V), for that given size class, as follows:

If $r_{\mathrm{s}}k \leq 1$ then,

$$\psi = \frac{4\pi r_{\mathrm{s}}\sigma}{\varepsilon(1 + kr_{\mathrm{s}})} \tag{3.53}$$

however, if $r_s k > 1$ then,

$$\psi = \frac{2K_{\mathrm{B}}T}{e} \sinh^{-1} \frac{2\pi e\sigma}{\varepsilon k K_{\mathrm{B}}T} \tag{3.54}$$

The zeta potential, ζ (V) is related to the surface potential through the following equations:

$$\zeta = \left(\frac{2K_{\mathrm{B}}T}{z_+ e}\right) \ln\left(\frac{\exp(\lambda) + 1}{\exp(\lambda) - 1}\right) \tag{3.55}$$

with λ given as:

$$\lambda = k\delta_{\mathrm{s}} + \ln\left(\frac{\exp(\lambda_1) + 1}{\exp(\lambda_1) - 1}\right) \tag{3.56}$$

and with λ_1 given as:

$$\lambda_1 = \frac{z_+ e\psi}{2K_{\mathrm{B}}T} \tag{3.57}$$

where δ_{s} is the Stern layer thickness (m).

Repulsion Potential

The repulsion potential, Φ_R (Joules), is calculated using the Healy-Hogg-Fursteneau equa-

tion:

$$\Phi_R(d) = \frac{\varepsilon r_{si} r_{sj}(\zeta_i^2 + \zeta_j^2)}{4(r_{si} + r_{sj})} \left[\frac{2\zeta_i \zeta_j}{\zeta_i^2 + \zeta_j^2} \ln\left(\frac{1 + e^{-kd}}{1 - e^{-kd}}\right) + \ln(1 - e^{-2kd}) \right] \tag{3.58}$$

where d is defined as the interface distance between two swollen particles, i and j, with swollen radii r_{si} and r_{sj}.

Attraction Potential

The attractive potential is attributed to the Wan der Waal's attractive potential, and is given as:

$$\begin{aligned} \Phi_A(D) &= \frac{-A_L}{6}\left[\frac{2r_{si}r_{sj}}{D^2 - (r_{si} + r_{sj})^2} + \frac{2r_{si}r_{sj}}{D^2 - (r_{si} - r_{sj})^2}\right. \\ &+ \left. \ln\left(\frac{D^2 - (r_{si} + r_{sj})^2}{D^2 - (r_{si} - r_{sj})^2}\right)\right] \end{aligned} \tag{3.59}$$

where D is the distance between particle centres, related to d as:

$$D = d + (r_{si} + r_{sj}) \tag{3.60}$$

The net interaction potential, Φ is given as:

$$\Phi = \Phi_A + \Phi_R \tag{3.61}$$

Fuch Stability Ratio

The maximum value for the net interaction potential, Φ_{max}, represents the energy barrier that the particles must overcome in order to coagulate. Φ_{max} is used to calculate the Fuch stability ratio:

$$W_{ij} = \frac{r_{si} + r_{sj}}{4kr_{si}r_{sj}} \exp\left(\frac{\Phi_{max}}{K_B T}\right) \tag{3.62}$$

where W_{ij} is the Fuch stability ratio between two swollen particles, i and j.

Using the Fuch stability ratio, the following equation gives the intrinsic coagulation

rate, B_{ij} ($\ell \cdot \mathrm{mol}^{-1} \cdot \mathrm{s}^{-1}$) between 2 particles, i and j:

$$B_{ij} = \frac{2K_{\mathrm{B}}T}{3\eta W_{ij}} \left(2 + \frac{r_{\mathrm{s}i}}{r_{\mathrm{s}j}} + \frac{r_{\mathrm{s}j}}{r_{\mathrm{s}i}}\right) \tag{3.63}$$

where η is the viscosity of the latex.

3.2 PSD Model Solution

It is possible to solve the previous model using an OCFE technique. This has been done by Immanuel at el.[69] The stiff integrators necessitated by the resultant system of DAEs resulted in an average solution time of about 38 minutes even without coagulation. Due to the limited applicability to on-line control applications, it was decided to use an alternative and more efficient solution technique developed by Immanuel et al.[71] Here only a brief description of the solution will be given with salient elements explained and emphasis placed on portions specifically relating to this work.

A fine discretisation mesh is applied to the particle size domain with 250 bins spanning a 2-500 nm particle radius range [Figure 3.1 (a)]. Each step within the time domain is split into 5 sub-steps for integration [Figure 3.1 (b)], in order to employ a 5th order predictor-corrector method.

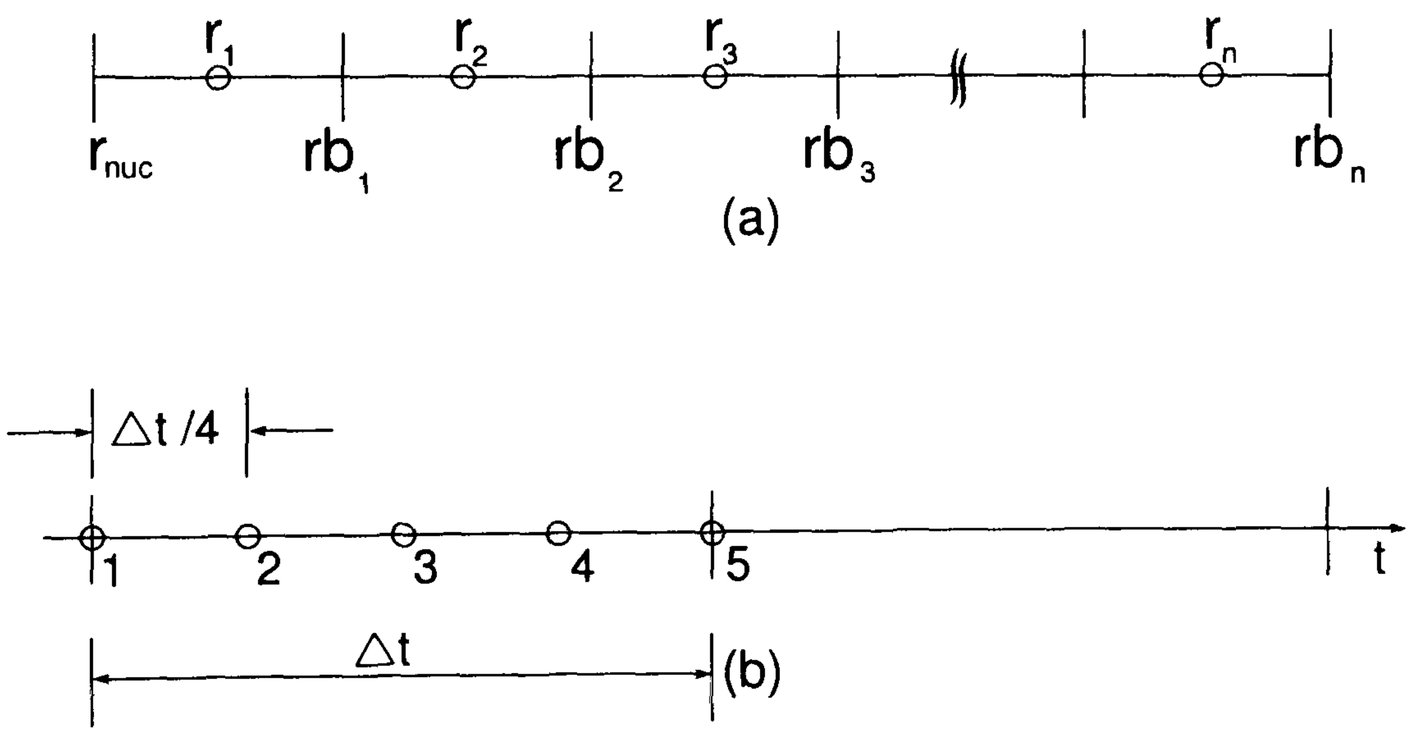


Figure 3.1: a) Discretisation of particle size domain and b) time domain

The fine particle discretisation grid (2 nm bin width) allows for a high resolution to be obtained for PSD. r_{nuc} is the size of a nucleated particle, with rb_j as the upper boundary

size for bin j. r_j is the representative size for bin j, and falls at the mid point of the bin. An important consideration is the distribution of particles within bins, here assumed to be uniform, hence implying a constant density. Based on this discretisation, the total amount of particles within a bin j is defined as $F_1 = \int_{r_{\text{nuc}}}^{rb_1} F(r,t)dr$ and $F_j = \int_{rb_{j-1}}^{rb_j} F(r,t)dr$ for $j = 2, 3, ..., n$. The following transformation can be applied to the original PBE (Eq. (3.26)):

$$\int_{rb_{j-1}}^{rb_j} \frac{\partial}{\partial t} F(r,t)dr + \int_{rb_{j-1}}^{rb_j} \frac{\partial}{\partial r}\left(F(r,t)\frac{dr}{dt}\right)dr = \int_{rb_{j-1}}^{rb_j} \Re_{\text{nuc}}\delta(r - r_{\text{nuc}})dr + \int_{rb_{j-1}}^{rb_j} \Re_{\text{coag}}dr \tag{3.64}$$

$$\frac{d}{dt}F_j + \left(F_j\frac{dr}{dt}\right)|_{rb_j} - \left(F_{j-1}\frac{dr}{dt}\right)|_{rb_{j-1}} = \delta_{j=1}\Re_{\text{nuc}}(t) + \int_{rb_{j-1}}^{rb_j} \Re_{\text{coag}}dr \tag{3.65}$$

The entire set of system equations (including MWD equations) is solved within a hierarchical solution scheme as shown in Figure 3.2. The decomposition algorithm involves the first tier of calculation of the individual rates of nucleation, growth and coagulation, whilst holding the PSD constant. In order to calculate these rates, the concentrations of the various system components are needed as well as the number of radicals per particle and the particle density. The mass balances over the system components and partitioning equations are evaluated as follows:

- Monomer mass balances: *ODEs*: 5° predictor-corrector technique
- Monomer partitioning: *non-linear algebraic system*: Newton-Raphson technique
- Surfactant partitioning: *Quadratic equation*
- CTA mass balance: *ODE*: 5° predictor-corrector technique
- CTA partitioning: *algebraic equation*
- Initiator mass balance: *ODE*: 5° predictor-corrector technique

- Aqueous phase radical balances: (*steady state assumed*) *non-linear algebraic system*: modified Powell hybrid method (based on Newton & scaled gradient method)

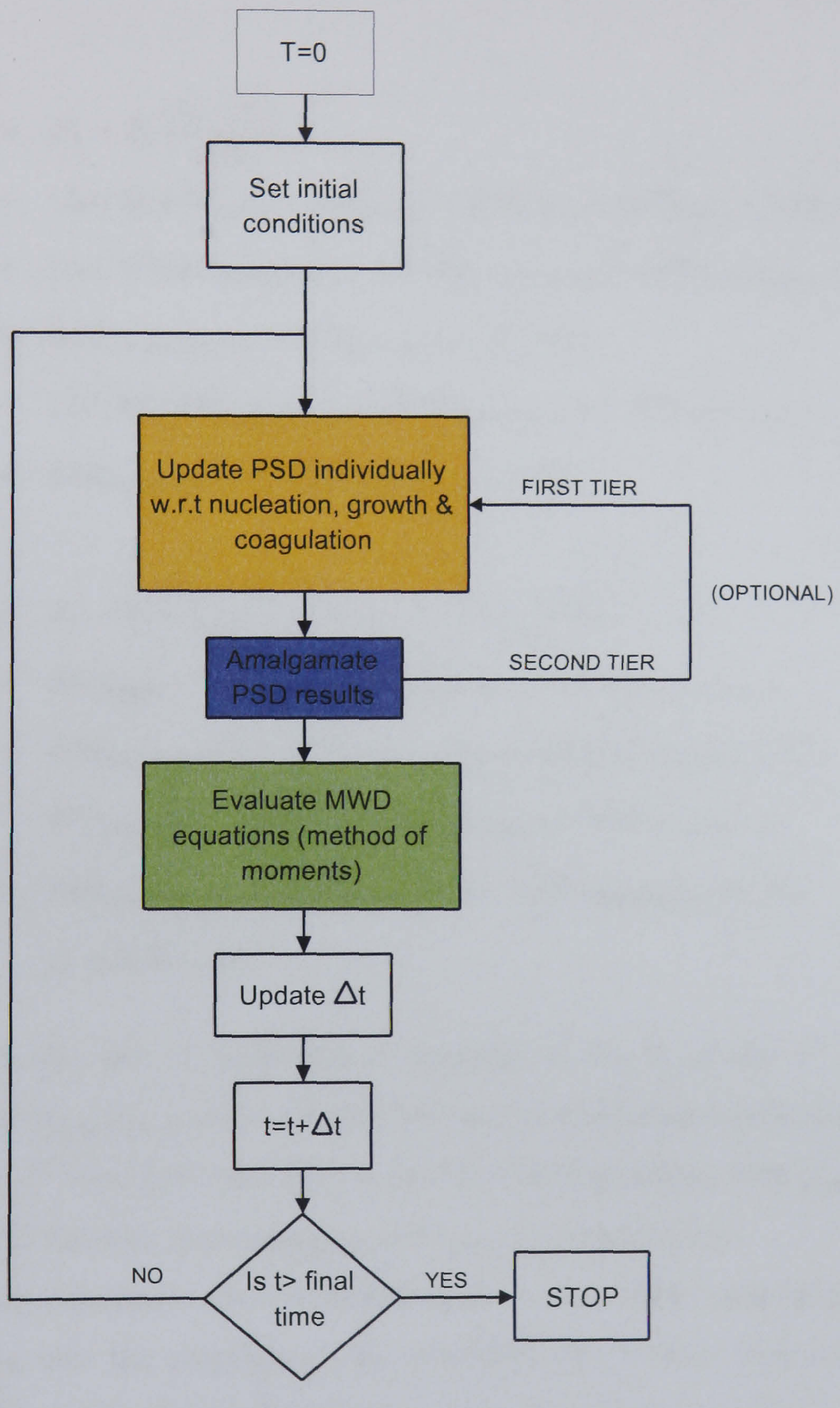


Figure 3.2: Hierarchical 2-tier algorithm for PSD/MWD model solution

For solution of the time varying system dynamics, a time step Δt is defined, and divided into 4 intervals, as shown in Figure 3.1(b). The solution of the ODEs (as above) is performed at stages corresponding to each time sub-step, providing values for the rates

of nucleation, growth and coagulation at each sub-step. This is done prior to the PSD update stage. The next sequential stage [see second-tier in Figure 3.2] involves the update of the PSD, based on the rates previously calculated, according to the following update scheme:

$$\begin{aligned}
F_{\text{new},1} &= F_1 - F_1\frac{rb_1 - ri_1}{\Delta R_1} \\
&+ (\Delta t/4)(14\Re_{\text{nuc},1} + 64\Re_{\text{nuc},2} + 24\Re_{\text{nuc},3} + 64\Re_{\text{nuc},4} + 14\Re_{\text{nuc},5})(1/45) \\
&+ (\Delta t/4)(14\Re_{\text{formation},1,1} + 64\Re_{\text{formation},1,2} + 24\Re_{\text{formation},1,3} \\
&+ 64\Re_{\text{formation},1,4} + 14\Re_{\text{formation},1,5})(1/45) \\
&- (\Delta t/4)(14\Re_{\text{depletion},1,1} + 64\Re_{\text{depletion},1,2} + 24\Re_{\text{depletion},1,3} \\
&+ 64\Re_{\text{depletion},1,4} + 14\Re_{\text{depletion},1,5})(1/45) \qquad (3.66)
\end{aligned}$$

$$\begin{aligned}
F_{\text{new},j} &= F_j - F_j\frac{rb_j - ri_j}{\Delta R_j} + F_(j-1)\frac{rb_{j-1} - ri_{j-1}}{\Delta R_{j-1}} \\
&+ H(j_{\text{upper}} - j)(\Delta t/4)(14\Re_{\text{formation},j,1} + 64\Re_{\text{formation},j,2} \\
&+ 24\Re_{\text{formation},j,3} + 64\Re_{\text{formation},j,4} + 14\Re_{\text{formation},j,5})(1/45) \\
&- H(j_{\text{cut-off}} - j)(\Delta t/4)(14\Re_{\text{depletion},j,1} + 64\Re_{\text{depletion},j,2} \\
&+ 24\Re_{\text{depletion},j,3} + 64\Re_{\text{depletion},j,4} + 14\Re_{\text{depletion},j,5})(1/45) \\
&(j = 2, 3, ..., n) \qquad (3.67)
\end{aligned}$$

where $\Re_{\text{nuc},i}$ is the rate of nucleation of particles in bin 1, at the ith time sub-step, $\Re_{\text{formation},j,i}$ and $\Re_{\text{depletion},j,i}$ are the respective rates of formation and depletion of particles in bin j at the ith time sub-step, $H(.)$ is the Heaviside function, with j_{upper} and $j_{\text{cut-off}}$ corresponding to the bins housing r_{upper} and $r_{\text{cut-off}}$, respectively.

The term ri_j represents the cut-off size within a bin, with particles larger than this value relocating into the neighboring bin (to RHS) at the next time step. This term enables the PSD update due to the continuous growth of particles, through evaluation of the fraction of particles in a bin that will grow into the adjacent bin, at each time step. The particular value of ri_j is determined by the growth rate values over the time sub-steps.

Following the update of the PSD, the MWD equations are evaluated (explained later). Δt is then updated based on the propagation of error in evaluation of component dynamics.

Also incorporated into this model solution is the algorithmic development made by Sun et al.[72] Here, a multi-level discretisation is applied to the particle size domain, based on an appreciation of the sensitivities of the individual rate-processes of nucleation, growth and coagulation to finite element width. Nucleation and growth are modelled based on a finer discretisation of the particle size domain, while coagulation is modelled based on a coarser discretisation. The results are then amalgamated to obtain the PSD. More details on these algorithms can be found in the original references.[71,72] These algorithms are incorporated into a standard FORTRAN code that is adopted for the present study.

3.3 MWD Model Structure

The MWD model formulation developed here uses a similar pseudohomopolymer approximation to that used by Saldivar et al.[77] in order to simplify the copolymer system. Saldivar et al.[77] developed population balances for MWD based on the density of live and dead polymer chains of different length that exist in a particle housing a certain number of radicals ($N_n^l(r,t)$ and $D_n^l(r,t)$). In the present work, a single particle is focussed on for the derivation of the population balance for live and dead chains, allowing the index describing the particle state to be dropped.

A kinetic scheme consistent with that developed for the PSD case is applied here. Population balances are formulated for the live and dead polymer population chain length distributions as follows.[77,152] The main assumptions that have been made in the MWD model include a one-way coupling with the PSD model, insensitivity of the MWD to the coagulation phenomenon[152] and the general validity of pseudo-bulk conditions.

The live polymer population, $N^l(r,t)$ is defined as the concentration of radicals (in ℓ^{-1}) of length l in a particle of size r at time t, given by Eqs. (3.68), (3.69) and (3.70):

$$\begin{aligned}\frac{\partial}{\partial t}N^0(r,t) &= \sum_{i=1}^{2} e_i^0 p_{\mathrm{w}i}[P_{\mathrm{w}}^0]/V_{\mathrm{p}}N_{\mathrm{A}} - \bar{k}_{\mathrm{p}}N^0 + \bar{k}_{\mathrm{tr}}(\bar{n}-N^0) + \bar{k}_{\mathrm{trA}}(\bar{n}-N^0) \\ &- \bar{k}_{\mathrm{t}}\bar{n}N^0 - \sum_{j=1}^{2} k_{\mathrm{dM}j}p_j N^0 \end{aligned} \tag{3.68}$$

$$\frac{\partial}{\partial t}N^l(r,t) = \sum_{i=1}^{2} e_i^l p_{\mathrm{w}i}[P_{\mathrm{w}}^l]/V_{\mathrm{p}}N_{\mathrm{A}} + \bar{k}_{\mathrm{p}}(N^{l-1} - N^l) - \bar{k}_{\mathrm{tr}}N^l - \bar{k}_{\mathrm{trA}}N^l - \bar{k}_t\bar{n}N^l \quad (1 \leq l < j_{\mathrm{cr}}) \tag{3.69}$$

$$\frac{\partial}{\partial t}N^l(r,t) = \bar{k}_{\mathrm{p}}(N^{l-1} - N^l) - \bar{k}_{\mathrm{tr}}N^l - \bar{k}_{\mathrm{trA}}N^l - \bar{k}_t\bar{n}N^l \quad (j_{\mathrm{cr}} \leq l < \infty)) \tag{3.70}$$

The first term on the right of Eq. (3.68) accounts for the entry of an oligomer of length 0 (monomeric radical derived from chain transfer to monomer) from the aqueous phase into particle of size r. The second term accounts for loss of monomeric radicals from a particle of size r when a monomeric radical propagates with a monomer unit to form a radical of length 1. The third and fourth terms account for the chain transfer reactions to both monomer and to chain transfer agent (CTA) in a particle of size r. The term '$-N^0$' accounts for the net cancellation of the effect of chain transfer to a monomeric radical on the number of monomeric radicals. The fifth term on the right of Eq. (3.68) accounts for termination reactions, whereby a monomeric radical can terminate with any length radical in a particle of size r (negative contribution to N^0 balance). The final term accounts for desorption of monomeric radicals from a particle of size r. j_{cr} is the critical chain length of aqueous phase oligomers, representing the aqueous phase solubility limit, beyond which homogenous nucleation occurs. Thus, no radicals with chain length beyond $j_{\mathrm{cr}} - 1$ are found in the aqueous phase, accounting for the absence of the entry term in Eq. (3.70). The notation e_i^l is the rate of entry into a particle of a radical of type i and length l, $[P_{\mathrm{w}}^l]$ is the concentration of oligomers of length l in the aqueous phase, N_{A} is the Avogadro number, $[A_{\mathrm{p}}]$ is the concentration of CTA in the particle phase, $[M_{\mathrm{p}}]$ is the concentration of monomer in the particle phase, p_i is the pseudo-homopolymer probability of finding a radical with an end unit of type i in the particle phase, $p_{\mathrm{w}i}$ is the pseudo-homopolymer probability of finding a radical with an end unit of type i in the aqueous phase and $k_{\mathrm{dM}j}$ is the desorption rate constant for a monomeric radical of type j.

The dead chain population is defined as the concentration (in mol$\cdot\ell^{-1}$) of polymer

chains of length l in a particle of size r at time t, given in Eq. (3.71):

$$\begin{aligned}\frac{\partial}{\partial t}D^l(r,t) &= \bar{k}_{\mathrm{tr}}N^l + \bar{k}_{\mathrm{trA}}N^l + \bar{k}_{\mathrm{td}}\bar{n}N^l \\ &+ \sum_{i=1}^{2}\sum_{j=1}^{2}\frac{\bar{k}_{tc}}{2}\sum_{m=0}^{l}N^m N^{l-m}\end{aligned} \tag{3.71}$$

In Eq. (3.71) the first two terms account for chain transfer to monomer and CTA respectively, and the last two terms account for termination reactions by disproportionation and combination respectively.

3.4 Method of Moments for MWD

It should be theoretically possible to directly solve for the full distribution for live and dead chain population balances using an extension of a technique developed by Crowley and Choi,[153] wherein discrete chain length intervals are used to simplify calculations. However in this case, a solution is pursued which evaluates the average molecular weight over a discretised particle size domain, through evaluation of the leading moments of the chain balances for each particle size class. The aforementioned solution strategy takes into account the fact the solution of the combined PSD and MWD model is highly computation-intensive, and serves as a good starting point to validate the model. Thus, the kth moment of the live and dead chains inside particles of size r is defined, respectively, by Eqs. (3.72) and (3.73):

$$\lambda_{\mathrm{N}k}(r,t) = \sum_{l=0}^{\infty} l^k (N_{\mathrm{p}}^l(r,t)) \tag{3.72}$$

$$\lambda_{Dk}(r,t) = \sum_{l=0}^{\infty} l^k (D_{\mathrm{p}}^l(r,t)) \tag{3.73}$$

The zeroth moment of the live radical population is linearly related to the average number of radicals/particle, $\bar{n}$. Thus, the zeroth moment in a particle of size r at time t is defined as in Eq. (3.74):

$$\lambda_{N0}(r,t) = \bar{n}(r,t)/V_{\mathrm{p}}N_{\mathrm{A}} \tag{3.74}$$

Here V_{p} is the volume of a particle of size r defined as $\frac{4}{3}\pi r^3$. The first live moment of the live radical balance $\lambda_{N1}(r,t)$ is derived as follows: The first moment of the live radical balance is derived as follows. Summing the contributions from individual equations for live radicals:

$$\begin{aligned}\frac{\partial}{\partial t}\lambda_{N1}(r,t) &= \frac{\partial}{\partial t}\sum_{l=0}^{\infty} lN^l(r,t) \\ &= \frac{\partial}{\partial t}lN^0(r,t) + \frac{\partial}{\partial t}\sum_{l=1}^{j_{\mathrm{cr}}-1} lN^l(r,t) + \frac{\partial}{\partial t}\sum_{l=j_{\mathrm{cr}}}^{\infty} lN^l(r,t) \qquad (3.75)\end{aligned}$$

Considering the contributions from individual rates to Eq. (3.75),

$$\frac{\partial}{\partial t}\lambda_{N1} = \tilde{\Re}_{\mathrm{entry}} + \tilde{\Re}_{\mathrm{prop}} + \tilde{\Re}_{\mathrm{tr}} + \tilde{\Re}_{\mathrm{trA}} + \tilde{\Re}_{\mathrm{termin}} + \tilde{\Re}_{\mathrm{des}} \qquad (3.76)$$

where $\tilde{\Re}_{entry}$ is the rate contribution from particle entry events, $\tilde{\Re}_{prop}$ is the rate contribution from propagation, $\tilde{\Re}_{tr}$ is the rate contribution from chain transfer to monomer, $\tilde{\Re}_{trA}$ is the rate contribution from chain transfer to CTA, $\tilde{\Re}_{termin}$ is the rate contribution from termination within a particle and $\tilde{\Re}_{des}$ is the rate contribution from desorption from a particle. These rate term are derived as follows:

$$\tilde{\Re}_{entry} = \sum_{l=1}^{j_{\mathrm{cr}}-1}\sum_{i=1}^{2} le_i^l p_{\mathrm{w}i}[P_{\mathrm{w}}^l]/V_{\mathrm{p}}N_{\mathrm{A}} \qquad (3.77)$$

$$\begin{aligned}\tilde{\Re}_{prop} &= \bar{k}_{\mathrm{p}}N^0 l + \sum_{l=1}^{\infty} l\bar{k}_{\mathrm{p}}(N^{l-1} - N^l) \\ &= \bar{k}_{\mathrm{p}}\left[\sum_{l=1}^{\infty} l(N^{l-1}) - \sum_{l=1}^{\infty} lN^l\right] \\ &= \bar{k}_{\mathrm{p}}[(N^0 + 2N^1 + 3N^2\ldots) - (N^1 + 2N^2\ldots)] \\ &= \bar{k}_{\mathrm{p}}[(N^0 + N^1 + N^2\ldots)] \\ &= \bar{k}_{\mathrm{p}}\lambda_{n0} \qquad (3.78)\end{aligned}$$

$$\begin{aligned}\tilde{\Re}_{ct} &= \bar{k}_{\mathrm{tr}}(\lambda_{N0}-N^0)l-\sum_{l=1}^{\infty}\bar{k}_{\mathrm{tr}}N^l l\\ &= -\bar{k}_{\mathrm{tr}}\left[0N^0+\sum_{l=1}^{\infty}lN^l\right]\\ &= -\bar{k}_{\mathrm{tr}}[0N^0+1N^1+2N^2...]\\ &= -\bar{k}_{\mathrm{tr}}\lambda_{N1}\end{aligned} \tag{3.79}$$

$$\begin{aligned}\tilde{\Re}_{\mathrm{trA}} &= \bar{k}_{\mathrm{trA}}(\lambda_{N0}-N^0)l-\sum_{l=1}^{\infty}\bar{k}_{\mathrm{trA}}N^l l\\ &= -\bar{k}_{\mathrm{trA}}\left[0N^0+\sum_{l=1}^{\infty}lN^l\right]\\ &= -\bar{k}_{\mathrm{trA}}\left[0N^0+1N^1+2N^2...\right]\\ &= -\bar{k}_{\mathrm{trA}}\lambda_{N1}\end{aligned} \tag{3.80}$$

$$\begin{aligned}\tilde{\Re}_{\mathrm{termin}} &= -\bar{k}_{\mathrm{t}}N^0\lambda_{N0}l-\sum_{l=1}^{\infty}\bar{k}_{t}N^l\lambda_{N0}l\\ &= -\bar{k}_{\mathrm{t}}\lambda_{N0}\left[0N^0+\sum_{l=1}^{\infty}lN^l\right]\\ &= -\bar{k}_{\mathrm{t}}\lambda_{N0}\left[\sum_{l=0}^{\infty}lN^l\right]\\ &= -\bar{k}_{\mathrm{t}}\lambda_{N0}\lambda_{N1}\end{aligned} \tag{3.81}$$

$$\tilde{\Re}_{\mathrm{des}}=\sum_{j=1}^{2}k_{\mathrm{dn}j}p_jN^0l=0 \tag{3.82}$$

Giving the first moment of the live radical balance:

$$\begin{aligned}\frac{\partial}{\partial t}\lambda_{N1}(r,t) &= \sum_{l=1}^{j_{\mathrm{cr}}-1}\sum_{i=1}^{2}le_i^lp_{\mathrm{w}i}\frac{[P_{\mathrm{w}}^l]}{V_{\mathrm{p}}N_{\mathrm{A}}}+\bar{k}_{\mathrm{p}}\lambda_{N0}-\bar{k}_{\mathrm{tr}}\lambda_{N1}\\ &- \bar{k}_{\mathrm{trA}}\lambda_{N1}-\bar{k}_{\mathrm{t}}\lambda_{N0}\lambda_{N1}\end{aligned} \tag{3.83}$$

The other moments are derived in a similar fashion as shown in Eqs. (3.84) to (3.87).

Note that the system of moments is closed for these simple kinetics.

$$\begin{aligned}\frac{\partial}{\partial t}\lambda_{N2}(r,t) &= \sum_{l=1}^{j_{\mathrm{cr}}-1}\sum_{i=1}^{2} l^2 e_i^l p_{\mathrm{w}i}\frac{[P_{\mathrm{w}}^l]}{V_{\mathrm{p}}N_{\mathrm{A}}} + \bar{k}_p(2\lambda_{N1}+\lambda_{N0}) - \bar{k}_{\mathrm{tr}}\lambda_{N2} \\ &- \bar{k}_{\mathrm{trA}}\lambda_{N2} - \bar{k}_{\mathrm{t}}\lambda_{N0}\lambda_{N2} \end{aligned} \tag{3.84}$$

$$\frac{\partial}{\partial t}\lambda_{D0}(r,t) = \bar{k}_{\mathrm{tr}}\lambda_{N0} + \bar{k}_{\mathrm{trA}}\lambda_{N0} + (\bar{k}_{\mathrm{tc}}/2 + \bar{k}_{\mathrm{td}})\lambda_{N0}^2 \tag{3.85}$$

$$\frac{\partial}{\partial t}\lambda_{D1}(r,t) = \bar{k}_{\mathrm{tr}}\lambda_{N1} + \bar{k}_{\mathrm{trA}}\lambda_{N1} + \bar{k}_{\mathrm{t}}\lambda_{N0}\lambda_{N1} \tag{3.86}$$

$$\frac{\partial}{\partial t}\lambda_{D2}(r,t) = \bar{k}_{\mathrm{tr}}\lambda_{N2} + \bar{k}_{\mathrm{trA}}\lambda_{N2} + \bar{k}_{\mathrm{t}}\lambda_{N0}\lambda_{N2} + \bar{k}_{\mathrm{tc}}\lambda_{N1}^2 \tag{3.87}$$

The number-average chain length (NACL) and the weight-average chain length (WACL) are defined in Eqs. (3.88) and (3.89), respectively:

$$\mathrm{NACL}(r,t) = \frac{\lambda_{D1}(r,t)}{\lambda_{D0}(r,t)} \tag{3.88}$$

$$\mathrm{WACL}(r,t) = \frac{\lambda_{D2}(r,t)}{\lambda_{D1}(r,t)} \tag{3.89}$$

As a further step, since a copolymer system is being modelled, a measure of the copolymer composition is necessary to determine the average molecular weight. The instantaneous copolymer composition corresponding to type i monomer units (I_i) is given by Eq. (3.90) and Eq. (3.91):[152,154]

$$I_1 = \frac{f_1(\vartheta_1 f_1 + f_2)}{f_1(\vartheta_1 f_1 + f_2) + f_2(\vartheta_2 f_2 + f_1)} \tag{3.90}$$

$$I_2 = 1 - I_1 \tag{3.91}$$

where ϑ_i is the reactivity ratio of monomers and f_i is the mole fraction of monomer i in the particle phase.

The number-average molecular weight (NAMW) in each particle size class is given in

Eq. (3.92):

$$\mathrm{NAMW}(r,t) = (I_1\mathrm{MW}_1 + I_2\mathrm{MW}_2)\mathrm{NACL}(r,t) \tag{3.92}$$

Similarly, the weight-average molecular weight is given by Eq. (3.93):

$$\mathrm{WAMW}(r,t) = (I_1\mathrm{MW}_1 + I_2\mathrm{MW}_2)\mathrm{WACL}(r,t) \tag{3.93}$$

The global number-average molecular weight, (N_{glob}) and the global weight-average molecular weight, (W_{glob}) for the entire system, are defined in Eqs. (3.94) and (3.95), respectively:

$$N_{\mathrm{glob}}(r,t) = \frac{\int_{r_{\mathrm{nuc}}}^{r_{\mathrm{max}}} \mathrm{NAMW}(r,t)\lambda_{D0}(r,t)F(r,t)dr}{\int_{r_{\mathrm{min}}}^{r_{\mathrm{max}}} \lambda_{D0}F(r,t)dr} \tag{3.94}$$

$$W_{\mathrm{glob}}(r,t) = \frac{\int_{r_{\mathrm{nuc}}}^{r_{\mathrm{max}}} \mathrm{WAMW}(r,t)\lambda_{D1}(r,t)F(r,t)dr}{\int_{r_{\mathrm{min}}}^{r_{\mathrm{max}}} \lambda_{D1}F(r,t)dr} \tag{3.95}$$

In order to solve the partial differential equations representing the live and dead moments given in this section, a discretisation grid is chosen similar to the one used in the PSD model solution. The grid equally divides the entire particle size domain into discrete bins. Within each bin a representative particle size is chosen (mid-point). The MWD model is formulated focussing on a single particle and so, using the representative particle size, a separate set of moments can be derived for each bin (250 bins, from 2 nm– 500 nm radius particles). This results in a system of ordinary differential equations, which are solved in combination with the PSD model within the hierarchical two-tier algorithm [See Figure 3.2 in Section 3.2]. The differential equations that describe the evolution of the MWD moments are solved using the same time steps as defined by the PSD model; it is found sufficient that only the error in solving the component material balance ODEs be used to manipulate Δt, rather than using a measure of the error from the solution of the MWD moment ODEs. At each time step, the PSD model is solved first and then the MWD moment equations –that depend on the PSD– are integrated. The ODEs describing the moments of live chains involve fast kinetics, therefore a pseudo-steady state is applied to these equations (consistent with the calculation of $\bar{n}$). Therefore the effect of

particle growth is unimportant in solving the live radical moments. A first order predictor-corrector technique is used for the evaluation of the ODEs describing the moments of dead chains. Neglecting particle growth effects could lead to widely different model predictions for the dead chain moments, as will be shown later. This makes it important to account for growth in solving the dead chain moment balances. This is done by setting the initial condition of the dead chain moments at the start of a discrete time step in a particular bin equal to the value at the end of the previous time step in a preceding bin as determined by the growth rates. This will require the initial condition of the dead chain moments in the first bin to be set to zero. The method is again a sequential decomposition algorithm that builds the population-level behavior by examining individual particle behavior.

3.5 Semi-batch Emulsion Polymerisation Simulation: PSD Results

A semi-batch copolymerisation of vinyl acetate (VAc) and butyl acrylate (BuA) was simulated with input trajectories as shown in Figure 3.3. The initiator is potassium persulphate, surfactant is sodium dodecyl sulphate (SDS) and the CTA is dodecyl mercaptan. VAc, BuA and CTA are fed at constant flow rates of 6×10^{-4} and 3×10^{-4} and 1×10^{-4} mol·s^{-1}, respectively. The initiator and surfactant are fed in as aqueous solutions of concentrations 1% and 5% respectively, while CTA is simulated as 1 % on total monomer. Figures 3.4- 3.6 present the PSD simulation results. The nominal parameter values used in this analysis are shown in Table 3.1 and 3.2.

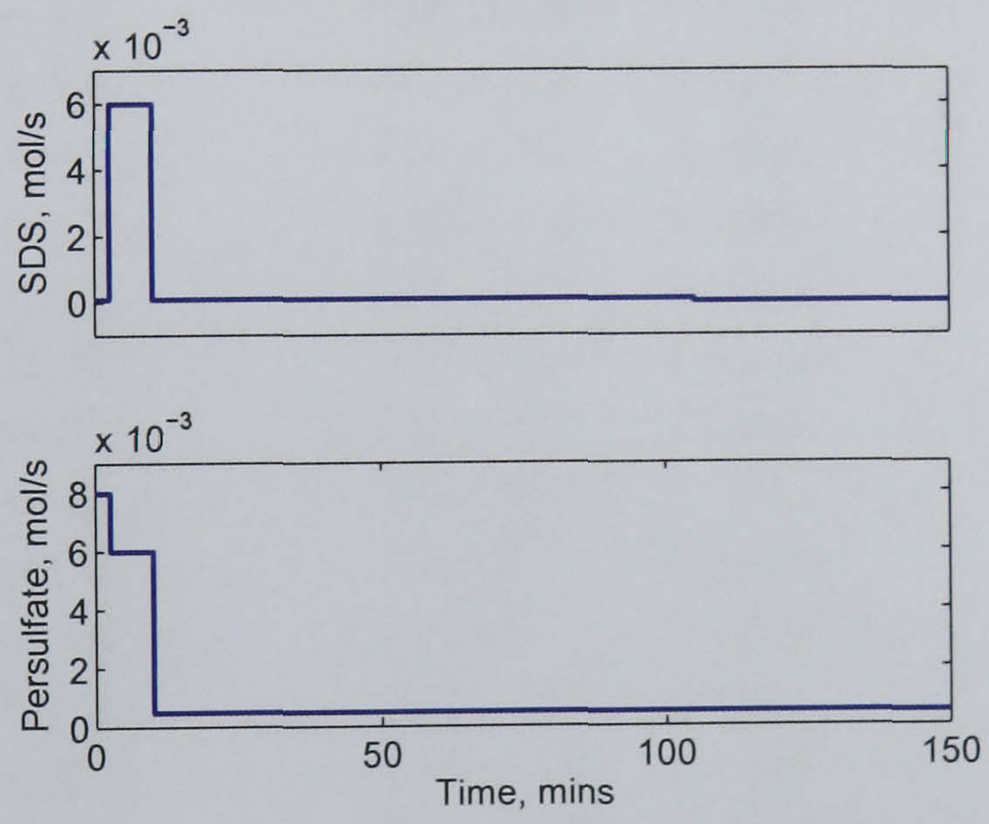


Figure 3.3: Simulation base-case input flow rates

Table 3.1: Nominal values for kinetic parameters used in model.

Kinetic Parameter	Value	Units	Ref.
$k_{p11} = k^{w}_{p11}$	3.29×10^{3}	$\ell \cdot mol^{-1} \cdot s^{-1}$	[69]
$k_{p12} = k^{w}_{p12}$	8.9×10^{4}	$\ell \cdot mol^{-1} \cdot s^{-1}$	[69]
$k_{p21} = k^{w}_{p21}$	3.9×10^{1}	$\ell \cdot mol^{-1} \cdot s^{-1}$	[69]
$k_{p22} = k^{w}_{p22}$	2.47×10^{2}	$\ell \cdot mol^{-1} \cdot s^{-1}$	[69]
$k_{tr11} = k^{w}_{tr11}$	9.3×10^{-3}	$\ell \cdot mol^{-1} \cdot s^{-1}$	[69]
$k_{tr12} = k^{w}_{tr12}$	9.3×10^{-3}	$\ell \cdot mol^{-1} \cdot s^{-1}$	[69]
$k_{tr21} = k^{w}_{tr21}$	5.3×10^{-4}	$\ell \cdot mol^{-1} \cdot s^{-1}$	[69]
$k_{tr22} = k^{w}_{tr22}$	9.3×10^{-3}	$\ell \cdot mol^{-1} \cdot s^{-1}$	[69]
$k_{trA1} = k^{w}_{trA1}$	1×10^{0}	$\ell \cdot mol^{-1} \cdot s^{-1}$	
$k_{trA2} = k^{w}_{trA2}$	1×10^{0}	$\ell \cdot mol^{-1} \cdot s^{-1}$	
$k_{t11} = k^{w}_{t11}$	1.05×10^{7}	$\ell \cdot mol^{-1} \cdot s^{-1}$	[69]
$k_{t12} = k^{w}_{t12}$	2.36×10^{5}	$\ell \cdot mol^{-1} \cdot s^{-1}$	[69]
$k_{t21} = k^{w}_{t21}$	2.36×10^{5}	$\ell \cdot mol^{-1} \cdot s^{-1}$	[69]
$k_{t22} = k^{w}_{t22}$	1.6×10^{3}	$\ell \cdot mol^{-1} \cdot s^{-1}$	[69]
k_{r1}	1	$\ell \cdot mol^{-1} \cdot s^{-1}$	
k_{r2}	1	$\ell \cdot mol^{-1} \cdot s^{-1}$	
k_{d}	7.2×10^{-7}	s^{-1}	[108]

Table 3.2: Nominal values for physical constants used in model.

Physical Constant	Nominal value	Units	Ref.
$K_{\mathrm{p}}^{\mathrm{A}}$	15		[69]
$K_{\mathrm{d}}^{\mathrm{A}}$	0		[69]
K_{p1}	32		[69]
K_{p2}	460		[69]
K_{d1}	46		[69]
K_{d2}	2140		[108]
K_{ad}	2100	$\ell \cdot \mathrm{mol}^{-1}$	[108]
K_{s}	0		
$K_{\mathrm{s}}^{\mathrm{d}}$	0		
cmc	3×10^{-3}	$\mathrm{mol} \cdot \ell^{-1}$	[108]
Γ_{∞}	3.95×10^{-6}	mol^2	[108]
α_{ms}	42×10^{-20}	m^2	[108]
D_{w1}	30 (n=2)	$\mathrm{cm} \cdot s^{-1}$	[69]
D_{w2}	55 (n=2)	$\mathrm{cm} \cdot s^{-1}$	[69]
$r_{\mathrm{nuc}} = r_{\mathrm{micelle}}$	5	nm	[69]
$r_{\mathrm{nuc}} = r_{\mathrm{micelle}}$	5	nm	[69]
ρ_{p}	1120	$\mathrm{g} \cdot \ell^{-1}$	[69]
j_{cr}	5	monomer units	[69]
ρ_{M1}	934	$\mathrm{g} \cdot \ell^{-1}$	
ρ_{M2}	894	$\mathrm{g} \cdot \ell^{-1}$	
MW_1	86.09	$\mathrm{g} \cdot \mathrm{mol}^{-1}$	
MW_2	128.17	$\mathrm{g} \cdot \mathrm{mol}^{-1}$	
N_{A}	6.023×10^{23}		
MW_{surf}	288.5	$\mathrm{g} \cdot \mathrm{mol}^{-1}$	
MW_{ini}	238	$\mathrm{g} \cdot \mathrm{mol}^{-1}$	

3.5.1 PSD and Nucleation

A bimodal PSD is generated in this semi-batch operation as shown in Figure 3.4(a). There are no micelles early on in the process ($t < 1s$) as the surfactant concentration is below the critical micelle concentration (cmc) as shown in Figure 3.4(b). Thus, no micellar nucleation takes place before 1 s. The radicals generated in the aqueous phase by decomposition of the initiator react with monomer to produce oligomers. These oligomers propagate until they reach their limit of aqueous phase solubility, j_{cr}. Upon reaching j_{cr}, homogenous nucleation takes place at very early times (see Figure 3.4(c)) and the resultant mode of particles is seen in Figure 3.4(a) (large peak centred around 30 nm). The particles generated by the first homogenous nucleation event are seen clearly in Figure 3.4(d). The

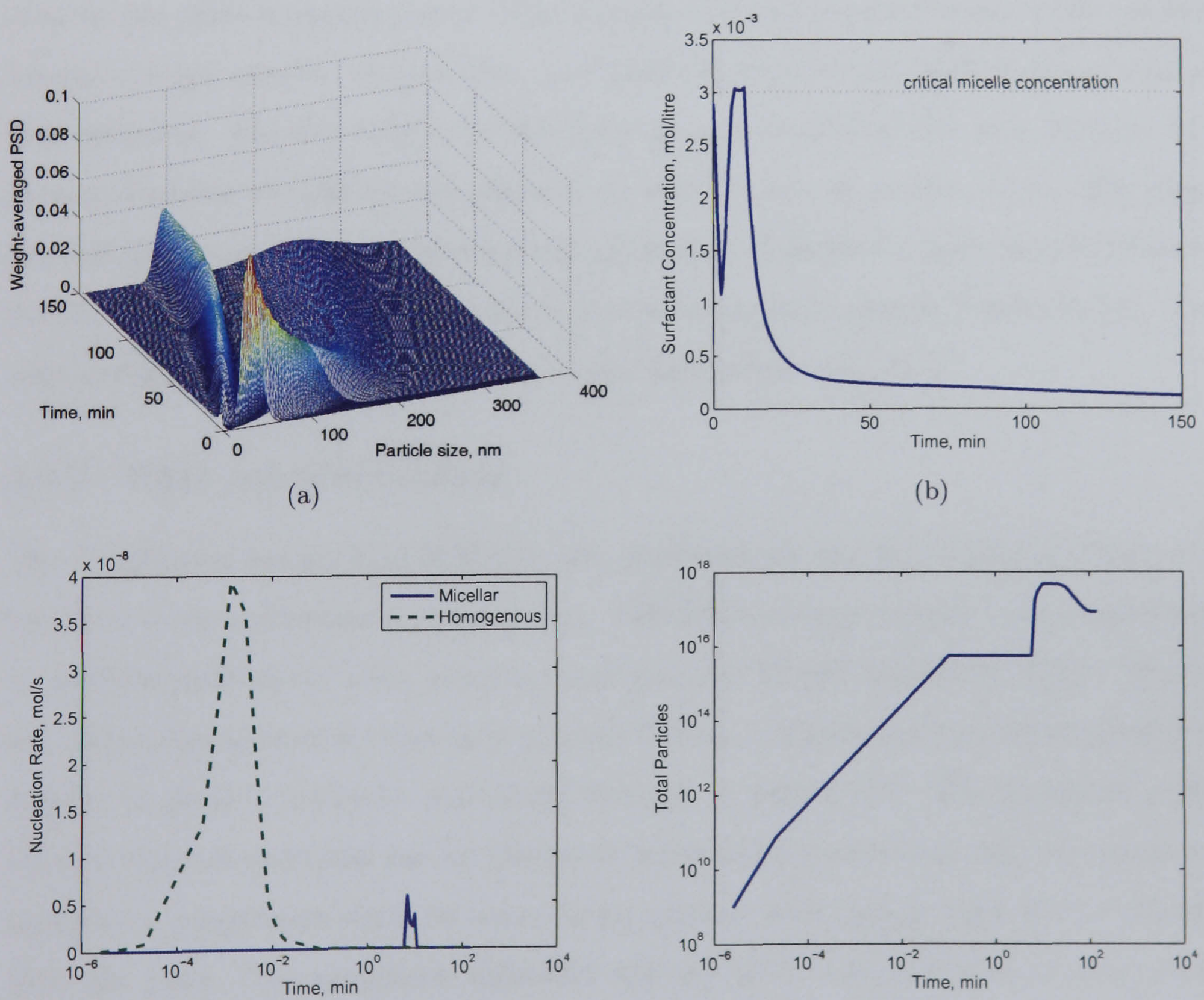


Figure 3.4: PSD evolution and the corresponding trends of surfactant concentration, nucleation rates and particle number.

homogenous nucleation results in a drop in surfactant concentration (see Figure 3.4(b)). which is due to surfactant molecules adsorbing onto the surface of the newly formed particles. The homogenous nucleation dies off due to the entry of the aqueous phase oligomers into the existent particles, rather than achieving the critical chain length.

Due to an increase in the surfactant feed rate as seen in Figure 3.3. the surfactant concentration exceeds the cmc at around 10 minutes (see Figure 3.4(b)). This results in the micellar nucleation seen in Figure 3.4(c) causing the appearance of a bimodal distribution. This results in a fairly steep increase in the number of particles as indicated by Figure 3.4(d), between 10^0 and 10^2 minutes. Following the micellar nucleation of the second mode of particles, the surfactant level drops rapidly as it is absorbed by the newly formed particles. The secondary nucleation of the large number of particles results in a drop in the particle growth rates. This is partly due to the partitioning of the monomers among a large number of particles, and hence a drop in the particle-phase monomer concentration. Another reason for the drop in growth rates is due to a decrease in the average number of radicals per particle, as will be seen in section 3.5.3. The drop in the surfactant concentration that follows the second nucleation results in reduced particle stabilisation, as evident by the drop in the total particles seen in Figure 3.4(d), due to coagulation. This aspect is elaborated in the next sub-section 3.5.2.

3.5.2 PSD and Coagulation

The coagulation kernel is modelled on the principles set out in the DLVO theory and is sensitive to the surfactant concentration. The DLVO theory considers the contributions to particle stability by ionic repulsive and Van der Waals' attractive forces. The total net interaction potential (repulsion potential minus attraction potential) is plotted with respect to particle interface separation distance in Figure 3.5. The maximum positive value of this net potential can be likened to a potential barrier that must be overcome in order for a coagulation event to occur. If no positive value exists, then rapid coagulation will take place. The maximum values for the net interaction potential (Joules) at 0.6 s and 1800 s are indicated in Figure 3.5, by the lines labeled 'a' and 'b', respectively. The particular example shown here deals with the interaction of two particles of minimum size, r_{nuc} (where r_{nuc} is the radius of a nucleated particle). The maximum value of the net

potential is larger at the beginning of the process (t=0.6 s) than compared to its value at 1800 s, meaning that the particles will be less likely to coagulate at the beginning of the process with high surfactant concentration and therefore the coagulation kernel will assume a lower value at the start.

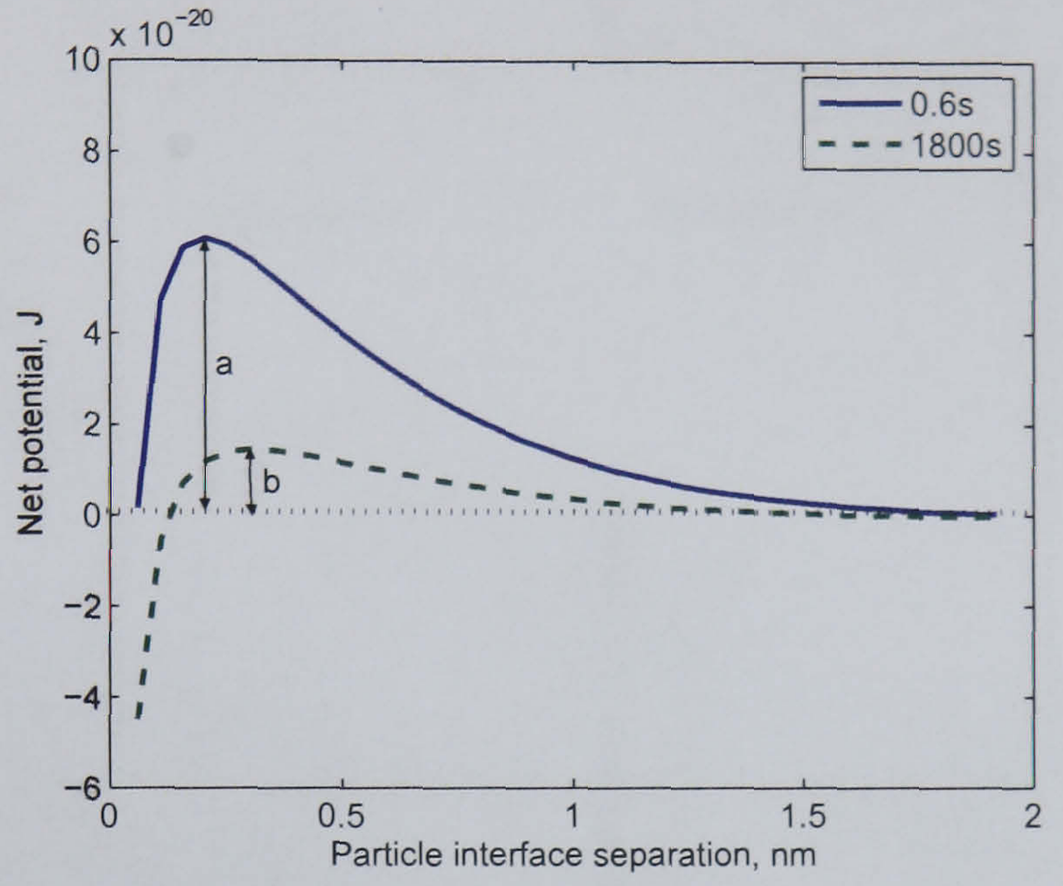
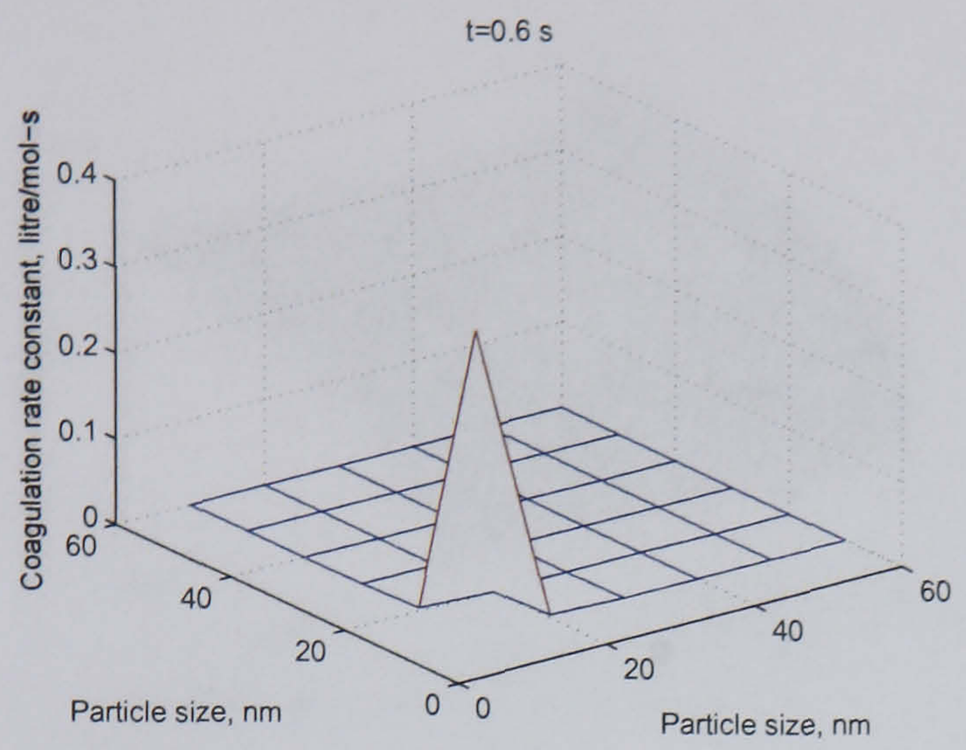
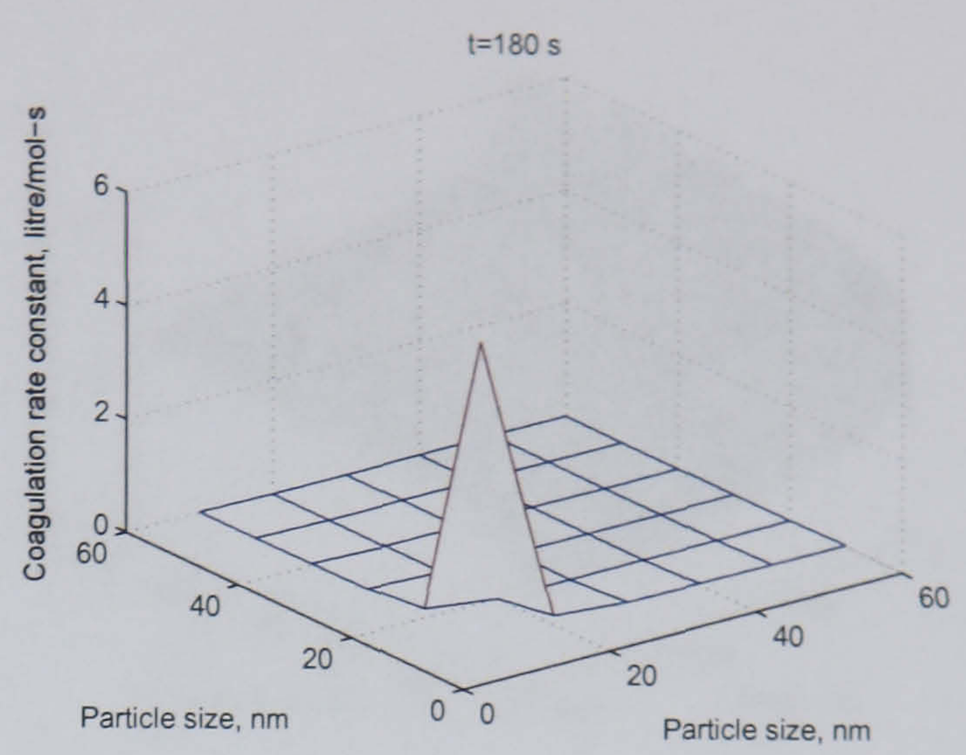


Figure 3.5: Net interaction potential between particles of size r_{nuc} at 0.6 s and 1800 s.

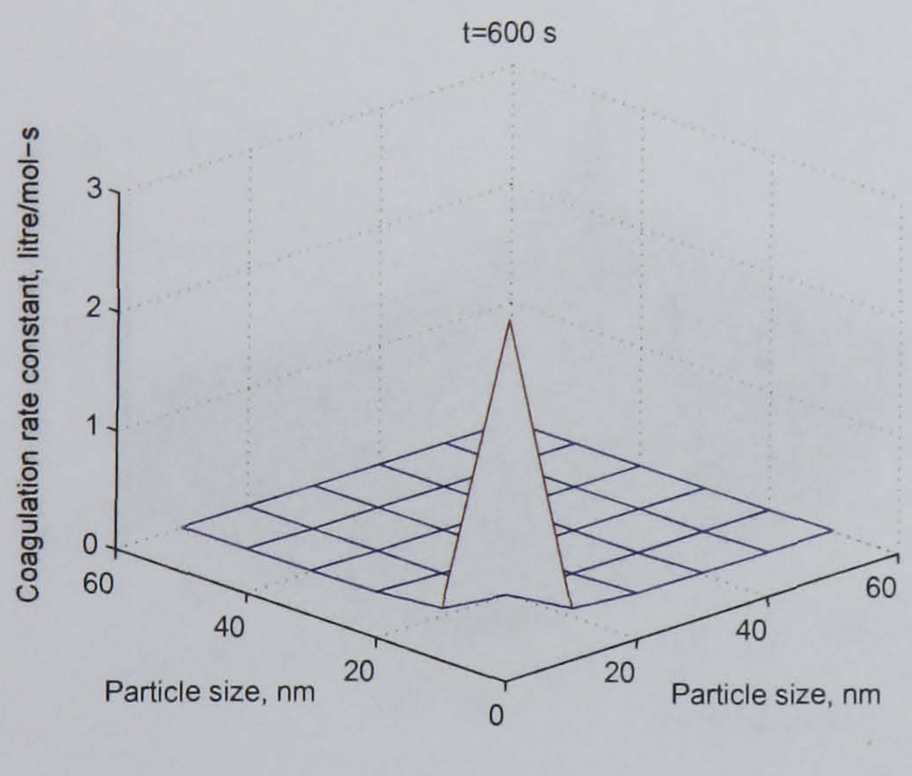
The plots of the size-dependent and time-varying coagulation kernel in Figures 3.6(a)-(d) confirm this drop in stability (increase in coagulation kernel value). Please note that the kernel plots in Figure 3.6 are more compact depictions of the stability traits between particles of different size combinations. The coagulation kernel at an early time, t=0.6 s (but after the initial homogenous nucleation phase), is low, indicating stable particles due to a high concentration of surfactant. The surfactant concentration reaches a minimum at about 180 s as seen in Figure 3.4(b), resulting in the higher coagulation rate constants shown in Figure 3.6(b). After about 200 s the surfactant level begins to rise due to an injected impulse at that time (see inputs in Figure 3.3) and then reaches a plateau at around 400 s. The coagulation rate constants on this plateau (at 600 s, Figure 3.4(b)) are lower as expected (see Figure 3.6(c)). From this point on, the surfactant level decreases steadily and the coagulation constant rises accordingly (see Figure 3.6(d)) due to there being insufficient surfactant to stabilise the particles.



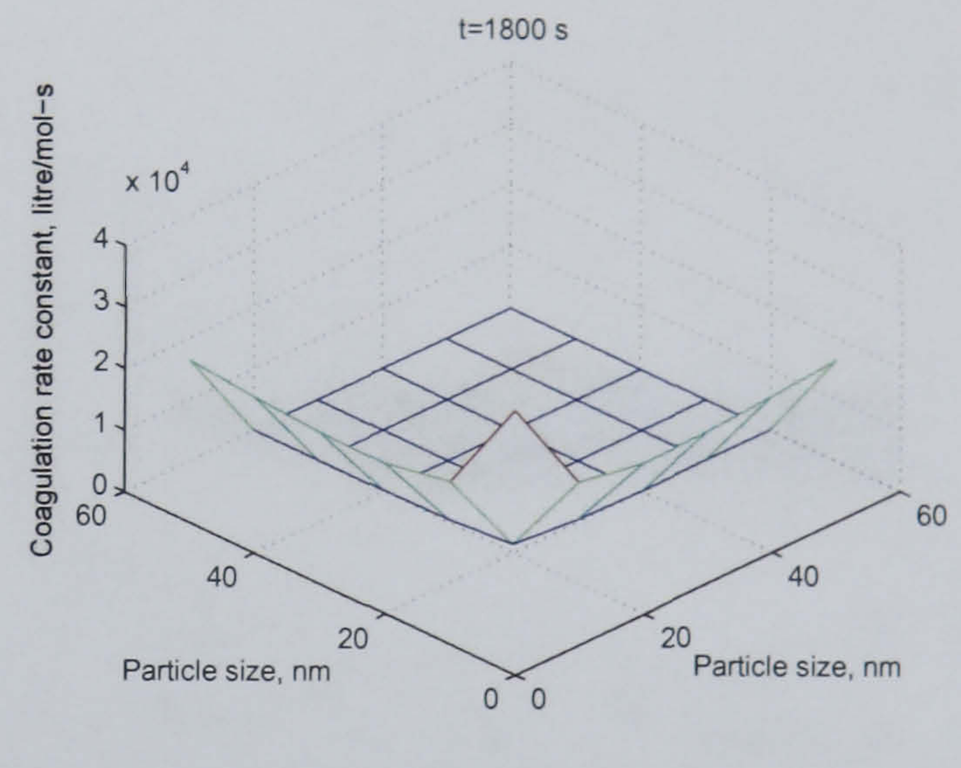
(a)



(b)



(c)

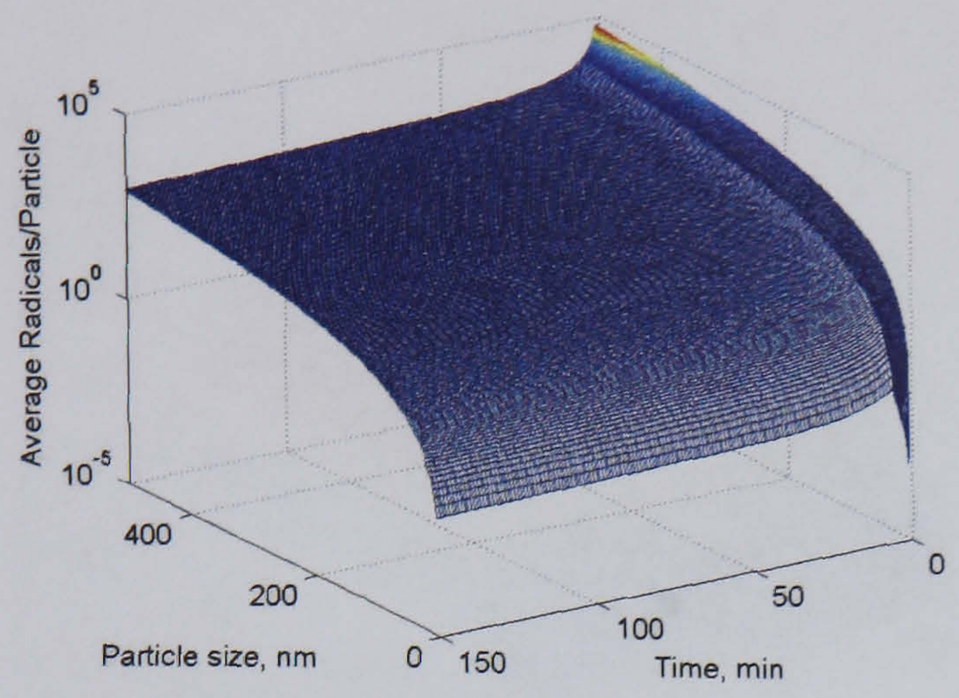


(d)

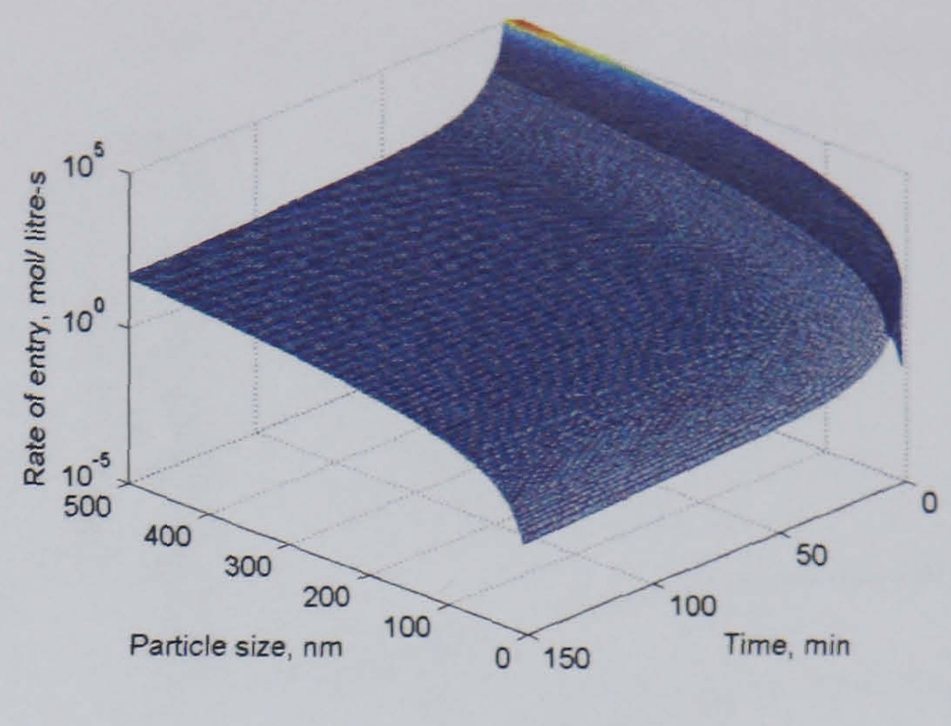
Figure 3.6: Coagulation rate constants corresponding to critical changes in surfactant concentration.

3.5.3 PSD and Average Number of Radicals/Particle

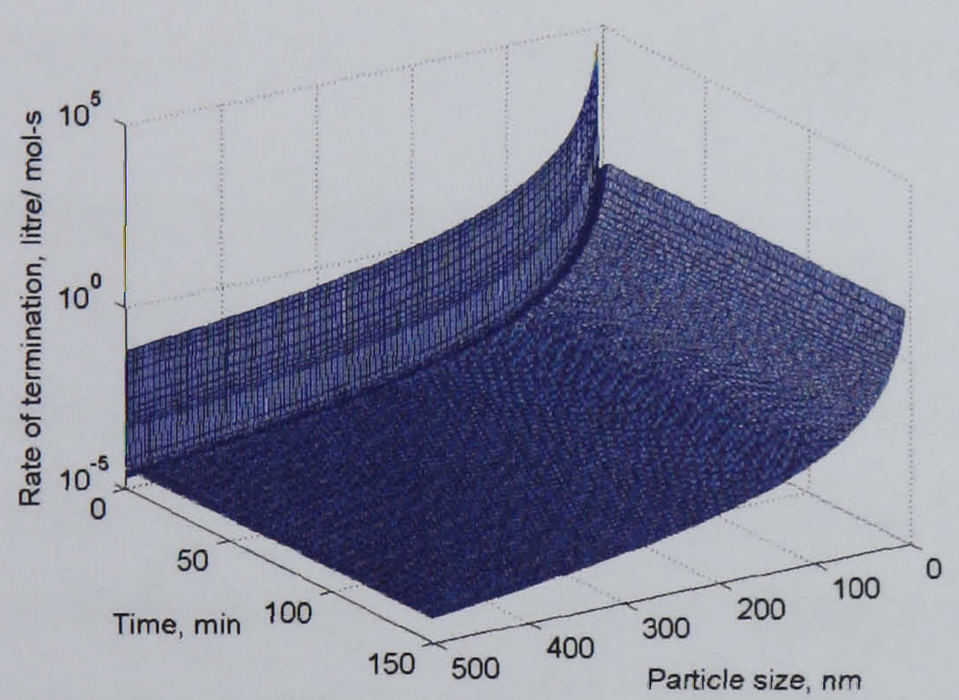
Figure 3.7(a) indicates that the average number of radicals per particle, $\bar{n}(r,t)$, is highly size dependent. It is seen that larger particles attain higher values of $\bar{n}(r,t)$. It is realised that the values shown for $\bar{n}(r,t)$ in the larger sized particles are inconsistent with the practical space limitations that exist in particles. The $\bar{n}(r,t)$ values shown here are based on a simulation using nominal parameter values (requiring further tuning) and as a result are somewhat overestimates. Despite this, the overall general trends exhibited are believed to be true. The reason for this size-dependence can be seen in Figures 3.7(b) and 3.7(c). Figure 3.7(b) shows that larger particles have larger entry rates, attributed to the collision entry model with entry rates proportional to the square of the particle radius.[69] Likewise,



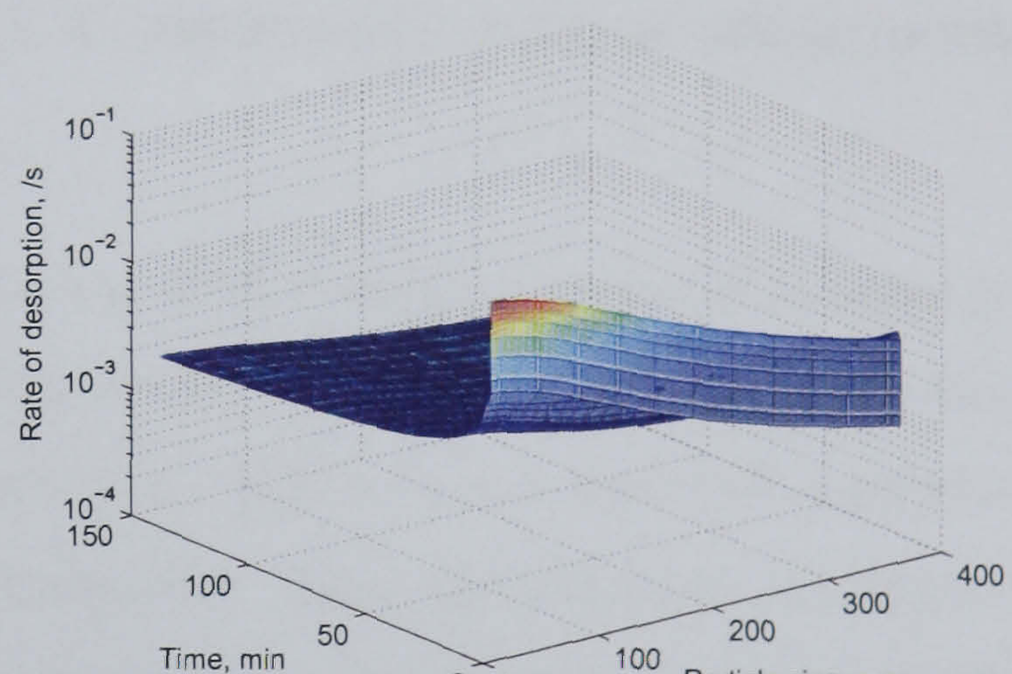
(a)



(b)



(c)



(d)

Figure 3.7: The average number of radicals/particle, the rate of entry, the rate of termination and the rate of desorption.

Figure 3.7(c) shows that the termination rate also exhibits size-dependence, with the termination rate decreasing with increase in particle size. The rate of desorption presented in Figure 3.7(d) indicates a reduced size-dependence compared to the rates of entry and termination. Figure 3.8 shows results to examine the pseudo-bulk vs. zero-one compartmentalisation expected for the system under investigation. Figure 3.8(a) shows that the ratio of entry rate to termination rate remains above unity. Referring to Figure 3.8(b) one notices that the value of the global average number of radicals (see Eq. (3.29)) always assumes a fairly high value and does not drop below 1 except at very early times. One could therefore argue that pseudo-bulk kinetics best describe this system. However the effect of $\bar{n}$ and its inherent assumptions on the evolution of PSD and MWD will be examined

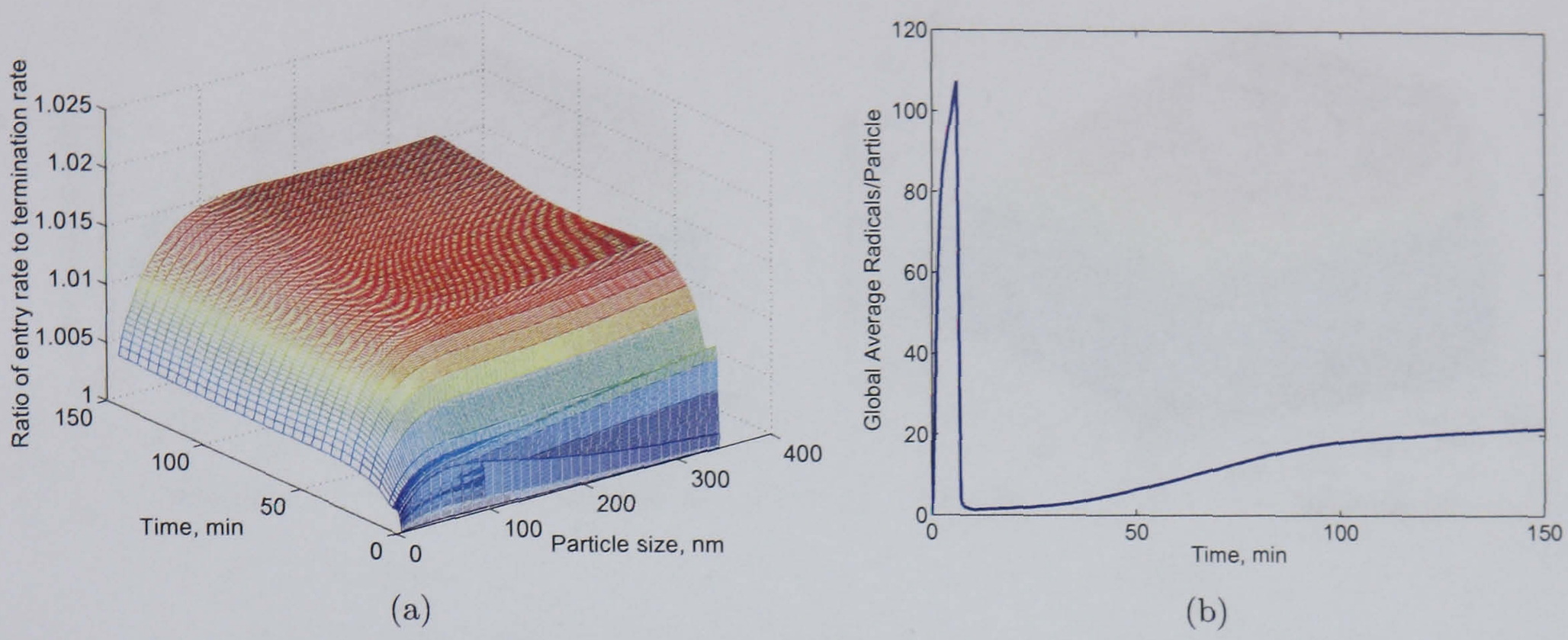


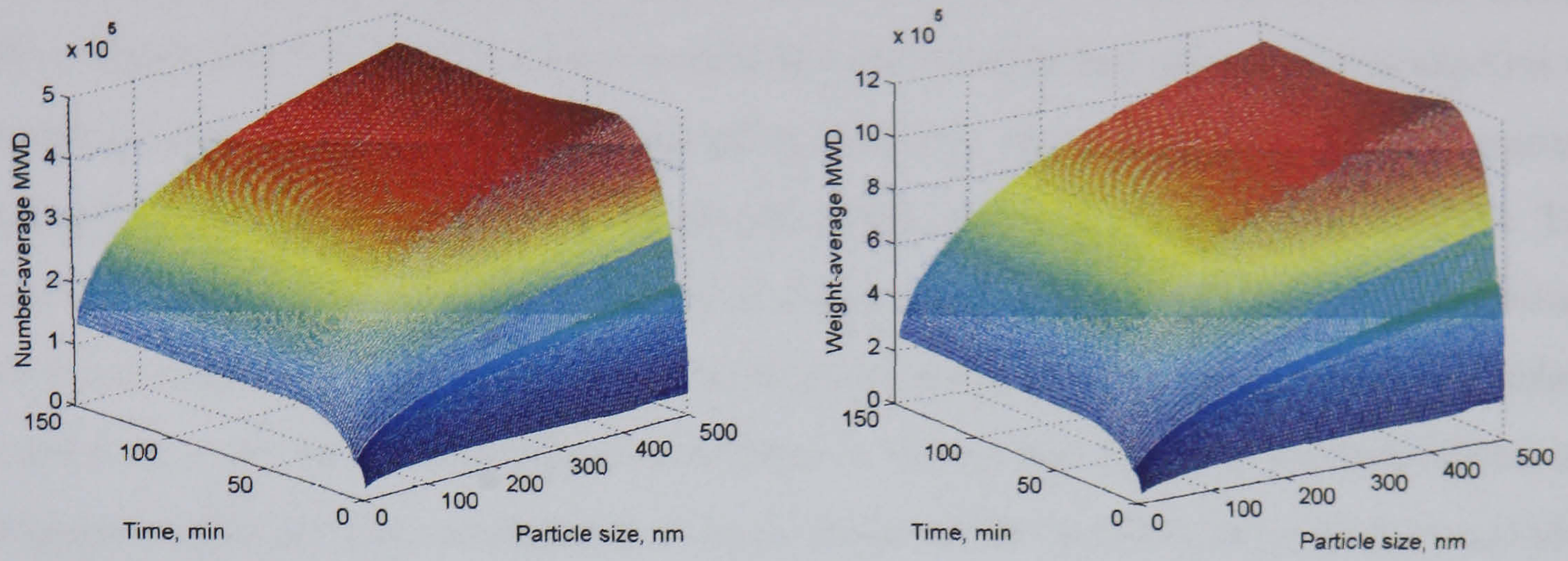
Figure 3.8: The ratio of entry to termination and the global average number of radicals/particle.

further in a forthcoming section.

A final comment is due on the time variation of the average number of radicals per particle. It is seen in both Figure 3.7(a) and 3.8(b) that the $\bar{n}$ value increases to very large values at the early times (before about 10 minutes). This is due to the small number of particles formed by the initial homogenous nucleation. Thus, the net entry of oligomers into each particle is high. Subsequent to the micellar nucleation at around 10 minutes, the large increase in the number of particles leads to reduced entry rates into any given particle, resulting in a net drop in the $\bar{n}$ values (both at the single-particle scale and the global scale).

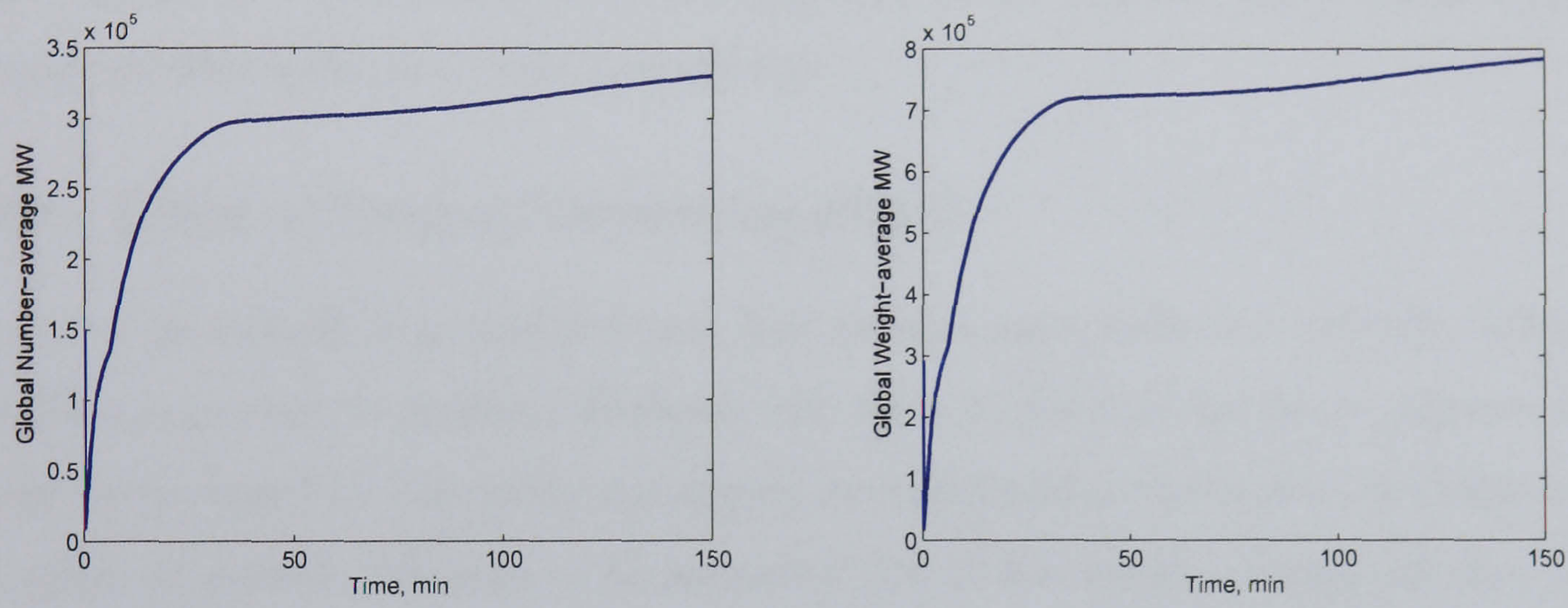
3.6 MWD: Semi-batch Simulation Results

A semi-batch simulation produced the following MWD plots (see Figures 3.9-3.10). Figures 3.9(a) and 3.9(b) show that MWD increases with time for approximately the first 40 minutes of reaction, after which little increase in MWD is observed. The same figures also elucidate the distinct size dependance of the MWD in both the number-average and weight-average cases. The molecular weight increases with increasing particle size. This can be associated with the increased chance that radicals have to grow via propagation reactions in large particles, until they undergo any of the other reactions (e.g. termination, chain transfer) which lead to cessation of growth.

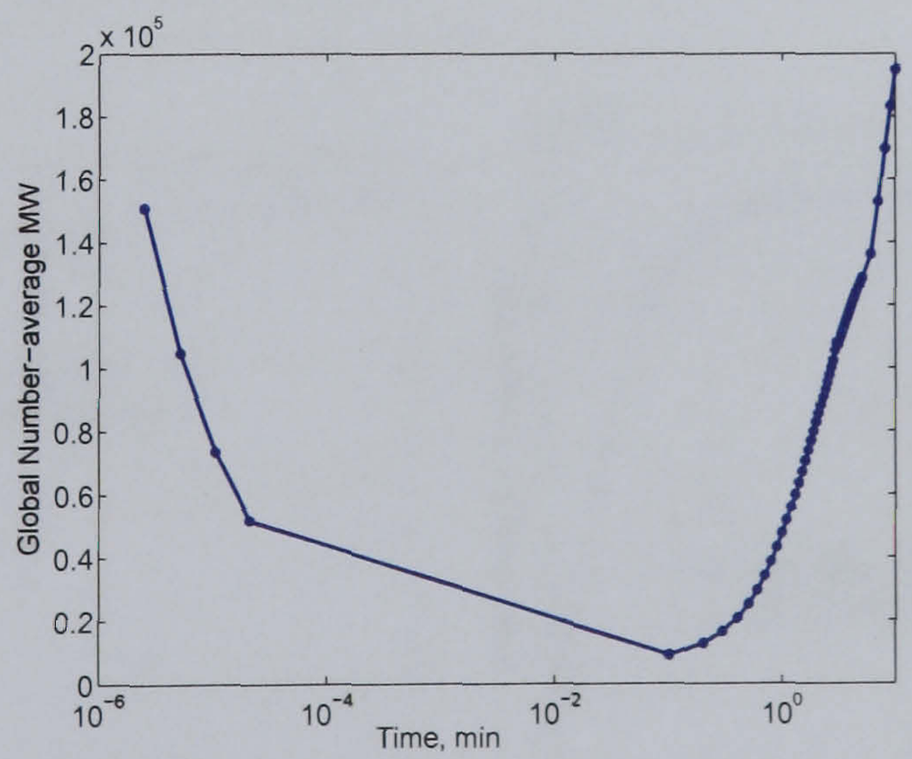


(a) (b)

Figure 3.9: Number-average and Weight-average MWD evolution.



(a) (b)



(c)

Figure 3.10: Global Number-average and Global Weight-average MW evolution and an initial time plot of the Global number-average MW evolution.

The global average molecular weights are shown in Figure 3.10, which exhibit a similar time evolutionary trend to that observed for the distribution evolutions; during the first 40 minutes a rapid increase in molecular weight is observed, after which there is a very gradual increase, reaching a number-average molecular weight value of approximately 300,000. The behavior at very early times is indicated in Figure 3.10(c) for the global number-average molecular weight. It is seen that there is an initial jump in the average molecular weight followed by a decrease as homogenous nucleation occurs and as more polymer chains are initiated. A similar trend is observed at early times in the distribution plots (not included in Figure 3.9 for clarity). As homogenous nucleation is completed, the average molecular weight begins to increase. As discussed previously, the increase is monotonic after this time, except for a momentary decrease in growth rates between 7-10 minutes, when the second micellar nucleation event is underway.

3.6.1 Effect of Particle Growth on MWD

As stated previously, it is assumed that fast kinetics govern the live radicals, therefore a pseudo-steady state is applied. However, the same is not true for dead polymer chains, which are governed by differential equations. As mentioned at the beginning of this section, the effect of growth will need to be accounted for in the model of dead polymer chains. Figure 3.11 shows the effect of accounting for growth in the MWD model. The growth

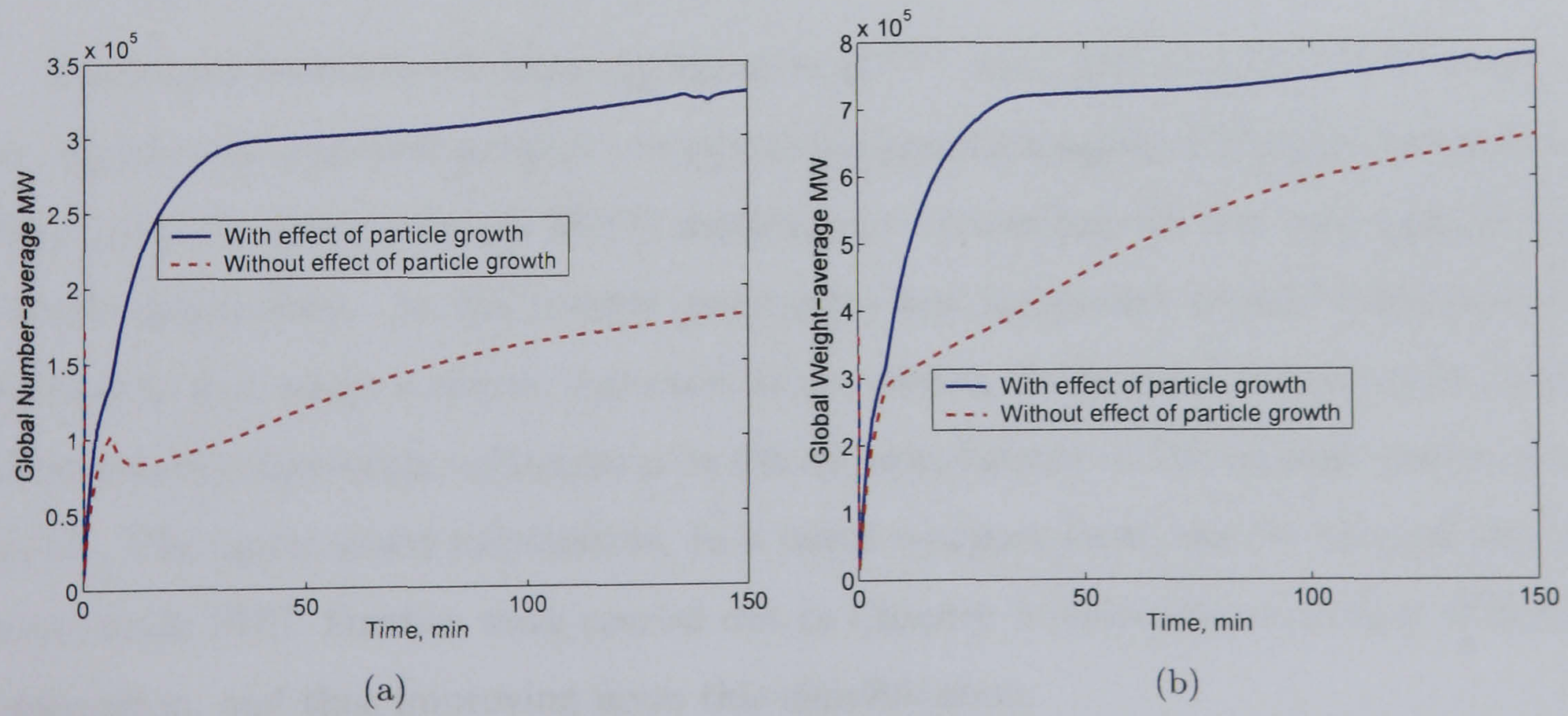


Figure 3.11: Global average molecular weight evolutions analysing the effect of particle growth.

of particles is considered in evaluating PSD and radical number in both cases shown. however the difference lies in the solution applied to the dead moment ODEs. In the 'without growth' case ODEs are solved as normal. In the 'with growth' case the initial condition of the dead chain moments at the start of a discrete time step in a particular bin is set equal to the value at the end of the previous time step in a preceding bin as determined by the growth rates. The growth effect can be seen to cause a prolonged initial increase in both the global average molecular weights. This results in a higher eventual molecular weight value than would have been predicted based on neglecting growth. For the global number-average molecular weight, an increase of approximately 100% is seen when growth is accounted for. In the case of global weight-average molecular weight, an increase of approximately 25% is observed. These results illustrate the importance of accounting for the particle growth from the PSD model in the MWD model.

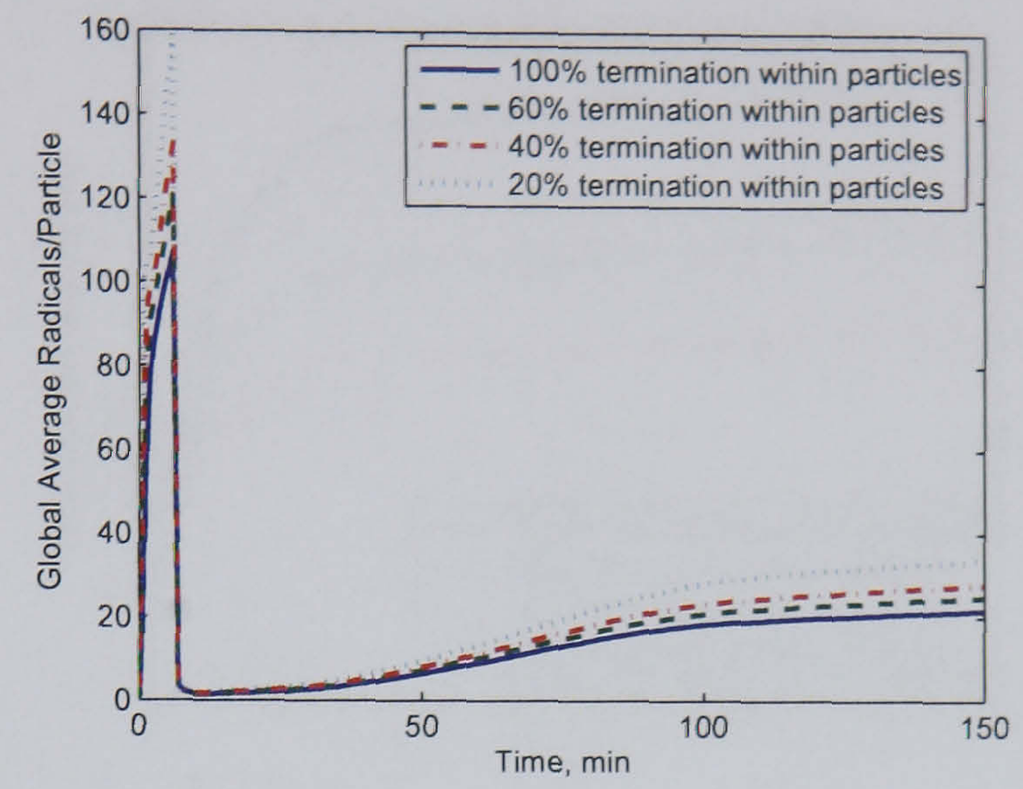
3.6.2 Effect of Compartmentalisation on Termination Rates: Sensitivity on PSD and MWD

A factor, f, was introduced into Eq. (3.28) to account for the possible variations in bimolecular termination, serving as a preliminary investigation into the system-wide effect of compartmentalisation on the process.

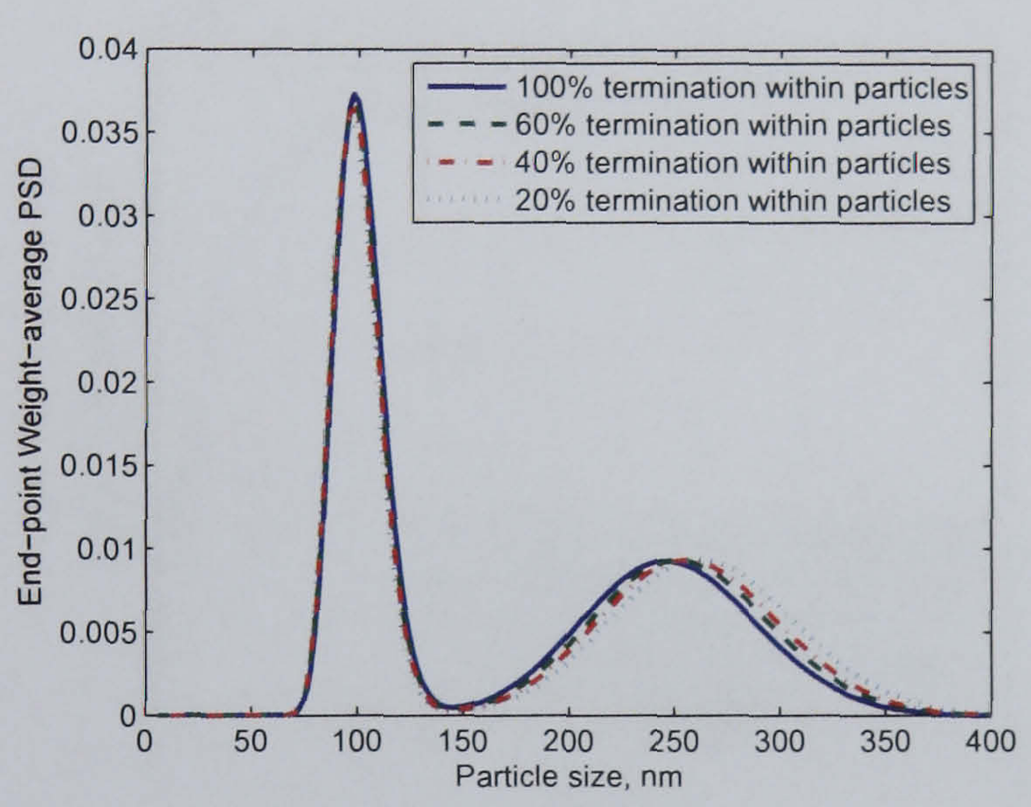
$$\frac{\partial \bar{n}(r,t)}{\partial t} = \Re'_{entry}(r) - \Re'_{desorp}(r) - f2\Re'_{termin}(r) \tag{3.96}$$

There have been notable works by Lichti et al.[121] and Ghielmi et al.,[122,123] which use the 'doubly-distinguished particle' concept to perform an analysis with a similar objective. They, however focus only on MWD models, not accounting for any interactions via a particle distribution. In the current generalised and integrated model framework, it is justified to first adopt a simple approach incorporating the factor f, which could be used to summarise meso-scale information in closed form kernels in the current (macro-scale) model. The summarised information, in a small compact form, can be plugged into the macro-scale PBE. Further work carried out in Chapter 5 looks into extraction of further information, and thus improving upon this simplification.

It is seen in Figure 3.12(a) that the global average number of radicals per particle



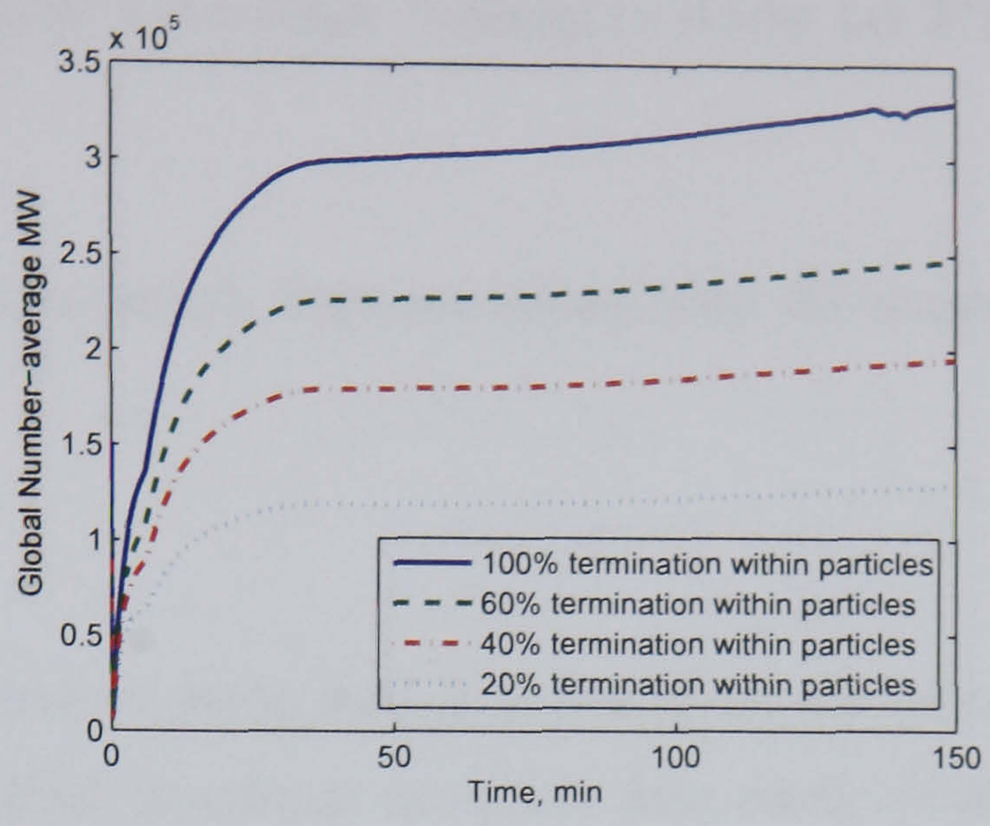
(a)



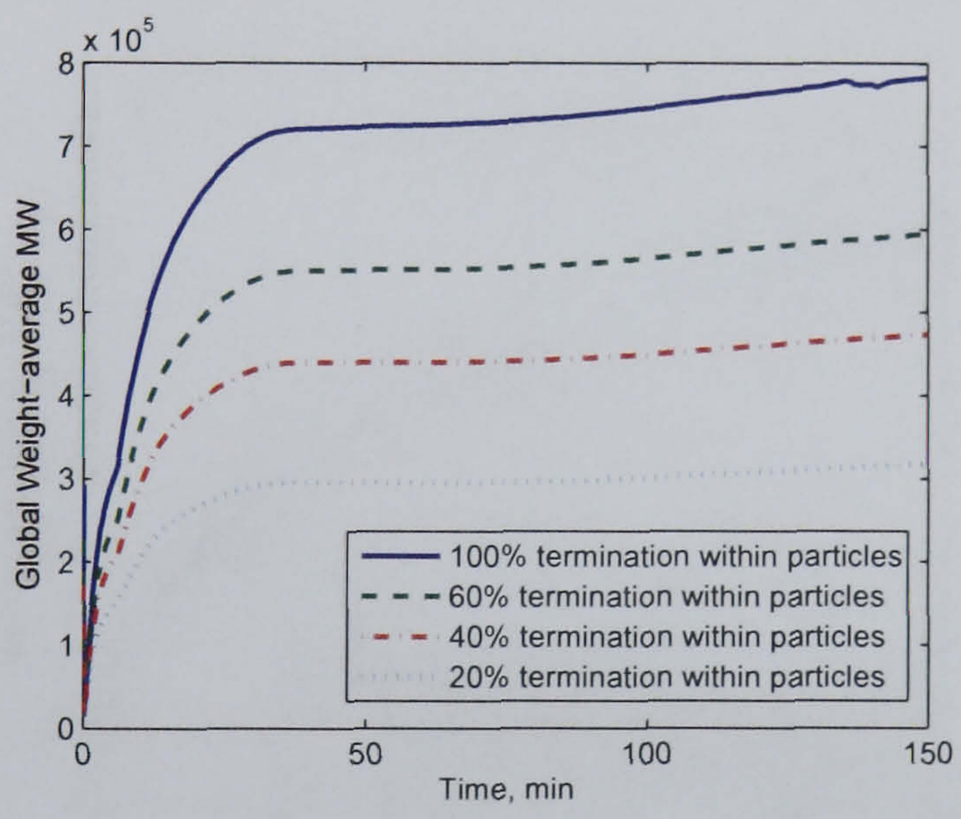
(b)

Figure 3.12: The effect of introducing a termination correction factor in the calculation of $\bar{n}$ on the global average number of radicals per particle and the end-point PSD.

increased as the factor f was decreased. The reduction in termination means that the net effect of entry is made stronger as depicted in Figure 3.12(a). This in turn results in larger growth rates and hence larger particle sizes as is seen in Figure 3.12(b). The net effect on the molecular weight is seen in Figure 3.13. With a reduction in termination, lower global average molecular weights are observed. When the termination is reduced by 40% (from 100% to 60%) the end molecular weight that is achieved is approximately 20% lower. When the termination is reduced a further 20% (from 60% to 40%), the end molecular weight is reduced by approximately 20%. When the termination is reduced a further 20% (from 40% to 20%), the end molecular weight is reduced by approximately 35%. These approximate



(a)



(b)

Figure 3.13: The effect of introducing a termination correction factor in the calculation of $\bar{n}$ on the global average molecular weight evolutions.

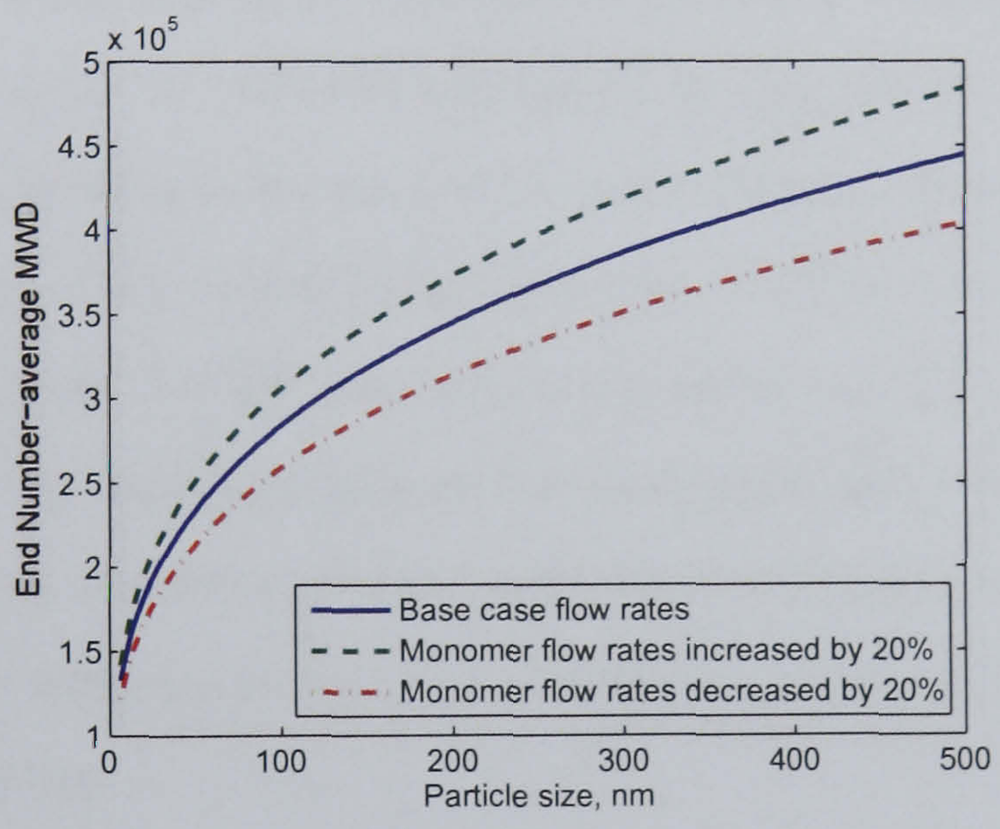
values indicate a non-linear relation between the termination factor and molecular weight. It is clear from the results that the decrease in the termination rate plays the dominant role in determining the molecular weights compared to any of the cascaded effects of a reduction in f. Over the range of f employed the particle number does not change to an appreciable degree, which signifies that the reduction of combination reactions occurring between long radicals is the active mechanism in reducing the molecular weight.

3.7 Macroscopic Process Sensitivities to Process Manipulations

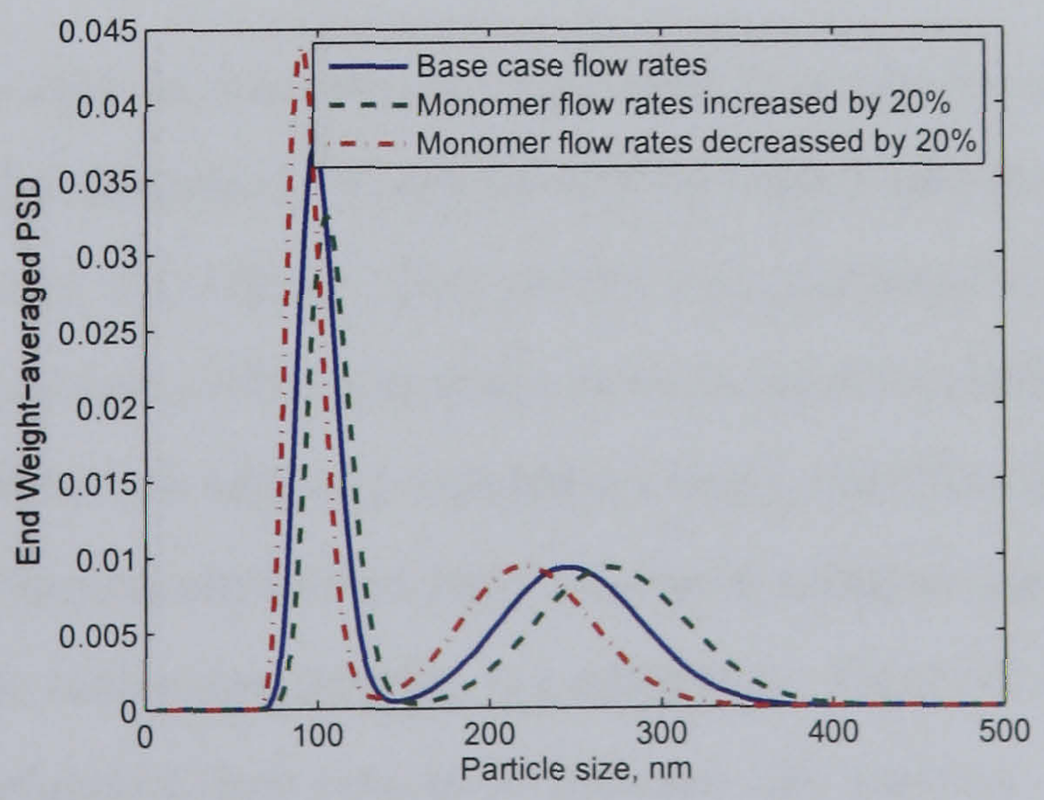
The flow rates of process inputs were perturbed from the nominal values shown in Figure 3.3.

Monomer

In the case of monomer flow rates, both VAc and BuA were changed in equal ratio. Figure 3.14(a) indicates that increasing monomer flow rates by 20% increases the MWD. Whilst increasing the monomer would lead to more aqueous oligomers, hence entry of



(a)



(b)

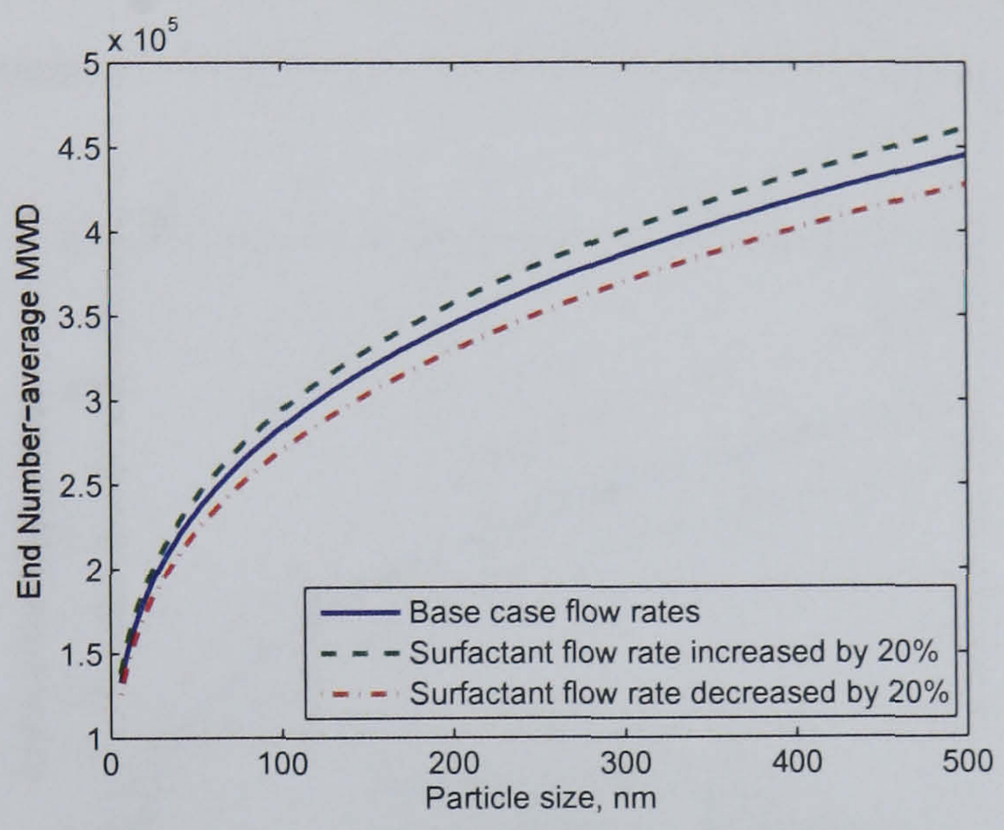
Figure 3.14: The effect of perturbations in monomer flow rates on end-time PSD and MWD.

small chains into particles, lowering the average molecular weight. the effect of a larger monomer concentration in particles has a stronger effect. This leads to a higher polymerisation rate of chains inside particles, hence increasing the average chain length. Lowering the monomer flow rate results in a lower concentration in particles and has the opposite effect, lowering the molecular weights. Figure 3.14(b) indicates that increasing monomer flow rate results in a shift of all modes of particles to the right, due to increased growth rates. It also shows the general trend of peaks shifting to left when monomer flow rate is decreased, due to decreased growth rates. If one focusses on the mode of particles centred around about 250 nm (homogeneously nucleated), upon increasing monomer flow rate this peak shifts up due to increased monomer concentration and hence growth. The opposite movement is observed upon decrease in monomer flow rate. There seems to be little change in the number of particles contained in this mode, which means that there is no alteration in the homogenous nucleation rate, despite the increased aqueous phase monomer concentration. This points to the fact that the initiation of monomer maybe the limiting factor in this case. In the case where the monomer flow rate is increased, there is an initial period of increased growth of the homogenously nucleated particles. These growing particles adsorb more surfactants onto their surfaces, resulting in less monomer being available for the subsequent micellar nucleation, observed in the smaller peak centred around about 110 nm.

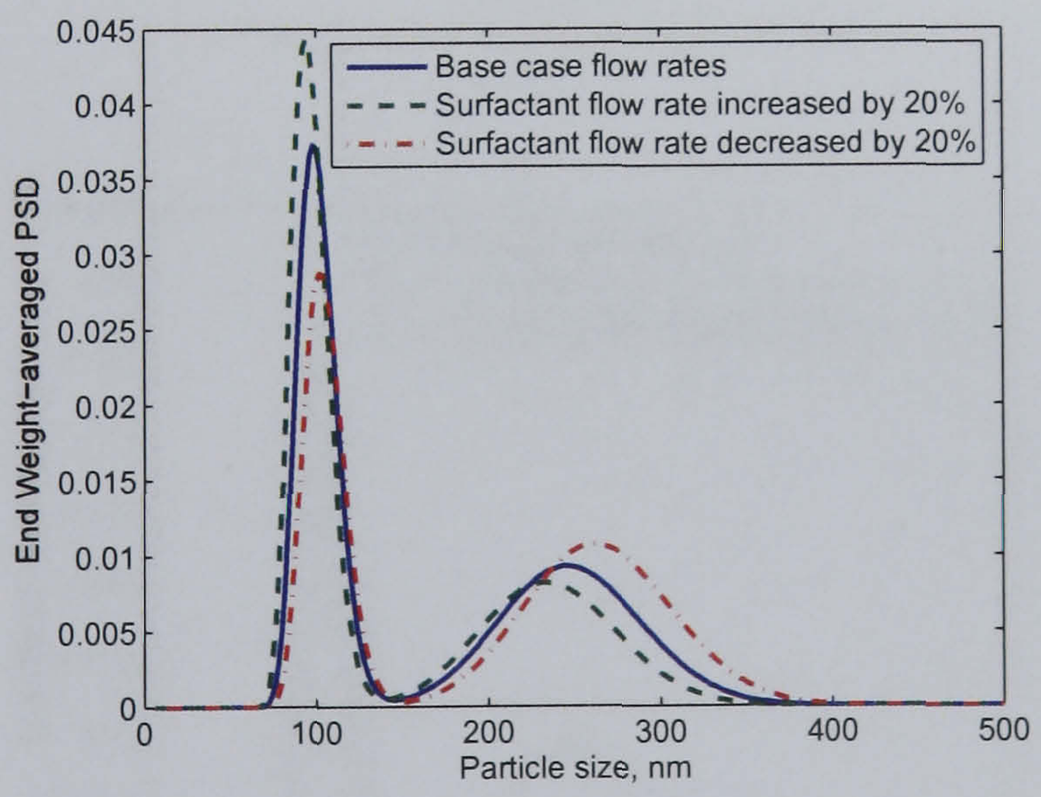
Surfactant

Figure 3.15(a) shows that an increase in surfactant flow rate results in a small increase in MWD. The increased surfactant level leads to an increased micellar nucleation, which leads to larger overall number of particles. This results in a decreased value of the global average number of radicals/particle. With less radicals to terminate inside a particle, polymerisation occurs for longer and at higher propagation rates, therefore higher molecular weights are observed. A decrease in surfactant level results in a higher number of radicals/particle on average and lower molecular weights are observed. Figure 3.15(b) shows that the effect of increasing surfactant flow rate is to increase the number of particles produced by micellar nucleation (see larger peak magnitude centred around approximately 100 nm). Decreasing surfactant flow rate results in the same peak becoming smaller in magnitude

(i.e. less micellar nucleation). The amount of homogenous nucleation that occurs at the start of the process is the same in the different cases. In the increased surfactant case, the base case homogenously nucleated peak (solid line, centred around 250 nm) becomes slightly smaller and shifts to the left due to a decreased level of growth subsequent to the larger micellar nucleation. When the surfactant level is decreased the converse effect is observed.



(a)



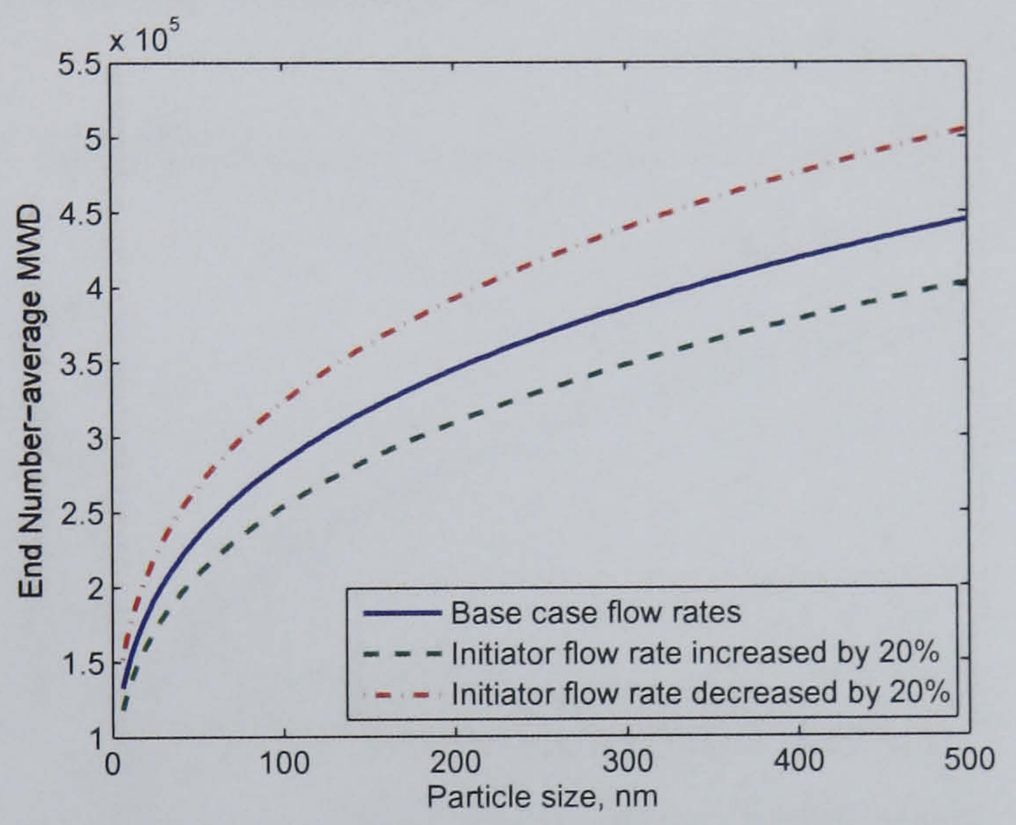
(b)

Figure 3.15: The effect of perturbations in surfactant flow rate on end-time PSD and MWD.

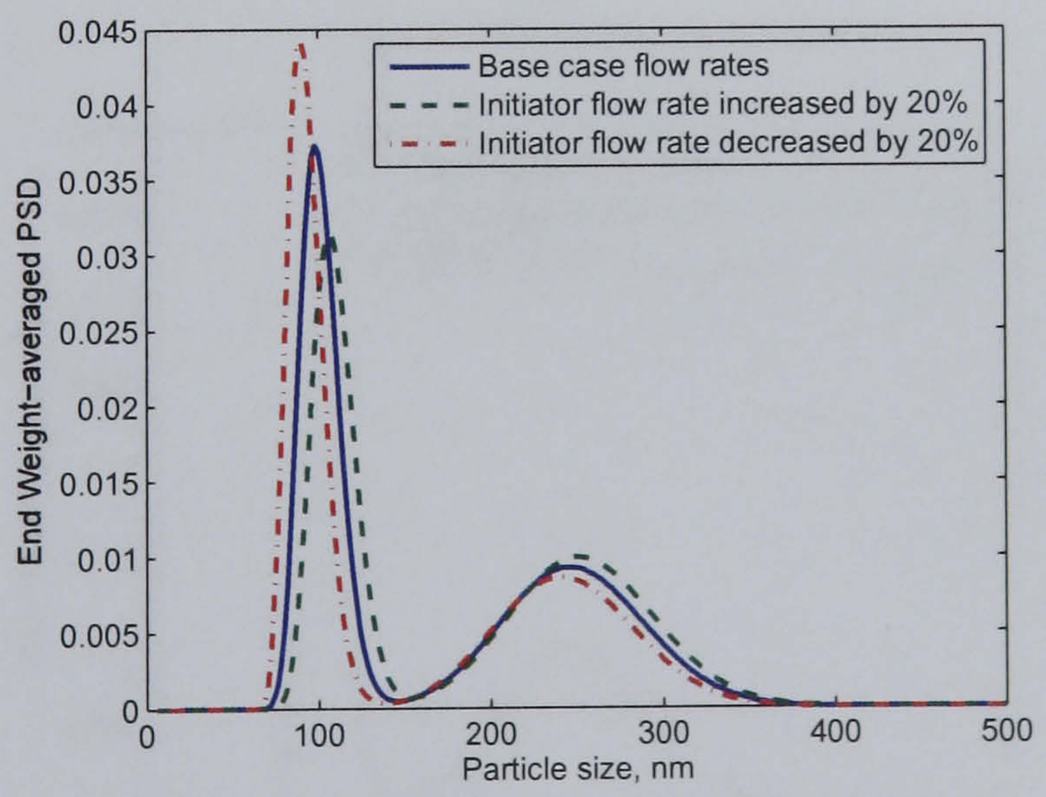
Initiator

Figure 3.16(a) shows a different trend to those seen previously. It indicates that as initiator flow rate is increased, MWD decreases. This effect is due to the increased concentration

of aqueous phase oligomer. The increased entry rate of oligomers into particles has a negative effect on MWD. A decrease in initiator flow rate has the opposite effect. The corresponding PSDs are shown in Figure 3.16(b). As the initiator flow rate is increased the level of aqueous phase oligomers increases, resulting in a larger homogenously nucleated peak (see peak on right, centred around approximately 260 nm). Therefore, the subsequent micellar nucleation is smaller (see peak on left, centered around approximately 110 nm). Decreasing the initiator flow rate results in a smaller homogenously nucleated peak and a larger micellar nucleation.



(a)

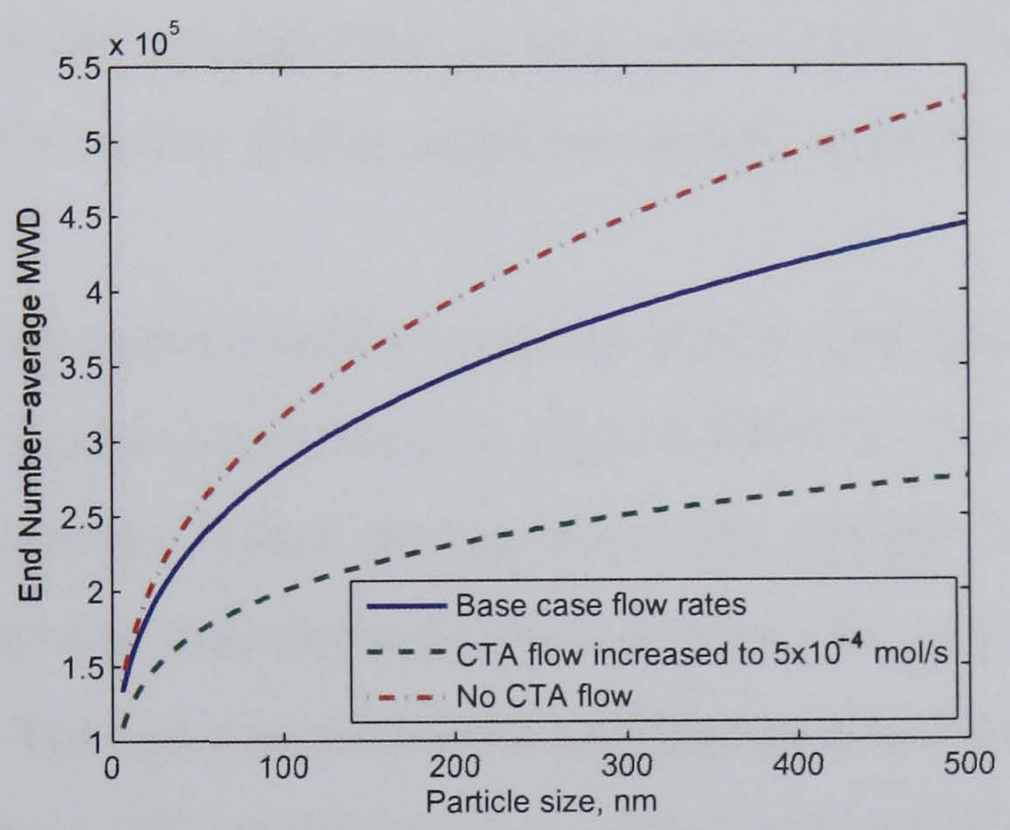


(b)

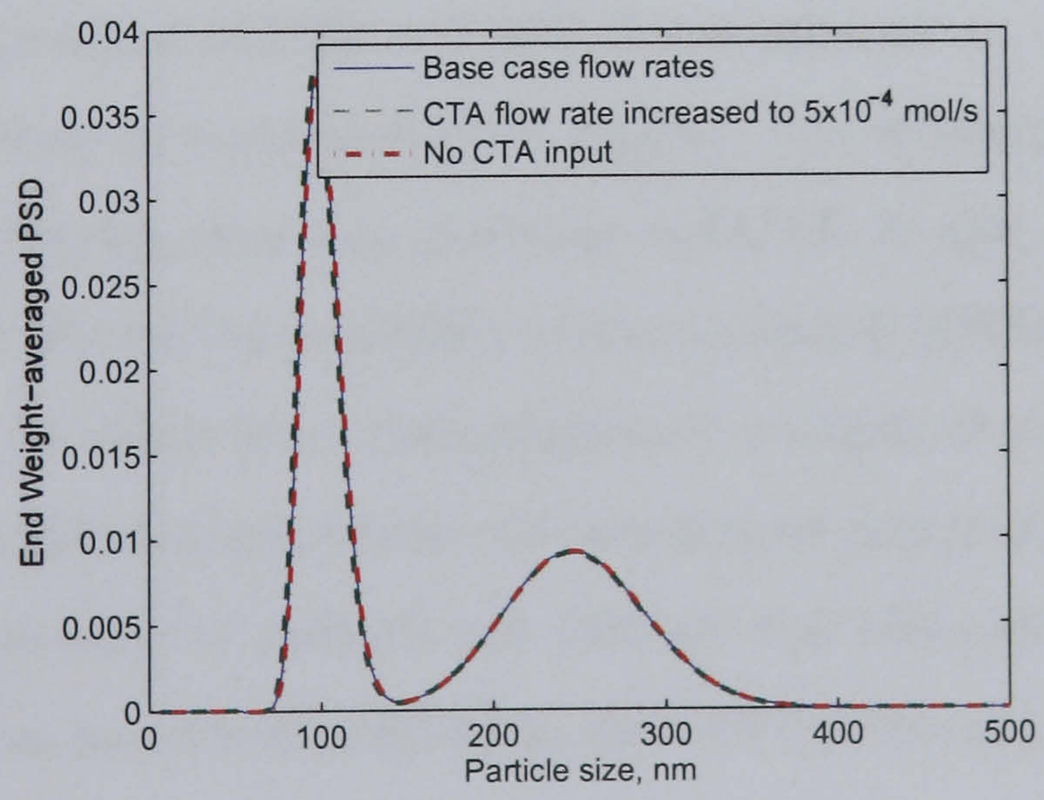
Figure 3.16: The effect of perturbations in initiator flow rate on end-time PSD and MWD.

CTA

The effect of perturbations to CTA flow rates is seen in Figure 3.17. With respect to the MWD plot in Figure 3.17(a), an increase in CTA flow rate results in a decrease in MWD, as expected. If CTA is not used in the process, then radicals within particles are more likely to achieve longer chain lengths, resulting in a higher MWD. Figure 3.17(b) indicates that CTA perturbations have negligible effect on PSD development. This result demonstrates that CTA provides the mechanism to manipulate MWD, without altering the PSD, leading to more a flexible control regime. This trend will also be seen in the experimental results presented in chapter 4.



(a)



(b)

Figure 3.17: The effect of perturbations in CTA flowrate on end-time PSD and MWD.

3.8 Chapter Summary

This section details a comprehensive model that simultaneously accounts for both PSD and MWD. The multi-scale dynamic model incorporates inputs for two monomers, CTA and a thermal initiator system. Coagulation dynamics are incorporated for an ionic surfactant stabilised system. Both homogenous and micellar nucleation are modelled. Partitioning of reaction components amongst the heterogenous system is considered. The pseudo-homopolymer approximation is used to simplify equations for a multi-monomer system. Further, a mechanistic formulation describing the average number of radicals per particle is used. The PSD model is solved using a decomposition algorithm, which enables a semi-analytical solution for the full PBE at each particle bin. The method of moments is used to solve the MWD model, giving molecular weight approximations for each discrete particle bin.

The results of a semi-batch emulsion polymerisation simulation elucidate the effect of process variables and model parameters on PSD and MWD. The MWD was shown to be highly size dependent, where larger average molecular weights were seen in larger particles. A so-called hierarchial two-tier solution technique was employed for the solution of the combined model. The solution technique resulted in a computational time of approximately 30 seconds (for a 150 minute semi-batch process) on a contemporary computer, consisting of a dual core 3.4 Ghz Intel pentium D processor with 1 GB of memory. The sensitivity of the objectives of PSD and MWD was assessed in relation to perturbations in monomer, surfactant, initiator and CTA inputs. The strongest effects on MWD were seen in the cases of varying monomer, initiator and CTA. In this constant monomer/CTA feeding regime, CTA offered the possibility of manipulating MWD, without changing PSD. The main points to be taken from the preliminary analysis of the effect of compartmentalisation, through a direct manipulation of bimolecular termination in particles, was that the global average number of radicals per particle was effected and hence so was PSD. Also a large effect was noted with respect to the MWD. This aspect will be elaborated on in Chapter 5.

Chapter 4

Experimental Studies & Model Validation

4.1 Introduction

It has been long established that important yet hard to measure macroscopic properties, such as optical properties and rheology are strongly influenced by PSD.[6,155] In addition, the particular MWD is thought to be well correlated with end-use properties such as rheology[12] and mechanical strength.[156] This motivates tighter control on product specifications. Multi-objective and distribution control are therefore extremely important in emulsion polymerisation.

It is difficult to maintain a complete and independent control over the entire range of important product properties in emulsion polymerisation due in the coupling effects that exist between PSD and MWD. As highlighted in Chapter 2, a literature review discussing the topic of controllability, the interaction between PSD and MWD in emulsion polymerisation has received little attention. To effect a tight and robust control in emulsion polymerisation, one aspect that necessitates a full understanding is the relationship between control objectives and operating conditions. This chapter will detail investigations into the simultaneous controllability of PSD and MWD– the beginning of a vast research problem. It will aim to elucidate the process interactions that determine the feasible regions for PSD and MWD. The dependence of PSD and MWD on operating conditions, and

the coupling between the two will be assessed through experimental sensitivity analysis on the main process manipulations: initiator, CTA, monomer and surfactant. In addition, the experimental data will be compared to the predictions of the model developed in Chapter 3. This comparison will enable model validation, as well as further elucidating important process mechanisms. The contents of this chapter are accepted for publication in the Macromolecular Reaction Engineering Journal.[157]

4.2 Experimental System

A schematic of the experimental facility employed in this study is shown in Figure 4.1 (supplement to the facility reported by Fan et al.[158]). The system comprises a 0.7 ℓ round-bottomed cylindrical stainless steel reaction vessel. Attached to the top of the vessel is an AE MagneDrive®II agitation device fitted with an impeller, the configuration of which is shown in Figure 4.1. The MagneDrive agitator is driven by an electric motor (Teco: 0.37 KW) via a drive belt (Fenner SP2 950). The gearing between the agitator and motor unit is 1:1. The motor is controlled by an A.C. variable speed drive (Teco Speecon 7200 Minicon E2 Series: 220 V, 0.4 KW). Heat transfer is provided by means of a thermal oil which is circulated between an external stainless steel jacket and the reaction vessel. A Single™Temperiertechnik ST01-6-12-DM heat exchanger unit provides temperature control and circulation of the heat transfer medium. There is a borosilicate glass coil reflux condenser (Quickfit, CX3/04) connected to the top of the reactor vessel. Reactants are fed via peristaltic pumps (a Pharmacia LKB P-1 and a Watson Marlow 505s). A 100 mL glass burette is also used to feed ingredients into the reactor (shot fashion) using pressurised nitrogen as the driving force. There is a sampling port at the lower end of the reactor.

Latex samples are characterised in terms of PSD using a capillary hydrodynamic fractionator (CHDF) from Matec Applied Sciences (CHDF 2000), equipped with a C-204 fractionation cartridge. MWD is measured using a triple-detector equipped gel permeation chromatography (GPC) system from Polymer Labs, combining refractive index, light scattering and viscometry measurements. The particular system used consists of a PL-GPC 50 with 2 pLgel 5μm Mixed-D columns (29°C) and a viscometer in conjunction

with a multi-angle light scattering detector from Wyett (Dawn 8). The solvent used is tetrahydrofuran (THF).

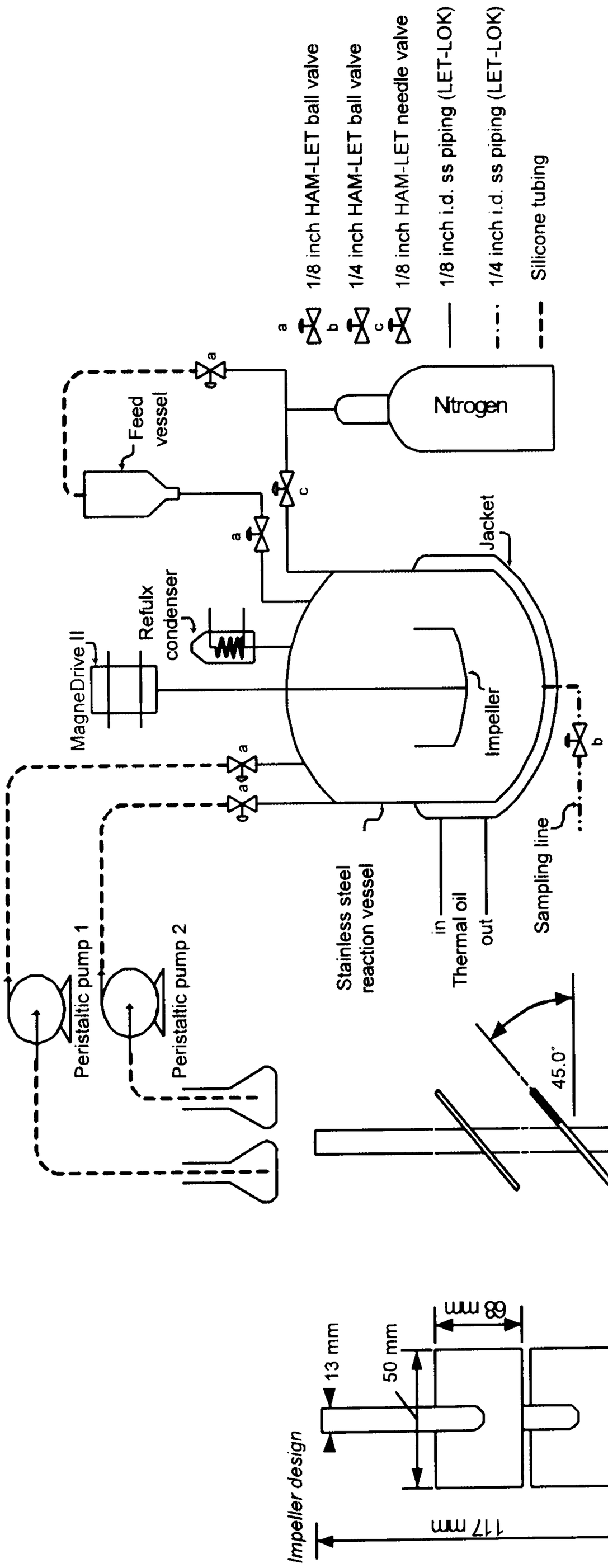


Figure 4.1: Schematic of experimental facility and impeller design.

4.3 Recipe and Operating Conditions

A semi-batch addition strategy is implemented for the set of experiments, following previous studies by Boutti et al.[159] and Immanuel et al[33]. Due to the nature of the monomer addition (shotwise) the reaction operates in both flooded and starved regimes depending on the monomer conversion. The monomers used in this study are vinyl acetate (VAc) from Fluka (>99%) and butyl acrylate (BuA) from Aldrich (>99%). The ionic emulsifier used is sodium dodecyl sulphate (SDS) from Aldrich. The thermal initiator used is sodium persulphate from Aldrich. The CTA used is 1-dodecanethiol from Aldrich. The quenching agent used is hydroquinone from Sigma. All chemicals are used as received from the manufacturer. Water used is deionised from an Elga Option 4 water purifier.

Reagents are prepared at room temperature. The amount of water in the initial charge [see Table 4.1] is heated to the reaction temperature (75°C in all cases). Isothermal conditions within the reactor are maintained via manual adjustment of the set point of the heat exchanger. Additional initial reactants [see 'Initial' column of Table 4.1] are added upon attaining reaction temperature. The agitator is set at a rotational speed corresponding to an A.C. variable-speed drive setting (13) that was found to be adequate for thorough mixing. Agitation is constant throughout the heating and reaction stages. The initial mixture addition defines the reaction time of t=0 min. Component feeds [see 'Feed' column of Table 4.1 and Figure 4.2] are started and are maintained manually as close as possible to target feed rates. Initiator (constant 1%) and surfactant (see Figure 4.2 for concentrations) aqueous solutions are fed via the peristaltic pumps. Monomer is fed shotwise via the pressurised glass burette. The initial and subsequent monomer feed is supplemented with the corresponding amount of CTA [see Table 4.1: weight basis per total monomer]. Latex samples are collected at certain times from the sampling port so as to maintain a satisfactory resolution of process outputs. Samples are immediately quenched with 2 wt% hydroquinone solution. The total batch time is 120 mins.

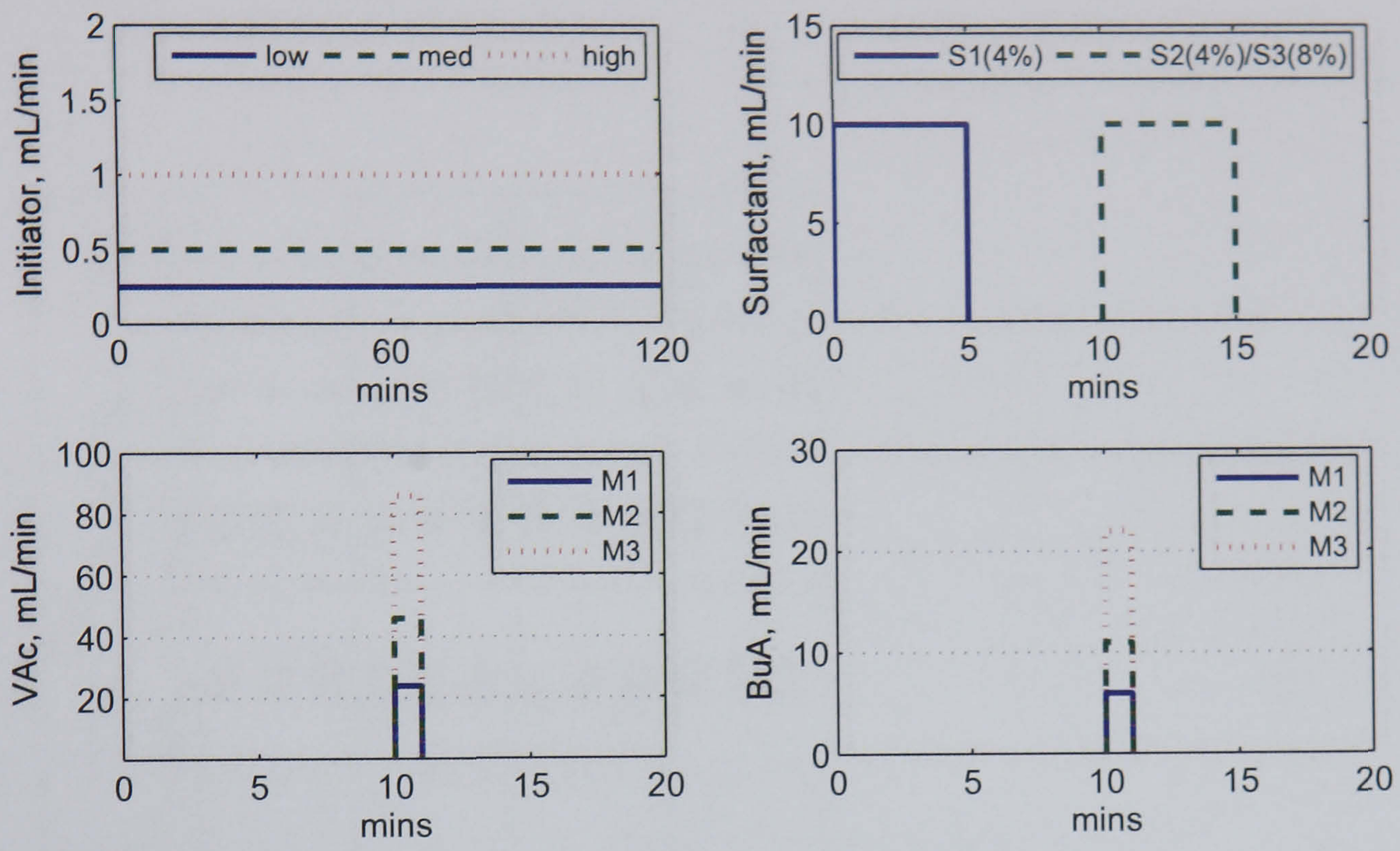


Figure 4.2: Experimental feed rates.

Table 4.1: Experimental inputs for initial reactants and feeds.

		Initial					Feed				
Process input	case ref	water (g)	Ini (g)	VAc (mℓ)	BuA (mℓ)	CTA wt%	Ini(1%) (mℓ · min^{-1})	Surf [Fig.4.2]	VAc (mℓ)	BuA (mℓ)	CTA wt%
Initiator	low	300	0.6	46	11	1	0.25	S2	24	6	1
	med	300	1.2	46	11	1	0.5	S2	24	6	1
	high	300	2.4	46	11	1	1.0	S2	24	6	1
Monomer	M1	300	1.2	46	11	1	0.5	S2	24	6	1
	M2	300	1.2	46	11	1	0.5	S2	46	11	1
	M3	300	1.2	46	11	1	0.5	S2	86	22	1
Surfactant	S1	300	1.2	46	11	1	0.5	S1	86	22	1
	S2	300	1.2	46	11	1	0.5	S2	86	22	1
	S3	300	1.2	46	11	1	0.5	S3	86	22	1
CTA	0%	300	1.2	46	11	0	0.5	S2	24	6	0
	1%	300	1.2	46	11	1	0.5	S2	24	6	1
	3%	300	1.2	46	11	3	0.5	S2	24	6	3

4.3.1 Latex Characterisation

The latex PSD is analysed using CHDF. A fraction of the sample obtained is diluted with DI water such that it is within the acceptable range for the CHDF 2000 device (0.1 to 5% solids). A 25 $\mu\ell$ sample loop is then filled with diluted sample ready for injection. The particular eluent used is GR500-1X from Matec. Sample injection to the CHDF 2000 column and elution is controlled via computer. The residence time of a sample is approximately 12 minutes. Solids content data is obtained via gravimetry. Particle number is calculated using PSD and solids content data (for more details see[33]).

The procedure used to determine the MWD of the latex samples is as follows: 1-2 mℓ of sample is left to dry at room temperature in an aluminium trough. Once dry (after approximately 24 hours when no further weight decrease is observed) a fraction of the sample is scraped from the trough and deposited into a glass vial. THF solvent from the GPC device is used to dissolve the sample. Polymer and THF are weighed such that a concentration of 1.5 to 2 mg·mℓ^{-1} is attained. The sample is left for 24 h to properly dissolve, after which the polymer solution is filtered, using a 0.2 μm PTFE filter, into a clean glass vial ready for GPC analysis. The analysis of filtered polymer solution via GPC is then carried out. The sample vial is placed in the GPC autosampler, and the data collection software is set to run. Cirrus software from Polymerlabs is used for data collection and to analyse the collected data. Elution time is approximately 35 minutes per sample. MWD traces are expressed as Differential Log Molecular Weight Distributions:

$$\left(\frac{dw}{d(\log \mathrm{MW_p})}\right)_i = \frac{\%dw_i}{dV_{ei}} \times \frac{dV_{ei}}{d(\log \mathrm{MW_p})_i} \tag{4.1}$$

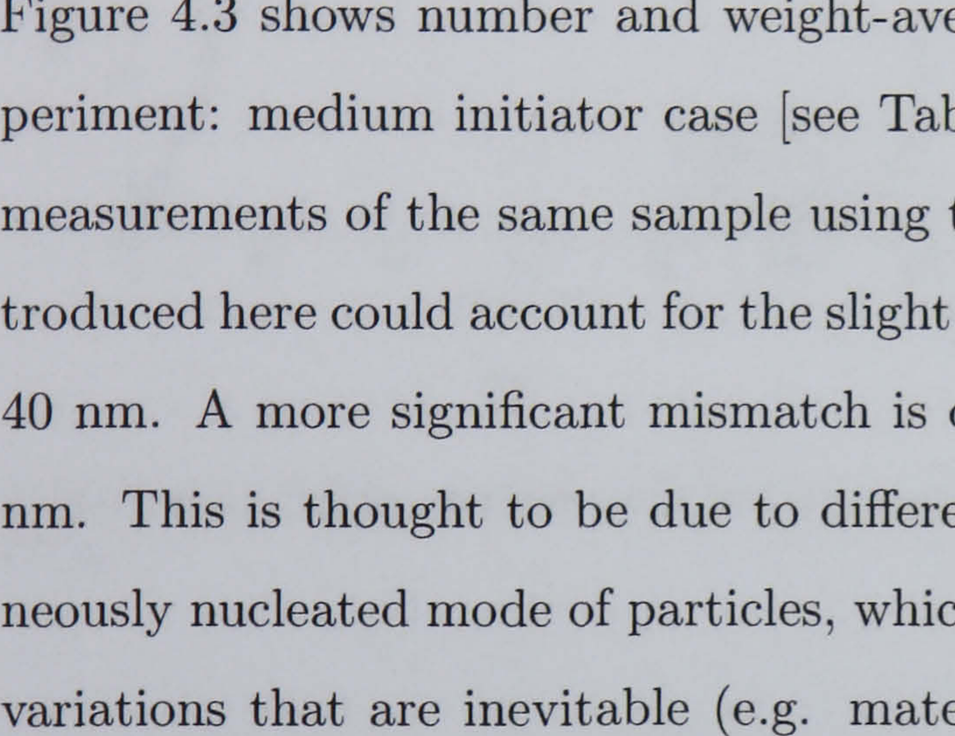
where $\mathrm{MW_p}$ is the molecular weight, w is the weight fraction of polymer, V_e is the elution volume and the indice i denotes the increment number of the discretised elution volume, used to calculate MWD. The first term on RHS of Eqn.4.1 represents the fractional concentration response of the unknown polymer sample and the second term on RHS of Eqn.4.1 represents the slope of the fitted MW calibration curve.

4.4 Experimental Results & Discussions

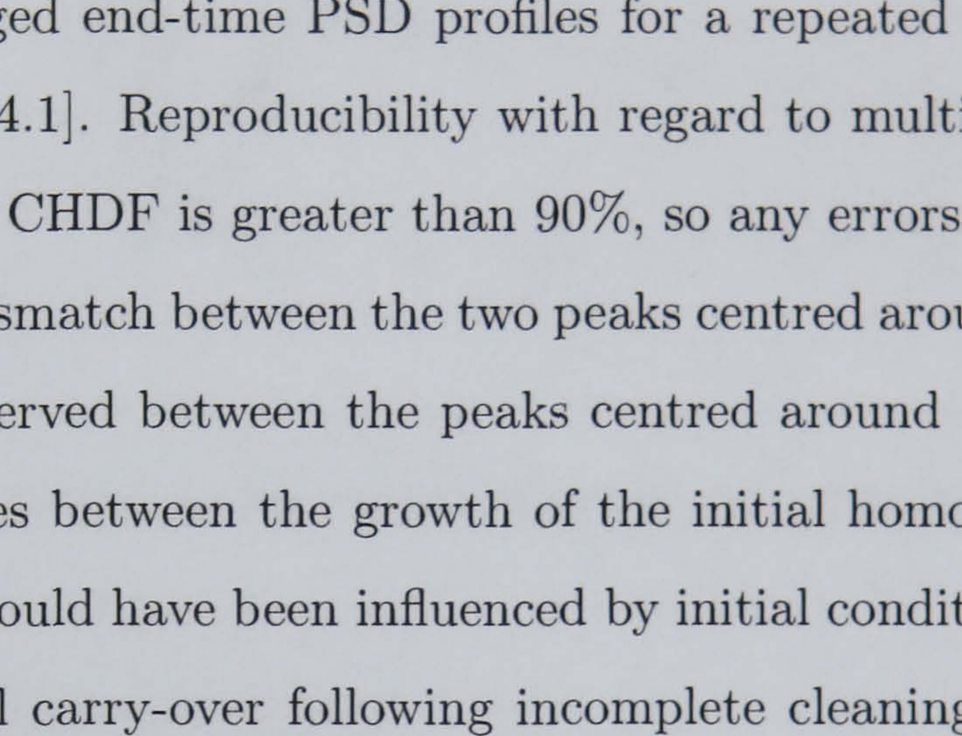
This section examines the effect of manipulated variable perturbations on PSD, MWD and other important latex attributes. A repeatability analysis of the experimental system is first presented.

4.4.1 Repeatability Analysis: PSD, solids content and number of particles

Figure 4.3 shows number and weight-averaged end-time PSD profiles for a repeated experiment: medium initiator case [see Table 4.1]. Reproducibility with regard to multiple measurements of the same sample using the CHDF is greater than 90%, so any errors introduced here could account for the slight mismatch between the two peaks centred around 40 nm. A more significant mismatch is observed between the peaks centred around 125 nm. This is thought to be due to differences between the growth of the initial homogeneously nucleated mode of particles, which could have been influenced by initial condition variations that are inevitable (e.g. material carry-over following incomplete cleaning of the reactor).



(a)

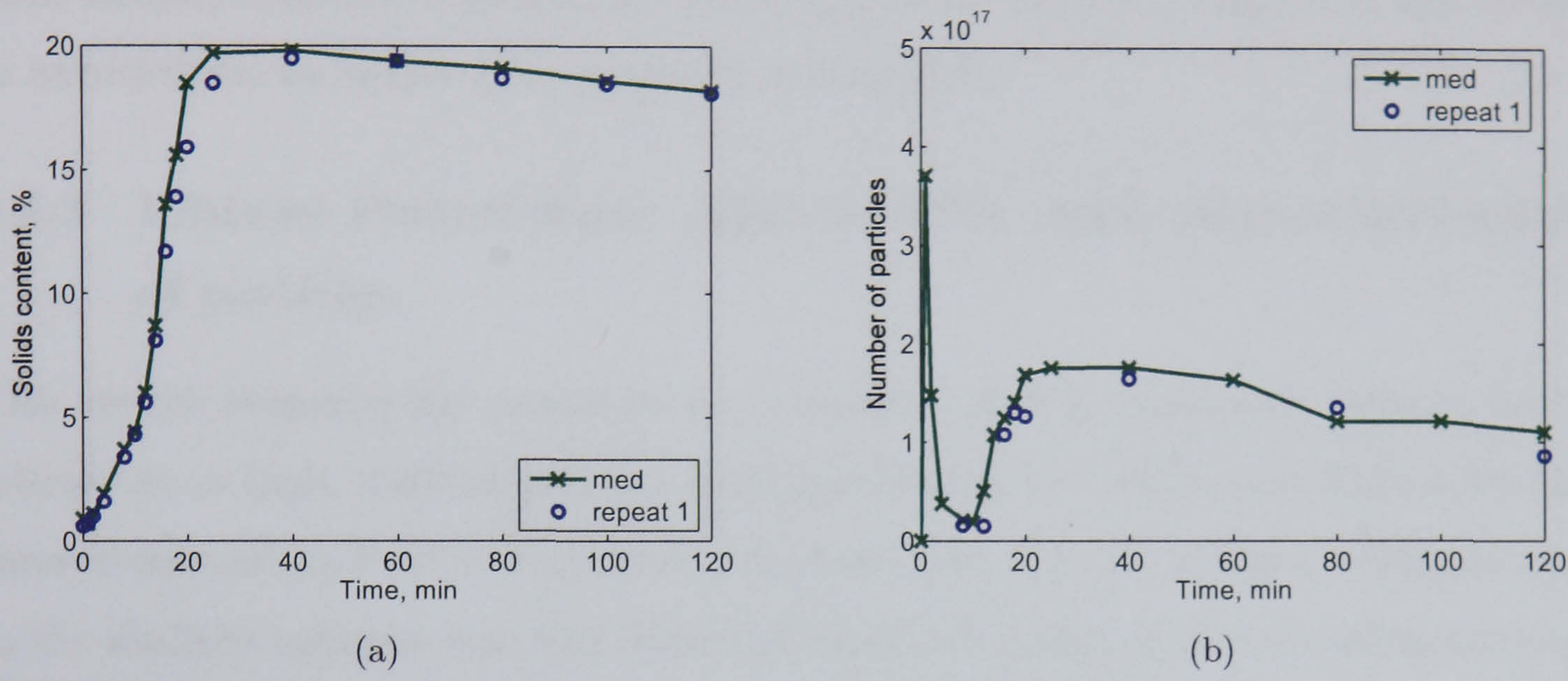


(b)

Figure 4.3: Number and weight-averaged end-time PSD profiles for medium initiator case with 1 wt% CTA.

Figure 4.4(a) shows that there is a very close match between the solid contents for two runs of the medium initiator perturbation case. The gravimetry technique used to measure solids has a typical reproducibility for multiple measurements of the same sample

of more than 95%. Particle number evolution [see Figure 4.4(b)] is calculated using a combination of PSD and solids data, and despite the small differences in PSD the particle number profile data is well matched.



(a) (b)

Figure 4.4: Solids content and particle number evolutions for medium initiator case with 1 wt% CTA.

4.4.2 Repeatability Analysis: Molecular weight

Figures 4.5(a) and 4.5(b) show number-averaged MW and end-time MWD respectively for the medium initiator case and a repeat of the same experiment. Good accord between repeated experiments is shown for the two MW variables, except for the initial

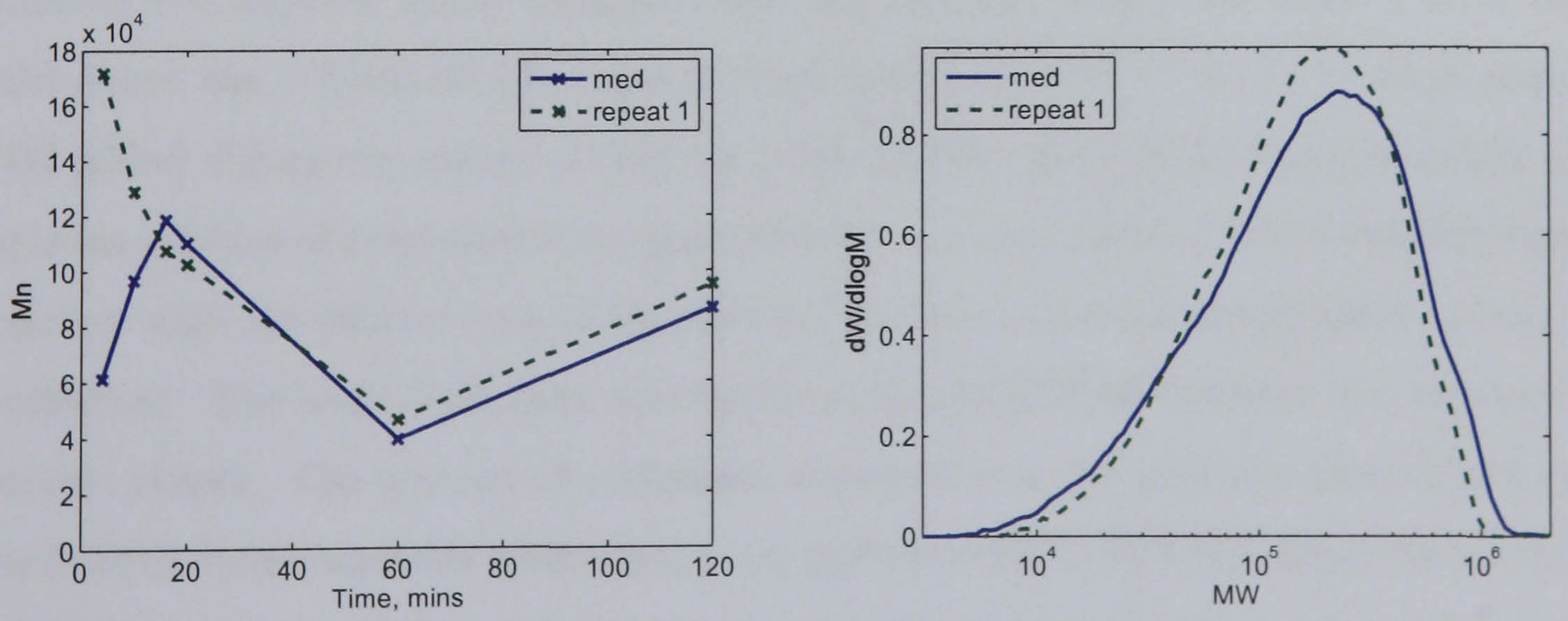


Figure 4.5: a) Number-averaged MW evolutions and b) End-time MWD profiles for medium initiator case with 1 wt% CTA.

number-averaged MW. This could be due to there being maximum temperature fluctuations during the beginning of an experiment whilst reactants take time to reach a constant temperature, and material carryover as mentioned. Upon multiple GPC analysis of the same sample, approximately 5% error was experienced between MWD measurements due to uncertainties in device calibration and post-analysis.

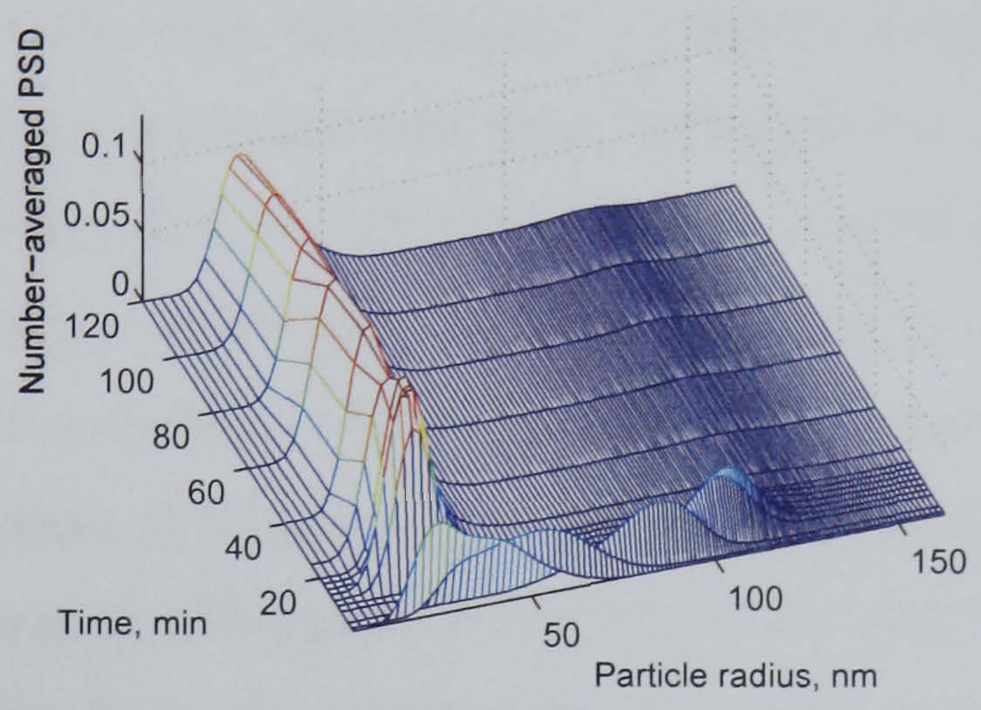
4.4.3 Initiator Perturbation: effect on PSD, solids content and number of particles

This section examines the results from experiments aiming to perturb initiator, and are referred to as high, medium and low initiator cases [as per Table 4.1]. Figure 4.6 shows the evolution of the PSD over a 2 hour, semi-batch run. The particular experiment relates to the medium initiator case, the details of which are shown in the preceding section. A bimodal PSD can be seen to develop in both the number and weight-averaged PSD plots. The first mode of particles (centred around 50 nm at the early times) can be attributed to a homogeneous nucleation event. Homogeneous nucleation is caused by the sparing amount of dissolved monomer polymerising to form short chain radicals, the hydrophobic character of which increases upon chain lengthening, causing them to collapse out of the aqueous phase and form a separate polymer particle phase.

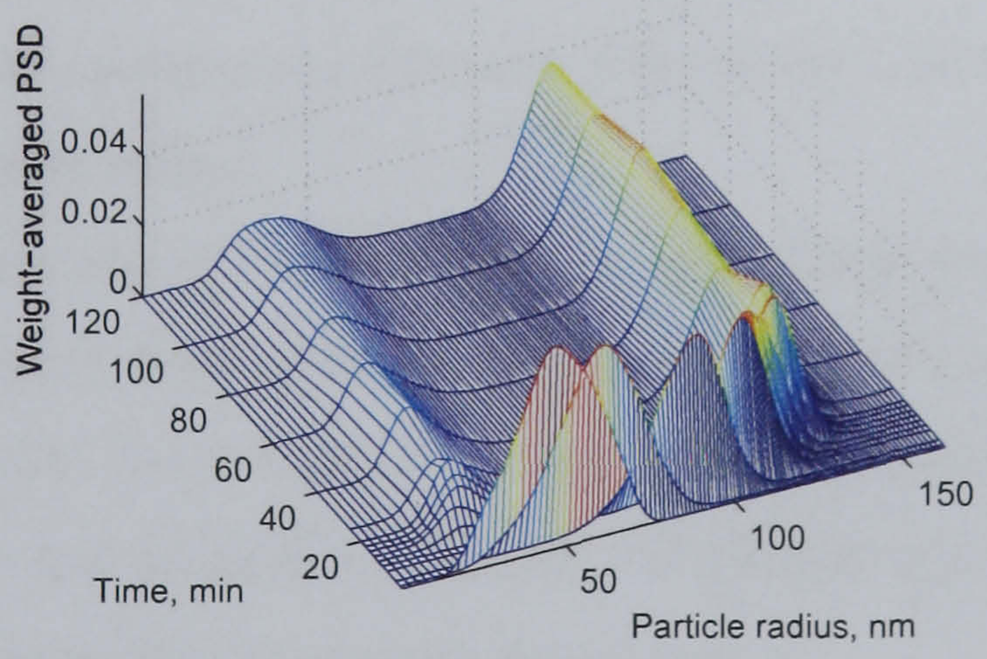
At around 10 mins, the emergence of a second peak is observed (centred around 25 nm). These particles are most likely to originate via a micellar nucleation mechanism, whereby the aqueous phase radicals enter the micelles, which are formed from excess SDS above the critical micelle concentration (cmc: $\sim 3\text{x}10^{-3}$ mol$\cdot\ell^{-1}$). Note that the SDS added during the course of reaction (step increase from 10-15 mins) amounts to an aqueous solution of a concentration approximately 6 times the cmc. The level of surfactant together with the surface area of the polymer particles determines the nature of micellar nucleation. The ionic surfactant will maintain an equilibrium between the aqueous and particle phases. The amount of surfactant adsorbed onto the particles directly influences the level of excess aqueous surfactant, so as particle surface area increases, the surfactant available to create micelles and nucleate new particles decreases. Throughout the reaction a continuous re-partitioning of monomer between the different sized particles will also occur. Excess monomer above the saturation value of the particles present in the system

will exist as a separate monomer droplet phase.

The number-averaged PSD evolution [Figure 4.6(a)] shows that the number of particles generated by the secondary micellar nucleation is greater than that generated by the initial homogeneous nucleation. The weight-averaged PSD evolution [Figure 4.6(b)] indicates that the total mass of particles contained in the mode corresponding to the homogeneous nucleation is greater than that of the mode created via the micellar mechanism.



(a)



(b)

Figure 4.6: Number and weight-averaged PSD evolution profiles for medium initiator case with 1 wt% CTA.

The initial (0 to 20 mins) dynamic nucleation and growth period, which results in the two modes of particles and determines their relative magnitude, precedes a period (20 to 120 mins), in which isothermal conditions are maintained and initiator is fed at a constant rate to ensure that any residual monomer is converted, as is common practice in industry.

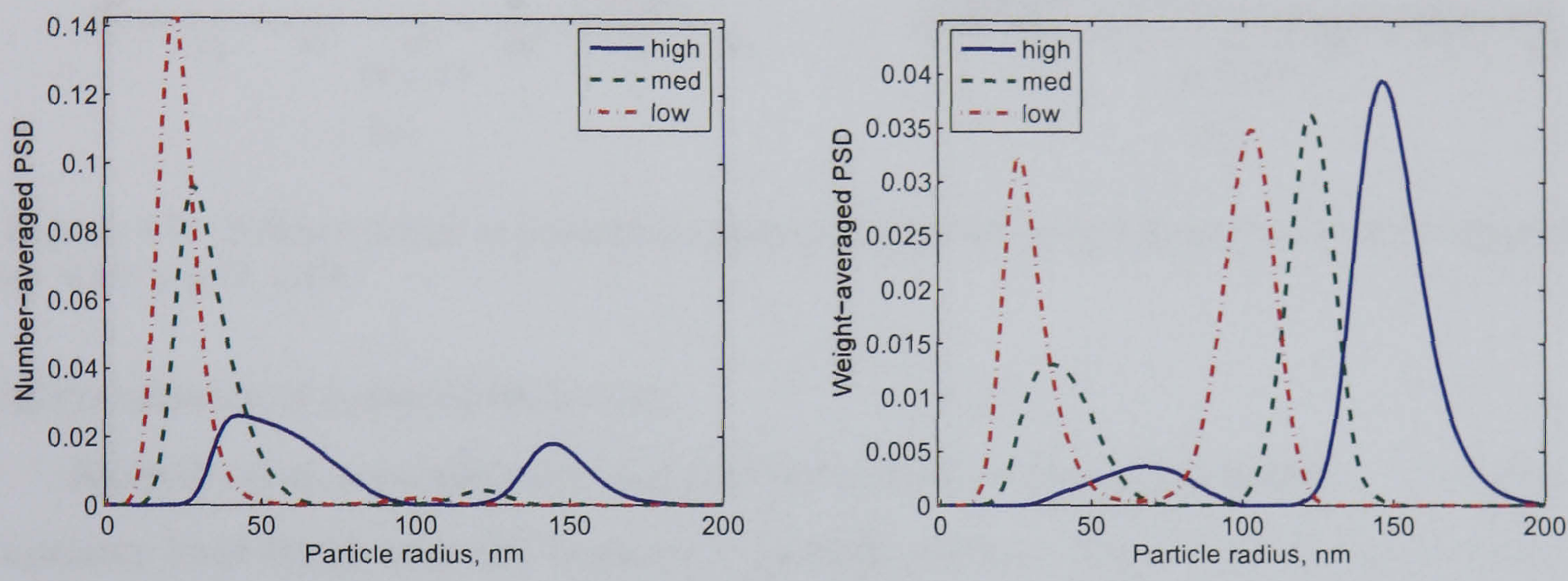
A slight broadening of the peaks is seen during this period.

The particular PSD engineered in this case has similarities to cases produced by Sajjadi and Brooks[160] and Immanuel et al.[33]. Sajjadi and Brooks studied a semi-batch BuA emulsion polymerisation using sodium lauryl sulfate as emulsifier and potassium persulphate as initiator. They used no surfactant in the initial reactor charge. A bimodal PSD was engineered by injecting a shot of surfactant after the initial nucleation event. The ratio of primary to secondary nucleation events was altered by varying initiator and emulsifier concentrations in the feed, temperature, or monomer concentration in the charge. A large enough initial nucleation however led to a monomodal PSD. Despite attempts to produce multimodal PSDs, this was not achieved. Immanuel et al.[33] studied a VAc/BuA semi-batch system, using a redox initiator pair with initial monomer, but no surfactant. to produce an initial homogeneous nucleation. The reduced stability of the primary mode of particles in the absence of surfactant was noted. Stability was thought to be brought about via *in situ* generated surfactants during this stage, which resulted in a decrease in particle number as seen here. A second mode of particles was generated via surfactant addition during the reaction together with a monomer feed. The bimodal system studied in these papers and the case presented here are very similar in character, in that particles are first generated in the absence of surfactant, followed by a period of nucleation resulting from radical entry into micelles.

Figure 4.7 compares the end-time number- and weight-averaged PSDs from the high, medium, and low initiator cases. Referring to Figure 4.7(a) the effect of increasing persulphate levels is as follows: the particles contained within micellar nucleated mode (centred around 25 nm for the low initiator case: dash-dotted line) grow larger (right shift) and become more polydisperse with increasing initiator feed.

The particles within the homogeneously nucleated mode (centered around 100 nm for the low initiator case: dash-dotted line) are also observed to grow larger. The homogeneous mode becomes relatively larger in comparison to the micellar mode as initiator level is increased. This behaviour is partly due to the increased magnitude of initial homogeneous nucleation occurring at higher initial persulphate levels. With more initial persulphate the number and surface area of the homogeneously nucleated particles increases, therefore due to surfactant partitioning effects explained above, the amount of surfactant available

for secondary nucleation decreases (resulting in a smaller micellar nucleation). In addition, increased initiator generates more aqueous phase radicals by reaction with sparing monomer, leading to higher numbers of radicals per particle and increasing growth rates. The increased growth rates during the reaction effect the relative end-time PSDs, and are responsible for the right shift of the homogeneously nucleated particle mode, as well as the micellar nucleated mode.

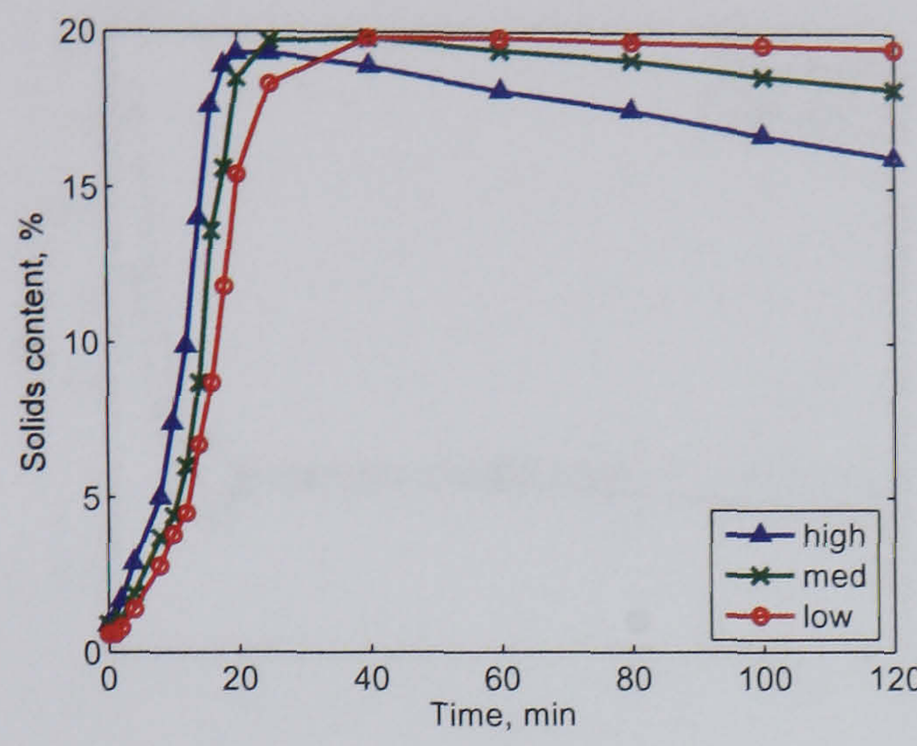


(a) (b)

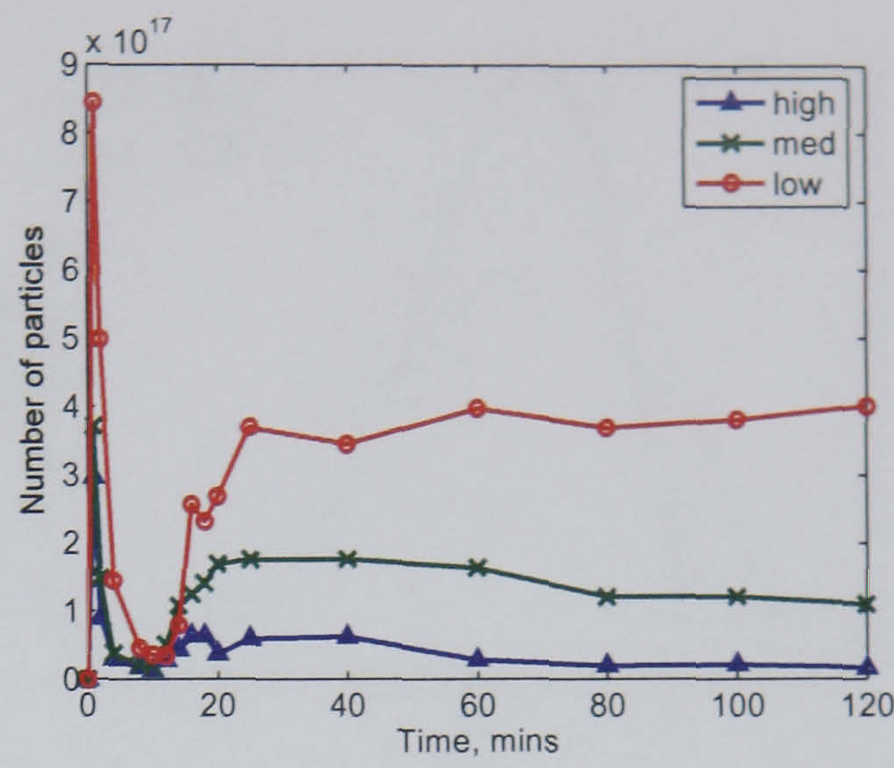
Figure 4.7: Number and weight-averaged end-time PSD profiles for initiator perturbation experiment set with 1 wt% CTA.

Figure 4.8(a) shows the solids content evolution. For higher initiator levels, solids content is seen to increase more rapidly and the maximum is achieved sooner, consistent with higher growth rates. The maximum achieved solids content value is similar for all three cases: approx. 20% and coincides with 100% conversion, at around 20 mins. After most of the monomer has been converted, solids content decreases due to the additional water input that constitutes the persulphate feed solution, causing a dilution of the reactor contents while little or no monomer exists to polymerise and counter this action. The rate of decrease is most for the higher initiator cases.

Figure 4.8(b) shows the evolution of particle number for the initiator perturbation experiment set. After a maximum particle number is reached all experiments show a rapid decrease in particle number, attributed to coagulation effects. Persulphate level appears to have little effect on the magnitude of the decrease, an indication of a dominant coagulation effect early on in the process, a result of the initial weak particle stabilisation



(a)



(b)

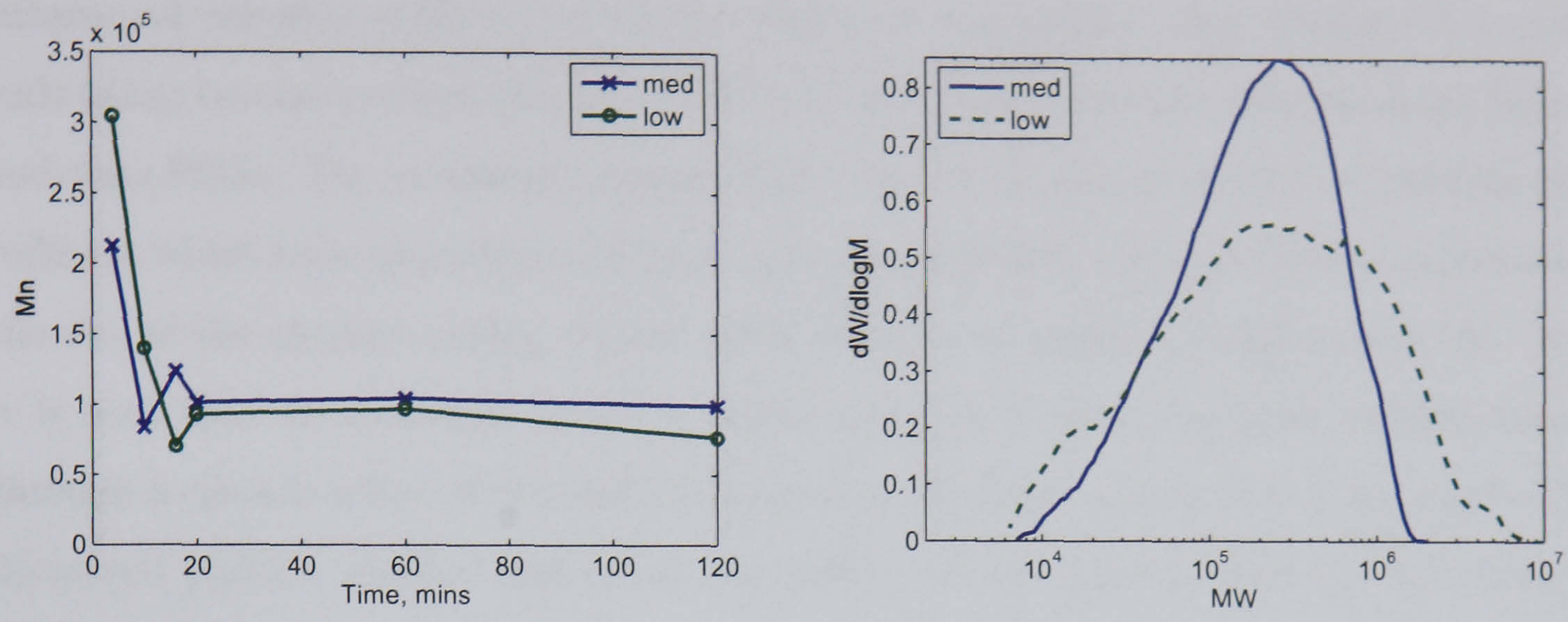
Figure 4.8: Solids content and particle number evolutions for initiator perturbation experiment set with 1 wt% CTA.

in the absence of external surfactant.

After 10 mins, secondary micellar nucleation influences particle number. The lower the initiator level the greater the increase in particle number. This is due to the fact that the smaller initial homogeneous nucleation and lower growth rates, typical of the low initiator levels, result in smaller and less numerous homogeneously-nucleated particles, than those homogeneous modes of particles that result from higher initiator levels. Therefore, upon addition of surfactant, more is used to stabilise the larger surface area presented by the particles in the high initiator case, leaving less surfactant available for the secondary nucleation (observed as a lower final particle number value). Minimal coagulation is observed to take place after the surfactant addition due to its strong stabilisation effect.

4.4.4 Initiator Perturbation: effect on MWD

Figure 4.9(a) shows that, within experimental error bounds, the number-averaged MW remains relatively unchanged for the low and medium initiator cases. However, as can be seen from Figure 4.9(b) the actual distributions (with similar number-average properties), are in fact different. The MW results for the high initiator case are missing here as GPC analysis was precluded due to polymer insolubility in the THF solvent, possibly due to a high degree of gel formation. This was despite CTA being used at 1 wt% per total monomer, which would act to subdue gel formation by reducing the number of branches per



(a) (b)

Figure 4.9: a) Number-averaged MW evolution and b) End-time MWD profiles for medium and low initiator cases: with 1 wt% CTA.

chain (for more details see next section: CTA perturbation). As increasing initiator levels meant that the homogeneously nucleated fraction of particles was greater, it is possible that reactions occurring within the larger particles were influential in gel formation (there is more polymer to accept radicals from donating chains). Therefore, the gel fraction would be greater in cases of high initiator, at least for the initiator range employed in this experiment set.

The polydispersities of low and medium initiator cases are 7 and 2.8 respectively. This is reflected in the MWDs in Figure 4.9(b). The lower initiator case produces a larger fraction of high molecular weight chains. This can be explained by looking at the relative total particle number for the low and medium initiator cases: after 10 mins, the particle number decreases for increasing initiator (c.f. explanation in preceding section). The decreased particle number and increased generation of radicals leads to a higher number of radicals being present in particles. Therefore, the MW achievable, before termination occurs, is lower. On the other hand, decreased initiator leads to decreased radical numbers inside particles, resulting in a larger fraction of high molecular weight chains.

4.4.5 Summary of Initiator Effects

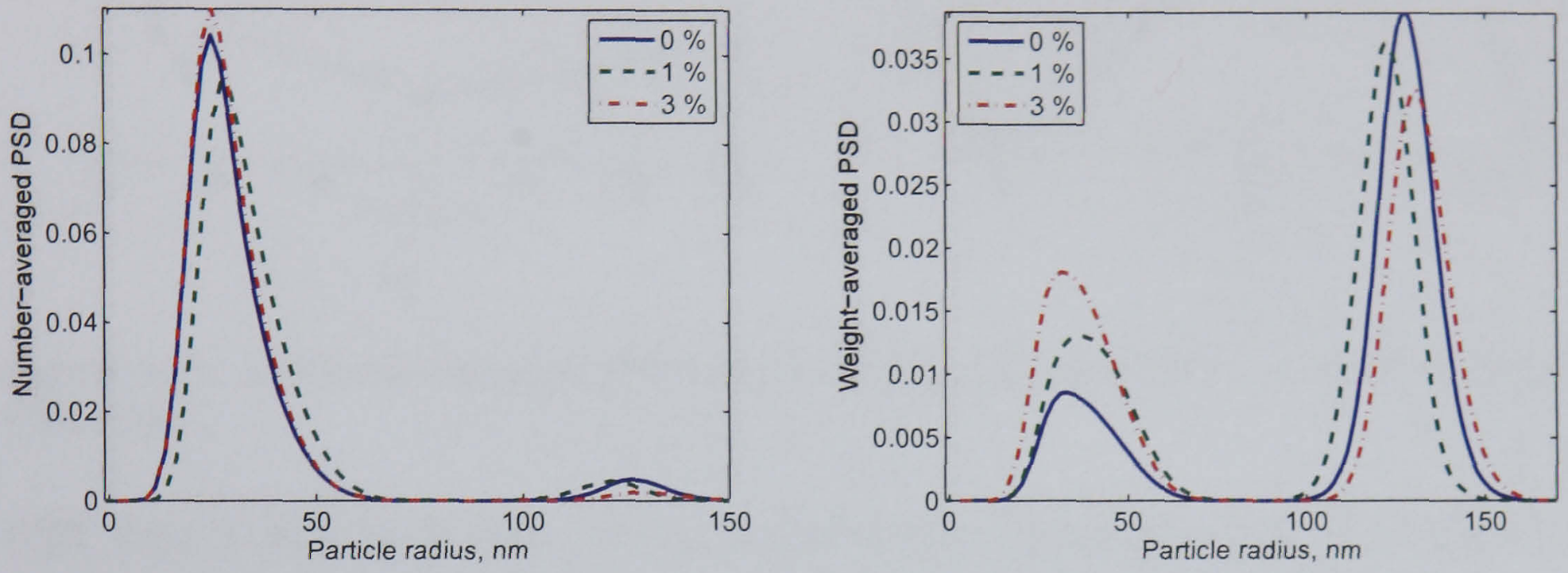
By increasing the amount of initiator used in the initial reaction charge, the magnitude of the homogeneous nucleation is increased. Through surfactant partitioning effects, the

subsequent micellar nucleation event is reduced in magnitude. The differences in magnitude of the two nucleations directly effects the ratio of the two peaks shown in the bimodal end-time PSDs. The increased initiator feed leads to an increased level of aqueous phase radicals, which enter particles causing an increase in growth rates and hence an increase in the size of the particle modes. Where GPC analysis is possible (medium and low cases), it is seen that an increased initiator level results in a lower end-time particle number through a cascade effect of increased homogeneous nucleation on micellar nucleation. The decreased particle number and hence increased radicals entering each particle from the aqueous phase results in a decreased fraction of high MW chains in the MWD. Increased initiator level also results in a more rapid increase in solids content of the latex, due to increased growth meaning a maximum conversion is reached in less time.

4.4.6 CTA Perturbation: effect on PSD & MWD

Dried latex samples from experiments without CTA apparently reached impractically high molecular weights precluding their dissolution in organic solvent (THF), a step required for the determination of molecular weight. It seems that chain transfer to polymer (producing long-chain branching), typical for VAc[161] and recently found in BuA,[162] was most probably occurring in the absence of CTA (which would otherwise compete with the polymers for chain transfer reactions), therefore, together with prevalent cross-linking reactions via combination, produced a gel. As mentioned, the model developed for this process does not account for chain transfer to polymer, therefore in light of the findings of these experiments it is important to realise the model limitations in cases wherein CTA is not used. To reduce the amount of gel formation, CTA was added to the monomer at various concentrations. CTA partitions between the phases and provides a highly reactive site for chain-transfer of active radicals from growing polymer chains. CTA reduces the amount of gel formation by influencing the radical dynamics such that the dead polymer molecules are shorter on average and it reduces the average life time of a polymer chain. thereby possibly reducing the number of cross-links per polymer chain and the length of the branches. Upon transfer to CTA the resultant species will polymerise by free radical chain addition in much the same fashion as a short chain radical produced from monomer. It was speculated that increased levels of CTA would provide an increased concentration

of chain transfer sites, with the effect of reducing overall molecular weight. With CTA addition, the latex produced readily dissolved in THF and could be processed for molecular weight determination using GPC. The effect of perturbing CTA concentration on PSD and MWD was studied [Table 4.1: 0%, 1%, 3% cases].

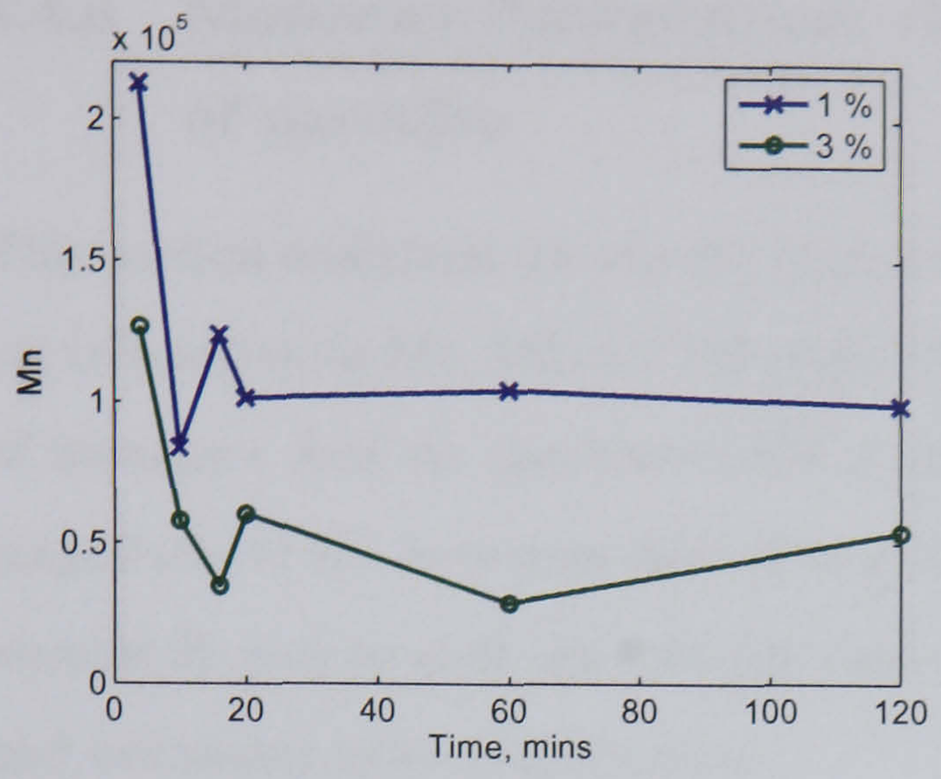


(a) (b)

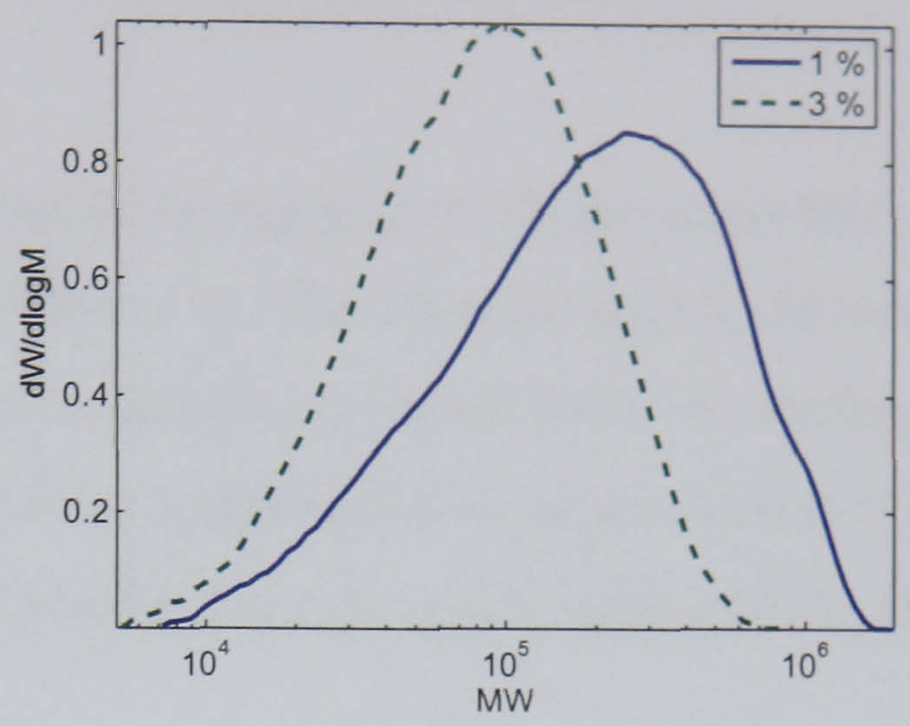
Figure 4.10: End-time PSD profiles for CTA perturbation experiment set.

Figure 4.10 shows the effect of CTA concentration on end-time PSD profiles. The number-averaged PSD profiles [Figure 4.10(a)] show minimal response to varying CTA level. A more discernable effect is visible in the weight-averaged PSDs [Figure 4.10(b)]. As CTA concentration is increased the magnitude of the micellar peak (centred around 35 nm) increases. This is due to the dynamic interactions between the processes of particle entry and desorption. The increased chain-transfer reactions, a result of increased CTA concentration, favours desorption from preexisting particles (those generated by homogeneous nucleation). Thereby, when the critical micelle concentration is reached, there will be a greater chance of aqueous phase oligomers entering the generated micelles, resulting in a larger number of micellar nucleated particles. Figure 4.10 shows that there is little difference in the sizes of homogeneous modes. This is due to the CTA effect being most predominant at the highest concentration: upon addition of monomer feed at 10 mins. This also coincides with the surfactant feed, therefore the main effect of CTA is on desorption around this time, greatly impacting the level of micellar nucleation.

The 0 wt% CTA case resulted in a high insoluble gel fraction (>60%), precluding MW measurement. Figure 4.11(a) indicates the effect on number-averaged MW of increasing



(a)



(b)

Figure 4.11: a) Number-averaged MW evolution and b) End-time MWD profiles for 1 and 3 wt% CTA cases.

CTA from 1 wt% to 3 wt%. At the lowest CTA concentration the end-time number-averaged MW is approx. 100 k, halving to approx. 50 k when CTA is increased to 3 wt%. The MWDs [Figure 4.11(b)] highlight the large reduction in long chains and increase in short chains, a direct effect of the strong CTA influence on chain-transfer reactions. This means that the entire MWD becomes less positively skewed and decreases in polydispersity as a result of CTA action.

4.4.7 Summary of CTA Effects

Increasing CTA concentration positively effects short chain production, therefore increasing desorption levels. This factor increases the level of aqueous phase radicals which then enter micelles upon surfactant addition, and thereby cause a marked increase in the number of micellar nucleated particles across the experiment set. With the current experiments, the growth of particles is not effected due to the shotwise addition of CTA coinciding with surfactant addition, thus the CTA effect is limited to nucleation events. Increasing CTA imparts a considerable and more direct effect on MWD. This effect is a consequence of increased chain transfer, limiting the growth of chains via polymerisation within particles and decreasing MW.

4.4.8 Monomer Perturbation: effect on PSD, solids content and number of particles

This section examines the results from experiments aiming to perturb monomer feed, and are referred to as M1, M2 and M3 cases [as per Table 4.1]. The effect of varying the amount of monomer feed on end-time PSD is elucidated clearly by Figure 4.12. Increasing the magnitude of the monomer feed causes the micellar nucleated mode of particles (centered around 35 nm) to shift towards the right and broaden i.e. the particles are growing larger and becoming more polydisperse.

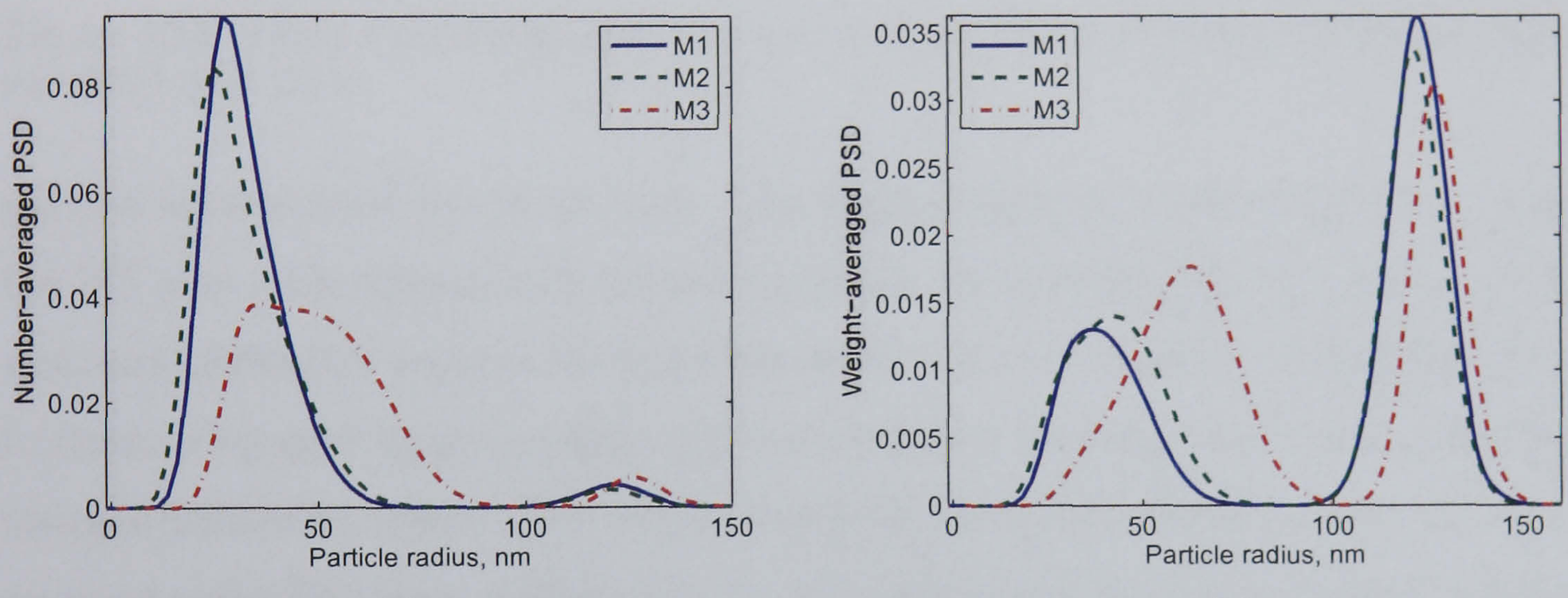
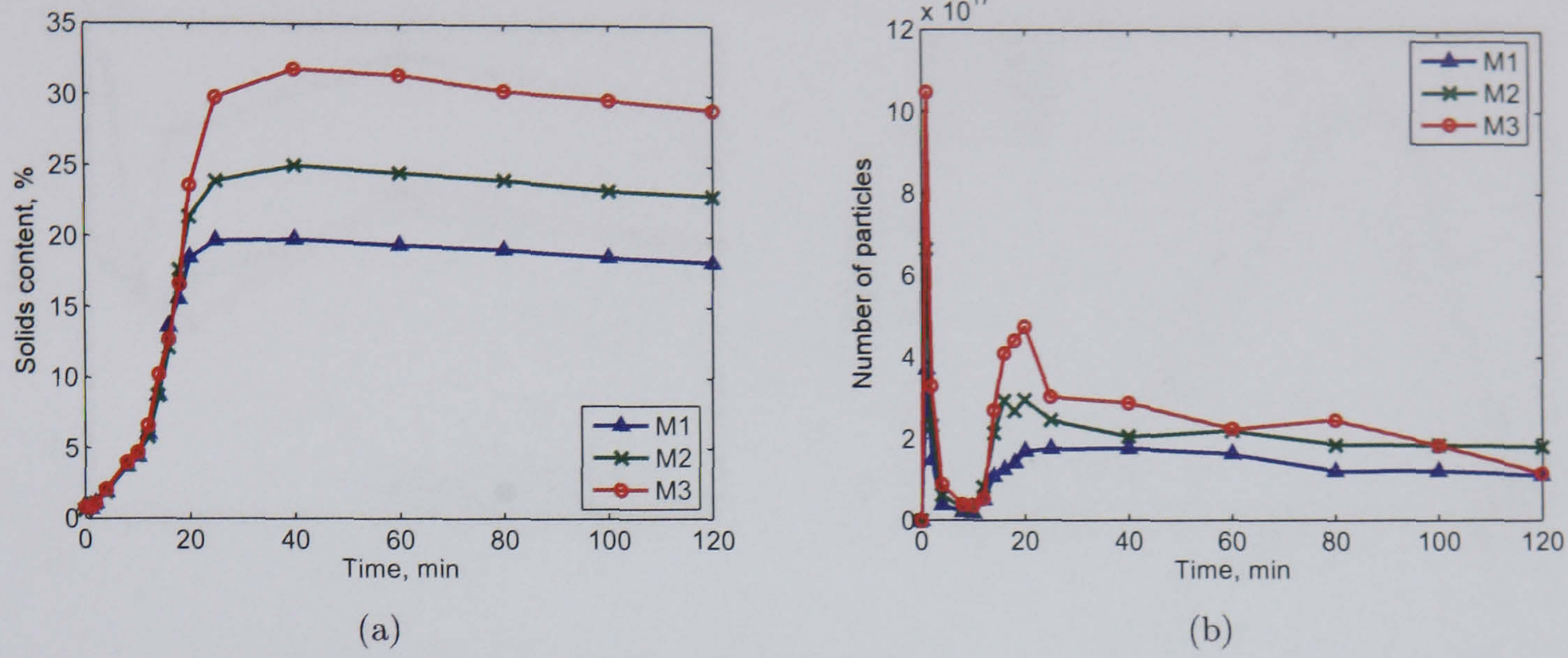


Figure 4.12: End-time PSD profiles for monomer perturbation experiment set with 1 wt% CTA.

Solids content evolutions are shown in Figure 4.13(a). Solids are observed to increase rapidly, the rate of increase being similar for all three cases (this is expected as recipes are identical until monomer feed at 10 min). Case M1 reaches a maximum of ~20% solids at around 25 min. Case M2 has a prolonged increase in solids content due to additional monomer supplied, and reaches a maximum slightly later than M1 at a value of ~25%. Case M3 shows a further increase in maximum solids achieving a maximum value of ~32%. The monomer reaches total conversion within 30 mins in all cases, with a slower rate of approach to maximum conversion for a larger monomer feed capacity.

Figure 4.13(b) shows the evolution of particle number for the monomer perturbation experiment set. The particle number profiles are similar for all cases for times up to ~10 min. After 10 min, at the time of the monomer and emulsifier feed commencing, the



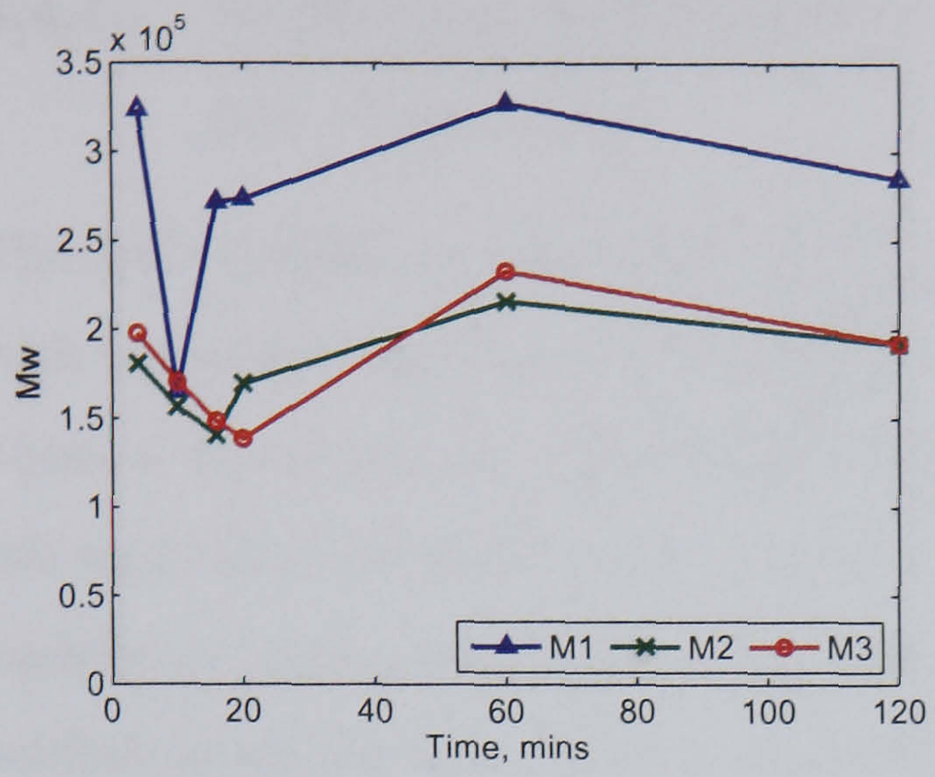
(a) (b)

Figure 4.13: Solids content and particle number evolution for monomer perturbation experiment set with 1 wt% CTA.

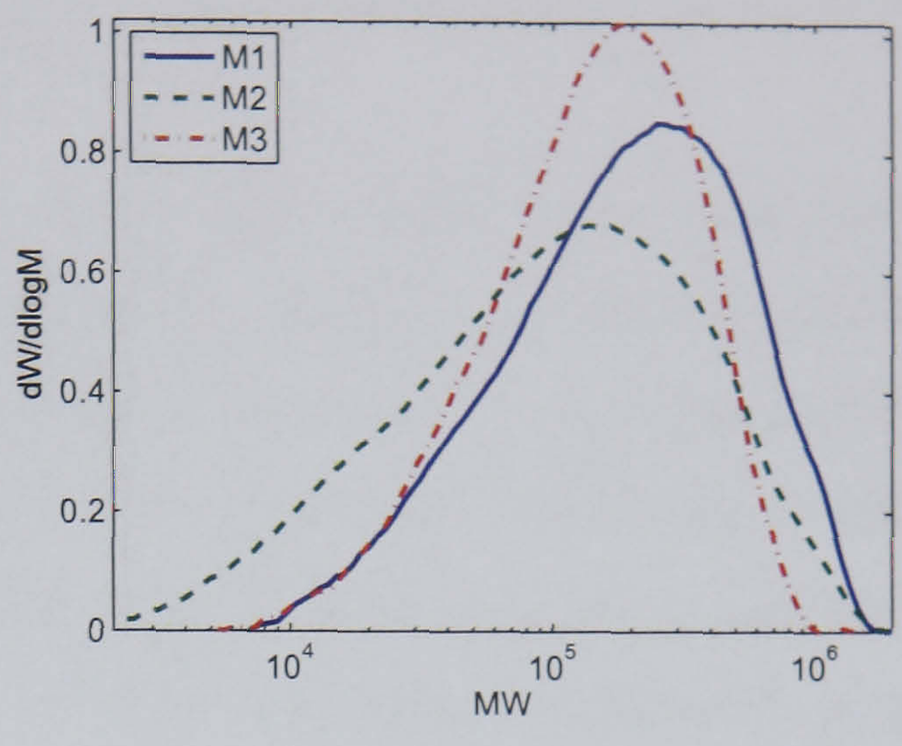
particle number increases in all cases. The largest increase in particle number is seen in the M3 case with progressively smaller increases for M2 and M1. At 20 min there is a maximum difference between the 3 cases in terms of particle number. This difference is due to there being more aqueous phase oligomers at higher monomer feed levels enhancing the micellar nucleation event. After the maximum disparity in particle number, the fact that more particles have been nucleated in the M3 case means that there is lower coverage by surfactant and as a result we see a large decrease in particle number due to coagulation for M3, and a progressively smaller decrease for smaller monomer feeds (case M2 then M1). Due to this differential coagulation phenomena, the particle number difference between the three cases is greatly reduced.

4.4.9 Monomer Perturbation: effect on MWD

Figure 4.14(a) indicates that as the monomer feed is increased in magnitude from M1 to M2 case, the weight-averaged MW decreases considerably (end-time values are approx. 290 k for M1 and 200 k for M2). Case M3 does not decrease any further in terms of weight-averaged MW. The MWDs in Figure 4.14(b) allow interpretation of the average MW data. In theory the first stage of all the reactions in this set should be identical, until the addition of the monomer feed (at 10 mins). The results show that by increasing the magnitude of the monomer feed, the proportion of high MW chains in the MWD decreases. The



(a)



(b)

Figure 4.14: a) Weight-averaged MW evolution and b) End-time MWD profiles for monomer perturbation experiment set with 1 wt% CTA.

increased monomer feed resulted in a prolonged particle and aqueous saturation period. The aqueous phase radicals would therefore be present for a longer period, thereby entering particles and increasing the relative chance of termination, reducing the average MW. The latter effect was apparently greater than the effect of increased monomer concentration, which would be expected to increase MW.

4.4.10 Summary of Monomer Effects

Increasing the monomer feed affects the system in terms of increased micellar nucleation and particle growth within this mode. The homogeneously nucleated particles are somewhat less affected. The rate of conversion is similar in all cases, however a proportionally higher maximum solids content is attained for higher monomer feeds. Increased monomer feed leads to a higher jump in particle number due to enhanced micellar nucleation, however the difference in particle number is short lived due to a limited surfactant concentration and associated coagulation, even reversing the trend. With respect to MW of the latex, increased monomer feed leads to higher entry rates for a prolonged period, thereby limiting the fraction of high MW chains achievable. In this experiment set, monomer perturbation is seen to strongly effect both PSD and MWD.

4.4.11 Surfactant Perturbation: effect on PSD, solids content and number of particles

The PSD profiles in Figure 4.15 indicate that the S1 case results in a monomodal PSD with a shoulder evident in the number-averaged plot, whilst S2 and S3 both give clear bimodal distributions. The timing of the surfactant feed in S1 is such that instead of two sequential nucleation events (as in all other cases), a combined homogeneous/micellar nucleation takes place early in the reaction. The large, singular nucleation event in S1 is evident in the particle number profile [Figure 4.16(b)]. Approximately 2.5×10^{18} particles are nucleated in the S1 case, clearly more than in the other two cases. These particles, due to their large surface area undergo rapid coagulation, until a time when they reach a state in which the surface coverage by surfactant is able to provide more effective stabilisation. The PSDs [Figure 4.15] of S2 and S3 are bimodal, due to there being sufficient time between the initial homogeneous nucleation event and subsequent surfactant addition. The surfactant feed profiles in S2 and S3 are the same, however the concentration of S3 (8%) is double that of S2 (4%). The extra surfactant molecules in case S3 are responsible for an increased aqueous phase micelle concentration at around 10 mins. Due to there being more micelles in S3, there is a greater chance of aqueous oligomers entering micelles than particles, leading to a larger micellar nucleation event. Hence, the relative size difference between the micellar and homogeneous peaks in S3 is reduced further from that

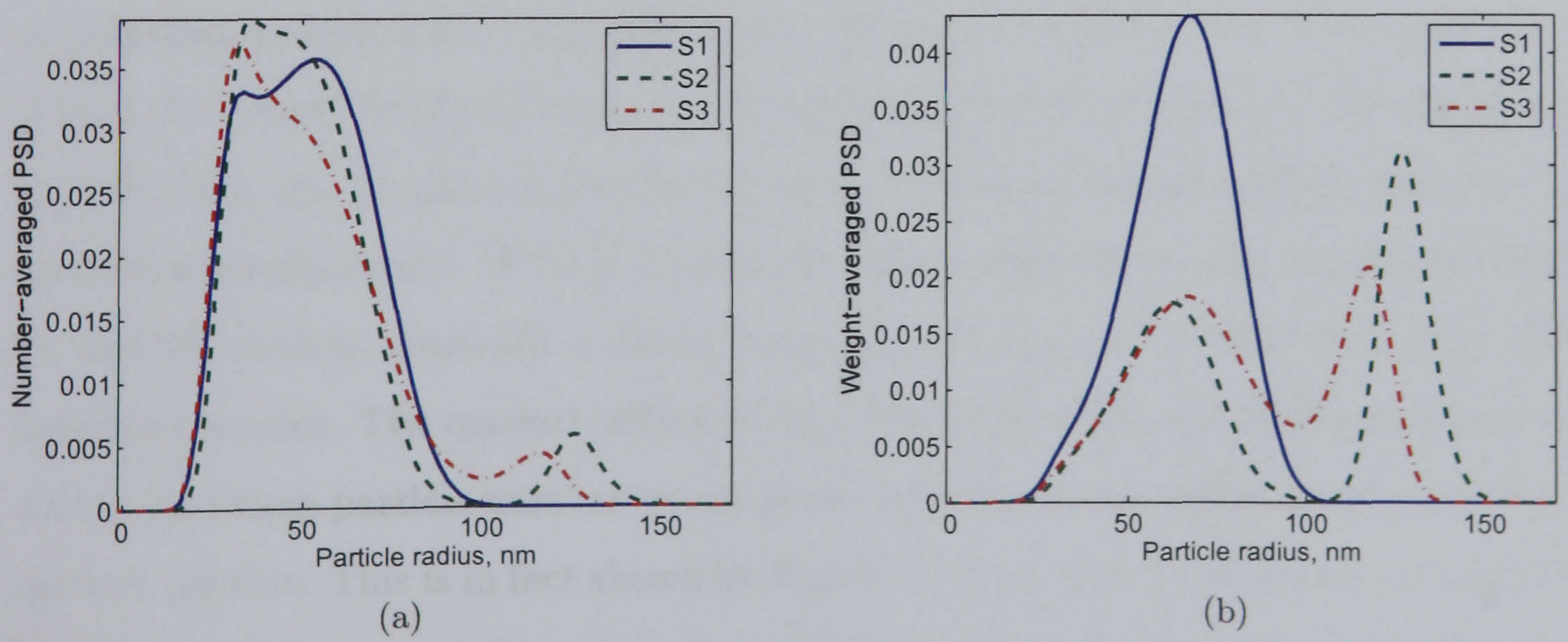
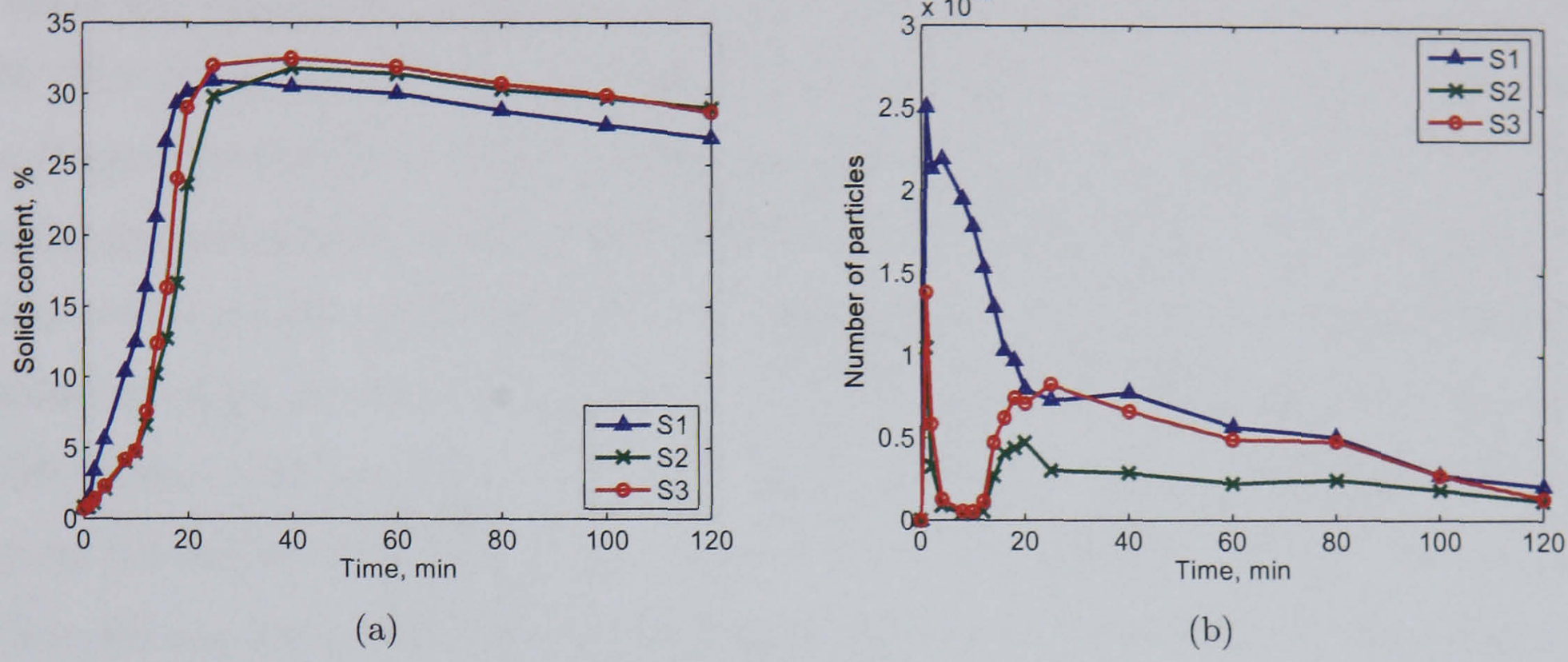


Figure 4.15: End-time PSD profiles for surfactant perturbation experiment set with 1 wt% CTA.

displayed in case S2.



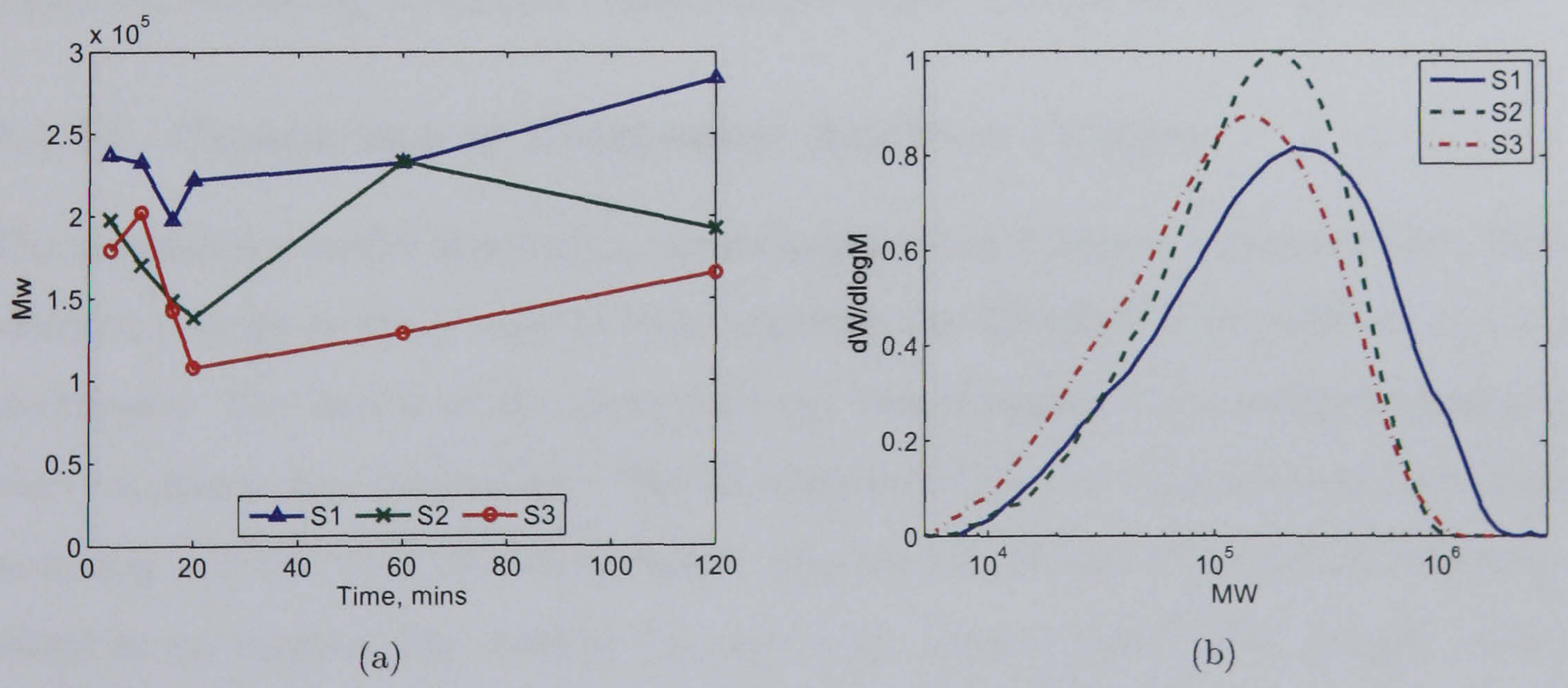
(a) (b)

Figure 4.16: Solids content and particle number evolution for surfactant perturbation experiment set with 1 wt% CTA.

Figure 4.16(b) shows the larger micellar nucleation event of S3 in terms of a greater particle number increase after approx. 10 min. S3 reaches a particle number almost twice that of S2 at around 20 mins. In Figure 4.16(b), case S2 shows a greater degree of coagulation than S3 immediately after the micellar nucleation event, due to less stabilisation from surfactant. The particle number in S2 then stabilises, and indicates a lower rate of coagulation than S3. This effect occurs due to there being a greater magnitude of micellar nucleation in S3, resulting in a disparity between the increased particle surface area and increased surfactant level, with a non-linear effect existing between the degree of increased stabilisation provided and the surface area. S1 shows a similar level of coagulation to S3 during the period following the micellar nucleation event, despite the increased amount of surfactant, due to the relative size of particles and increased surface area over which surfactant could adsorb. What is interesting here, is that all particle number profiles, S1, S2 and S3, seem to approach a similar value towards the end of reaction due to different coagulation rates. The marked difference in PSDs between S1 and S2/S3, together with a similar end-time particle number would seem to indicate that solids must be different to account for this. This is in fact shown by Figure 4.16(a), with S1 achieving a slightly lower maximum solids content than the other reactions. The rate of increase in solids content up to the maximum is higher in S1 than in the other two cases.

4.4.12 Surfactant Perturbation: effect on MWD

Figure 4.17 shows that weight-averaged MW is highest for case S1 and is lowest in case S3. The reason for case S1 reaching the highest average molecular weight, reflected in the largest fraction of high-MW chains in the MWD [Figure 4.17(b)], is due to the large initial particle number and small particle size. The large number of particles means that there will be a lower number of radicals per particle to promote growth via polymerisation. Before 20 mins, the particle number in cases S2 and S3 is considerably lower than in S1. This is due to the combined nucleation event resulting from the surfactant level being above the cmc at early times in S1 compared to the homogenous nucleation in S2 and S3. Thus, there is likely to be more radicals per particle in general, promoting termination and lowering MW. Comparing the MWDs of case S2 and S3, there is a decrease in the high MW and an increase in the low MW fraction of the MWD [Figure 4.17(b)] as surfactant concentration is increased. This is due to the ratio of number of homogeneous and micellar nucleated particles. The more predominant micellar mode of particles in case S3 means that the rate of entry will be altered such that more radicals exist within smaller particles lowering MW due to increased termination and lower monomer concentration.



(a) (b)

Figure 4.17: a) Weight-averaged MW evolution and b) End-time MWD profiles for surfactant perturbation experiment set with 1 wt% CTA.

4.4.13 Summary of Surfactant Effects

The timing of surfactant was the most important factor in determining the nature of the PSD (i.e. whether a bimodal PSD was produced or not). When surfactant addition is sufficiently delayed following the initial homogeneous nucleation period, a bimodal PSD is produced. It is important to understand the mechanisms governing the production of bimodal PSDs considering that they have been shown to lead to improved end-product properties (e.g. viscosity and packing fraction). If this delay period is too short, a combined nucleation results in a large, single mode of particles. When two distinct nucleation events are engineered, an increased surfactant concentration leads to an enhanced micellar nucleation event increasing the relative size of the micellar particle mode in the end-time PSD and leading to a greater increase in particle number. The increased availability of surfactant molecules results in a smaller drop in particle number immediately following micellar nucleation. The rate of conversion is fastest in the case where a monomodal PSD is produced. Early surfactant addition results in the highest initial number of particles, therefore the radical number per particle is low promoting growth of polymer chains, leading to an increased fraction of high MW chains in the MWD. Where a bimodal PSD is produced, increasing surfactant concentration causes a small decrease in final MW.

4.4.14 Comparison of Component Addition Policies

The preliminary model simulation results presented in Chapter 3 demonstrated different addition policies to those used in these experiments, therefore it is pertinent to compare the results. The model at this point had not been compared to experiment and parameters consisted of a nominal set. The simulation in Chapter 3 incorporated a continuous monomer addition over the whole batch, whereas in this experimental set monomer was added in an impulse like fashion (i.e over a far more compact time frame). The shot feeding policy was chosen as a convenient and proven method to produce bimodal PSDs, a favorable type of distribution typical of many industrial operations for reasons explained earlier. The difference in feeding caused the particles contained within the homogeneously nucleated peak (to the RHS of the distribution) in Figure 3.14 to grow larger, the cascaded effect of which reduced the magnitude of the subsequent micellar nucleation (i.e.

the relative size of the peak to the LHS of the distribution decreases). In the experimental case [Figure 4.12] the homogeneously nucleated peak also shifts to the right, however the micellar peak (the LH peak of the distribution) becomes larger and shifts to the right, highlighting the effect of partitioning of the monomer impulse amongst the distribution of particles in the system. With respect to the molecular weight indicated by the simulation case in Chapter 3 (continuous monomer feed), the system distribution of molecular weight increases as the monomer feed is increased. This is in contrast to the apparent decrease in final weight-averaged molecular weight as demonstrated by the experimental system.

The difference in feeding policy of CTA appears to effect the PSD results. In Chapter 3 (simulation case), where CTA was added in a continuous fashion over the batch, the perturbation of CTA seems only to effect MWD results, with minimal effect on PSD. A larger effect on PSD is seen when CTA is added in a concentrated form together with monomer feed, as in the experimental case. This effect should be taken into account wherein CTA is desired to be used as a control variable to impart change to MWD without effecting PSD.

Finally, in the case of initiator perturbation, for the experimental set the concentration of initiator feed was increased in proportion to the initial amount of initiator. The simulation in Chapter 3 only involved an increase of initiator feed rate and showed the same trend in PSD as in the experiment, but to a far lesser extent. This shows that in controlling PSD, the initial level of initiator has a greater effect than initiator feed rate due to the extent that the initial mode of particles impacts subsequent nucleation events.

4.5 Preliminary Model Validation Results

The experimental studies presented above illustrate the ability to independently control both PSD and MWD. They also illustrate the complexity of the interaction that exists between PSD and MWD, and the plethora of intricate mechanisms that define the emergence of these distributed features. A mechanistic model of PSD and MWD will benefit from comparison to the experimental data, and on the other hand, once sufficient mechanistic knowledge is incorporated, can provide a facility to aid experimental design. A model may also provide a means to quantify the restrictions on simultaneous control of

PSD and MWD and to map out reachable regions.

The emulsion polymerisation model described in Chapter 3 was used to simulate the conditions used in the preceding experiments. The objective was to deduce the capability of the model to reproduce experimental trends in response to perturbations in process manipulations. A preliminary comparison will be made to verify the model features and suggest further refinement. Those parameters tuned are highlighted in Table 4.2 and 4.3. A single case ('high' initiator) was used to tune minimal parameters by hand, with no further tuning done for comparison to further cases, making this a good test of model capability. Only the values different to the nominal parameter set indicated in Chapter 3 are shown. The following sections compare experimental results and model predictions.

Table 4.2: Tuned values for kinetic parameters used in model.

Kinetic Parameter	Value	Units	Ref.
$k_{p11} = k^{w}_{p11}$	16.45×10^{3}	$\ell \cdot mol^{-1} \cdot s^{-1}$	
$k_{p12} = k^{w}_{p12}$	44.5×10^{4}	$\ell \cdot mol^{-1} \cdot s^{-1}$	
$k_{p21} = k^{w}_{p21}$	19.5×10^{1}	$\ell \cdot mol^{-1} \cdot s^{-1}$	
$k_{p22} = k^{w}_{p22}$	12.35×10^{2}	$\ell \cdot mol^{-1} \cdot s^{-1}$	
$k_{tr11} = k^{w}_{tr11}$	46.5×10^{-3}	$\ell \cdot mol^{-1} \cdot s^{-1}$	
$k_{tr12} = k^{w}_{tr12}$	46.5×10^{-3}	$\ell \cdot mol^{-1} \cdot s^{-1}$	
$k_{tr21} = k^{w}_{tr21}$	26.5×10^{-4}	$\ell \cdot mol^{-1} \cdot s^{-1}$	
$k_{tr22} = k^{w}_{tr22}$	46.5×10^{-3}	$\ell \cdot mol^{-1} \cdot s^{-1}$	
$k_{trA1} = k^{w}_{trA1}$	9.54×10^{3}	$\ell \cdot mol^{-1} \cdot s^{-1}$	[163]
$k_{trA2} = k^{w}_{trA2}$	9.54×10^{3}	$\ell \cdot mol^{-1} \cdot s^{-1}$	[163]
$k_{t11} = k^{w}_{t11}$	5.25×10^{7}	$\ell \cdot mol^{-1} \cdot s^{-1}$	
$k_{t12} = k^{w}_{t12}$	11.8×10^{5}	$\ell \cdot mol^{-1} \cdot s^{-1}$	
$k_{t21} = k^{w}_{t21}$	11.8×10^{5}	$\ell \cdot mol^{-1} \cdot s^{-1}$	
$k_{t22} = k^{w}_{t22}$	8×10^{3}	$\ell \cdot mol^{-1} \cdot s^{-1}$	
k_{r1}	100	$\ell \cdot mol^{-1} \cdot s^{-1}$	
k_{r2}	100	$\ell \cdot mol^{-1} \cdot s^{-1}$	
k_{d}	28.8×10^{-7}	s^{-1}	

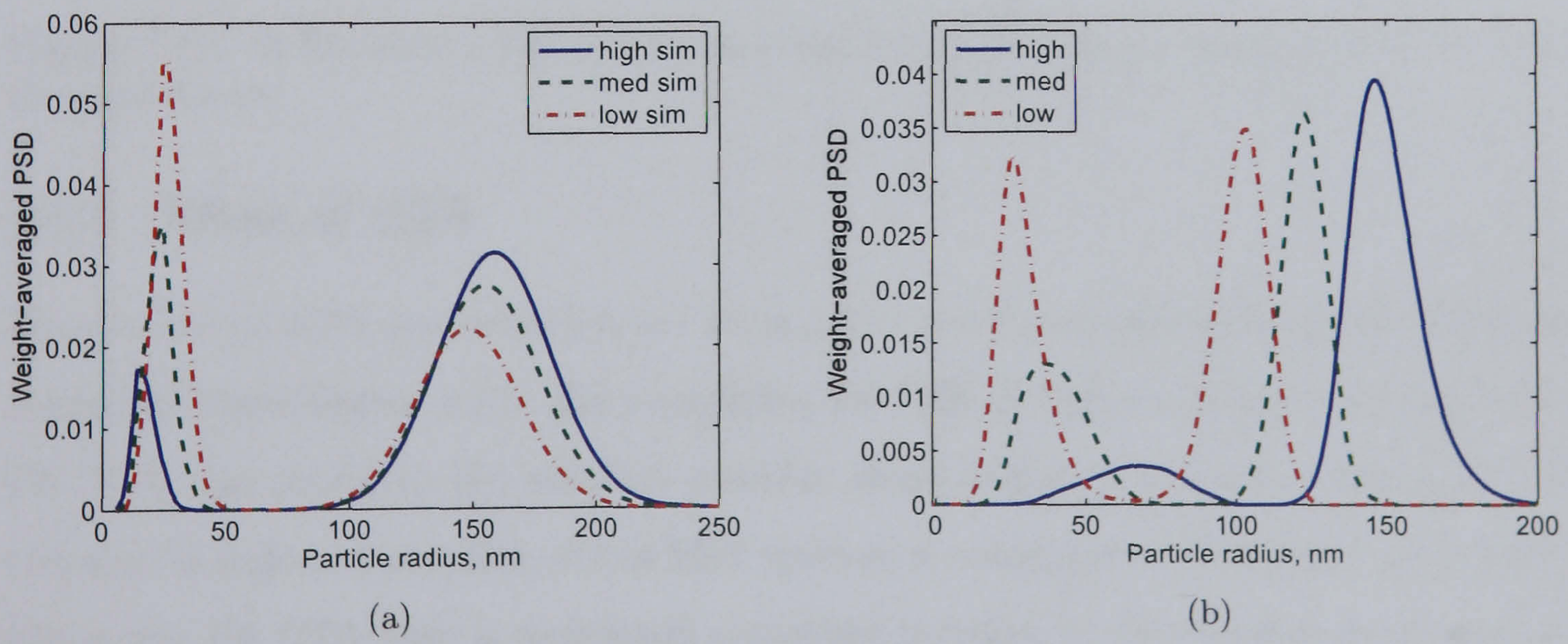
Table 4.3: Tuned values for physical constants used in model.

Physical Constant	Value	Units
cmc	1.5×10^{-3}	$mol\ell^{-1}$
α_{ms}	42×10^{-19}	m^2
D_{w1}	6 (n=2)	$cm \cdot s^{-1}$
D_{w2}	11 (n=2)	$cm \cdot s^{-1}$

4.5.1 Effect of Initiator

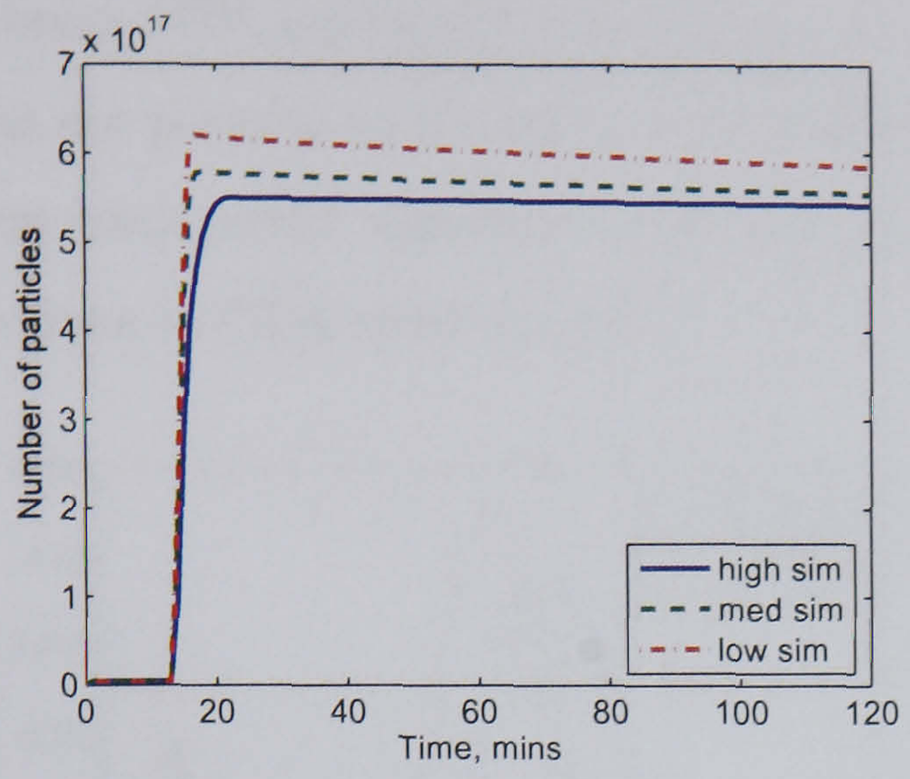
The end-time weight-averaged PSD profiles in Figure 4.18(a), resulting from a tuned simulation, are representative of those produced experimentally [Figure 4.18(b)] in that they indicate an increasing initial homogeneous nucleation for increasing initiator levels. Simulations also show that subsequent micellar nucleation events, reflected in particle number evolutions [Figure 4.19], are effected in a similar fashion to that demonstrated by experiment i.e. micellar nucleation decreases for increasing initiator. The simulation however does not appear to be able to properly capture the sharp initial increase in particle number due to homogenous nucleation which may account for some of the discrepancy in PSD. Similar ratios between PSD peaks are shown in both cases. The simulation however appears to show less growth in the micellar nucleated modes than is shown experimentally, suggesting a need to improve the growth model and its parameters.

The experimental average MWs shown in Figure 4.20(b) were too close to allow definitive deductions to be made, however the model predictions [Figure 4.20(a)] clearly indicate an increase in end-time average MW, for a decrease in initiator levels. This would seem to be confirmed in the experimental results for MWD where an increasing fraction of high MW chains is produced in the MWD for lower initiator levels [see Figure 4.9(b)]. The experimental result for the molecular weight in the high persulphate case was not obtainable due to gel formation as explained earlier.

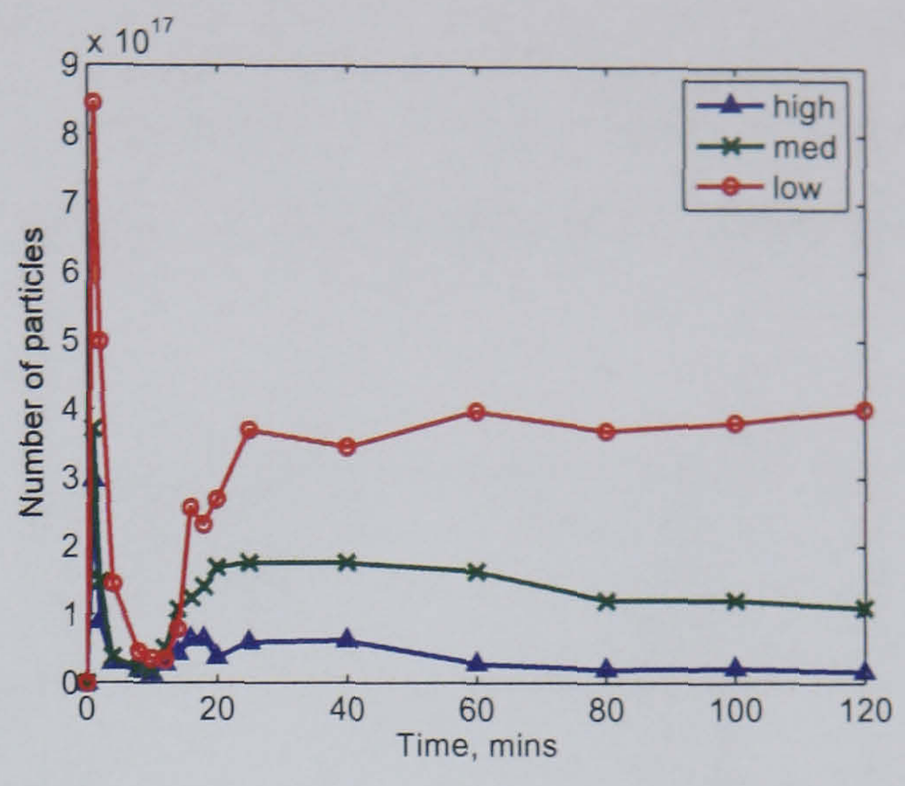


(a) (b)

Figure 4.18: a) Simulation and b) Experimental results for end-time weight-averaged PSD for initiator perturbation set.

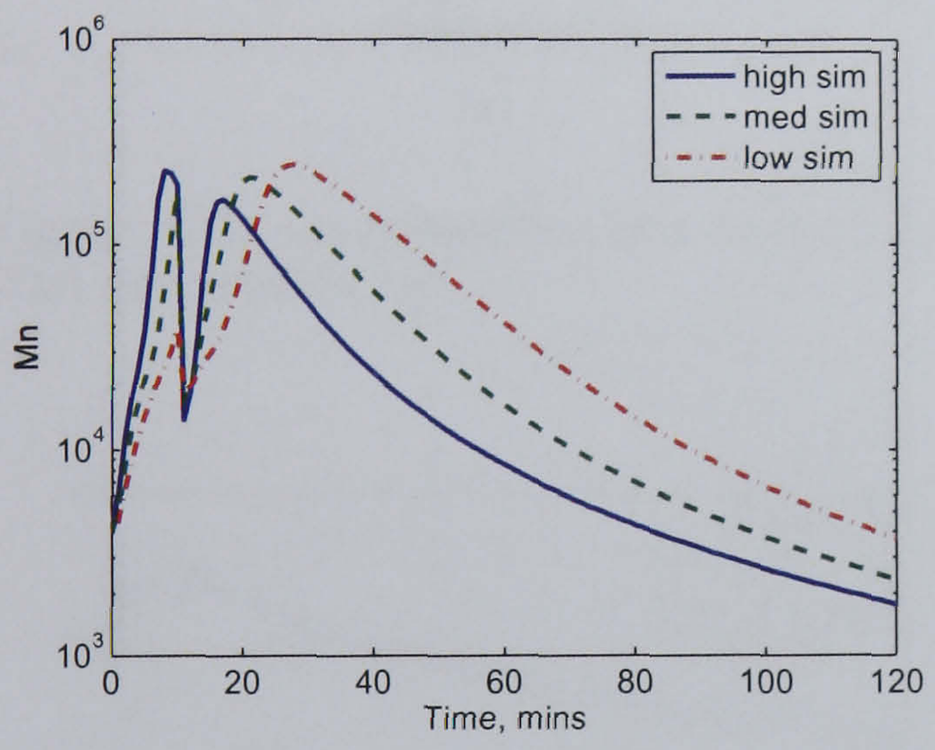


(a)

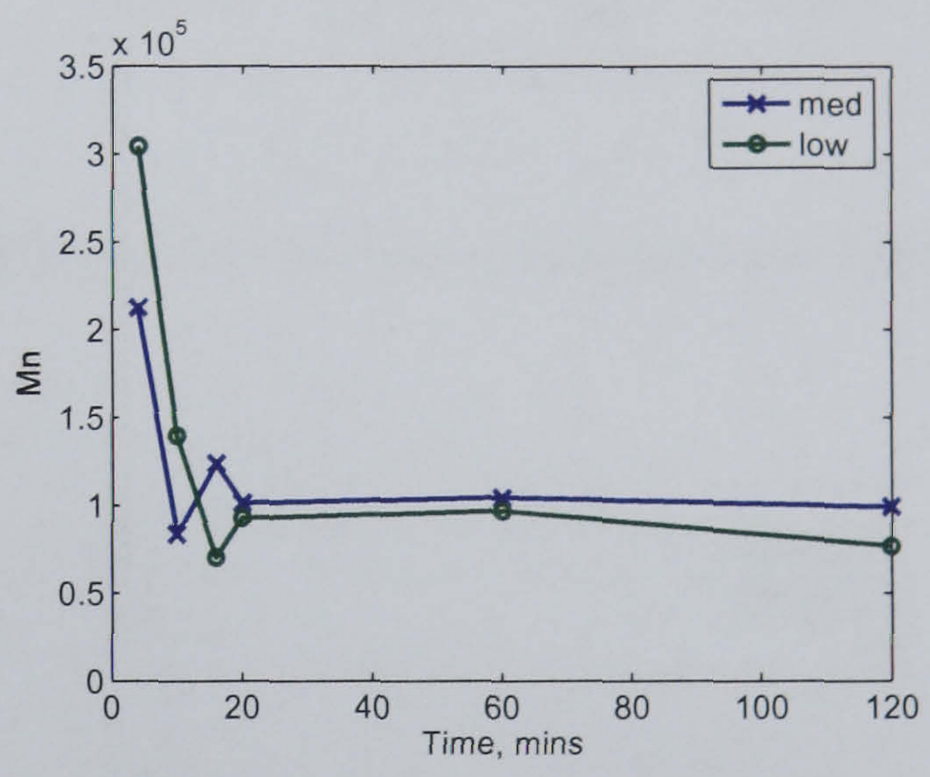


(b)

Figure 4.19: a) Simulation and b) Experimental results for particle number for initiator perturbation set.



(a)



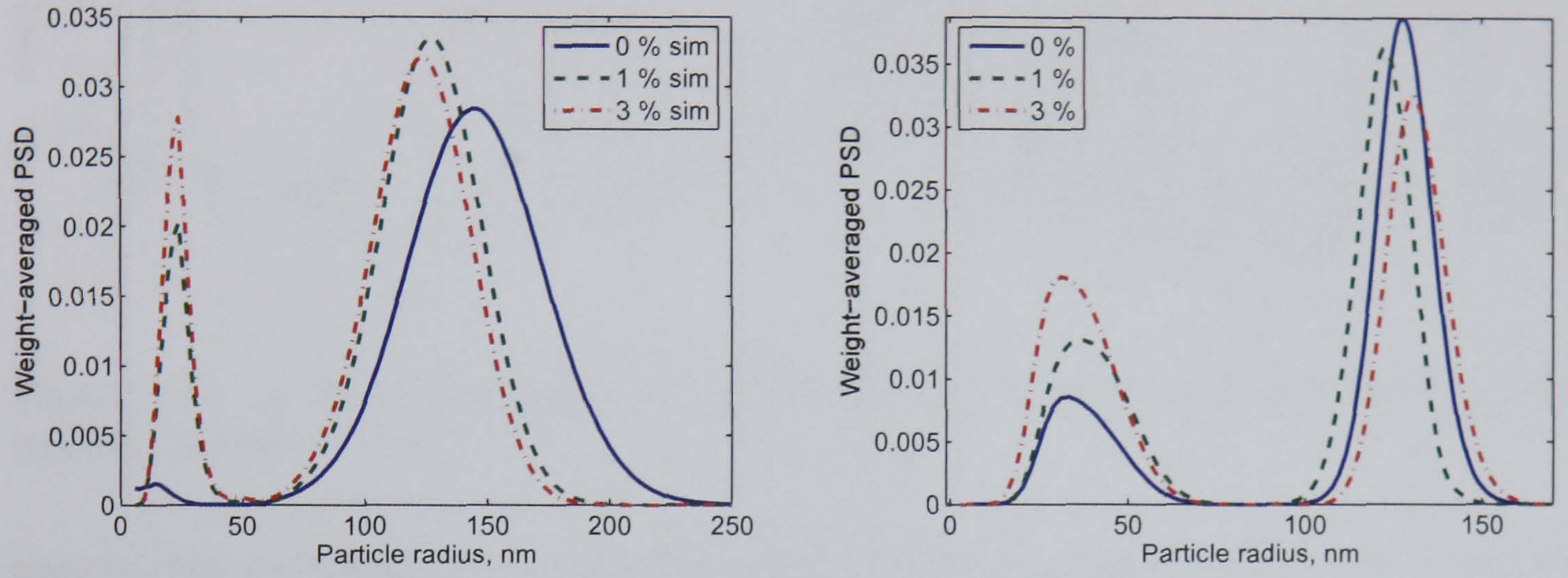
(b)

Figure 4.20: a) Simulation and b) Experimental results for number-averaged MW for initiator perturbation set.

4.5.2 Effect of CTA

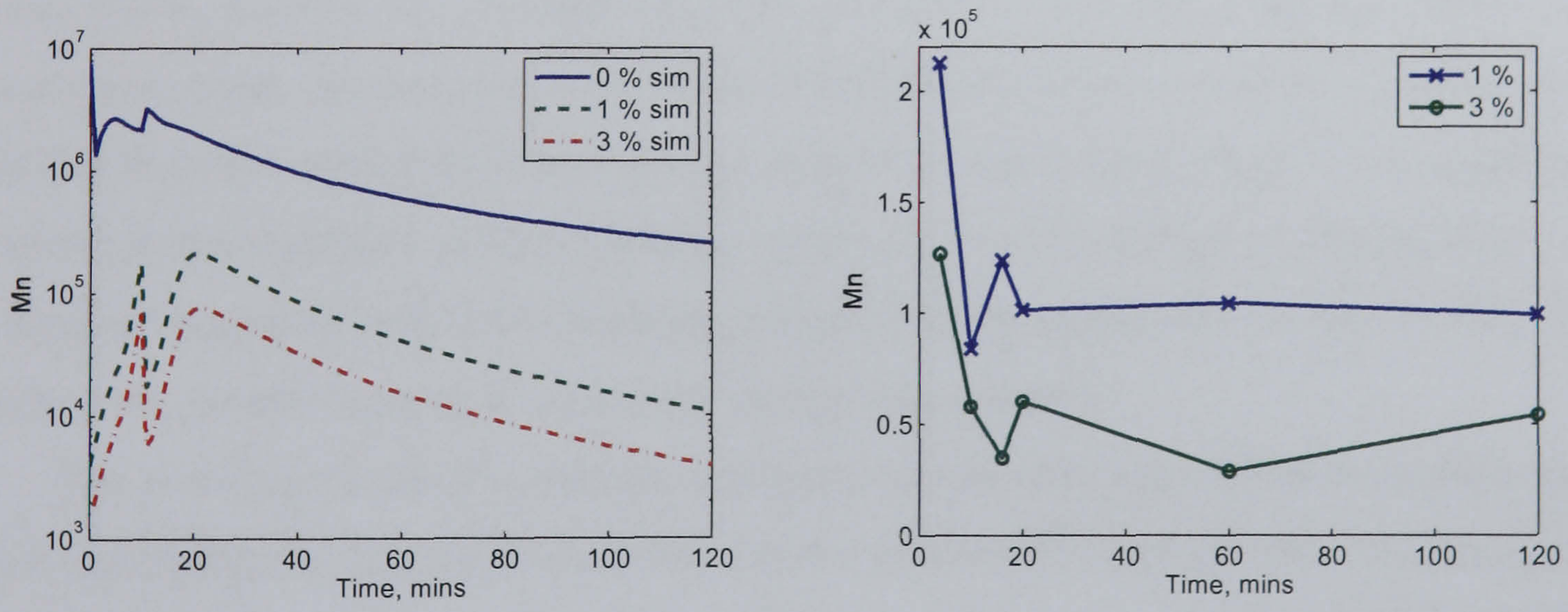
Simulations of CTA perturbation are all in accord with experimental trends as shown in Figure 4.21 and Figure 4.22. The simulation for PSD in Figure 4.21(a) indicates that the 0% CTA case produces the smallest micellar mode of particles (peak centred around 20 nm) due to lack of desorption of low MW species, a consequence of reduced chain transfer. When the 1% CTA case is simulated a marked increase in the micellar nucleated mode of particles results. A further increase in the same peak is observed for the simulated 3% CTA case, similar to that observed by experiment [Figure 4.21(b)]. With respect to

average MW, the model was able to simulate all three cases (0%, 1% and 3%), however it was not possible to obtain an experimental result for the 0% CTA case. Figure 4.22 shows that both model simulation and expermiment indicate a sizable decrease in MW for an increase in CTA concentration.



(a) (b)

Figure 4.21: a) Simulation and b) Experimental results for end-time weight-averaged PSD for CTA perturbation set.

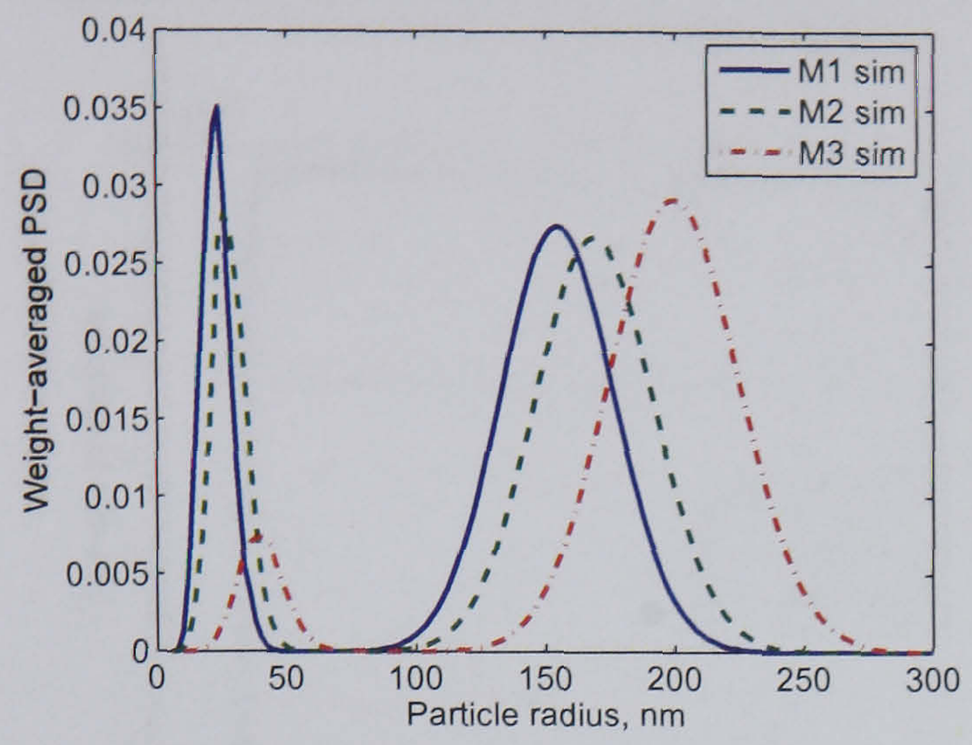


(a) (b)

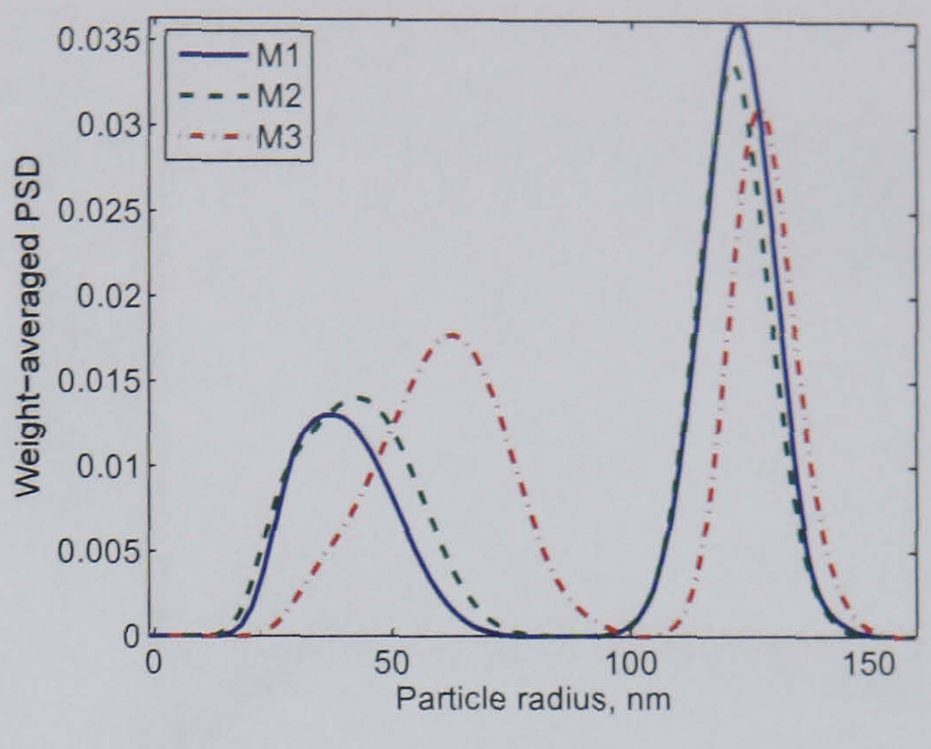
Figure 4.22: a) Simulation and b) Experimental results for number-averaged MW evolution for CTA perturbation set.

4.5.3 Effect of Monomer

Simulation of weight-averaged PSD for the monomer perturbation set [Figure 4.23(a)] demonstrated a bimodal nature similar to that observed experimentally [Figure 4.23(b)],



(a)



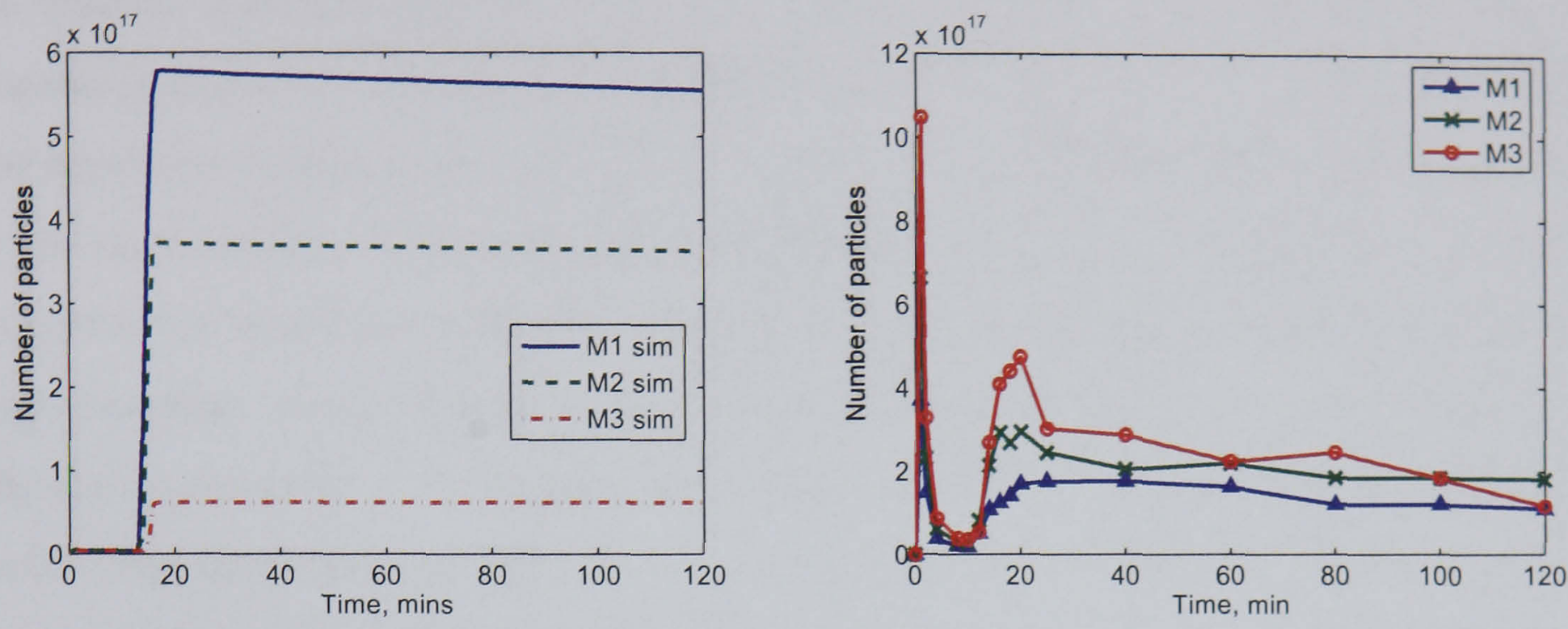
(b)

Figure 4.23: a) Simulation and b) Experimental results for end-time weight-averaged PSD for monomer perturbation set.

however the magnitude of the micellar nucleation was underestimated. This is due to the level of conversion predicted by simulation being far lower than the experimental value around the time of the micellar nucleation event. In the experimental system, where there is a very low amount of monomer present around the micellar nucleation time, a mechanism exists, whereby an increased monomer feed at this time can positively influence the nucleation event. In the model, conversion is much lower and we do not see the same effect. In fact there is a reduction in free aqueous surfactant due to the increased surface area presented by the monomer swollen particles, negatively influencing the micellar nucleation at increased monomer feed rates [compare particle number evolutions in Figure 4.24]. Thus again, the growth aspects of the model require improvement.

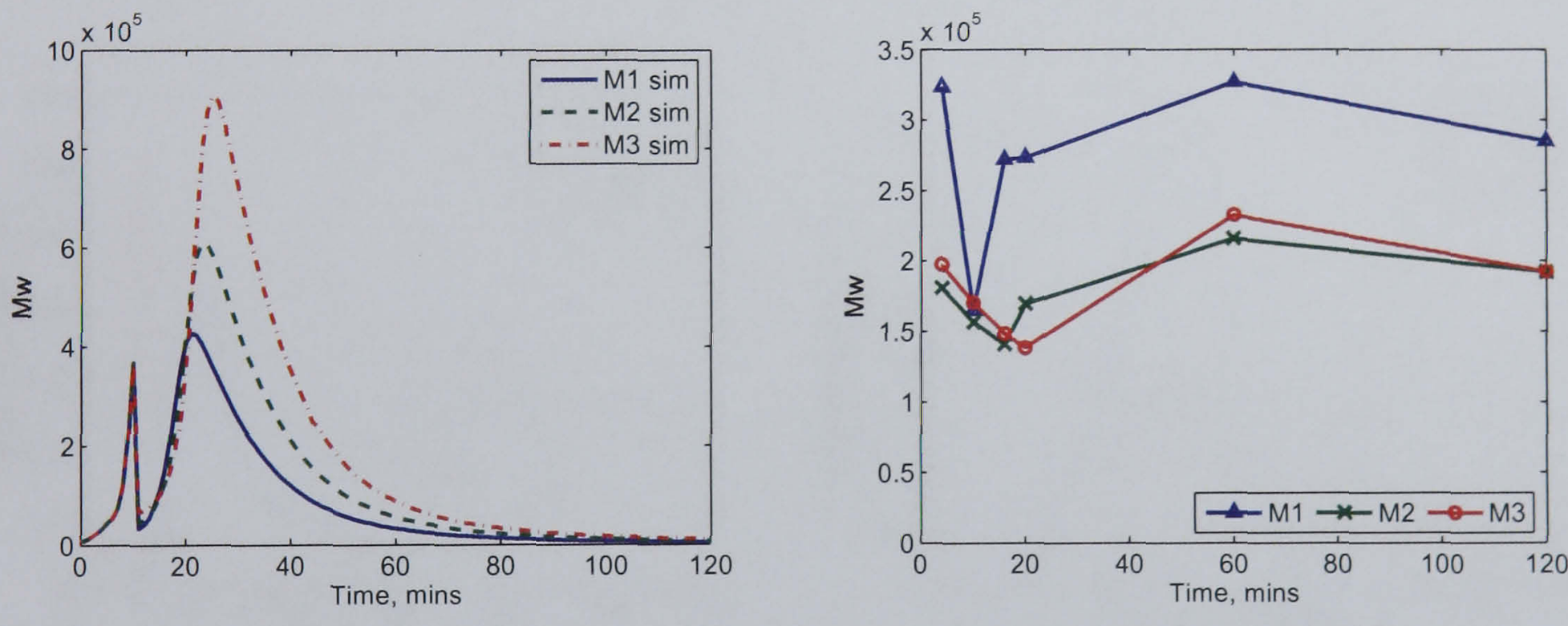
The reduction in micellar nucleation impacts on the simulated values for particle number; decreasing for increasing monomer, thereby affecting the average MWs in a manner inconsistent with experiment [Figure 4.25]. The simulated average MWs [see Figure 4.25(a)] increase as monomer is increased. This is due to particle number considerations and their effect on radical flux into particles. Despite the end output differences, the overall model mechanistic approach still adequately represents the process, the differences in this case highlighting the cascaded effect that a different conversion can have on MWD (reflected through micellar nucleation, particle number and finally MW). By simulating the advanced conversion at the intermediate time prior to the monomer feed that is implied by

experiment, better results should be expected.



(a) (b)

Figure 4.24: a) Simulation and b) Experimental results for particle number for monomer perturbation set.



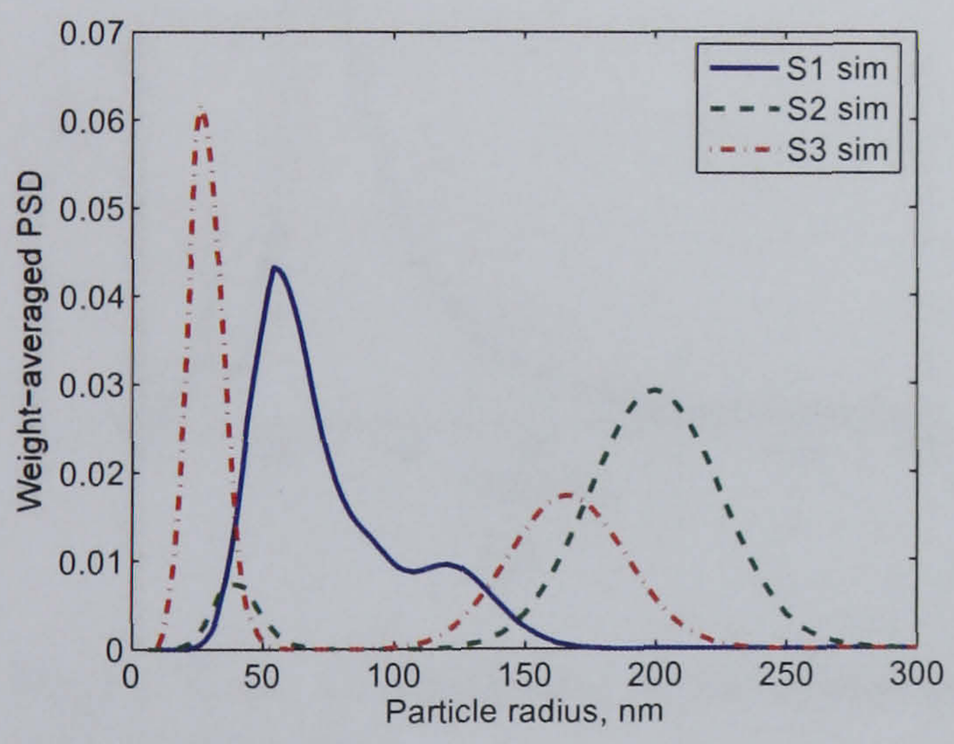
(a) (b)

Figure 4.25: a) Simulation and b) Experimental results for weight-averaged MW evolution for monomer perturbation set.

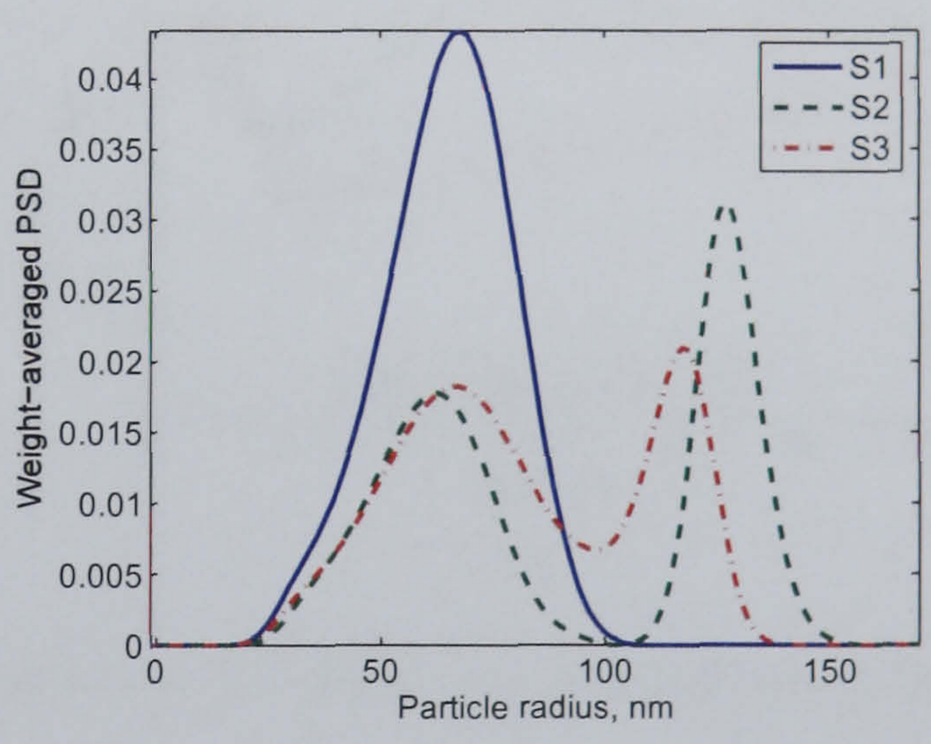
4.5.4 Effect of Surfactant

PSD simulation results for the surfactant perturbation experimental set are shown in Figure 4.26(a). The experimental results shown in Figure 4.26(b) suggest that compared to the S2 and S3 cases, in the S1 case, the micellar nucleation is advanced. In the S2 and S3 cases, micellar nucleation occurs around 15 min, whereas in the S1 case, it occurs early so as to present a single mode of particles. This can also be seen in the shoulder of the simulated

number-averaged PSD [Figure 4.15(a)]. While the model captures this advancement of the micellar nucleation in the S1 case, it is still not perfect, creating a slight shoulder (corresponding to the homogeneous particles) in the PSD, instead of a monomodal PSD. The experimental weight-averaged PSD trends for the S2 and S3 cases are well represented by the model; firstly, both have clearly defined bimodal PSDs, furthermore as surfactant concentration is increased, the relative magnitude of the micellar nucleated mode increases [Figure 4.26(a), mode centred around 40 nm]. This mode actually shifts slightly to the left, the opposite way to the experiment, again manifesting the discrepancies in the growth model. The simulated evolution of the number of particles [Figure 4.27(a)] approaches the same order of magnitude as the experiment [Figure 4.27(b)] and correctly indicates the timing of nucleation events, however the amount of micellar nucleation for case S3 is over-predicted due to incorrect surfactant levels. In relation to MWD [Figure 4.28] both experiments and simulations show a relative insensitivity to surfactant perturbations.



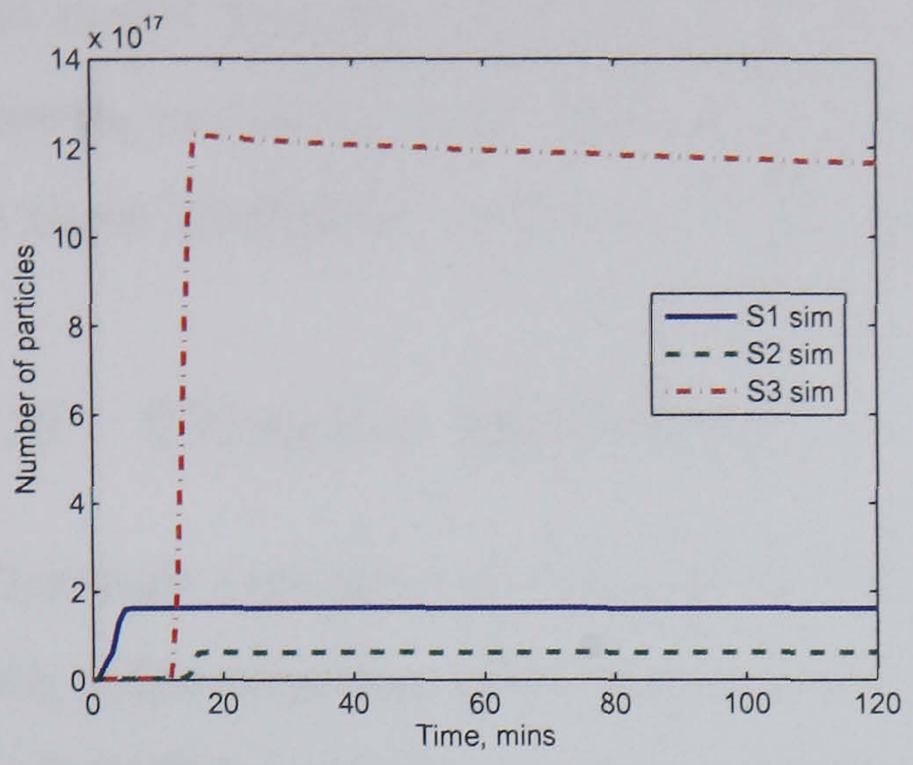
(a)



(b)

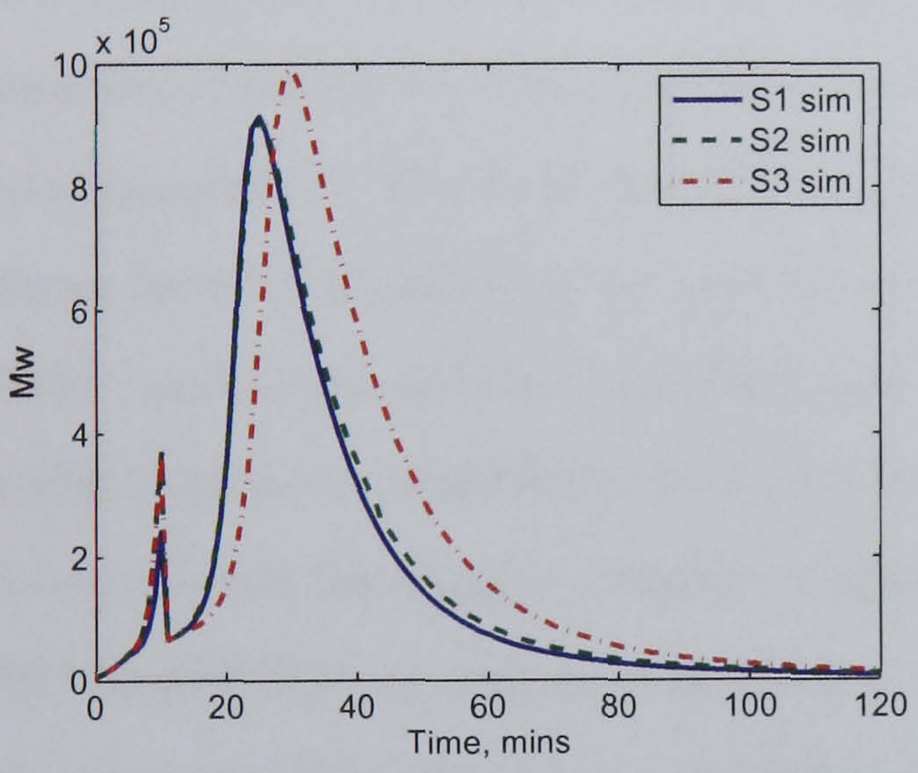
Figure 4.26: a) Simulation and b) Experimental results for end-time weight-averaged PSD for surfactant perturbation set.

Based on these preliminary comparisons, key discrepancies of the model have been identified. In particular, the growth model and its response to initiator is found to not match experiments well. This error cascades into further errors in nucleation. Also, errors have been identified in the nucleation model. Further, parametric uncertainties exist in the model. However, the qualitative correspondence in most cases is encouraging. There are a number of uncertain parameters that exist within the detailed model, and as mentioned



(a) (b)

Figure 4.27: a) Simulation and b) Experimental results for particle number for surfactant perturbation set.



(a) (b)

Figure 4.28: a) Simulation and b) Experimental results for weight-averaged MW for surfactant perturbation set.

at the beginning of this section, tuning has been carried out in so far as a few manually adjusted parameters to move simulation results into the same region as demonstrated by the experiment. The large number of critical parameters and the complex interactions that result from the mechanisms they govern, mean that manual parameter tuning is insufficient to provide a comprehensive fit with experimental results. Although the model embodies the required mechanisms to adequately describe the emulsion polymerisation process, a more formal and rigorous optimisation of uncertain model parameters is needed. As a further study it is proposed to use the experimental data to more accurately tune

the model focussing on parameters that govern the important underlying mechanisms: growth, nucleation and coagulation. This can be done using optimisation techniques such as those highlighted in Chapter 6: Future work.

4.6 Chapter Summary

This work highlights the complexity of the underlying mechanisms and reactions in emulsion polymerisation. This aspect is especially evident in the current scenario, where bimodal PSDs have been engineered to be representative of current industry trends. What sets emulsion polymerisation apart from other types of polymerisation is the particulate nature, the establishment and dynamics of which is clearly seen to affect the mechanisms that shape both PSD and MWD. The coupling between PSD and MWD evident from these experiments has been comprehensively discussed and summarised in each of the four cases presented. The same conditions used for experiments have been simulated using a comprehensive population balance model. While the model was able to reproduce some of the qualitative trends, it showed discrepancies in others. In such cases aspects of the model that need refinement were identified. The comparison between model and simulation allowed for a more detailed insight into how different process mechanisms effected PSD and MWD, as well as providing a platform for model improvement. The work confirmed that CTA was the most useful candidate for MWD manipulation, with minimal alteration of PSD. In contrast, for the manipulation of PSD with minimal alteration of MWD, no variable in particular stood out. This paper provides the starting point to further map in detail, the restrictions on attainable regions for simultaneous control of PSD and MWD. Also, the potentially erroneous mechanisms of the model that were identified, can be investigated for model improvement. One mechanism that certainly has the potential to effect model results through lack of accounting, as alluded to in Chapter 3, is compartmentalisation. The model presented in Chapter 3 assumes that pseudo-bulk kinetics apply, wherein each particle is assumed to act like a miniature bulk reactor. Chapter 5 looks further into the possible errors that may be introduced into such a PBE model via this assumption. Another factor that may have played a part in the disparities between model and experiment was the absence of chain transfer to polymer modelling, a reaction

that could be prevalent in this type of system.

Chapter 5

Compartmentalisation Analysis

5.1 Introduction

This chapter will further address the role of compartmentalisation in the previously developed model [Chapter 3]. In the literature there have been various attempts at accounting for the effects of compartmentalisation; for instance Butte et al.[124,125,126] developed a model for MWD, based on the concept of the doubly distinguished particle (theoretical precepts by Lichti et al.[121]) Assuming a monodisperse particle population, they highlighted some of the effects of compartmentalisation (i.e. short-long radical termination leading to bimodal MWDs) through accurate accounting for the lengths of radicals terminating within particles. Reynhout et al.[111] incorporated compartmentalisation into their seeded emulsion polymerisation model by introducing a compartmentalisation factor that modified the reaction rates according to a calculation of the fraction of particles that would actually house reactions, based on the possibilities for arrangement of the radicals that were distributed amongst them. The work in this chapter applies a model structure similar to that developed in the work of Saldivar et al. and Reynhout et al. i.e. distinguishing between discrete radical classes for each particle size. The novel aspect of this work lies in the fact that the two-dimensional representation of particles is solved directly (without further simplifications such as the pseudo-bulk assumption as in Salivar et al.[77]) within a comprehensive framework accounting for nucleation events (Reynhout et al. simplify their model by assuming a seeded system). The solution framework is based on a similar

rate decomposition algorithm to the one utilised in Chapter 3 as will be described in more detail later.

The PSD model developed in Chapter 3 consisted of 2 one-dimensional PBEs: a balance for particle density, and another for the average number of radicals per particle. A key assumption in this model is that pseudo-bulk kinetics hold. However, as demonstrated in Chapter 3 (section 3.6.2) through a simple manipulation of $\bar{n}$ via a compartmentalisation factor, the molecular weight calculations in the model were very sensitive to termination events in particles. At times when the number of radicals per particle is low, the validity of this assumption raises questions. The following model development will attempt to account in a rigorous manner for the termination events occurring within particles, and hence give a clearer indication of the impact of compartmentalisation when invoking the pseudo-bulk assumption.

The pseudo-bulk assumption is to be challenged by developing a model that accounts rigorously for each particle state in terms of the number of live radicals they contain and their size, circumventing the reliance of the PSD model on an average number of radicals. It is speculated that in developing a PSD model that accurately accounts for intra-particle kinetics, the coupled MWD will also be represented more accurately. The MWD model will still be coupled to the PSD model via a calculation of the average number of radicals per particle, therefore the forthcoming analysis does not completely simulate compartmentalised conditions. It does however provide a means to eliminate the over-accounting for termination by counting particles with 1 or less radicals, transferring this accurate picture to the MWD model.

It is clear that in creating a two-dimensional model from the previous one-dimensional model will allow a resolving of information on radical numbers. This will however be at the expense of computational time, therefore this two-dimensional model structure is suggested as means to analyse the impact of compartmentalisation, and not necessarily for application to on-line model-based control. If however there is considerable improvement in accuracy, one could foresee the model being subjected to algorithmic advances for speed-up its computation.

The layout of this chapter is as follows: first the 2D PSD model will be developed, then the solution technique will be given. This will be followed by an account of the

MWD model and its solution. Key simulation results will then be shown, comparing the previously developed PSD/MWD model and the one developed in this chapter.

5.2 2D PSD Model Framework

The general structure of the previously developed PSD model consisted of a one-dimensional PBE for particle density ($F(r,t)$) and another for the average number of radicals per particle ($\bar{n}(r,t)$). The model developed in this chapter uses a combination of these two approaches, resolving individual particles in terms of their size and the number of radicals they contain (radical class).[77] The two-dimensional particle density, $F_n(r,t)$, which is defined as the amount of particles containing n radicals and is of size r, at time t (where n is an integer). The rigorous accounting for intra-particle dynamics at a PSD level (i.e. no termination in particle with less than 2 radicals), will allow a more accurate picture of MW to be obtained.

The same overall *kinetic scheme* as tabulated in Chapter 3 is used here, as are the *pseudo-homopolymerisation* approximations.

5.2.1 PSD Model: System PBE

The PBE equation used to describe the polymer particles $F_n(r,t)$ is given as:

$$\frac{\partial F_n(r,t)}{\partial t} + \frac{\partial}{\partial r}\left(F_n(r,t)\frac{dr(n)}{dt}\right) =$$

$$\delta_{n=1}\delta(r-r_{\text{nuc}})\Re_{\text{nuc}} + (\Re''_{\text{entry}} + \Re''_{\text{desorp}} + \Re''_{\text{termin}}) \tag{5.1}$$

where,

$$\Re''_{\text{entry}} = \sum_{i=1}^{2}\sum_{l=0}^{j_{cr}-1} e_i^l(r)p_{\text{w}i}[P_{\text{w}}^l]\Big(F_{n-1}(r) - F_n(r)\Big) \tag{5.2}$$

$$\Re''_{\text{desorp}} = \frac{1}{N_{\text{A}}}\sum_{j=1}^{2} k_{\text{dM}j}(r)\frac{\sum_{i=1}^{2}(k_{\text{tr}ij}[M_{\text{p}j}]+k_{\text{trA}i}[A_{\text{p}j}])p_i n}{k_{\text{dM}j}(r)+\sum_{l=1}^{2}k_{\text{p}jl}[M_{\text{p}l}]}\Big(F_{n+1}(r) - F_n(r)\Big) \tag{5.3}$$

$$\Re''_{\text{termin}} = \frac{1}{2N_{\text{A}}V_{\text{p}}(r)}\sum_{i=1}^{2}\sum_{j=1}^{2} p_i p_j k_{tij}\Big((n+2)(n+1)F_{n+2} - n(n-1)F_n\Big) \tag{5.4}$$

This preliminary framework does not include coagulation dynamics, so as to not further complicate the model. The terms, $\Re''_{\text{entry}}$, $\Re''_{\text{desorp}}$ and $\Re''_{\text{termin}}$ on the RHS of the system PBE describe the particle radical class changing events. In the previous 1D model, terms representing similar mechanisms were used to evaluate an average number of radicals per particle, which was in turn used to evaluate size-dependent particle growth. The terms in the 2D model appear in the overall PBE on the RHS, as they are linked to discrete events that determine the exact number of radicals present in a particle. The term $\Re''_{\text{entry}}$ represents the entry of radicals into particles, and has a positive effect on the population of particles F_n upon entry into a particle with one radical less than the class in question (F_{n-1}). The term negatively effects F_n, upon radical entry into a similar class of particle. The term $\Re''_{\text{desorp}}$ represents the desorption of radicals from particles. and as can be seen from the equation above, has the opposite effect on F_n to the entry term described above, i.e. it negatively effects F_n upon desorption from a similar class particle, and positively effects F_n upon desorption from particles with one more radical than this class (F_{n+1}). The third term, $\Re''_{\text{termin}}$ represents the bimolecular termination reactions that occur between radicals in particles, and since it involves two radicals, positively effects F_n when termination occurs in a particle with two more radicals than the class in question (F_{n+2}). The term imparts a negative effect on F_n when termination occurs inside a particle of similar class. The growth of particles in the 2D model is then evaluated for each discrete radical class, involving an assumption that Eq. (3.37) holds for the low number of radicals considered. Future work may aim to address this issue and therefore model growth in a more applicable framework, perhaps adopting a probabilistic Monte Carlo approach.

5.2.2 PSD Model: Component Balances

Monomer

The same partitioning equations as presented in Chapter 3 were used to describe the equilibrium state of monomers in the system. A modification was needed for the calculation of particle volume, as follows:

$$V_{\text{p}} = N_{\text{A}} \int_{r=r_{\text{nuc}}}^{r_{\text{max}}} \frac{4}{3}\pi r^3 \sum_{n=0}^{n_{\text{max}}} F_n(r,t)dr \tag{5.5}$$

The mass balance over monomer is given as:

$$\begin{aligned}\frac{dM_j}{dt} &= u_{\mathrm{M}j} - \sum_{i=1}^{2}(k^{\mathrm{w}}_{\mathrm{p}ij} + k^{\mathrm{w}}_{\mathrm{tr}ij})p_{\mathrm{w}i}[M_{\mathrm{w}j}]\sum_{n=o}^{j_{\mathrm{cr}}-1}[P^n_{\mathrm{w}}]V_{\mathrm{aq}} \\ &- \sum_{i=1}^{2}(k_{\mathrm{p}ij} + k_{\mathrm{tr}ij})p_i[M_{\mathrm{p}j}]\int_{r=r_{\mathrm{nuc}}}^{r_{\mathrm{max}}}\sum_{n=0}^{n_{\mathrm{max}}} nF_n(r,t)dr \quad (j=1,2) \end{aligned} \tag{5.6}$$

Surfactant

The same partitioning equations as presented in Chapter 3 were used to describe the equilibrium state of surfactant in the system. A modification was needed for the calculation of particle surface area, as follows:

$$A^{\mathrm{s}}_{\mathrm{p}} = \int_{r_{\mathrm{nuc}}}^{r_{\mathrm{max}}} 4\pi r_{\mathrm{s}}^2 N_{\mathrm{A}} \sum_{n=0}^{n_{\mathrm{max}}} F_n(r,t)dr \tag{5.7}$$

CTA

The same partitioning equations as presented in Chapter 3 were used to describe the equilibrium state of CTA in the system. The mass balance over CTA is given as:

$$\begin{aligned}\frac{dA}{dt} &= u_{\mathrm{A}} - \sum_{i=1}^{2}(k^{\mathrm{w}}_{\mathrm{trA}i})p_{\mathrm{w}i}\sum_{n=o}^{j_{\mathrm{cr}}-1}[P^n_{\mathrm{w}}][A_{\mathrm{w}}]V_{\mathrm{aq}} \\ &- \sum_{i=1}^{2}(k_{\mathrm{trA}i})p_i[A_{\mathrm{p}}]\int_{r=r_{\mathrm{nuc}}}^{r_{\mathrm{max}}}\sum_{n=0}^{n_{\mathrm{max}}} nF_n(r,t)dr \end{aligned} \tag{5.8}$$

5.2.3 Aqueous Phase Oligomer Balance

The same pseudo-homopolymer rate constants given in Chapter 3 are used in the following aqueous phase radical balances.

$$\begin{aligned}\frac{d([P^1_{\mathrm{w}}]V_{\mathrm{aq}})}{dt} &= V_{\mathrm{aq}}\sum_{i=1}^{2}k_{\mathrm{r}i}[R_{\mathrm{w}}][M_{\mathrm{w}i}] - V_{\mathrm{aq}}\bar{k}^{\mathrm{w}}_t[P^1_{\mathrm{w}}]\left(\sum_{l=0}^{j_{\mathrm{cr}}-1}[P^l_{\mathrm{w}}] + [R_{\mathrm{w}}]\right) \\ &- \left(\bar{k}^{\mathrm{w}}_{\mathrm{p}} + \bar{k}^{\mathrm{w}}_{\mathrm{tr}} + \bar{k}^{\mathrm{w}}_{\mathrm{trA}}\right)[P^1_{\mathrm{w}}]V_{\mathrm{aq}} + \bar{k}^{\mathrm{w}}_{\mathrm{p}}[P^0_{\mathrm{w}}]V_{\mathrm{aq}} \\ &- \sum_{i=1}^{2}e^1_{\mathrm{m},i}p_{\mathrm{w}i}[P^1_{\mathrm{w}}]C_{\mathrm{micelle}}V_{\mathrm{aq}} \\ &- \int_{r=r_{\mathrm{nuc}}}^{r_{\mathrm{max}}}\sum_{i=1}^{2}e^1_i(r)[P^1_{\mathrm{w}}]\sum_{n=0}^{n_{\mathrm{max}}}F_n(r,t)dr \end{aligned} \tag{5.9}$$

$$\begin{aligned}
\frac{d([P_{\mathrm{w}}^{0\mathrm{T}}]V_{\mathrm{aq}})}{dt} &= \left(\bar{k}_{\mathrm{tr}}^{\mathrm{w}} + \bar{k}_{\mathrm{trA}}^{\mathrm{w}}\right) \sum_{l=1}^{j_{\mathrm{cr}}-1} [P_{\mathrm{w}}^{l}]V_{\mathrm{aq}} - \bar{k}_{\mathrm{p}}^{\mathrm{w}}[P_{\mathrm{w}}^{0\mathrm{T}}]V_{\mathrm{aq}} \\
&- \bar{k}_{\mathrm{t}}^{\mathrm{w}}[P_{\mathrm{w}}^{0\mathrm{T}}] \left(\sum_{l=0}^{j_{\mathrm{cr}}-1} [P_{\mathrm{w}}^{l}] + [R_{\mathrm{w}}] \right) V_{\mathrm{aq}} - \sum_{i=1}^{2} e_{\mathrm{m},i}^{0} p_{\mathrm{w}i} [P_{\mathrm{w}}^{0\mathrm{T}}] C_{\mathrm{micelle}} V_{\mathrm{aq}} \\
&- \int_{r=r_{\mathrm{nuc}}}^{r_{\mathrm{max}}} \sum_{i=1}^{2} e_{i}^{0}(r) p_{\mathrm{w}i} [P_{\mathrm{w}}^{0\mathrm{T}}] \sum_{n=0}^{n_{\mathrm{max}}} F_n(r,t) dr \\
&+ \left(\bar{k}_{\mathrm{tr}}^{\mathrm{w}} + \bar{k}_{\mathrm{trA}}^{\mathrm{w}}\right) \int_{r=r_{\mathrm{nuc}}}^{r_{\mathrm{max}}} \frac{\sum_{n=0}^{n_{\mathrm{max}}} n F_n(r,t) k_{\mathrm{dM}j}(r) dr}{k_{\mathrm{dM}j}(r) + \sum_{l=1}^{2} k_{\mathrm{p}il}[M_{\mathrm{pl}}]}
\end{aligned} \tag{5.10}$$

$$\begin{aligned}
\frac{d([P_{\mathrm{w}}^{n}]V_{\mathrm{aq}})}{dt} &= \bar{k}_{\mathrm{p}}^{\mathrm{w}} \left([P_{\mathrm{w}}^{n-1}] - [P_{\mathrm{w}}^{n}] \right) V_{\mathrm{aq}} - \bar{k}_{\mathrm{tr}}^{\mathrm{w}}[P_{\mathrm{w}}^{n}]V_{\mathrm{aq}} \\
&- e_{\mathrm{m},i}^{n} p_{\mathrm{w}i} [P_{\mathrm{w}}^{n}] C_{\mathrm{micelle}} V_{\mathrm{aq}} \\
&- \int_{r=r_{\mathrm{nuc}}}^{r_{\mathrm{max}}} \sum_{i=1}^{2} e_{i}^{n}(r) p_{\mathrm{w}i} [P_{\mathrm{w}}^{n}] \sum_{n=0}^{n_{\mathrm{max}}} F_n(r,t) dr \\
&- \bar{k}_{t}^{\mathrm{w}}[P_{\mathrm{w}}^{n}] \left(\sum_{l=0}^{j_{\mathrm{cr}}-1} [P_{\mathrm{w}}^{l}] + [R_{\mathrm{w}}] \right) V_{\mathrm{aq}} \\
& n = 2, 3, ..., j_{\mathrm{cr}-1}
\end{aligned} \tag{5.11}$$

5.2.4 Average Radical Number per Particle

For model comparison purposes, the equivalent value to $\bar{n}$ for the 1D model (Eq. (3.27)) was calculated from the 2D model by integrating over n for each r, then multiplying by the respective n, to give the total number of radicals present in particles of size r. This number was then divided by the total number of particles of size r, calculated by summing over n for each r, as follows:

$$\bar{n}(r,t) = \frac{\sum_{n=0}^{n_{\mathrm{max}}} n F_n(r,t)}{\sum_{n=0}^{n_{\mathrm{max}}} F_n(r,t)} \tag{5.12}$$

The global average number of radicals, n_{glob} [see Eq. (3.29) for 1D model] was calculated from the 2D model via a similar method to that above, except the denominator and nominator were both summed over n, as shown below:

$$n_{\mathrm{glob}}(t) = \frac{\int_{r=r_{\mathrm{nuc}}}^{r_{\mathrm{max}}} \sum_{n=0}^{n_{\mathrm{max}}} n F_n(r,t) dr}{\int_{r=r_{\mathrm{nuc}}}^{r_{\mathrm{max}}} \sum_{n=0}^{n_{\mathrm{max}}} F_n(r,t) dr} \tag{5.13}$$

5.3 2D PSD Model Solution

To solve the model given above, a modified solution strategy was developed. based on that used for the previous model.[71] The particle radius domain was discretised according to a similar grid (250 bins, spanning 2 to 500 nm radius particles). For computation, the grid was updated with a second dimension to account for the class of particle (i.e. how many integer radicals it contained). A section of the grid is shown in Figure 5.1. A variable describing the maximum number of radicals in a particle was introduced. such that the resultant set of equations could be solved. Analogous to Chapter 3, the total amount of particles in element j, with n radicals is defined as: $F_{j,n} = \int_{rb_{j-1}}^{rb_j} F_n(r.t)dr$ for $j = 2, 3, ..., 250$, $F_{1,n}(t) = \int_{r_{\text{nuc}}}^{rb_1} F_n(r,t)dr$ $(n = 0, 1, ..., n_{\text{max}})$.

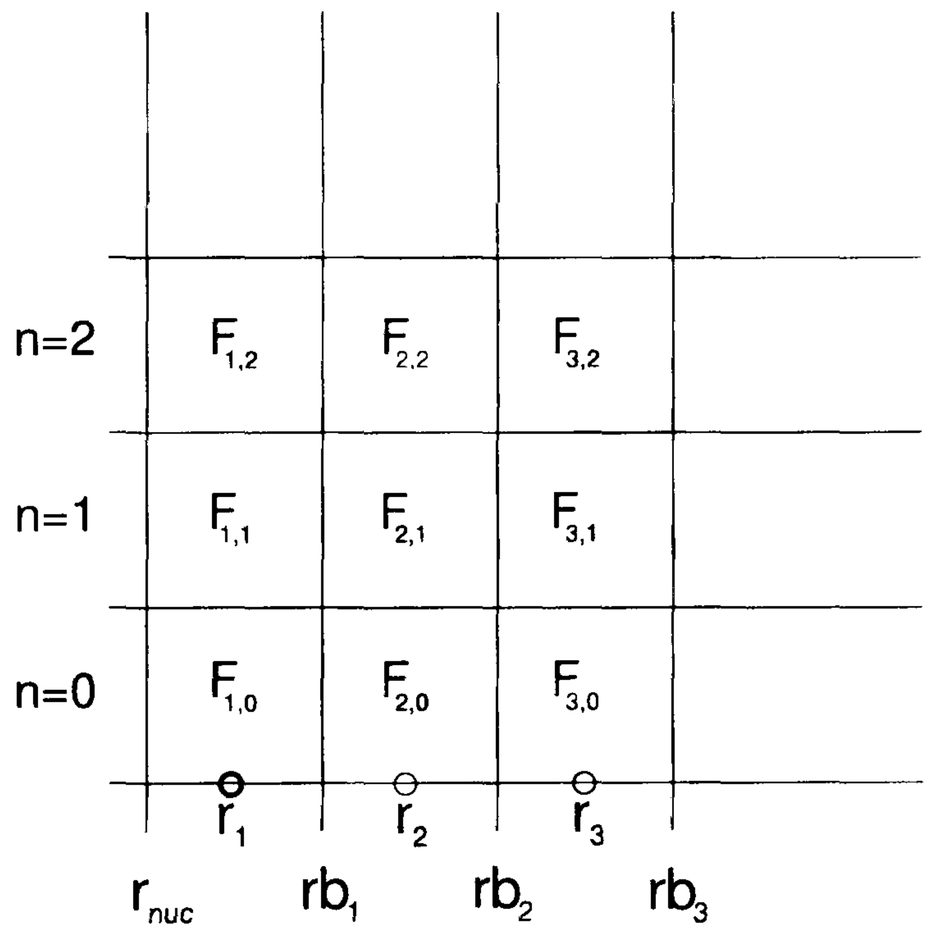


Figure 5.1: 2D discretisation grid for $F_n(r,t)$.

The hierarchical two-tier algorithm[71] is applied to the system of equations [see Figure 5.2], wherein the *first* tier the PSD is held constant enabling calculation of the rates of nucleation, growth, entry, desorption and termination. The next tier of calculation then involves the consolidation of the individual effects to obtain the cumulative 2D PSD using the following update scheme (Eqs. 5.14, 5.15. 5.12 and 5.17). Careful attention must be paid to which terms apply to each element of the grid [Figure 5.3]. for example no growth update will apply to the first row of the grid (where there are no radicals present).

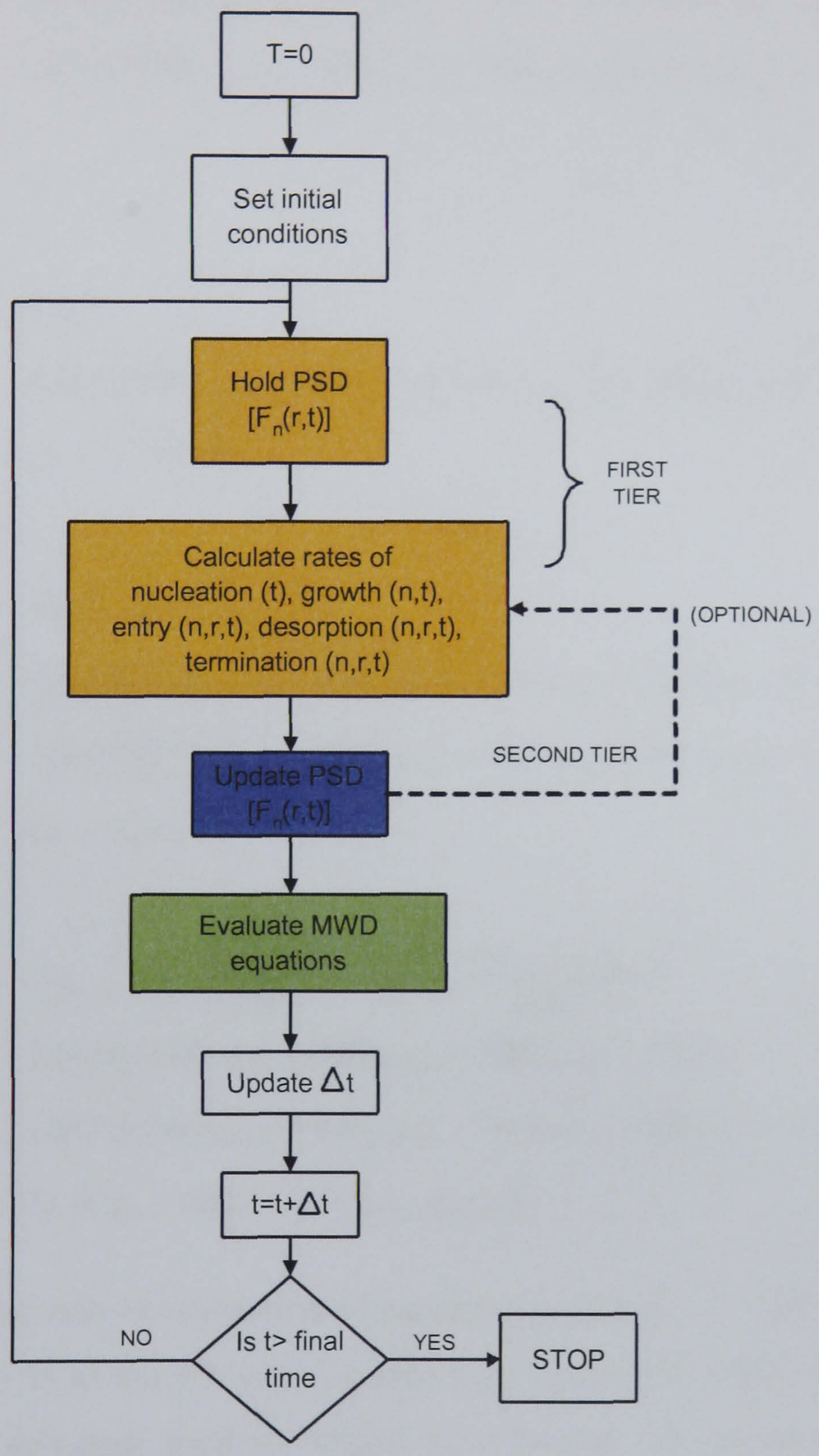


Figure 5.2: Adapted Hierarchical 2-Tier algorithm for 2D PSD/MWD model solution.

$$
\begin{aligned}
F_{\text{new},1,1} &= F_{1,1} - F_{1,1}\frac{rb_1 - ri_1}{\Delta R_1} \\
&+ (\Delta t/4)(14\Re_{\text{nuc},1} + 64\Re_{\text{nuc},2} + 24\Re_{\text{nuc},3} + 64\Re_{\text{nuc},4} + 14\Re_{\text{nuc}.5})(1/45) \\
&+ (\Delta t/4)(14n_{\text{com},1} + 64n_{\text{com},2} + 24n_{\text{com},3} + 64n_{\text{com},4} + 14n_{\text{com},5})(1/45)
\end{aligned} \tag{5.14}
$$

$$
\begin{aligned}
F_{\text{new},j,0} &= F_{j,0} \\
&+ (\Delta t/4)(14n_{\text{com},1} + 64n_{\text{com},2} + 24n_{\text{com},3} + 64n_{\text{com},4} + 14n_{\text{com},5})(1/45) \\
&(j = 1, ..., 250)
\end{aligned} \tag{5.15}
$$

$$
\begin{aligned}
F_{\text{new},1,k} &= F_{1,k} - F_{1,k}\frac{rb_1 - ri_1}{\Delta R_1} \\
&+ (\Delta t/4)(14\Re_{\text{nuc},1} + 64\Re_{\text{nuc},2} + 24\Re_{\text{nuc},3} + 64\Re_{\text{nuc},4} + 14\Re_{\text{nuc},5})(1/45) \\
&+ (\Delta t/4)(14n_{\text{com},1} + 64n_{\text{com},2} + 24n_{\text{com},3} + 64n_{\text{com},4} + 14n_{\text{com},5})(1/45) \\
&(k = 2, n_{\max})
\end{aligned} \tag{5.16}
$$

$$
\begin{aligned}
F_{\text{new},j,k} &= F_{j,k} - F_{j,k}\frac{rb_1 - ri_1}{\Delta R_1} + F_{j-1,k}\frac{rb_{j-1} - ri_{j-1}}{\Delta R_{j-1}} \\
&+ (\Delta t/4)(14\Re_{\text{nuc},1} + 64\Re_{\text{nuc},2} + 24\Re_{\text{nuc},3} + 64\Re_{\text{nuc},4} + 14\Re_{\text{nuc},5})(1/45) \\
&+ (\Delta t/4)(14n_{\text{com},1} + 64n_{\text{com},2} + 24n_{\text{com},3} + 64n_{\text{com},4} + 14n_{\text{com},5})(1/45) \\
&(j = 2, ..., 250, \quad k = 1, ..., n_{\max})
\end{aligned} \tag{5.17}
$$

where $\Re_{\text{nuc},i}$ is the rate of nucleation of particles in element 1,1 (bin corresponding to $r = r_{nuc}$ and $n = 1$) at the ith time sub-step and $n_{\text{com},i}(r, n)$ is the combined rate term (at the ith time sub-step) used to update each element due to entry, desorption and termination, taking into account the specific particle class and the definition of a maximum number of radicals:

$$
n_{\text{com},i}(r, n) = \breve{\Re}_{entry}(r, n) + \breve{\Re}_{des}(r, n) + \breve{\Re}_{termin}(r, n) \tag{5.18}
$$

Here, for $n = 0$,

$$\breve{\Re}_{\text{entry},i}(r,n) = [A]\Big(- F_n(r)\Big) \tag{5.19}$$

$$\breve{\Re}_{\text{des},i}(r,n) = [B]\Big(F_{n+1}(r)\Big) \tag{5.20}$$

$$\breve{\Re}_{\text{termin},i}(r,n) = [C]\Big((n+2)(n+1)F_{n+2})\Big) \tag{5.21}$$

for $n = 1$,

$$\breve{\Re}_{\text{entry},i}(r,n) = [A]\Big(F_{n-1}(r) - F_n(r)\Big) \tag{5.22}$$

$$\breve{\Re}_{\text{des},i}(r,n) = [B]\Big(2F_{n+1}(r) - 1F_n(r)\Big) \tag{5.23}$$

$$\breve{\Re}_{\text{termin},i}(r,n) = [C]\Big((n+2)(n+1)F_{n+2})\Big) \tag{5.24}$$

for $n = 2, 3, .., n_{max} - 2$,

$$\breve{\Re}_{\text{entry},i}(r,n) = [A]\Big(F_{n-1}(r) - F_n(r)\Big) \tag{5.25}$$

$$\breve{\Re}_{\text{des},i}(r,n) = [B]\Big((n+1)F_{n+1}(r) - nF_n(r)\Big) \tag{5.26}$$

$$\breve{\Re}_{\text{termin},i}(r,n) = [C]\Big((n+2)(n+1)F_{n+2} - n(n-1)F_n\Big) \tag{5.27}$$

for $n = n_{max} - 1$,

$$\breve{\Re}_{\text{entry},i}(r,n) = [A]\Big(F_{n-1}(r) - F_n(r)\Big) \tag{5.28}$$

$$\breve{\Re}_{\text{des},i}(r,n) = [B]\Big((n+1)F_{n+1}(r) - nF_n(r)\Big) \tag{5.29}$$

$$\breve{\Re}_{\text{termin},i}(r,n) = [C]\Big(- n(n-1)F_n\Big) \tag{5.30}$$

for $n = n_{max}$,

$$\breve{\Re}_{\text{entry},i}(r,n) = [A]\Big(F_{n-1}(r)\Big) \tag{5.31}$$

$$\breve{\Re}_{\text{des},i}(r,n) = [B]\Big(- nF_n(r)\Big) \tag{5.32}$$

$$\breve{\Re}_{\text{termin},i}(r,n) = [C]\Big(- n(n-1)F_n\Big) \tag{5.33}$$

with,

$$A = \sum_{i=1}^{2} \sum_{l=0}^{j_{\text{cr}}-1} e_i^l(r) p_{\text{w}i} [P_{\text{w}}^l] \tag{5.34}$$

$$B = \frac{1}{N_{\text{A}}} \sum_{j=1}^{2} k_{\text{dM}j}(r) \frac{\sum_{i=1}^{2} (k_{\text{tr}ij}[M_{\text{p}j}] + k_{\text{trA}i}[A_{\text{p}j}]) p_i}{k_{\text{dM}j}(r) + \sum_{l=1}^{2} k_{\text{p}jl}[M_{\text{p}l}]} \tag{5.35}$$

$$C = \frac{1}{2N_{\text{A}} V_{\text{p}}(r)} \sum_{i=1}^{2} \sum_{j=1}^{2} p_i p_j k_{\text{t}ij} \tag{5.36}$$

Figure 5.3 shows the update considerations that apply to each element of the 2D

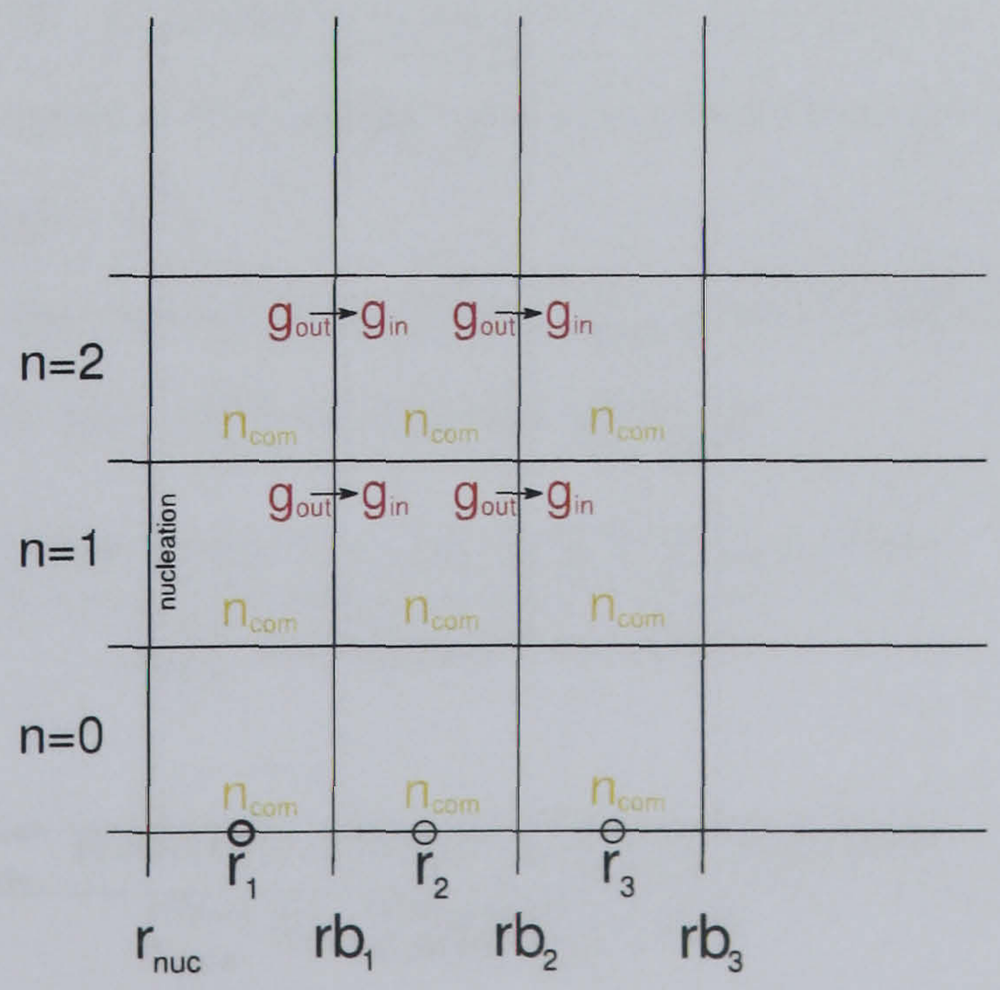


Figure 5.3: 2D grid update considerations.

discretisation grid proposed. The term g_{out} indicates that a particular element will contain a fraction of particles that grow into the adjacent element (to the right). The term g_{in} indicates that a particular element will receive particles from the element to the left (via growth). Nucleation is only applied to element $F_{1,1}$. The term n_{com} is used to update all elements including those with no radicals, according to the equations given in this section.

5.4 MWD Model and Solution

The MWD model structure developed in Chapter 3 was incorporated into the 2D PSD model. The solution technique involved application of the method of moments to the MWD population balances, in the same fashion as previously shown. Again, a one-way information flow was established between the PSD and MWD models, with $\bar{n}(r,t)$ being equated with the zeroth moment of the live polymer chain length population balance:

$$\lambda_{\mathrm{N0}}(r,t) = \sum_{l=0}^{\infty} l^0(N_{\mathrm{p}}^l(r,t)) = \bar{n}(r,t) \tag{5.37}$$

It is noted that although $\bar{n}(r,t)$ represents an average number of radicals per particle, the rigorous accounting for intra-particle kinetics through a 2D balance on $F_n(r,t)$ allows the effect of compartmentalisation, if any, on this system to be conferred through this term. The 2D PSD model is self-contained, relying on no calculation of $\bar{n}$. The set of ODEs that resulted from application of the method of moments to the MWD population balances were solved using a first order predictor-corrector integrator in the sequential algorithm shown in Figure 5.2.

The global number-average molecular weight, (N_{glob}^2), and the global weight-average molecular weight, (W_{glob}^2), for the entire system are given as:

$$N_{\mathrm{glob}}^2(r,t) = \frac{\int_{r_{\mathrm{min}}}^{r_{\mathrm{max}}} \mathrm{NAMW}(r,t)\lambda_{D0}(r,t)\sum_{n=0}^{n_{\mathrm{max}}} F_n(r,t)dr}{\int_{r_{\mathrm{min}}}^{r_{\mathrm{max}}} \lambda_{D0}\sum_{n=0}^{n_{\mathrm{max}}} F_n(r,t)dr} \tag{5.38}$$

$$W_{\mathrm{glob}}^2(r,t) = \frac{\int_{r_{\mathrm{min}}}^{r_{\mathrm{max}}} \mathrm{WAMW}(r,t)\lambda_{D1}(r,t)\sum_{n=0}^{n_{\mathrm{max}}} F_n(r,t)dr}{\int_{r_{\mathrm{min}}}^{r_{\mathrm{max}}} \lambda_{D1}\sum_{n=0}^{n_{\mathrm{max}}} F_n(r,t)dr} \tag{5.39}$$

5.5 PSD/MWD Results and Discussion

The original 1D PSD/MWD model described in Chapter 3 and the 2D model developed in this chapter, were used to simulate an emulsion polymerisation process, sharing identical inputs and parameter values (values used as per Table 3.1 and 3.2). This was done to observe the difference in results due to model structure i.e. pseudo-bulk assumption of the 1D PBE-based model verses the new 2D PBE-based model that rigorously accounts for intra-particle reactions for PSD.

The recipe simulated was the *medium initiator case* as indicated in Table 4.1. By using this particular recipe, information can be gained regarding the role of compartmentalisation in the model validation carried out in Chapter 4; also observations should be possible as to the effect of the impulse-like monomer feeding policy employed. Also, a comparison was made between the 1D model, 2D model and experimental results for PSD for each of the surfactant perturbation cases shown in Table 4.1.

5.5.1 Convergence of n

Since closure of the model equations, and therefore of the solution technique, requires a maximum value of n to be defined, a suitable maximum was obtained by simulating several cases for $n_{\max}$. The minimum value of $n_{\max}$, wherein PSDs fully converged, was taken as optimal for the current recipe and therefore used for further analytical simulations.

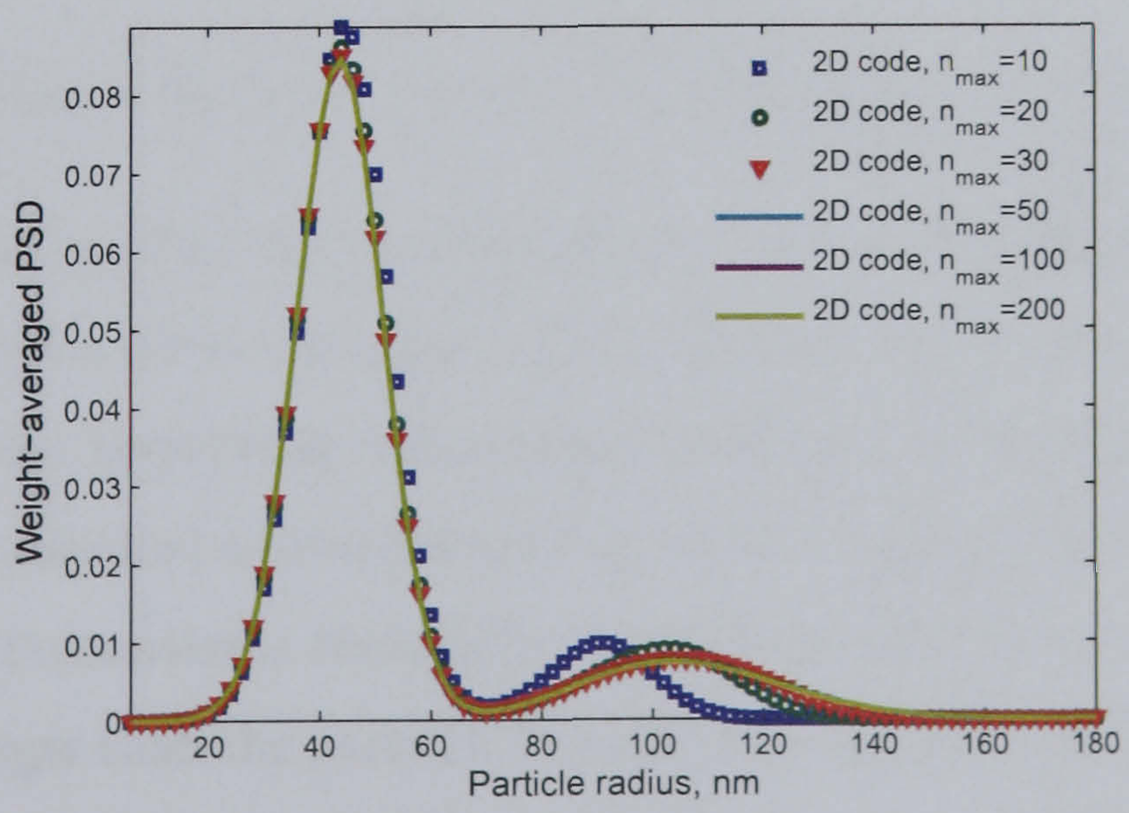
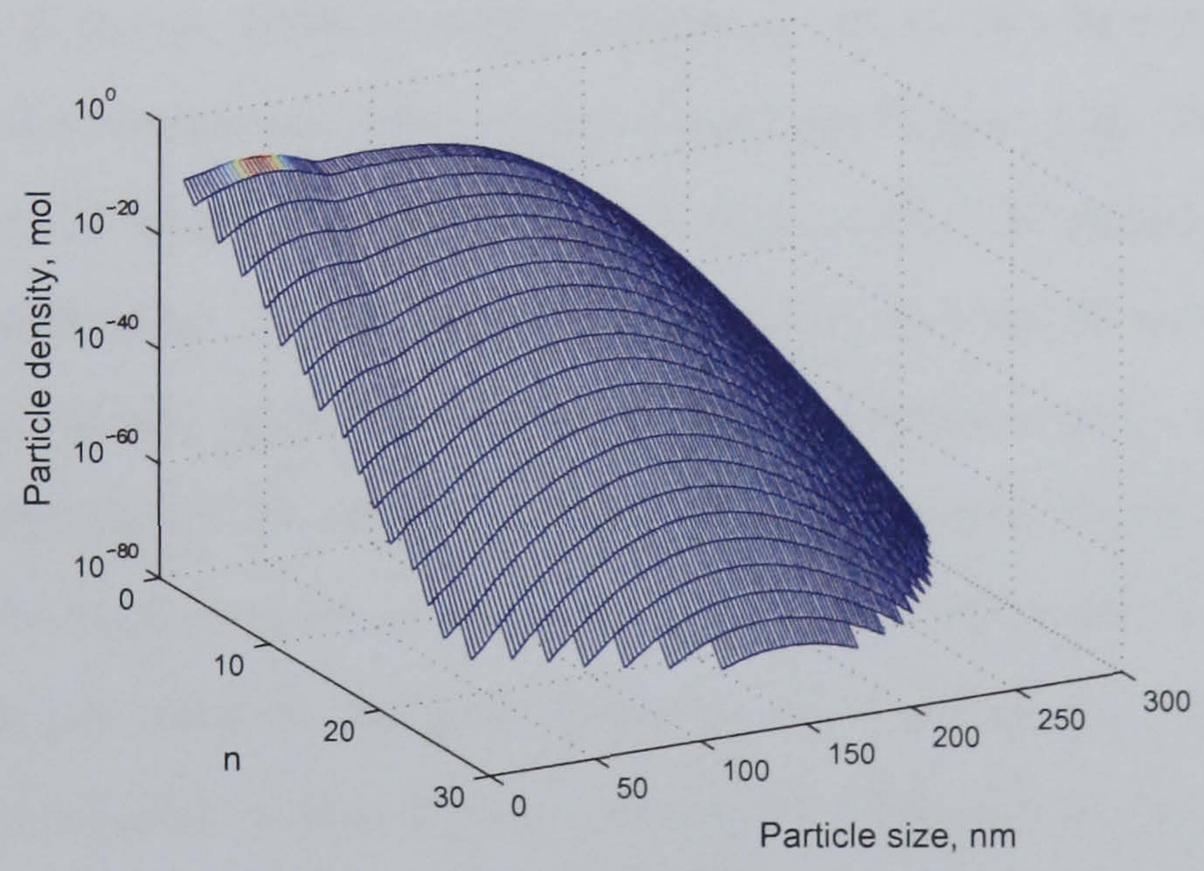


Figure 5.4: Convergence of weight-average PSD for increasing values of $n_{\max}$.

Figure 5.4 shows that convergence was obtained at a value of $n_{\max} = 30$. Solution time for the model (with no coagulation, single level discretisation and using the aforementioned algorithm) was approximately 4 hours on a dual core 2.4 Ghz processor with 4 GB of RAM.

5.5.2 PSD and MWD Model Results

Figure 5.5 shows the 2D model output for particle density, with respect to the size of particles, r, and the number of radicals contained, n. In order to compare with the output from the 1D model, n must be first summed over and further processing done to obtain the weight-averaged PSD.



(a)

Figure 5.5: End-time 2D model output for density of particles distributed over r and n.

Figure 5.6 (a) shows that the end-time PSDs are somewhat different when comparing the 1D and 2D versions of the emulsion polymerisation model. When comparing the data from both models it is noted that experimental error and uncertainty regarding exact PSD profiles that lead to desired end-use properties must be taken into account. The end-time PSD profiles both demonstrate bimodality, however the two modes of particles in the 2D case have grown larger than the particles simulated by the 1D model. Figure 5.6(c) and (d) shows the rate of both homogenous and micellar nucleation in the 2D case is less than that indicated by the 1D model, due to the effect of the particle radical balance on the overall

system dynamics. The influence on the number of particles is shown in Figure 5.6(b), where a lower number of particles is obtained for the 2D case (but of the same order of magnitude).

Figure 5.7(b) shows the overall number of radicals per particle predicted by the 2D model is greater than that of the 1D model. The end-time plot of $\bar{n}(r)$ [Figure 5.7(a)] for both models exhibits the same trend. The abrupt cut-off point shown by the 2D model is due to the way that the model only deals with radicals in existing particles, rather than calculating $\bar{n}(r,t)$ (see Eq. (3.27)) for all values of r, despite there being no particles of that size present in the system. This does not however effect the global average in the 1D model. The larger number of radicals/particle in the 2D case impacts particle growth causing the end-time PSD to shift further to the right than that of the 1D simulation [Figure 5.6]. The effect of the disparity between both models in terms of radicals/particle is seen to profoundly effect the monomer consumption rates [see Figure 5.8]. The rate of monomer consumption in the 2D model case is far higher than in the 1D model, therefore monomer becomes exhausted sooner. This increase in conversion rate would appear to coincide with experimental observations made in Chapter 4, wherein experimental monomer conversion appeared to be faster than that demonstrated by the 1D model. Figure 5.9(a) and (b) show the level of VAc and BuA present in the system. Since the 2D model has a generally higher number of radicals per particle, the more reactive monomer (BuA) becomes exhausted at around 40 mins, compared to 80 mins as indicated by the 1D model. At around 40 mins in the 2D model, the effect of having minimal BuA present is to positively influence the uptake of VAc (see spike in Figure 5.8(a) and the increase in negative gradient of 2D model plot in Figure 5.9(a)). This effect is based on the change in reactivities of a pure VAc system as compared to a VAc/BuA system (compare the propagation constants in Table 3.1).

The difference in radical number per particle and resultant monomer consumption between the two models has important consequences for the global-average MWD evolutions shown in Figure 5.10. A comparison of the initial trends (0 to 40 min) shown by the 1D and 2D models, show a close match, indicating that the assumptions made in deriving the 1D PSD model, although greatly effecting intermediate process variables such as the average number of radicals per particle, impart little effect on the overall MWD prediction.

During this time period, it is noted that the global-average number of radicals per particle is considerably high [see Figure 5.7], demonstrating the capacity of the 1D model to operate in regions in which radical number is high. A large disparity between the predicted global-average MWs occurs after around 40 min, due to the monomer levels at this time.

The MW begins to increase at around 40 mins in the 2D model, coinciding with the exhaustion of BuA. This signifies a switch between the dominating monomers (from BuA to VAc). Following this increase, the MW gradually decreases due to the exhaustion of monomers and the creation of monomer starved conditions, promoting the formation of low MW chains.

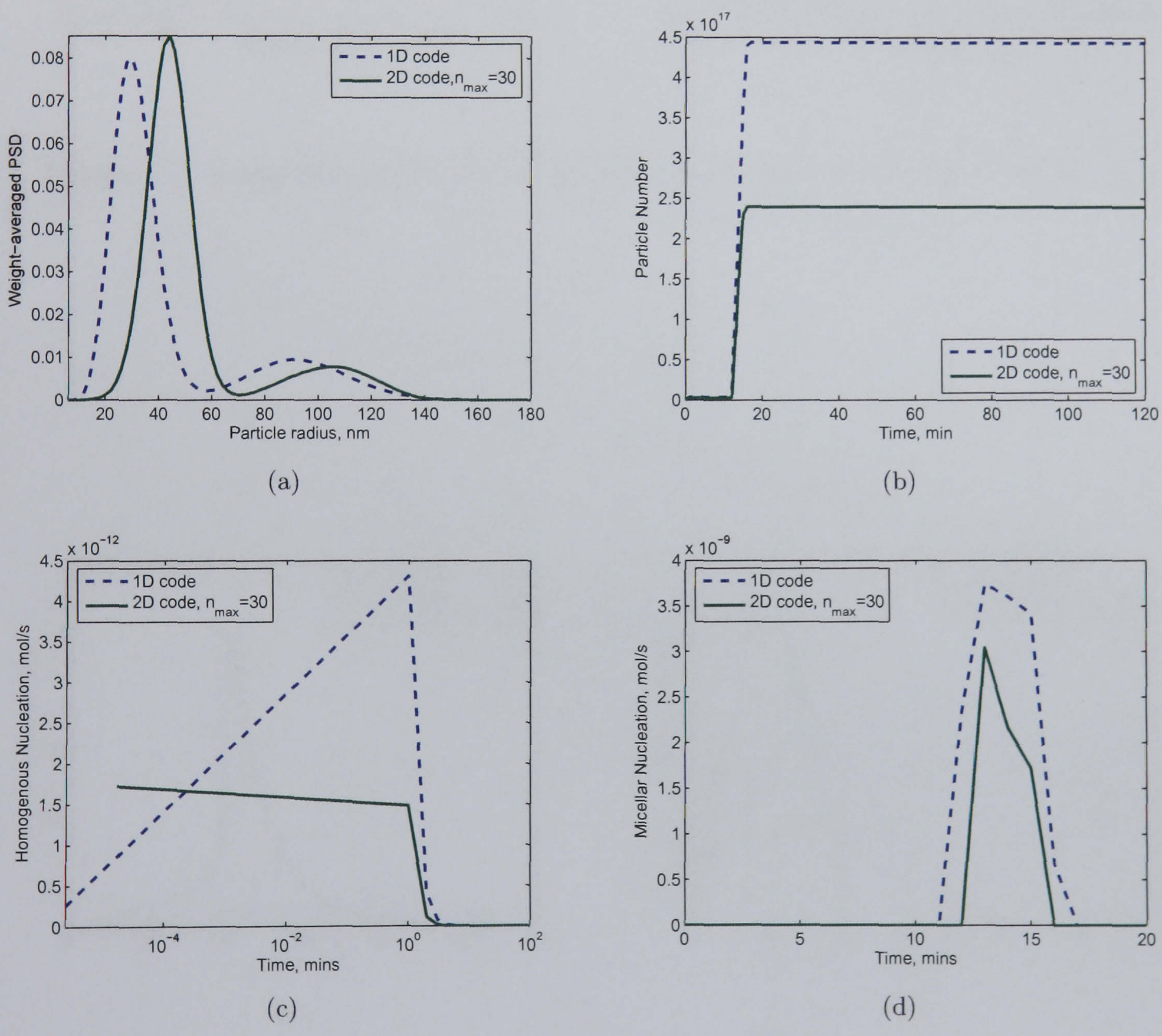
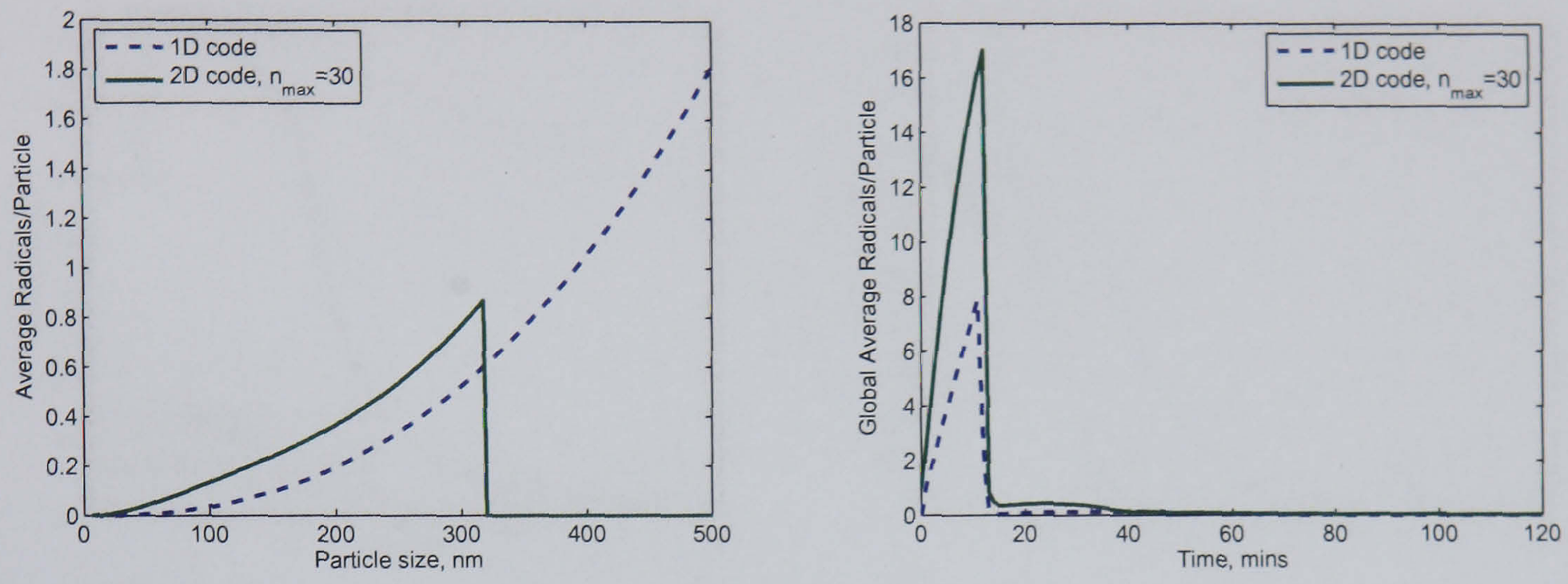
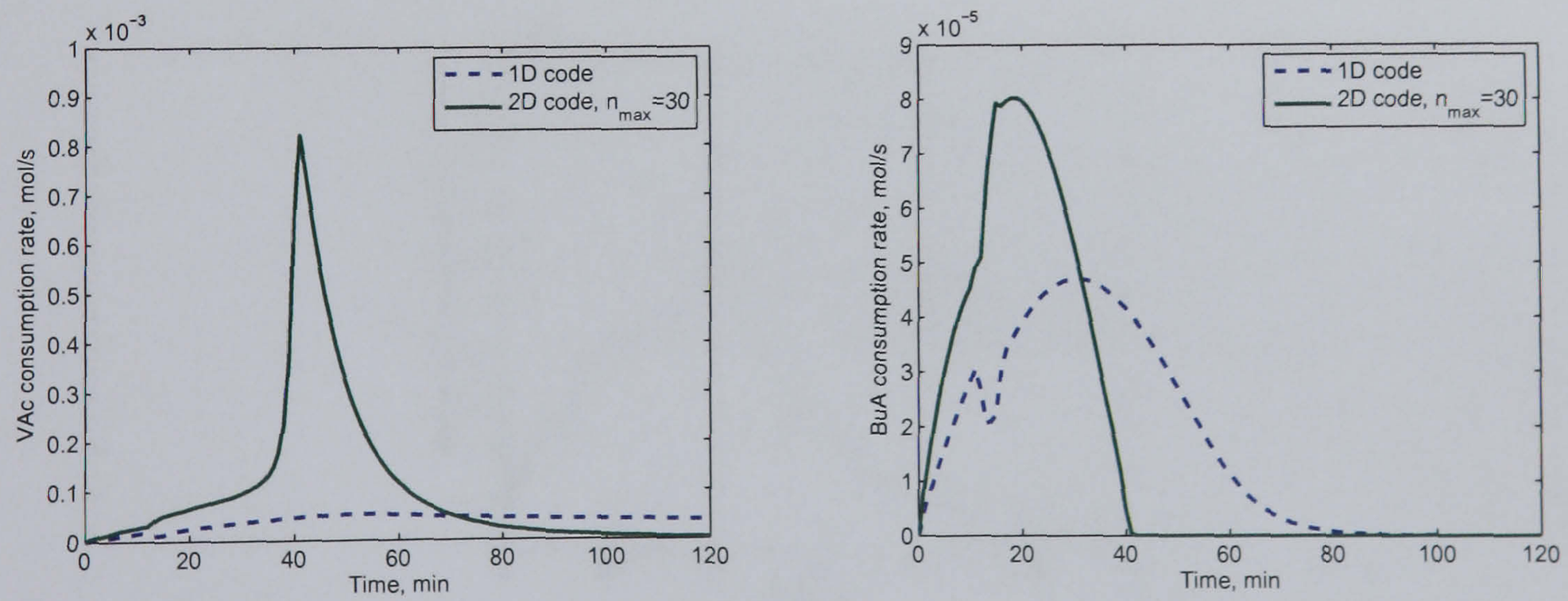


Figure 5.6: Comparison of 1D and 2D model results for a) Weight-average PSD b) Particle number c) Rate of homogenous nucleation and c) Rate of micellar nucleation.



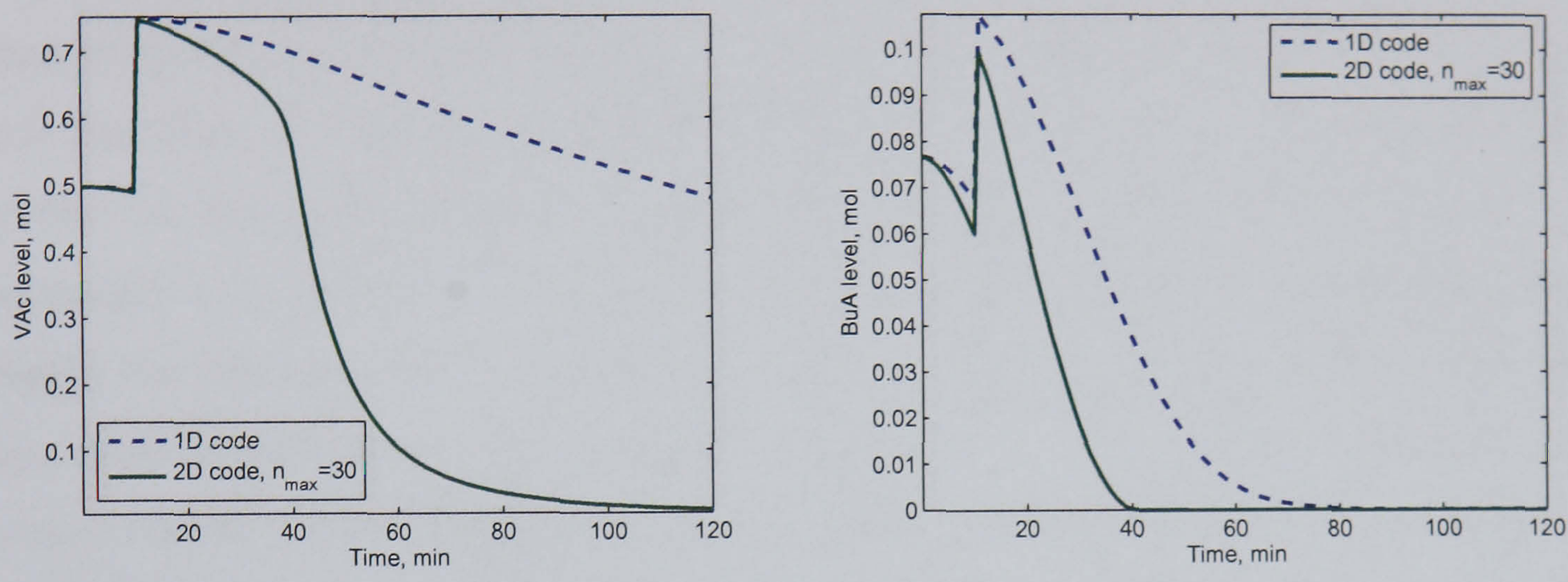
(a) (b)

Figure 5.7: Comparison of 1D and 2D model results for a) end-time $\bar{n}(r,t)$ and b) n_{glob}.



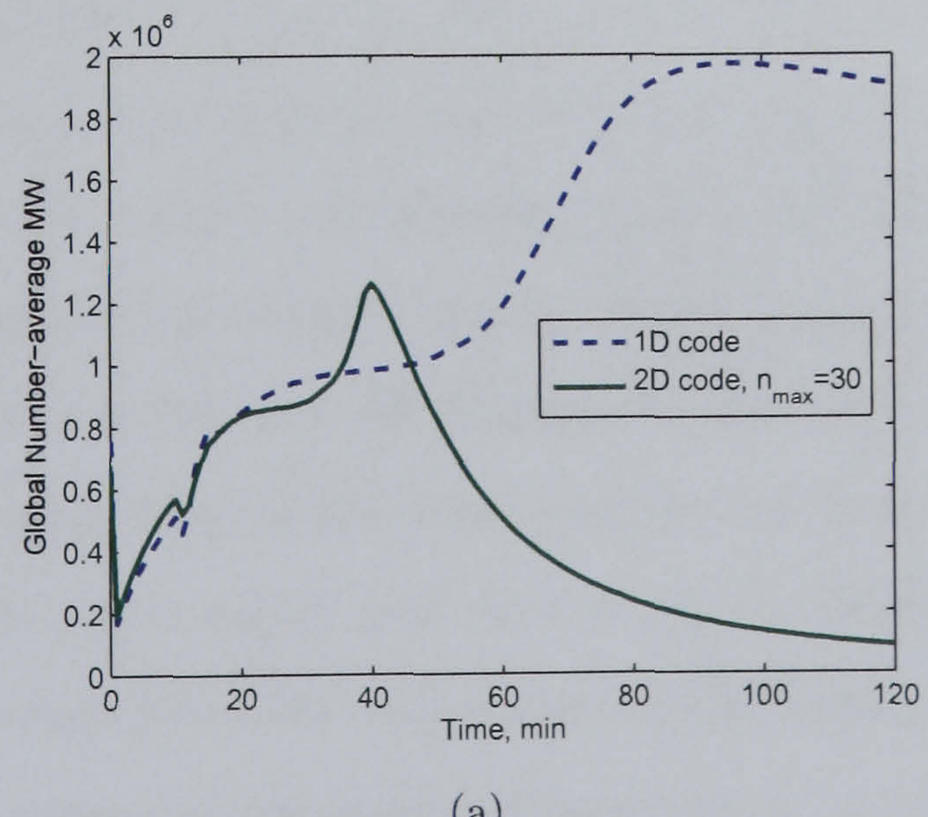
(a) (b)

Figure 5.8: Comparison of 1D and 2D model results for a) VAc and b) BuA consumption rates.



(a) (b)

Figure 5.9: Comparison of 1D and 2D model results for the amount of a) VAc and b) BuA in the system.



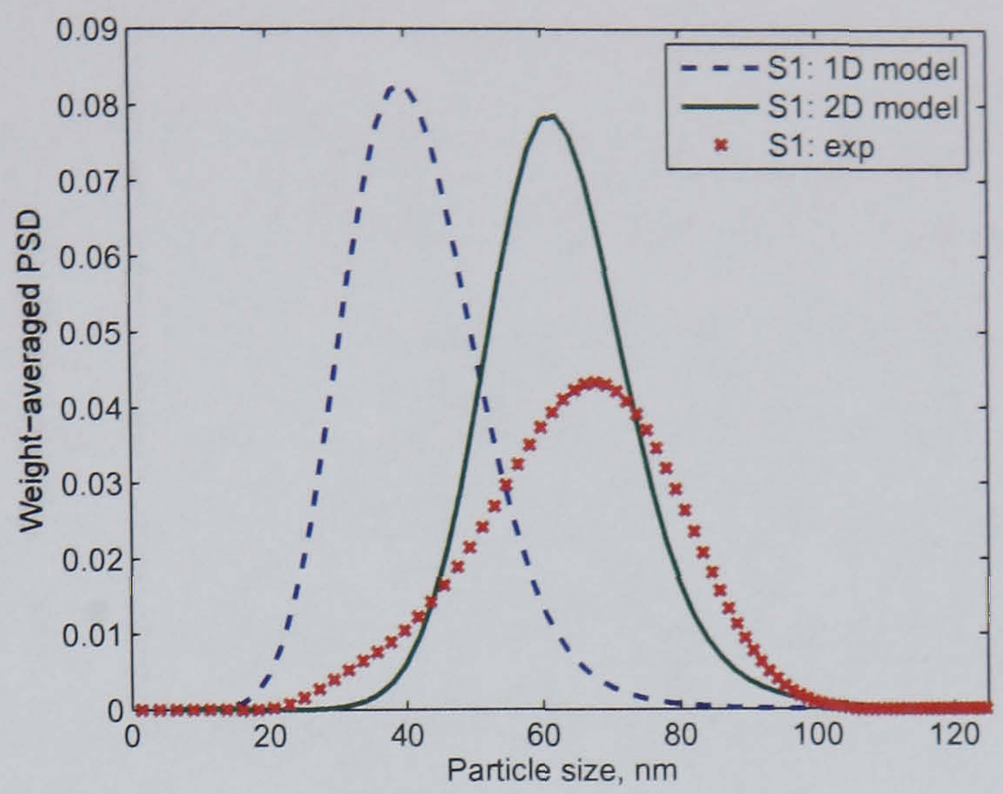
(a)

Figure 5.10: Comparison of 1D and 2D model results for global number-average MW.

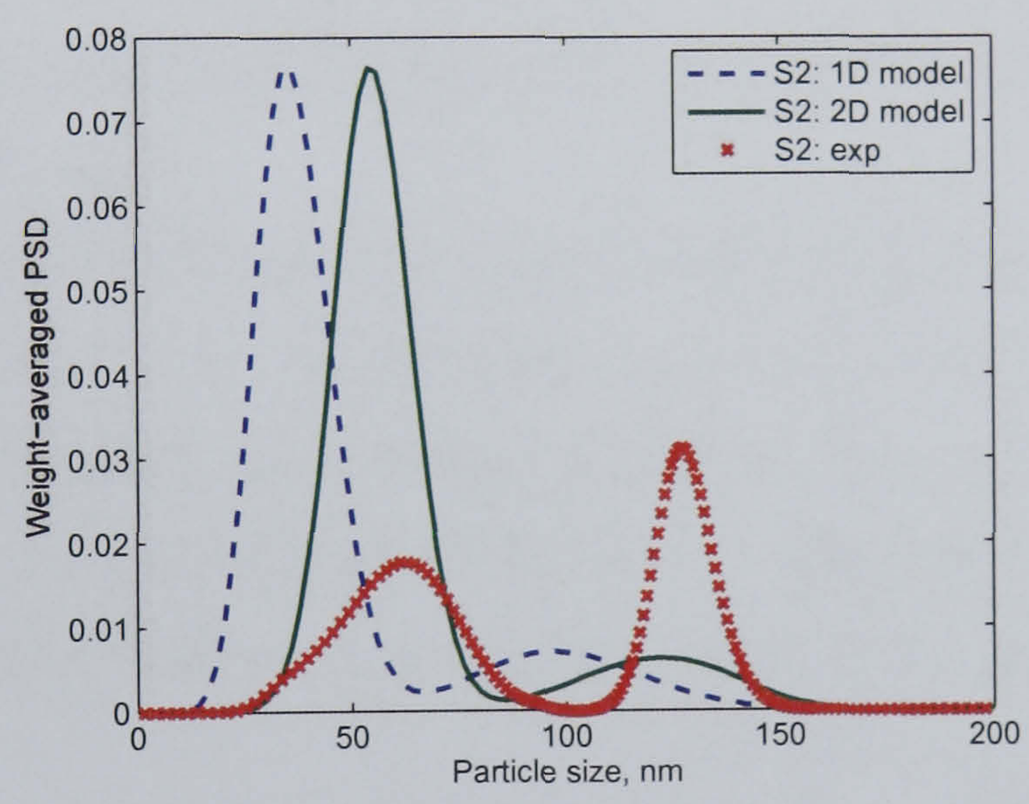
5.5.3 1D Model, 2D Model and Experiment Comparison

In the 1D model validation section of Chapter 4, some of the disparities that arose between model and experimental results were identified as possibly being due to incorrect accounting for growth in the 1D model. The above analysis of 1D and 2D models shows that the effect of compartmentalisation on the model predictions is to somewhat under-predict the amount of radicals being present in particles in the case of the 1D model. The potentially improved prediction of the radicals/particle in the 2D model might favourably impact the rate of growth of particles. It is therefore pertinent to examine what effect rigorously accounting for the inter-particle dynamics in the 2D model has on the match between model and the previously discussed experimental results. The inputs for cases S1, S2 and S3 [Table 4.1] have been implemented in the 1D model developed in Chapter 3 and the 2D model developed in this chapter, the weight-average PSD results from which have been overlaid with experimental results [see Figures 5.11(a),(b) and (c)]. The intention here is to observe whether accounting for compartmentalisation has a substantial effect on the PSD results (it should be noted that the aspect of coagulation is absent from the models).

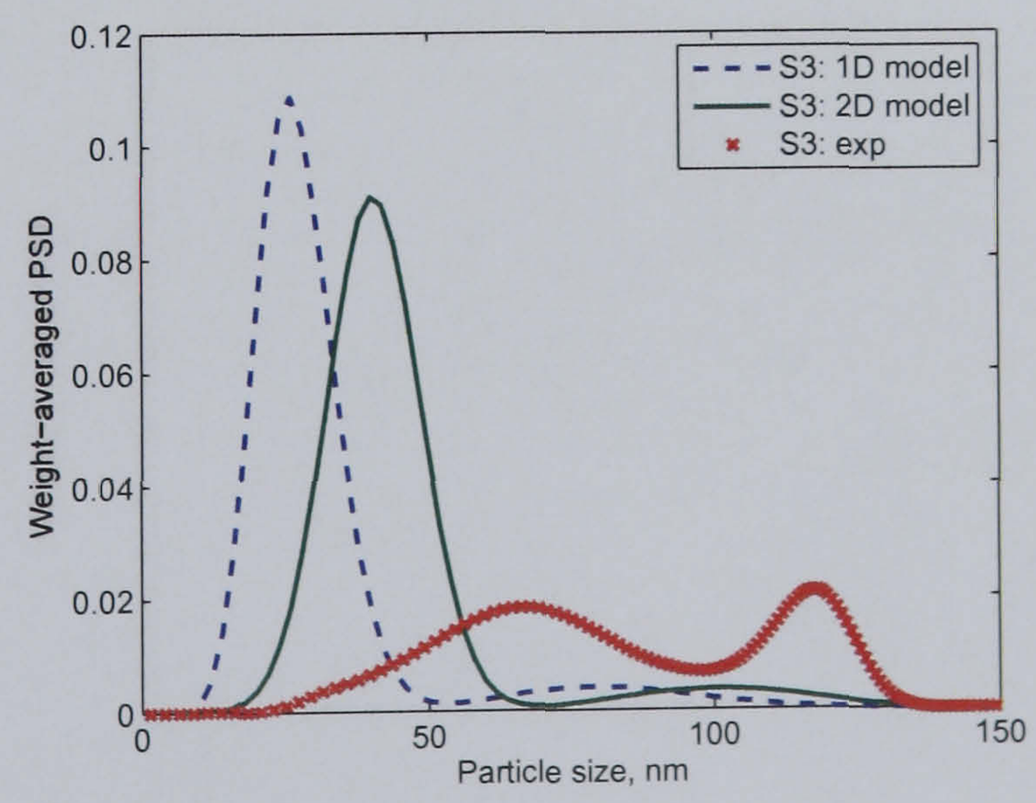
For case S1 [Figure 5.11(a)], the 1D model shows a monomodal PSD similar to experiment, however the simulated particles are smaller than those produced experimentally. The 2D model, although still not perfect due to lack of coagulation (and possibly parametric errors), has simulated a mode of particles that are of similar size to those in the experiment. The improved match between simulation and experiment is due to the 2D model better accounting for the radical number/particle, and hence growth is more accurately captured. For case S2 and S3 [Figure 5.11(b) and (c)] both models and the experiment show a bimodal distribution due to surfactant feed timing, and again a better correlation is observed between model and experiment for the 2D model, due to improved growth simulation. It is expected that coagulation would lead to a further improved match, however due to the 2D nature of the model, this would be a substantial development.



(a)



(b)



(c)

Figure 5.11: Comparison of 1D and 2D model and experimental results for weight-averaged PSD for a) case S1 b) case S2 and c) case S3.

5.6 Chapter Summary

In this chapter two models were compared: a 1D PSD/MWD model and a 2D PSD/MWD model. Analysis of the simulation results showed a slight difference in PSD predictions and a marked difference in the global-average number of radicals per particle. This caused a large difference in the monomer consumption profiles, leading to disparities between global number-average MW profiles. This study gives an insight into the effect of compartmentalisation on the individual mechanisms that shape PSD and MWD. PSD results were compared from the 1D and 2D models and experiment for the surfactant perturbation set described in chapter 4. The 2D model showed that in properly accounting for inter-particle dynamics, a more accurate picture was obtained for the number of radicals per particle, more faithfully reproducing experimental trends in growth, in comparison to the 1D (pseudo-bulk) model.

The direct solution of this 2D model could be exploited for a more systematic accounting of compartmentalisation in the 1D model framework. Future work may aim to systematically capture the compartmentalisation effect on the correction factor 'f' described in Chapter 3 allowing a more rigorous derivation of this correction factor for insertion into the balance for $\bar{n}(r,t)$. A suggestion of how this may be done can be found in Chapter 6

Chapter 6

Conclusions and Future Work

6.1 Thesis Conclusions

The final chapter will review the questions asked at the beginning of the thesis, and conclude as to the extent to which they were answered. Firstly, a summarised account of the contributions from this thesis will be given. The simultaneous controllability of PSD and MWD in emulsion polymerisation was assessed through experimental studies. The objective of this work was to provide a starting point for the quantification of control effect on important product characteristics. A comprehensive population balance modelling framework was developed for the process, which incorporated factors such as a coagulation kernel for ionic surfactants and thermal initiator. A new MWD model was developed, which was solved coupled to the PSD model. The model was developed with on-line control application in mind (about 30 s solution time was obtained). Upon model validation, accord with experimental data trends was encouraging, however it was apparent that growth rates were under-predicted, prompting a study into the effect of compartmentalisation. To assess this factor, a 2D version of the model was built, similar in form to the full unsimplfied model by Saldivar et al.[77] Instead of assuming a pseudo-bulk situation. with information loss regarding radical activity inside particles, the model was solved in its full 2D form, with an adaption for the 2D model of the decomposition algorithm for PBE solution. Comparison of the output from this 2D model. with the 1D model and experimental data, showed growth modelling improvements in the 1D model were probably

needed, with the 2D model providing a systematic method for doing this.

(1) The first question sought to be addressed in this study related to the *viability of simultaneously controlling PSD and MWD, given process limitations*:

Elsewhere, it has been established that PSD and MWD strongly influence important end-product properties. It is therefore important to understand the influence that control action has on these variables. It is generally understood that emulsion polymerisation is described by unique reaction mechanisms, the interaction of which may lead to extremely complicated behaviour, therefore elucidation of such interactions in a controllability sense presents a useful source of information. Chapter 4 of this thesis presented an experimental study into the simultaneous controllability of PSD and MWD, through perturbation of several commonly used manipulated variables. The work analysed the practical limitations on the attainability of PSD and MWD, through a set of experiments designed to effectively manipulate all inputs. A bimodal PSD was first engineered through two distinct nucleation events, one initial surfactant-free homogenous nucleation event at early times and a micellar nucleation event via an impulse feed of monomer and surfactant some time later during the reaction. The summarised information that the experimental work provided is presented for each perturbed input:

Initiator: increasing the concentration of initiator feed increased the magnitude of the initial homogenous nucleation, effecting the relative size of the subsequent micellar nucleation. The decrease in the overall number of particles led to a smaller fraction of high MW chains in the MWD.

CTA: increasing the concentration of CTA caused a slight change in the homogenously nucleated mode of particles in the weight-averaged PSD profile, at the same time causing a large decrease in the MW.

Monomer: increasing the monomer feed led to an increase in the magnitude of micellar nucleation and growth of this mode, also limiting the fraction of high MW chains in the MWD

Surfactant: the timing of surfactant feed was seen to effect the modality of the PSD produced (bimodal or monomodal). In the case where a bimodal PSD was produced, increasing surfactant caused a small decrease in the final MW. Hence, this manipulated

variable possibly offers the best opportunity to manipulate PSD with minimal change to the final MW.

The chapter therefore answers the question above by demonstrating and analysing the various combinations of mechanisms that act to shape PSD and MWD profiles. The range of experiments carried out clearly indicated the operation of individual mechanisms in the simultaneous formation of PSD and MWD. Inferential control of important end-product properties would therefore be carried out by implementing a form of distribution control for PSD and MWD as pointed out in the Future Work section.

(2) The second question related to the *possibility and practicality of modelling the emulsion polymerisation reactor, accounting simultaneously for both PSD and MWD*:
Chapter 3 shows the mechanistic development of a combined PSD and MWD model for a copolymerisation system with ionic surfactant and thermal initiation. The incorporation of coagulation kinetics in a comprehensive framework was also carried out. The feasibility of model solution was demonstrated by producing a detailed range of process results, including weight-average PSD and NAMW for all particle sizes. The subsequent analysis of PSD and MWD results, showed that the model structure was fully capable of simulating the required process mechanisms. The practicality of the model was demonstrated with an overall solution time of approximately 30 s for simulation of a typical semi-batch polymerisation reaction. The minimal solution time was a result of the use of an efficient model structure, applying a selection of historical developments, such as the pseudo-homopolymer approximation, the pseudo-bulk assumption, and the method of moments for MWD solution, in parallel to an efficient solution strategy e.g. hierarchial 2-tier algorithm and multi-level discretisation. The model was certainly practical enough for use in control applications, as alluded to in the introduction section.

In Chapter 4, validation of the dynamic model was carried out by comparison to a range of experimental data for all model inputs, representing a rigorous test platform. The model was first tuned using the results of one experiment, and then without further tuning, subjected to a range of experimentally conducted recipe manipulations. The model demonstrated capacity to simulate perturbations in *initiator*, *CTA*, *monomer* and *surfactant*. A qualitative agreement for both PSD and global MW was obtained for per-

turbations in initiator and CTA. Qualitative agreement was obtained for PSD in the case of surfactant perturbations. MW results via simulation of surfactant perturbations however did not match experimentally obtained values, highlighted as being caused by growth errors that arose from incorrect predictions for the number of radicals per particle. PSD and MW results from experiments that perturbed monomer were not captured well by the model. This was again thought to be due to incorrect accounting for the number of radicals per particle, and hence growth, and was therefore investigated further in Chapter 5.

Chapter 5 goes on to analyse the effect of compartmentalisation on the model, and in fact demonstrates that some error seen in the validation effort was most probably due to the ill-accounting of the compartmentalised nature of the process. A 2D model was developed with the intention of highlighting differences in model simulation capacity compared to the 1D model, based on the proper accounting for intra-particle reactions. The 1D model developed in Chapter 3 was shown to be sensitive to compartmentalisation, which caused differences in the number of radicals per particle, effecting growth rates. The insight given by this chapter provided a basis for the future incorporation of a correction factor into the dynamic radical balance to allow the 1D model to simulate conditions were compartmentalisation has a large effect. The model development and analysis therefore proves that it is possible and very practical to model both PSD and MWD.

(3) The third question was related to the *evaluation of a framework to formulate such a PSD/MWD model*:
This question is also inherently answered under the previous question. The framework used to model PSD/MWD, as described in Chapter 3, consisted of 2 one-dimensional PBEs– a balance for particle density, and another for the average number of radicals per particle. This was combined with a separate set of discrete population balances for the number of live and dead chains existing within particles, distributed with respect to their length. Moments of these population balances were derived. The tractability of this mathematical framework was shown to be good, providing a model solution over a manageable time scale (i.e. for on-line control application). Validation of this model was done in a comprehensive manner with qualitative agreement with experiment obtained.

and answers given where agreement was not obtained. A more rigorous 2D model structure was developed, whereby the effect of compartmentalisation on the 1D model was assessed. This suggested that the 1D model structure was indeed capable of modelling PSD and MWD, with the incorporation of a correction factor. The development of this correction factor will require more work, and will be elaborated among the proposals for future.

6.2 Future work

Attention is now focussed on the specific corollaries, which build on the contributions from this thesis:

(1) In question 3, it was mentioned that the application of moments to the MWD framework led to a feasible model. In the next stage, the MWD model can be developed further such that it is solved directly to give a full MWD output, instead of the average MWs across the particle size domain. This should, however, be weighted against the fact that an experimental measurement of MWD across size is very difficult at present. It is speculated that although the MWD model equations rely on an average number of radicals per particle, therefore cannot intrinsically account for compartmentalisation, a suitable correction factor for this value can be derived based on future work to be described later (point 3). If the chain length balances are to be solved directly using an update scheme like that used for the PSD the problem would most likely become too large for effective application to on-line control, and therefore it would be useful to pursue simplification techniques such as those which aim to solve for discrete bands of chains, rather than each individual chain length.[164,153] Alternative methods have been used to obtain full MWD via reconstruction from moments of the distribution, e.g. the numerical fractionation technique.[165,166]

(2) It is recognised that the model match with experimental data, whilst being of sufficient quality to allow conclusions to be made about process interactions, was not perfect. To improve the model accuracy, it is first suggested that more systematic evaluation of model parameters be carried out. In the current model the parameters were adjusted manually, and since there are several important parameters that greatly effect results, altering these

together, and observing the effect on multiple outputs, was not easy (despite the quick solution time). Therefore, it is proposed that a more formal parameter estimation study be carried out. The parameter estimation would involve the process model being embedded within an optimisation scheme. The objective function would involve the discretised experimental PSD and MWD and solids fraction data as targets. The objective function would seek to minimise the difference or squared difference between model output and experimental data, via the manipulation of chosen model parameters (subject to physical constraints). It is suggested that a commercially available optimisation routine may be used, such as the gradient based technique used in the work of Bianco and Immanuel.[167]

(3) As alluded to during discussions of the model fit with experimental data, a compartmentalisation factor (f) could be developed to modify radical dynamics, and therefore allow the correct accounting for intra-particle radical dynamics, influencing particle growth, and therefore PSD as well as MWD. It is proposed to use the 2D model to simulate cases where number of radicals per particle is low (i.e. < 2). Using data for the 2D distribution of radicals in particles, it can be conceived to evaluate the proportions of particles of a particular size that will actually house certain reactions e.g. bimolecular termination will only occur in the fraction of particles with more than two radicals. This would allow a more fundamental analysis to underpin a correction factor that would either directly correct reaction rate constants[108], or modify the radical balance. Alternatively, a simultaneous approach could be adopted to model f, wherein f is dynamically evaluated at each time step as a closed-form function (to be determined) that would summarise mechanistic information about compartmentalisation.

(4) The model developed incorporates micellar and homogenous nucleation. However, as mentioned in chapter 3, there is also evidence for coagulative nucleation[24,21,144,145] playing a part in particle formation, the modelling[25,26,168,169] of which could be included as a possible model improvement step. Another theory of nucleation they may warrant model inclusion is the so-called 'micellisation' mechanism modelled by Song and Poehlein,[170,171] which, as the authors point out, is similar to homogenous nucleation with the exception of the size of the nucleated particles.

(5) Another proposal for future work relates to the development of strategies for the simultaneous control of PSD and MWD, which has been shown to be possible in this work. It is envisioned to first continue studies into quantifying the limitations on control of PSD and MWD by carrying out further experiments to analyse different feed regimes. Since the experiments carried out in this work involve mainly impulse feeding of monomer, it would be useful to employ a more continuous monomer feed.

Further, it is proposed to use the model to map out attainable regions in terms of PSD and MWD, in a reachability analysis akin to[137,172,173]. The model would be utilised to perform a sensitivity analysis to evaluate the feasible regions, for example, in terms of average molecular weight versus particle diameter (or ratio of peaks for a bimodal PSD). This would serve as part of a comprehensive methodology for the effective design of material properties.

(6) As a means to develop an effective and systematic process control scheme for the emulsion polymerisation process, it is pertinent to adopt a model-based approach. The combined PSD and MWD model developed in this work could be used for open-loop optimisation: it has already been shown that optimal recipes can be generated for an emulsion polymerisation by solving multi-objective dynamic optimisation problems towards target PSD, number of particles and solids content.[174,175,176,177,178,167,179] It is expected that optimal recipes may be generated for particular multi-objective problems, encompassing PSD, MWD and solids fraction.

Further work towards a comprehensive process control scheme would involve incorporation of the model within a model predictive control (MPC) framework,[180,181,68] such that the optimiser described above would be run at each available process measurement interval (currently about 10 mins for PSD). A state estimator would be used to correct for process disturbances and/or model errors, and a new (corrected) set of feed trajectories defined at each measurement interval. On-line MPC with a target consisting of MWD would be difficult due to the low measurement frequency possible for MWD. Use of a model as a soft-sensor [state estimator] would perhaps allow for more frequent indirect measurements to be taken. An alternative would be on-line feedback/control for PSD and

a batch-to-batch feedback control for MWD.

Bibliography

[1] R. F. Dunbrook in *Synthetic Rubber* (G. S. Whitby, C. C. Davis, and R. F. Dunbrook, eds.), ch. 2, New York: Wiley, 1954.

[2] W. P. Hohenstein and H. Mark, "Polymerization of olefins and diolefins in suspension and emulsion. part i.," *International Journal of Mass Spectrometry and Ion Processes*, vol. 1, pp. 127–145, 1946.

[3] P. A. Lovell and M. S. El-Aasser, eds., *Emulsion Polymerization and Emulsion Polymers*. Wiley, 1997.

[4] G. Belfort, R. H. Davis, and A. L. Zydney, "Review the behavior of suspensions and macromolecular solutions in crossflow microfiltration," *Journal of Membrane Science*, vol. 96, pp. 1–58, 1994.

[5] "Vinylidene chloride-based latex and process for producing the same," 2001. US Patent 6172158.

[6] P. F. Luckham and M. A. Ukeje, "Effect of particle size distribution on the rheology of dispersed systems," *J Colloid Interface Sci*, vol. 220, pp. 347–356, 1999.

[7] R. Greenwood, P. F. Luckham, and T. Gregory, "Minimising the viscosity of concentrated dispersions by using bimodal particle size distributions," *Colloids and Surfaces: A: Physiochemical and Engineering Aspects*, vol. 144, pp. 139–147, 1998.

[8] M. D. Amaral, S. Van Es, and J. M. Asua, "Effect of the particle size distribution on the low shear viscosity of high-solid-content latexes," *Journal of Polymer Science: Part A: Polymer Chemistry*, vol. 42, pp. 3936–3946, 2004.

[9] R. W. Nunes, J. R. Martin, and J. F. Johnson, "Influence of molecular weight and molecular weight distribution on mechanical properties of polymers," *Polymer Engineering and Science*, vol. 22, pp. 205–228, 1982.

[10] D. I. Lee in *Polymeric Dispersions: Principles and Applications* (J. M. Asua, ed.), Kluwer Academic, 1996.

[11] O. Elizalde, M. Vicente, C. Plessis, J. R. Leiza, and J. M. Asua, "Knowledge-based control of emulsion polymerization: Tailoring adhesive properties," *JCT Research*, vol. 1, pp. 45–51, 2004.

[12] J. E. Puskas, P. Chan, K. B. McAuley, G. Kaszas, and S. Shaikh *Polymer Reaction Engineering VI conference*, vol. Halifax, Canada, p. May, 2006.

[13] B. K. Dietrich, W. A. Pryor, and S. J. Wu, "Chain transfer constants of mercaptans in the emulsion polymerization of styrene," *Journal of Applied Polymer Science*, vol. 36, pp. 1129–1141, 1988.

[14] W. D. Harkins, "A general theory of the mechanism of emulsion polymerization," *Journal of The Americal Chemical Society*, vol. 69, no. 6, pp. 1428–1444, 1947.

[15] H. Benoit and P. Rempp, eds., *Macromolecules*. Pergamon Press.

[16] W. J. Priest, "Particle growth in the aqueous polymerization of vinyl acetate," *J Phys Chem*, vol. 56, pp. 1077–1082, 1952.

[17] F. K. Hansen and J. Ugelstad, "Particle nucleation in emulsion polymerization. i. a theory for homogeneous nucleation," *J Polym Sci: Polym Chem Ed*, vol. 16, pp. 1953–1979, 1978.

[18] A. S. Dunn, "Latex particle nucleation in emulsion polymerization," *Eur Polym J.* vol. 25, pp. 691–694, 1989.

[19] W. H. Smith and R. H. Ewart, "Kinetics of emulsion polymerization," *J.Chem.Phys.*, vol. 16, pp. 592–599, 1948.

[20] J. L. Gardon, "Emulsion polymerization. i. recalculation and extension of the smith-ewart theory," *J Polym Sci: Polym Chem*, vol. 6, pp. 623–641, 1968.

[21] I. Kuhn and K. Tauer, "Nucleation in emulsion polymerization: A new experimental study. 1. surfactant-free emulsion polymerization of styrene," *Macromolecules*, vol. 28, pp. 8122–8128, 1995.

[22] K. Tauer, R. Deckwer, I. Kuhn, and C. Schellenberg, "A comprehensive experimental study of surfactant-free emulsion polymerization of styrene," *Colloid Polymer Science*, vol. 277, pp. 607–626, 1999.

[23] A. P. Parker, P. A. Reynolds, A. L. Lewis, and L. Hughes, "Semi-continuous emulsion co-polymerisation of methylmethacrylate and butylacrylate using zwitterionic surfactants: Evidence of coagulative nucleation above the critical micelle concentration," *Colloids and Surfaces*, vol. 268, pp. 162–174, 2005.

[24] G. Lichti, R. G. Gilbert, and D. H. Napper, "The mechanisms of latex particle formation and growth in the emulsion polymerisation of stryene using the surfactant sodium dodecyl sulfate," *Journal of Polymer Science: Polymer Chemistry Edition*, vol. 21, pp. 269–291, 1983.

[25] P. J. Feeney, D. H. Napper, and R. G. Gilbert, "Coagulative nucleation and particle size distributions in emulsion polymerization," *Macromolecules*, vol. 17, pp. 2520–2529, 1984.

[26] P. J. Feeney, D. H. Napper, and R. G. Gilbert, "Surfactant-free emulsion polymerization: Predictions of the coagulative nucleation theory," *Macromolecules*, vol. 20, pp. 2922–2930, 1987.

[27] R. M. Fitch, *Polymer Colloids: A Comprehensive Introduction*. Academic Press, 1997.

[28] F. J. Schork, Y. Luo, W. Smulders, J. P. Russum, A. Butté, and K. Fontenot, *Polymer Particles, Advances in Polymer Science*, ch. Miniemulsion Polymerization, pp. 129–256. Springer-Verlag, Heidelberg, 2005.

[29] X. Q. Wu and F. J. Schork, "Batch and semibatch mini/macroemulsion copolymerization of vinyl acetate and comonomers," *Ind. Eng. Chem. Res.*, vol. 39, pp. 2855–2865, 2000.

[30] J. Ugelstad, M. S. El-Aasser, and J. W. Vanderhoff, "Emulsion polymerization: initiation of polymerization in monomer droplets.," *Journal of Polymer Science*, vol. 11, pp. 503–513, 1973.

[31] B. V. Derjaguin and L. D. Landau *Acta Physicochim.*, vol. 14, p. 633, 1941.

[32] E. J. W. Verwey and J. T. G. Overbeek, *Theory of the Stability of Lyophobic Colloids.* New York: Elsevier, 1948.

[33] C. D. Immanuel, T. J. Crowley, E. S. Meadows, C. F. Cordeiro, and F. J. Doyle III, "Evolution of multimodal particle size distribution in vinyl acetate/butyl acrylate emulsion copolymerizations," *J Polym Sci Part A: Polym Chem*, vol. 41, pp. 2232–2249, 2003.

[34] C. Kiparissides, , J. F. MacGregor, S. Singh, and A. E. Hamielec *Can. J. Chem Eng.*, vol. 58, pp. 65–71, 1980.

[35] M. Vicente, S. BenAmor, L. M. Gugliotta, J. R. Leiza, and J. M. Asua, "Control of molecular weight distribution in emulsion polymerization using on-line reaction calorimetry," *Ind. Eng. Chem. Res.*, vol. 40, pp. 218–227, 2001.

[36] M. S. El-Aasser, T. Makgawinata, J. W. Vanderhoff, and C. Pichot, "Batch and semicontinuous emulsion copolymerization of vinyl acetat-butyl acrylate. i. bulk, surface, and colloidal properties of copolymer latexes," *Journal of Polymer Science: Polymer Chemistry Edition*, vol. 21, pp. 2363–2382, 1983.

[37] A. Echevarría, J. R. Leiza, J. C. de la Cal, and J. M. Asua, "Molecular weight distribution control in emulsion polymerization," *AIChE Journal*, vol. 44, pp. 1667–1679, 1998.

[38] F. J. Schork in *Control of Polymerization Reactors* (F. J. Schork, P. B. Desphande, and K. W. Lefew, eds.), Dekker, 1993.

[39] H. U. Moritz in *Polymer Reaction Engineering* (K. H. Reichert and W. Geisler, eds.), VCH Verlag, 1989.

[40] E. D. Sudol, M. S. El-Aasser, F. J. Micale, and J. W. Vanderhoff, "Development and testing of a space-flight dilatometer/reactor," *Rev. Sci. Instrum.*, vol. 57, pp. 2332–2338, 1986.

[41] S. Canegallo, M. Apostolo, G. Storti, and M. Morbidelli, "On-line conversion monitoring through ultrasound propagation velocity measurements in emulsion polymerization," *Journal of Applied Polymer Science*, vol. 57, pp. 1333–1346, 1995.

[42] C. Wang, T. J. Vickers, J. B. Schlenoff, and C. K. Mann, "In situ monitoring of emulsion polymerization using fiber-optic raman spectroscopy," *Applied Spectroscopy*, vol. 46, pp. 1729–1731, 1992.

[43] C. Orr Jr and J. M. Dallavalle, *Fine Particle Measurement.* New York: Macmillan, 1959.

[44] T. Kourti, J. F. MacGregor, and A. E. Hamielec, "Minimum number of turbidity measurements required for the determination of particle size distributions," *Journal of Colloid and Interface Science*, vol. 120, pp. 292–295, 1987.

[45] B. E. Dahneke, ed., *Measurement of Suspended Particles by Quasi Elastic Light Scattering.* New York: Wiley-Interscience, 1983.

[46] J. A. Davidson, C. W. Macosko, and E. A. Collins, "Latex particle size analysis : I. flow ultramicroscopy," *Journal of Colloid and Interface Science*, vol. 25, pp. 381–388, 1967.

[47] J. Li, K. D. Caldwell, and W. Machtle, "Particle characterization in centrifugal fields : Comparison between ultracentrifugation and sedimentation field-flow fractionation," *Journal of Chromatography A*, vol. 517, pp. 361–376, 1990.

[48] J. G. DosRamos and C. A. Silebi, "The determination of particle size distribution of submicrometer particles by capillary hydrodynamic fractionation (chdf)." *Journal of Colloid and Interface Science*, vol. 135, pp. 165–177, 1990.

[49] E. A. Collins, "Measurement of particle size and particle size distribution," in *Emulsion Polymerization and Emulsion Polymers* (P. A. Lovell and M. S. El-Aasser, eds.), ch. 12, pp. 385–436, Wiley, 1997.

[50] R. J. Young and P. A. Lovell, *Introduction to Polymers.* London: Chapman and Hall, 1991.

[51] A. Meyer, N. Jones, S. Lyle, S. Venkataramani, J. Clark, and D. Kranbuehl, "Laser light-scattering molecular weight analysis of a poly(fluoro acrylate)." *Journal of Applied Polymer Science*, vol. 91, pp. 3447–3454, 2004.

[52] M. Karas, D. Bachmann, U. Bahr, and F. Hillenkamp, "Matrix-assisted ultraviolet laser desorption of non-volatile compounds," *International Journal of Mass Spectrometry and Ion Processes*, vol. 78, pp. 53–68, 1987.

[53] D. Britton, F. H. P. A, and Lovell, "13c nmr spectroscopy studies of branching and sequence distribution in copolymers of vinyl acetate and n-butyl acrylate prepared by semibatch emulsion copolymerization," *Macromolecules*, vol. 34, pp. 817–829, 2001.

[54] T. L. Clarke-Pringle and J. F. MacGregor, "Optimisation of molecular-weight distributionusing batch-to-batch adjustments," *Ind. Eng. Chem. Res.*, vol. 37, pp. 3660–3669, 1998.

[55] T. J. Crowley, C. A. Harrison, and F. J. Doyle III, "Batch-to-batch optimization of psd in emulsion polymerization using a hybrid model," *Proc. American Control Conf., Arlington, VA, Omnipress, Madison, WI*, vol. 2, pp. 981–986, 2001.

[56] S. M. Miller and J. B. Rawlings, "Model identification and control strategies for batch cooling crystallisers," *AIChE Journal*, vol. 40, pp. 1312–1327, 1994.

[57] V. Liotta, C. Georgakis, E. D. Sudol, and M. S. El-Aasser, "Real-time estimation and control of particle size in semi-batch emulsion polymerization," *Proceedings of the Americal Control Conference*, pp. 1172–1176, 1997.

[58] G. Fevotte, T. F. McKenna, S. Othman, and A. M. Santos, "A combined hardware/software sensing approach for on-line control of emulsion polymerisation processes," *Comp. Chem. Eng. Suppl.*, vol. 22, pp. 443–449, 1998.

[59] J. Dimitratos, C. Georgakis, M. S. El-Aasser, and A. Klein, "Dynamic modeling and state estimation for an emulsion copolymerization reactor," *Comp. Chem. Eng.*, vol. 13, pp. 21–33, 1989.

[60] D. G. Luenberger, "Observers for multivariate systems," *IEEE Trans. Autom. Control*, vol. 11, pp. 190–197, 1966.

[61] D. G. Luenberger, "An introduction to observers," *IEEE Trans. Autom. Control*, vol. 16, pp. 596–602, 1971.

[62] I. T. Cameron, F. Y. Wang, C. D. Immanuel, and F. Stepanek, "Process systems modelling and applications in granulation: A review," *Chemical Engineering Science*, vol. 60, pp. 3723–3750, 2005.

[63] D. Ramkrishna, *Population Balances: Theory and Applications to Particulate Systems in Engineering*. San Diego: Academic Press, 2000.

[64] H. Hulburt and S. Katz, "Some problems in particle technology: A statistical mechanical formulation," *Chemical Engineering Science*, vol. 19, pp. 555–574, 1964.

[65] D. L. Ma, D. K. Tafti, and R. D. Braatz, "High resolution simulation of multi-dimensional crystallization," *Industrial and Engineering Chemistry Research*, vol. 41, pp. 6217–6223, 2002.

[66] T. Crowley, E. Meadows, and F. Doyle III, "Numerical issues in solving population balance equations for particle size distribution control in emulsion polymerization," *Proceedings of the 1999 American control conference*, 1999.

[67] F. Gelberd and J. H. Seinfeld, "Numerical solution of the dynamic equation for particulate systems," *Journal of Computational Physics*, vol. 28, pp. 357–375, 1978.

[68] T. J. Crowley, E. S. Meadows, E. Kostoulas, and F. J. Doyle III, "Control of particle size distribution described by a population balance model of semibatch emulsion polymerization," *J. Process Control*, vol. 10, pp. 419–432, 2000.

[69] C. D. Immanuel, C. F. Cordeiro, S. S. Sundaram, E. S. Meadows, T. J. Crowley, and F. J. Doyle III, "Modeling of particle size distribution in emulsion co-polymerization:

comparison with experimental data and parametric sensitivity studies," *Comput Chem Eng*, vol. 26, pp. 1133–1152, 2002.

[70] Y. Liu and I. T. Cameron, "A new wavelet-based method for the solution of the population balance equation," *Chemical Engineering Science*, vol. 56, pp. 5283–5294, 2001.

[71] C. D. Immanuel and F. J. Doyle III, "Computationally efficient solution of population balance models incorporating nucleation, growth and coagulation: application to emulsion polymerization," *Chemical Engineering Science*, vol. 58, pp. 3681–3698, 2003.

[72] N. Sun and C. D. Immanuel, "Efficient solution of population balance models employing a hierarchical solution strategy based on a multi-level discretization," *Transactions of the Institute of Measurement and Control*, vol. 27, pp. 347–366, 2005.

[73] M. J. Hounslow, R. L. Ryall, and V. R. Marshall, "A discrete population balance for nucleation, growth and aggregation," *AIChE*, vol. 11, pp. 1821–1832, 1988.

[74] S. Kumar and D. Ramkrishna, "On the solution of population balance by discretization i: a fixed pivot technique," *Chemical Engineering Science*, vol. 51, pp. 1311–1332, 1996.

[75] K. W. Min and W. H. Ray, "On the mathematical modeling of emulsion polymerization reactors," *Journal of Macromolecular Science- Reviews in Macromolecular Chemistry and Physics*, vol. 2, pp. 177–255, 1974.

[76] J. B. Rawlings and W. H. Ray, "The modelling of batch and continuous emulsion polymerization reactors. part i: Model formulation and sensitivity to parameters," *Polymer Engineering and Science*, vol. 28, pp. 237–256, 1988.

[77] E. Saldívar, P. Dafniotis, and H. Ray, "Mathematical modeling of emulsion copolymerisation reactors. i. model formulation and application to reactors operating with micellar nucleation," *Journal of Macromolecular Science- Reviews in Macromolecular Chemistry and Physics*, vol. C38, pp. 207–325, 1998.

[78] W. D. Harkins, "A general theory of the reaction loci in emulsion polymerization." *J.Chem.Phys.*, vol. 13, no. 9, pp. 381–382, 1945.

[79] W. D. Harkins, "A general theory of the reaction loci in emulsion polymerization ii," *J.Chem.Phys.*, vol. 14, no. 1, pp. 47–48, 1946.

[80] W. H. Smith and R. H. Ewart, "Kinetics of emulsion polymerization," *J.Chem.Phys.*, vol. 16, pp. 592–599, 1948.

[81] J. L. Gardon, "Emulsion polymerization i. recalculation and extension of the smith-ewart theory," *Journal of Polymer Science: Part A: Polymer Chemistry*, vol. 6, no. 3, pp. 623–641, 1968.

[82] J. L. Gardon, "Emulsion polymerization ii. review of experimental data in the context of the revised smith-ewart theory," *Journal of Polymer Science: Part A: Polymer Chemistry*, vol. 6, no. 3, pp. 643–664, 1968.

[83] J. L. Gardon, "Emulsion polymerization iii. theoretical prediction of the effects of slow termination rate within latex particles," *Journal of Polymer Science: Part A: Polymer Chemistry*, vol. 6, no. 3, pp. 665–685, 1968.

[84] J. L. Gardon, "Emulsion polymerization iv. experimental verification of the theory based on slow termination rate within latex particles," *Journal of Polymer Science: Part A: Polymer Chemistry*, vol. 6, no. 3, pp. 687–710, 1968.

[85] J. L. Gardon, "Emulsion polymerization v. lowest theoretical limits of the ratio kt/kp," *Journal of Polymer Science: Part A: Polymer Chemistry*, vol. 6, no. 10, pp. 2853–2857, 1968.

[86] W. H. Stockmayer, "Note on the kinetics of emulsion polymerization," *Journal of Polymer Science*, vol. 24, pp. 314–317, 1957.

[87] J. T. OToole, "Kinetics of emulsion polymerization," *Journal of Applied Polymer Science*, vol. 9, pp. 1291–1297, 1965.

[88] M. Harada, M. Nomura, H. Kojima, W. Eguchi, and S. Nagata. "Rate of emulsion polymerization of styrene," *Journal of Applied Polymer Science*, vol. 16, no. 4, pp. 811–833, 1972.

[89] J. Dimitratos, C. Georgakis, M. S. El-Aasser, and A. Klein. "Dynamic modeling and state estimation for an emulsion copolymerization reactor," *Computers and Chemical Engineering*, vol. 13, pp. 21–33, 1989.

[90] J. Dimitratos, C. Georgakis, M. El-Aasser, and A. Klein, "An experimental study of adaptive kalman filtering in emulsion copolymerization," *Chemical Engineering Science*, vol. 46, pp. 3203–3218, 1991.

[91] A. Urretabizkaia, E. D. Sudol, M. S. El-Aasser, and J. M. Asua, "Calorimetric monitoring of emulsion copolymerization reactions," *Journal of Polymer Science: Part A: Polymer Chemistry*, vol. 31, pp. 2907–2913, 1993.

[92] M. Nomura, K. Yamamoto, I. Horie, and K. Fujita, "Kinetics of emulsion copolymerization. ii. effect of free radical desorption on the rate of emulsion copolymerization of styrene and methyl methacrylate," *Journal of Applied Polymer Science*, vol. 27, pp. 2483–2501, 1982.

[93] M. Nomura, M. Kubo, and K. Fujita, "Kinetics of emulsion copolymerization. iii. prediction of the average number of radicals per particle in an emulsion copolymerization system," *Journal of Applied Polymer Science*, vol. 28, pp. 2767–2776, 1983.

[94] J. Forcada and J. M. Asua, "Modeling of unseeded emulsion copolymerization of styrene and methyl methacrylate," *Journal of Polymer Science, Part A: Polymer Chemistry Edition*, vol. 28, pp. 987–1009, 1990.

[95] J. R. Richards, J. P. Congalidis, and R. G. Gilbert. "Mathematical modeling of emulsion copolymerization reactors," *Journal of Applied Polymer Science*, vol. 37, pp. 2727–2756, 1989.

[96] E. L. Casella, O. Araujo, and R. Giudici, "Mathematical modeling of batch emulsion

copolymerization processes," *Polymer Reaction Engineering*, vol. 11, pp. 869–910. 2003.

[97] J. Gao and A. Penlidis, "Mathematical modeling and computer simulator/database for emulsion polymerizations," *Progress in Polymer Science*, vol. 27. pp. 403–535. 2002.

[98] D. C. Sundberg and J. D. Eliassen, *Polymer Colloids.* New York: Plenum, 1971.

[99] C. Kiparissides, J. F. MacGregor, and A. E. Hamielec, "Continuous emulsion polymerization. modeling oscillations in vinyl acetate polymerization," *Journal of Applied Polymer Science*, vol. 23, pp. 401–418, 1979.

[100] J. D. Stevens and J. O. Funderburk, "Design models for continuous emulsion polymerization and preliminary experiment evaluation." *Ind. Eng. Chem. Process Des. Develop.*, vol. 11, pp. 360–369, 1972.

[101] P. H. H. Araujo, J. C. de la Cal, J. M. Asua, and J. C. Pinto, "Modeling particle size distribution (psd) in emulsion copolymerization reactions in a continuous loop reactor," *Macromolecular Theory and Simulation*, vol. 10. pp. 769–779, 2001.

[102] J. B. Rawlings and W. H. Ray, "The modelling of batch and continuous emulsion polymerization reactors. part ii: Comparison with experimental data from continuous stirred tank reaactors," *Polymer Engineering and Science*, vol. 28, pp. 257–274, 1988.

[103] G. Lichti, R. G. Gilbert, and D. H. Napper, "The growth of polymer colloids." *Journal of Polymer Science: Polymer Chemistry Edition*, vol. 15. pp. 1957–1971. 1977.

[104] S. Chen and K. Wu, "Emulsion polymerization: theory of particle size distribution in copolymerization systems," *Journal of Polymer Science, Part A: Polymer Chemistry Edition*, vol. 26, pp. 1487–1506, 1988.

[105] M. J. Ballard, D. H. Napper, and R. G. Gilbert, "Theory of emulsion copolymerization kinetics," vol. 19. pp. 939–954. 1981.

[106] G. Storti, S. Carra, M. Morbidelli, and G. Vita, "Kinetics of multimonomer emulsion polymerization. the pseudo-homopolymerization approach," *Journal of Applied Polymer Science*, vol. 37, pp. 2443–2467, 1989.

[107] E. Saldivar, O. Araujo, and R. Giudici, "Modeling and experimental studies of emulsion copolymerization systems. iii. acrylics," *Journal of Applied Polymer Science*, vol. 84, pp. 1320–1338, 2002.

[108] E. M. Coen, R. G. Gilebrt, B. R. Morrison, H. Leube, and S. Peach, "Modelling particle size distributions and secondary particle formation in emulsion polymerisation," *Polymer*, vol. 39, pp. 7099–7112, 1998.

[109] C. D. Immanuel, F. J. Doyle III, C. F. Cordeiro, and S. S. Sundaram. "Population balance psd model for emulsion polymerization with steric stabilizers," *AIChE Journal*, vol. 49, pp. 1392–1404, 2003.

[110] X. E. E. Reynhout, *Novel approaches for emulsion polymerization research and development.* PhD thesis, Technische Universiteit Eindhoven, 2004.

[111] X. E. E. Reynhout, J. Meuldijk, B. A. H. Drinkenburg, P. D. Iedema, and M. Wulkow, "A novel method to model emulsion polymerization kinetics: The explicit radical-particle size distribution approach," *Polymer-Plastics Technology and Engineering*, vol. 44, pp. 707–740, 2005.

[112] C. Sayer, P. H. H. Arajo, G. Arzamendi, J. M. Asua, E. L. Lima, and J. C. Pinto, "Modeling molecular weight distribution in emulsion polymerization reactions with transfer to polymer," *Journal of Polymer Science: Part A: Polymer Chemistry*, vol. 39, pp. 3513–3528, 2001.

[113] H. Tobita, Y. Takada, and M. Nomura, "Molecular weight distribution in emulsion polymerization," *Macromolecules*, vol. 27, pp. 3804–3811, 1994.

[114] E. Giannetti, G. Storti, and M. Morbidelli, "Emulsion polymerisations. ii. kinetics, molecular weight distributions. and polymer microstructure of emulsion copolymers," *Journal of Polymer Science: Part A: Polymer Chemistry*, vol. 26, pp. 2307–2343, 1988.

[115] G. Storti, G. Polotti, M. Cociani, and M. Morbidelli. "Molecular weight distribution in emulsion polymerization. i. the homopolymer case," *Journal of Polymer Science: Part A: Polymer Chemistry*, vol. 30, pp. 731–750, 1992.

[116] G. Storti, G. Polotti, P. Canu, and M. Morbidelli, "Molecular weight distribution in emulsion polymerization. ii. the copolymer case," *Journal of Polymer Science: Part A: Polymer Chemistry*, vol. 30, no. 5, pp. 751–777, 1992.

[117] K. W. Min, *The Modelling and Simulation of Emulsion Polymerization Reactors*. PhD thesis, State University of New York at Buffalo, 1976.

[118] G. Arzamendi, J. Forcada, and J. M. Asua, "Kinetics of long-chain branching in emulsion polymerization," *Macromolecules*, vol. 27, pp. 6068–6079, 1994.

[119] J. Villermaux and L. Blavier, "Free radical polymerization engineering-i. a new method for modeling free radical homogeneous polymerization reactions," *Chemical Engineering Science*, vol. 39, pp. 87–99, 1984.

[120] G. Arzamendi, C. Sayer, N. Zoco, and J. M. Asua, "Modeling of mwd in emulsion polymerisation: Partial distinction approach," *Polymer Reaction Engineering*, vol. 6, pp. 193–223, 1998.

[121] G. Lichti, R. G. Gilbert, and D. H. Napper, "Molecular weight distributions in emulsion polymerizations," *Journal of Polymer Science: Polymer Chemistry Edition*, vol. 18, pp. 1297–1323, 1980.

[122] A. Ghielmi, S. Fiorentino, G. StortI, M. Mazzotti, and M. Morbidelli, "Long chain branching in emulsion polymerization," *Journal of Polymer Science: Part A: Polymer Chemistry*, vol. 35, pp. 827–858, 1997.

[123] A. Ghielmi, G. Storti, and M. Morbidelli, "Molecular weight distribution in emulsion polymerization: Role of active chain compartmentalization," *Macromolecules*, vol. 31, pp. 7172–7186, 1998.

[124] A. Butte, G. Storti, and M. Morbidelli, "Evaluation of the chain length distribution in free-radical polymerization, 1: Bulk polymerization," *Macromolecular Theory and Simulations*, vol. 11, pp. 22–36, 2002.

[125] A. Butte, G. Storti, and M. Morbidelli, "Evaluation of the chain length distribution in free-radical polymerization, 2a: Emulsion polymerization." *Macromolecular Theory and Simulations*, vol. 11, pp. 37–52, 2002.

[126] A. Butte, A. Ghielmi, G. Storti, and M. Morbidelli, "Calculation of molecular weight distributions in free-radical polymerization with chain branching." *Macromolecular Theory and Simulations*, vol. 8, pp. 498–512, 1999.

[127] D. Semino and W. H. Ray, "Control of systems described by population balance equations i. controllability analysis," *Chem Eng Sci*, vol. 50. pp. 1805–1824. 1995.

[128] D. Semino and W. H. Ray, "Control of systems described by population balance equations ii. emulsion polymerization with constrained control action," *Chem Eng Sci*, vol. 50, pp. 1825–1839, 1995.

[129] T. J. Crowley, E. S. Meadows, E. Kostoulas, and F. J. Doyle III, "Control of particle size distribution described by a population balance model of semibatch emulsion polymerization," *Journal of Process Control*, vol. 10, pp. 419–432. 2000.

[130] E. S. Meadows, T. J. Crowley, C. D. Immanuel, and F. J. Doyle III, "Nonisothermal modeling and sensitivity studies for batch and semibatch emulsion polymerization of styrene," *Ind Eng Chem Res*, vol. 42, pp. 555–567, 2003.

[131] V. Liotta, C. Georgakis, E. D. Sudol, and M. S. El-Aasser, "Manipulation of competitive growth for particle size control in emulsion polymerization," *Ind Eng Chem Res*, vol. 36, pp. 3252–3263, 1997.

[132] S. M. Ahn, M. J. Park, and H. K. Rhee, "Extended kalman filter-based nonlinear model predictive control for a continuous mma polymerization reactor," *Ind Eng Chem Res*, vol. 38, pp. 3942–3949, 1999.

[133] T. J. Crowley and K. Y. Choi, "Experimental studies on optimal molecular weight distribution control in a batch-free radical polymerization process," *Chem Eng Sci*, vol. 53, pp. 2769–2790, 1998.

[134] A. Echevarria, J. R. Leiza, J. C. de la Cal, and J. M. Asua, "Molecular weight distribution control in emulsion polymerization," *AIChE*, vol. 44, pp. 1667–1679, 1998.

[135] M. Vicente, J. R. Leiza, and J. M. Asua, "Simultaneous control of the copolymer composition and mwd in emulsion copolymerization," *AIChE Journal*, vol. 47, pp. 1594–1606, 2001.

[136] M. Vicente, J. R. Leiza, and J. M. Asua, "Dynamic optimization of non-linear emulsion copolymerization systems: Open-loop control of composition and molecular weight distributions," *Chemical Engineering Journal*, vol. 85, pp. 339–349, 2002.

[137] C. D. Immanuel and F. J. Doyle III, "A sensitivity approach to reachability analysis for particle size distribution in semibatch emulsion polymerization," *Ind Eng Chem Res*, vol. 43, pp. 327–339, 2004.

[138] C. D. Immanuel, Y. Wang, and N. Bianco, "Feedback controllability assessment and control of particle size distribution in emulsion polymerisation," *Chemical Engineering Science*, vol. 63, pp. 1205–1216, 2008.

[139] J. Zeaiter, J. A. Romagnoli, G. W. Barton, V. G. Gomes, B. S. Hawkett, and R. G. Gilbert, "Operation of semi-batch emulsion polymerization reactors: modelling, validation and effect of operating conditions," *Chem Eng Sci*, vol. 57, pp. 2955–2969, 2002.

[140] J. Zeaiter, J. A. Romagnoli, and V. G. Gomes, "Online control of molar mass and particle-size distributions in emulsion polymerization," *AIChE*, vol. 52, pp. 1770–1779, 2006.

[141] S. J. Sweetman, C. D. Immanuel, T. Malik, S. Emmett, and N. Williams, "Population balance model for emulsion polymerisation under pseudo-bulk conditions: Combined particle size distribution and molecular weight distribution," *Macromol Symp*, vol. 243, pp. 159–178, 2006.

[142] N. M. Beylerian, L. R. Vardanyan, R. S. Harutyunyan, and R. L. Vardanyan, "Kinetics and mechanism of potassium persulfate decomposition in aqueous solutions

studied by a gasometric method," *Macromolecular Chemistry and Physics*, vol. 203, pp. 212–218, 2002.

[143] A. M. Santos, P. Vindevoghel, C. Graillat, A. Guyot, and J. Guillot, "Study of the thermal decomposition of potassium persulfate by potentiometry and capillary electrophoresis," *Journal of Polymer Science: Part A: Polymer Chemistry*, vol. 34, pp. 1271–1281, 1996.

[144] E. Ozdeger, E. D. Sudol, M. S. El-Aasser, and A. Klein, "Role of the nonionic surfactant triton-405 in emulsion polymerization. iii. copolymerization of styrene and n-butyl acrylate," *Journal of Polymer Science: Part A: Polymer Chemistry*, vol. 35, pp. 3837–3846, 1997.

[145] Y. H. Chang and Y. D. Lee, "Structural effects of a novel polymeric emulsifier- ssipm modified tetracarboxylic acid terminated polyester on the emulsion polymerization of butyl methacrylate," *Polymer*, vol. 40, pp. 5929–5937, 1999.

[146] S. Melis, M. Kemmere, J. Meuldijk, G. Storti, and M. Morbidelli, "A model for the coagulation of polyvinyl acetate particles in emulsion," *Chemical Engineering Science*, vol. 55, pp. 3101–3111, 2000.

[147] R. Hogg, T. W. Healy, and D. W. Fuerstenau, "Mutual coagulation of colloidal dispersions," *Transactions of the Faraday Society*, pp. 1638–1651, 1966.

[148] G. R. Wiese and T. W. Healy, "Effect of particle size on colloid stability," *Transactions of the Faraday Society*, pp. 490–499, 1970.

[149] R. O. Ottewill, "Emulsion polymerization," in *Emulsion Polymerization* (I. Piirma, ed.), New York: Academic, 1982.

[150] H. C. Hamaker, "The london van der waals attraction between spherical particles," *Physica*, vol. 4, pp. 1058–1072, 1937.

[151] A. S. Dunn and L. C. H. Chong, "Application of the theory of colliod stability to the problem of particle formation in aqueous solutions of vinyl acetate," *Br. Polym. J.*, vol. 2, pp. 49–58, 1970.

[152] M. Park, M. T. Dokucu, and F. J. Doyle III, "Modeling and sensitivity analysis of particle size distribution and chain length distribution in a semibatch emulsion copolymerization reactor," *Macromolecular Theory and Simulations*, vol. 14, pp. 474–490, 2005.

[153] T. J. Crowley and K. Y. Choi, "Calculation of molecular weight distribution from molecular weight moments in free radical polymerization," *Industrial Engineering Chemistry Research*, vol. 36, pp. 1419–1623, 1997.

[154] F. R. Mayo and F. M. Lewis, "Copolymerization. i. a basis for comparing the behavior of monomers in copolymerization; the copolymerization of styrene and methyl methacrylate," *Journal of the American Chemical Society*, vol. 66, pp. 1594–1601, 1944.

[155] C. Parkinson, S. Matsumoto, and P. Sherman, "The influence of particle-size distribution on the apparent viscosity of non-newtonian dispersed systems," *J Colloid Interface Sci*, vol. 33, pp. 150–160, 1970.

[156] S. C. Misra, C. Pichot, M. S. El-Aasser, and J. W. Vanderhoff, "Batch and semicontinuous emulsion copolymerization of vinyl acetate-butyl acrylate ii. morphological and mechanical properties of copolymer latex films," *J Polym Sci. Polym Chem Ed*, vol. 21, pp. 2383–2396, 1983.

[157] S. J. Sweetman, C. D. Immanuel, T. I. Malik, S. Emmett, and N. Williams, "Simultaneous controllability of PSD and MWD in emulsion polymerisation," *Macromolecular Reaction Enginering*, 2008. Accepted.

[158] S. Fan, S. P. Gretton-Watson, J. H. G. Steinke, and E. Alpay, "Polymerisation of methyl methacrylate in a pilot-scale tubular reactor: modelling and experimental studies," *Chemical Engineering Science*, vol. 58, pp. 2479–2490, 2003.

[159] S. Boutti, C. Graillat, and T. F. McKenna, "High solids content emulsion polymerisation without intermediate seeds. part ii. in situ generation of bimodal latices," *Polymer*, vol. 46, pp. 1211–1222, 2005.

[160] S. Sajjadi and B. W. Brooks, "Unseeded semibatch emulsion polymerization of butyl acrylate: Bimodal particle size distribution," *J Polym Sci Part A: Polym Chem*, vol. 38, pp. 528–545, 2000.

[161] M. S. El-Aasser and J. W. Vanderhoff, eds., *Emulsion Polymerisation of Vinyl Acetate*. Applied Science, London, 1981.

[162] P. A. Lovell, T. H. Shah, and F. Heatley, "Chains transfer to polymer in emulsion polymerization of n-butyl acrylate studied by 13c nmr spectroscopy and gpc," *Polym Comm*, vol. 32, pp. 98–103, 1991.

[163] J. Mendoza, J. C. De La Cal, and J. M. Asua, "Kinetics of the styrene emulsion polymerization using n-dodecyl mercaptan as chain-transfer agent," *Journal of Polymer Science: Part A: Polymer Chemistry*, vol. 38, pp. 4490–4505, 2000.

[164] B. Amaro, C. D. Immanuel, E. N. Pistikopoulos, A. Daiß, S. Müßig, K. Hungenberg, and P. A. Saraiva, "Molecular weight distribution in free-radical solution polymerisation - model development and process optimisation," *Macromolecular Reaction Engineering*, 2007. Submitted.

[165] G. Papavasiliou, Í. Birol, and F. Teymour, "Calculation of molecular weight distributions in non-linear free-radical polymerization using the numerical fractionation technique," *Macromol. Theory Simul.*, vol. 11, pp. 533–548, 2002.

[166] G. Papavasiliou, , and F. Teymour, "Reconstruction of the chain length distribution for vinyl-divinyl copolymerization using the numerical fractionation technique," *Macromol. Theory Simul.*, vol. 12, pp. 543–548, 2003.

[167] N. Bianco and C. D. Immanuel, "Optimal open-loop recipe generation for particle size distribution control in semi-batch emulsion polymerisation," in *Series on Computers and Operations Research* (I. D. L. Bogle and J. Zilinskas, eds.), vol. 7. World Scientific Publishing, 2006.

[168] P. J. Feeney, R. G. Gilbert, and D. H. Napper, "Periodic nucleation processes in emulsion polymerization systems," *Journal of Colloid and Interface Science*, vol. 107, pp. 159–173, 1985.

[169] C. S. Chern and C. H. Lin, "Particle nucleation in semi-batch surfactant-free emulsion polymerization of acrylic monomers," *Polymer International*, vol. 42, pp. 409–421, 1997.

[170] Z. Song and G. W. Poehlein, "Particle nucleation in emulsifier-free aqueous-phase polymerization: Stage 1," *Journal of Colloid and Interface Science*, vol. 128, pp. 486–500, 1989.

[171] Z. Song and G. W. Poehlein, "Particle formation in emulsifier-free aqueous-phase polymerization of styrene," *Journal of Colloid and Interface Science*, vol. 128, pp. 501–510, 1989.

[172] Y. Wang, C. D. Immanuel, and F. J. Doyle III, "Reachability of particle size distribution in emulsion batch polymerization under mid-course correction policies," *American Control Conference, IEEE*, pp. 2491–2496, 2003.

[173] C. D. Immanuel, J. H. G. Steinke, and J. S. Higgins, "An integrated model-based analysis of polymer chemistry and polymerisation reactors," *Macromolecular Symposia*, vol. 243, pp. 225–232, 2006.

[174] J. Flores-Cerrillo and J. F. MacGregor, "Iterative learning control for final batch product quality using partial least squares models," *Industrial and Engineering and Chemistry Research*, vol. 44, pp. 9146–9155, 2005.

[175] A. Kalani and P. D. Christofides, "Nonlinear control of spatially inhomogeneous aerosol processes," *Chemical Engineering Science*, vol. 54, pp. 2669–2678, 1999.

[176] K. Lee, J. H. Lee, D. R. Yang, and A. W. Mahoney, "Integrated run-to-run and on-line model-based control of particle size distribution in semibatch precipitation reactor," *Computers and Chemical Engineering*, vol. 26, pp. 1117–1131, 2002.

[177] Z. K. Nagy and R. D. Braatz, "Open-loop and closed-loop robust optimal control of batch processes using distributional and worts-case analysis," *Journal of Process Control*, vol. 14, pp. 411–422, 2004.

[178] E. E. Saldívar and W. Ray, "Control of semicontinuous emulsion copolymerization reactors," *A.I.Ch.E. Journal*, vol. 43, pp. 2021–2033, 1997.

[179] C. D. Immanuel and F. J. Doyle III, "Hierarchical multiobjective strategy for particle-size distribution control," *AIChE Journal*, vol. 49, pp. 2383–2399, 2003.

[180] D. Q. Mayne, J. B. Rawlings, C. V. Rao, and P. O. M. Scokaert, "Constrained model predictive control: Stability and optimality," *Automatica*, vol. 36, pp. 789–814, 2000.

[181] F. Allgower, T. Badgwell, J. Qin, J. Rawlings, and S. Wright, "Nonlinear predictive control and moving horizon estimation - an introductory overview," in *Advances in Control: Highlights of ECC '99* (P. Frank, ed.), ch. 12, pp. 391–449, New York: Springer-Verlag, 1999.

Appendix A

Nomenclature

Symbol	Description
r	radius of an unswollen polymer particle
r_j	representative particle radius for bin j
rb_j	upper boundary size for bin j
ri_j	cut-off size for bin j
r_s	radius of a swollen polymer particle
j_{cr}	critical chain length for a aqueous phase radical
I_{w}	aqueous phase initiator
$[I_{\mathrm{w}}]$	concentration of aqueous phase initiator
R_{w}	aqueous phase initiator radicals
$k_{\mathrm{r}j}$	rate constant for initiation of a type j monomer in aq. phase
$M_{\mathrm{w}j}$	monomer of type j in aq. phase
$M_{\mathrm{p}j}$	monomer of type j in particle phase
$[M_{\mathrm{w}j}]$	concentration of monomer of type j in aq. phase
$[M_{\mathrm{p}j}]$	concentration of monomer of type j in particle phase
$P^l_{\mathrm{w}i}$	polymer radicals of length l and type i in aq. phase
$P^0_{\mathrm{w}i}$	monomeric radicals of type i in aq. phase
$P^0_{\mathrm{wA}i}$	radicals derived from chain transfer to CTA in aq. phase
$N^l_{\mathrm{p}i}$	polymer radicals of length l and type i in particle phase
$N^0_{\mathrm{p}i}$	monomeric radicals of type i in particle phase

$N^0_{\mathrm{pA}i}$	radicals derived from chain transfer to CTA in particle phase
$[P^l_{\mathrm{w}i}]$	concentration of polymer radicals of length l and type i in aq. phase
$[P^0_{\mathrm{w}i}]$	concentration of monomeric radicals of type i in aq. phase
$[P^0_{\mathrm{wA}i}]$	concentration of radicals derived from chain transfer to CTA in aq. phase
$[N^l_{\mathrm{p}i}]$	concentration of polymer radicals of length l and type i in particle phase
$[N^0_{\mathrm{p}i}]$	concentration of monomeric radicals of type i in particle phase
$[N^0_{\mathrm{pA}i}]$	concentration of radicals derived from chain transfer to CTA in particle phase
D^l_{w}	dead polymer chains of length l in aq. phase
D^l_{p}	dead polymer chains of length l in particle phase
$[D^l_{\mathrm{p}}]$	concentration of dead polymer chains of length l in particle phase
A_{w}	CTA in aq. phase
A_{p}	CTA in particle phase
$[A_{\mathrm{w}}]$	concentration of CTA in aq. phase
$[A_{\mathrm{p}}]$	concentration of CTA in particle phase
p_i	pseudo-homopolymer probability that a radical if type i in particle phase
$p_{\mathrm{w}i}$	pseudo-homopolymer probability that a radical if type i in aq. phase
u_i	molar flow rate of initiator into reactor
u_{Mj}	molar flow rate of type j monomer into reactor
u_{A}	molar flow rate of CTA into reactor
V_{aq}	Volume of aq. phase
k_{d}	rate constant for decomposition in the aq. phase
$k^{\mathrm{w}}_{\mathrm{p}ij}$	rate constant for propagation of a radical of type i with a monomer of type j in aq. phase
$k^{\mathrm{w}}_{\mathrm{td}ij}$	rate constant for termination via disproportionation of a radical of type i with a radical of type j in aq. phase
$k^{\mathrm{w}}_{\mathrm{tc}ij}$	rate constant for termination via combination of a radical of type i with a monomer of type j in aq. phase
$k^{\mathrm{w}}_{\mathrm{tr}ij}$	rate constant for chain transfer from a radical of type i to a monomer of type j in aq. phase

$k^{\mathrm{w}}_{\mathrm{trA}ij}$	rate constant for chain transfer from a radical of type i to CTA in particle phase
$k_{\mathrm{p}ij}$	rate constant for propagation of a radical of type i with a monomer of type j in particle phase
$k_{\mathrm{td}ij}$	rate constant for termination via disproportionation of a radical of type i with a radical of type j in particle phase
$k_{\mathrm{tc}ij}$	rate constant for termination via combination of a radical of type i with a monomer of type j in particle phase
$k_{\mathrm{tr}ij}$	rate constant for chain transfer from a radical of type i to a monomer of type j in particle phase
$k_{\mathrm{trA}ij}$	rate constant for chain transfer from a radical of type i to CTA in particle phase
e^l_i	rate constant for entry into a particle of a length l oligomer
$e^l_{\mathrm{m},i}$	rate constant for entry into a micelle of a length l oligomer
$k_{\mathrm{dM}i}$	rate constant for desorption of a monomeric radical from a particle of type i
$\bar{k}^{\mathrm{w}}_{\mathrm{tr}}$	pseudo-homopolymer rate constant for chain transfer in aq. phase
$\bar{k}^{\mathrm{w}}_{\mathrm{p}}$	pseudo-homopolymer rate constant for propagation in aq. phase
$\bar{k}^{\mathrm{w}}_{t}$	pseudo-homopolymer rate constant for total termination in aq. phase
$\bar{k}^{\mathrm{w}}_{\mathrm{trA}}$	pseudo-homopolymer rate constant for chain transfer to CTA in aq. phase
$\bar{k}_{\mathrm{tr}}$	pseudo-homopolymer rate constant for chain transfer in particle phase
$\bar{k}_{\mathrm{trA}}$	pseudo-homopolymer rate constant for chain transfer to CTA in particle phase
$\bar{k}_{\mathrm{p}}$	pseudo-homopolymer rate constant for propagation in particle phase
$\bar{k}_{\mathrm{t}}$	pseudo-homopolymer rate constant for total termination in particle phase
$\bar{k}_{\mathrm{tc}}$	pseudo-homopolymer rate constant for combination termination in particle phase
$\bar{k}_{\mathrm{td}}$	pseudo-homopolymer rate constant for disproportionation

	termination in particle phase
MW_i	molecular weight of monomer i
$\rho_{\mathrm{M}i}$	density of monomer i
ρ_{p}	density of polymer
$\bar{n}$	average number of radicals per particle
$V_{j,\mathrm{p}}$	volume of type j monomer in particles
$V_{j,\mathrm{w}}$	volume of type j monomer in aqueous phase
$V_{j,\mathrm{d}}$	volume of type j monomer in droplet phase
V_{p}	volume of unswollen particles
$V_{\mathrm{p}}^{\mathrm{s}}$	volume of swollen particles
V_{w}	volume of water
$V_{\mathrm{w}}^{\mathrm{T}}$	total volume of aqueous phase
V_{d}	total volume of monomer droplets
$K_{\mathrm{p}i}$	coefficient for monomer partitioning between particles and water
$K_{\mathrm{d}i}$	coefficient for monomer partitioning between droplets and water
$S_{(w)}$	concentration of free surfactant in aq. phase
S_{T}	total amount of surfactant in reactor
K_{s}	coefficient for surfactant partitioning between particles and water
$K_{\mathrm{s}}^{\mathrm{d}}$	coefficient for surfactant partitioning between droplets and water
K_{ad}	Langmuir adsorption constant
Γ_{∞}	Langmuir adsorption constant
$A_{\mathrm{p}}^{\mathrm{s}}$	surface area of polymer particles
$K_{\mathrm{d}}^{\mathrm{A}}$	coefficient for CTA partitioning between droplets and water
$K_{\mathrm{p}}^{\mathrm{A}}$	coefficient for CTA partitioning between particles and water
$D_{\mathrm{w}i}$	particle/ micelle entry rate parameter
$\bar{D}_{\mathrm{w}j}$	diffusion coefficient for monomer j in the aqueous phase
C_{micelle}	concentration of micelles in reactor
α_{ms}	area occupied by a surfactant molecule
N_A	Avogadro number
σ_{gen}	charge arising due to adsorbed surfactant

σ_{surf}	charge arising due to initiator
z_+	counter-ion valence
e	charge on an electron
A_{s}	total area occupied by surfactant
k	inverse double layer thickness
K_{B}	Boltzmann's constant
T	absolute temperature
I_{s}	ionic strength
[elec]	concentration of electrolyte in aq. phase
ε_0	permittivity of free space
ε_r	relative permittivity of water
ψ	surface potential
ζ	zeta potential
δ_{s}	Stern layer thickness
Φ_R	repulsion potential
Φ_A	attraction potential
A_{L}	Hamaker constant
D	distance between particle centres
d	interface particle distance
W_{ij}	Fuch stability ratio between two particles, i and j
B_{ij}	intrinsic coagulation rate between two particles, i and j
$\lambda_{\text{N}k}$	k^{th} moment of live radical balance
λ_{Dk}	k^{th} moment of dead polymer chain balance
NACL	number average chain length
WACL	weight average chain length
I_i	copolymer composition corresponding to type i monomer units
ϑ_i	reactivity ratio of monomer i
f_i	mole fraction of monomer i in the particle phase
N_{glob}	global number-average molecular weight (1D model)
W_{glob}	global weight-average molecular weight (1D model)

$\mathrm{MW_p}$	molecular weight of polymer
w	weight fraction of polymer
V_e	elution volume
n	discrete number of radicals
$\Re_\mathrm{entry}$	rate of entry into particles
$\Re'_\mathrm{entry}$	"
$\Re''_\mathrm{entry}$	"
$\breve{\Re}_\mathrm{entry}$	"
$\Re_\mathrm{des}$	rate of desorption from particles
$\Re'_\mathrm{des}$	"
$\Re''_\mathrm{des}$	"
$\breve{\Re}_\mathrm{des}$	"
$\Re_\mathrm{termin}$	rate of termination inside particles
$\Re'_\mathrm{termin}$	"
$\Re''_\mathrm{termin}$	"
$\breve{\Re}_\mathrm{termin}$	"
N^2_glob	global number-average molecular weight (2D model)
W^2_glob	global weight-average molecular weight (2D model)

Appendix B

Experimental Studies

B.1 Emulsion Polymerisation Equipment

Figure B.1 shows the emulsion polymerisation rig (detailed in Chapter 4).

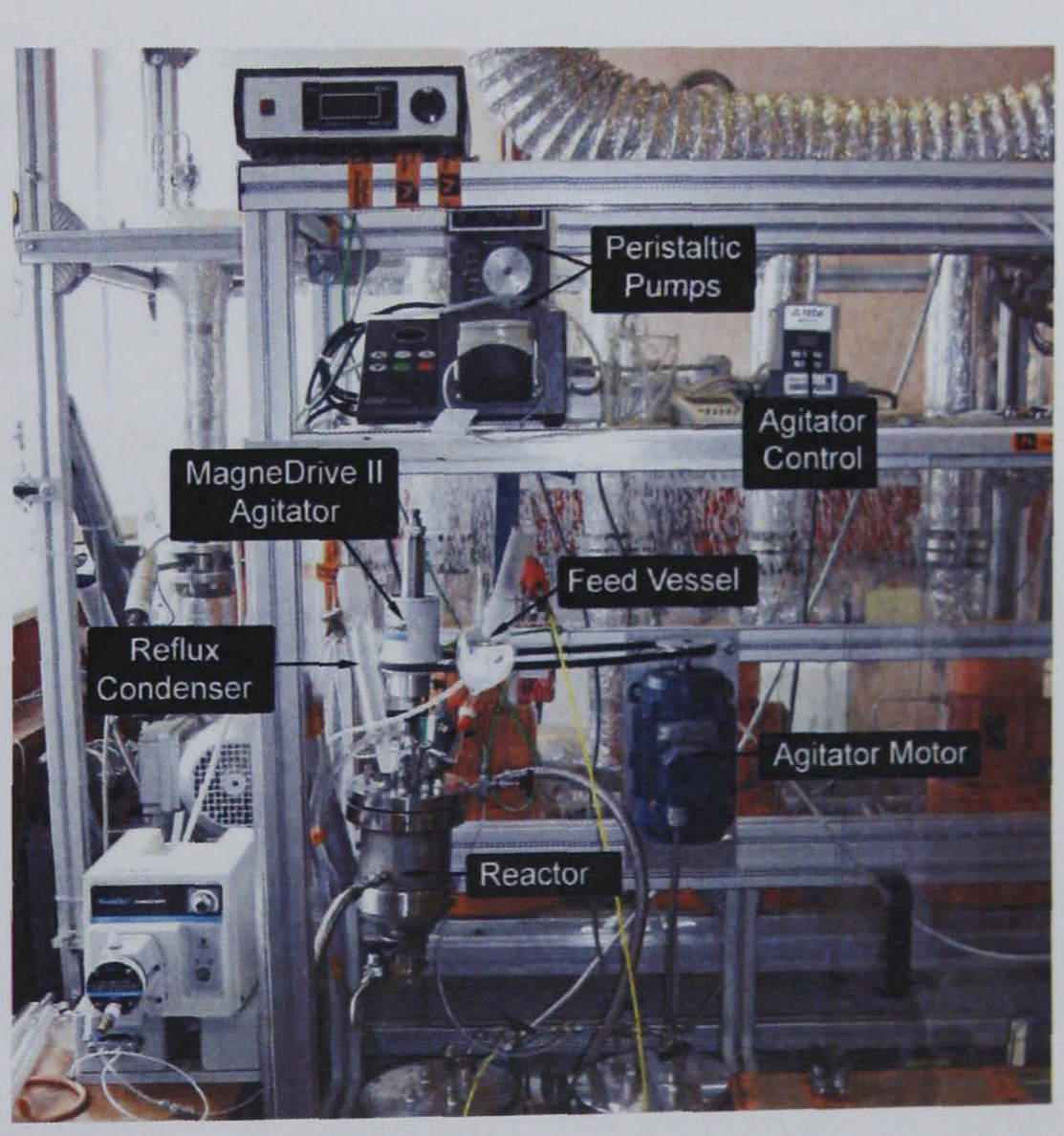


Figure B.1: Emulsion Polymerisation Experimental System system.

B.2 Capillary Hydrodynamic Fractionation: Measurement of PSD

The CHDF hardware setup is shown in Figure B.2.

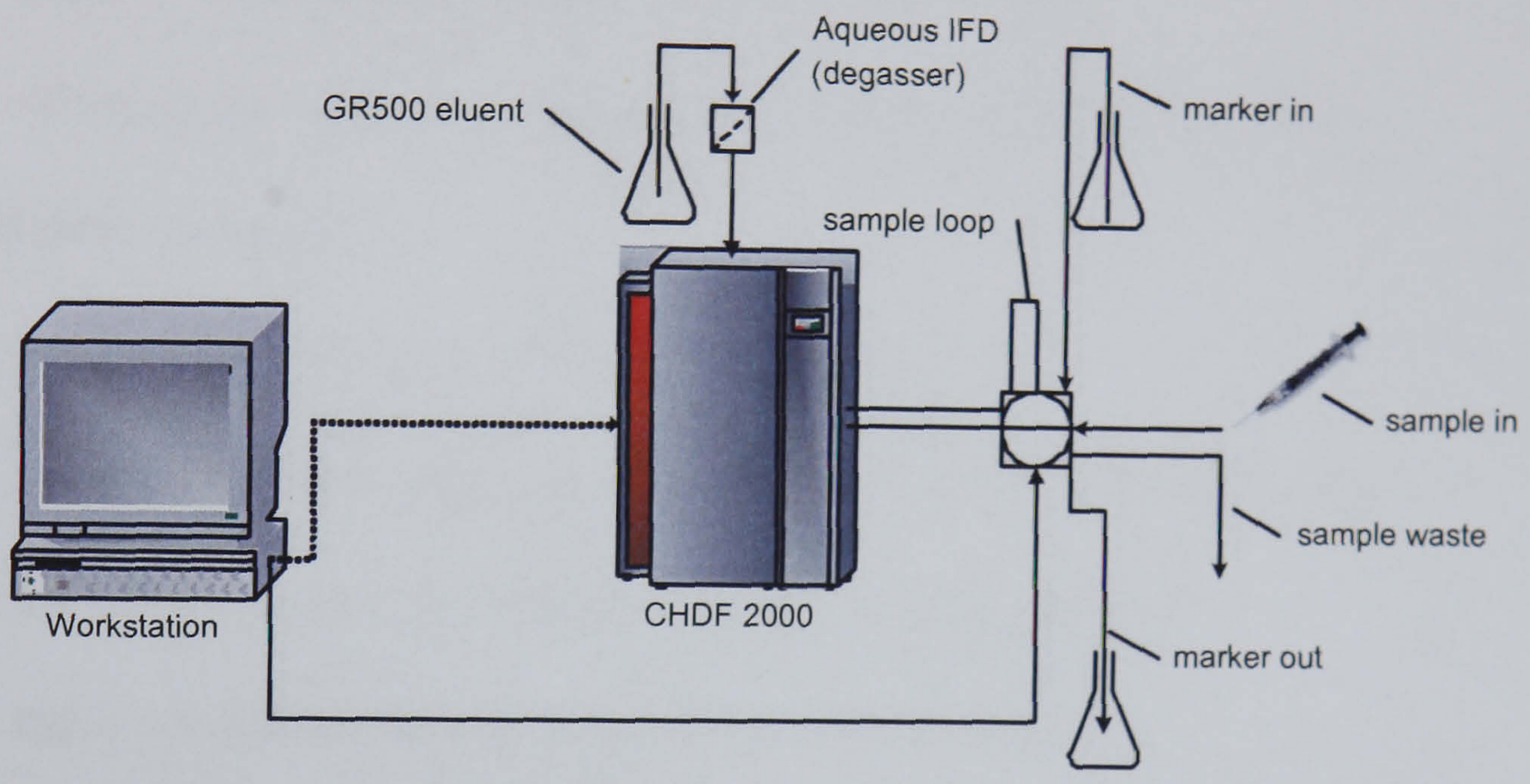


Figure B.2: Diagrammatic representation of CHDF system.

B.2.1 Materials and Methods

- *CHDF Hardware*: CHDF 2000 (Matec Applied Sciences)
- *Fractionation Cartridge*: C-204 Matec Applied Sciences)
- *Auto-injection device*: Rheodyne LabPRO PR700-102-01
- *Control/Analysis Software*: CHDF Version 3.2 (Matec Applied Sciences)
- *Eluent*: GR500 1x (Matec Applied Sciences), diluted 20:1 in DI water
- *Calibration Standards*: Nanosphere^{TM} Size Standards, 70nm, 600nm and multimodal 81, 199, 499 (Duke Scientific Corp.)
- *Marker fluid*: 0.005% sodium benzoate in water

CHDF Procedure

Sample preparation:

- fill glass vial with 5 mL sample from reactor
- mix 0.5 mL of 1% hydroquinone solution with sample
- dilute sample with eluent/DI water to within range (0.1–5% solids)

CHDF2000 operation

- ready CHDF device [see hardware User Guide v3.3]
- ready CHDF data collection software [see software User Guide v3.3]
- set marker running through auto-sampler (via gravity flow)
- inject sample into 25 μL sample loop, purge to waste
- run CHDF via software prompt
- data collection is now automatic (12 min/sample)

B.3 Gel Permeation Chromatography: Measurement of MWD

B.3.1 Materials and Methods

- *GPC Hardware*: PL-GPC 50 Integrated GPC system (Polymer Labs): refractive index and viscosity
- *GPC Hardware*: Dawn 8+ (Wyatt): light scattering
- *GPC Hardware*: PL Datastream high resolution data acquisition system (Polymer Labs)
- *Auto-sampler*: PL-AS RT GPC Autosampler (Polymer Labs)
- *Column Type*: 2 pLgel 5μm Mixed-D columns (29°C)
- *Control Software*: PL Instrument Control V2.0

- *Control Software*: Datastream monitor V1.2
- *Collection Software*: PL Astra V5.3.1.4 (collects RI and LS data)
- *Analysis Software*: Scirrus Multi-Online/Offline V3.0
- *Eluent*: Chromatography grade THF (Fisher)
- *Calibration Standards*: PL EasiVial PS-H

GPC Procedure

Sample preparation:

- fill glass vial with 5 mL sample from reactor
- mix 0.5 mL of hydroquinone solution with sample
- decant approx. 2 mL of sample into a shallow metal trough (maximising surface area to facilitate evaporation)
- dry sample at room temp until until no further weight change occurs
- using THF from GPC, make up 3mL polymer solution to approx. 1.5 mg/mL (exact concentration is required for analysis)
- allow 24 hours for dissolution of polymer

GPC operation

- ready GPC hardware [as above]. Samples must be placed in autosampler device.
- ready GPC data collection software [see PL software User Guide v3.3]
- begin measurement process (each sample takes approx. 35 mins)
- analyse data using analysis software (as above)

KING'S LONDON UNIV.